



# **THE TOXICOLOGY OF ANTIPSYCHOTIC DRUGS ON HUMAN NEURONAL CELLS**

By

**Israa Jameel Hakeem**

A thesis submitted to the University of Birmingham for the degree of  
DOCTOR OF PHILOSOPHY

School of Biosciences  
College of Life and Environmental Sciences  
University of Birmingham  
August 2018

UNIVERSITY OF  
BIRMINGHAM

**University of Birmingham Research Archive**

**e-theses repository**

This unpublished thesis/dissertation is copyright of the author and/or third parties. The intellectual property rights of the author or third parties in respect of this work are as defined by The Copyright Designs and Patents Act 1988 or as modified by any successor legislation.

Any use made of information contained in this thesis/dissertation must be in accordance with that legislation and must be properly acknowledged. Further distribution or reproduction in any format is prohibited without the permission of the copyright holder.

## **Abstract**

Antipsychotic medications are primarily used to manage several psychiatric disorders, such as schizophrenia and bipolar mania. They are also prescribed to manage neurodegenerative diseases symptoms including delusion, aggressiveness and agitation. Researches have suggested limiting the use of the first generation antipsychotics (FGAs) in elderly patients because of their adverse side-effects. The main aim of this study was to examine the effects of the first and second generation of antipsychotic drugs (SGAs) on neuronal (SH-SY5Y) and non-neuronal cells (COS7).

According to the  $LC_{50}$  values for the drugs investigated, chlorpromazine, trifluoperazine, olanzapine and quetiapine, they were specifically neurotoxic, since they were more potent in SH-SY5Y cells than in non-neuronal COS7 cells. In addition, of the FGAs tested in SH-SY5Y cells, they proved to be far more potent ( $LC_{50}$  5-6  $\mu$ M) compared to the SGA drugs tested ( $LC_{50}$  85-100  $\mu$ M). The major mechanism of cell death was apoptosis with regulated necrosis playing a minor role only with FGAs. Autophagy was not, however, involved. FGA induced apoptosis through the extrinsic pathway by activating caspase-8, and SGA induced cell death through the intrinsic pathway by activating caspase-9.

The involvement of  $Ca^{2+}$  pumps; SERCA2b and SPCA1a and the  $Ca^{2+}$  binding protein regucalcin (RGN) were investigated. From the results overexpression of SERCA2b and RGN showed a positive effect in the protection against the antipsychotic drug cell death, but no protection was observed with SPCA1a.

*This thesis is dictated to  
My father...  
My Love Dr. Basim Aljabhan*

## Acknowledgement

*“All praise is due to Allah, the Lord of the Worlds”*

Words cannot express my gratitude to all those who stood by me during this challenging scientific journey, but I shall try. First, I would like to thank my first supervisor, Prof. Frank Michelangeli, for his invaluable assistance and guidance throughout my PhD career. He is a wonderful supervisor and I consider myself lucky to have known him both professionally and personally. Also, I would like to thank my second supervisor, Dr. Nik Hodges, for his advice and crucial contribution in providing me with his guidance and emotional support especially in the last two years of my PhD.

I am also thankful to the Saudi Arabian Cultural Bureau for their generosity in sponsoring my PhD.

A big thanks to all of the staff in the Birmingham University School of Biosciences who helped me accomplish this research. A special thanks to all of my laboratory friends in the 8th, 4th and 7th floor for their continuous support. Special thanks goes to Noor, Abiola, Rachel, Mais, Shirikant and many others whom I have not mentioned here.

Most importantly, I am very grateful my husband Basim without whom I would have neither started nor finished this PhD. He is the rock in my world and I am the luckiest to have him by my side.

Last but not least, I am grateful for the limitless support of my family and friends. Especially I would like to express my love and appreciation to my mother Najia, my kids Battal and Miral who keep me grounded every step of the way. I am also grateful to all my friends especially Rawan who taught that it is normal to turn mental during my thesis writing.

With love,

Israa Hakeem

## Table of Contents

<b>Table of Contents</b> .....	<b>v</b>
<b>List of Abbreviations</b> .....	<b>xiii</b>
<b>1.1 Neurons</b> .....	<b>2</b>
<b>1.2 The Morphologically Defined Regions of a Neuron</b> .....	<b>2</b>
<b>1.3 Synapses</b> .....	<b>3</b>
<b>1.4 Neurotransmitters</b> .....	<b>5</b>
<b>1.5 Calcium Ions</b> .....	<b>7</b>
1.5.1 Neuronal Calcium Ions.....	9
<b>1.6 Calcium Transporters</b> .....	<b>11</b>
1.6.1 Calcium Pump .....	11
<b>1.7 Regucalcin</b> .....	<b>17</b>
1.7.1 RGN Functions.....	19
1.7.2 RGN in the Brain.....	20
<b>1.8 Alzheimer’s Disease</b> .....	<b>22</b>
<b>1.9 Cell Death</b> .....	<b>24</b>
1.9.1 Apoptosis.....	26
1.9.2 The Apoptosis Pathway.....	29
1.9.3 Necrosis.....	34
1.9.4 Regulated Necrosis.....	35
1.9.5 Autophagy .....	36
<b>1.10 Antipsychotic Drugs</b> .....	<b>38</b>
1.10.1 First-Generation Antipsychotics (FGAs) .....	39
1.10.2 Second-Generation Antipsychotics (SGAs) .....	40
1.10.3 Mechanism of Action .....	42
1.10.4 Chlorpromazine .....	43
1.10.5 Trifluoperazine .....	44
1.10.6 Olanzapine.....	45
1.10.7 Quetiapine .....	46
<b>2. Materials and Methods</b> .....	<b>49</b>
<b>2.1 Cell culture</b> .....	<b>49</b>
<b>2.2 Subculture</b> .....	<b>49</b>
<b>2.3 Cell Counting</b> .....	<b>50</b>
<b>2.4 Cryopreservation of Cells</b> .....	<b>51</b>
<b>2.5 MTT (3-(4,5-Dimethylthiazol-2-yl)-2,5-Diphenyltetrazolium Bromide) Cell Viability Assay</b> .....	<b>52</b>
<b>2.6 Crystal Violet</b> .....	<b>53</b>
<b>2.7 Sample Preparation</b> .....	<b>53</b>
2.7.1 Stock Solutions.....	53
2.7.2 Positive Control Solution .....	54
<b>2.8 Mechanism of Cell Death</b> .....	<b>54</b>
2.8.1 Apoptosis.....	54
2.8.2 Necrosis.....	56
2.8.3 Autophagy .....	57
<b>2.9 Preparation of Agar Plates and LB Broth Medium</b> .....	<b>58</b>

2.10 RGN-GFP Plasmid Preparation.....	59
2.11 Bacteria Recovery.....	60
2.12 Plasmid Maxi-Prep.....	61
2.13 Transient Transfection.....	61
2.14 Protein Extraction.....	62
2.15 Protein Estimation.....	63
2.16 Protein Separation by SDS Page.....	63
2.17 Western Blot Protein Transfer.....	64
2.18 Flow Cytometry.....	68
2.19 Co-Localisation.....	68
2.20 Confocal Microscopy.....	69
2.21 Differentiation of Sh-SY5Y Cells with Retinoic Acid.....	69
2.22 Statistics.....	70
<b>3. A Systematic Investigation of the Mechanisms of Cell Death Induced by Antipsychotic Drugs.....</b>	<b>72</b>
<b>3.1 Results.....</b>	<b>74</b>
<b>3.1.1 Cell Viability.....</b>	<b>74</b>
3.1.1.1 <i>Validity of MTT</i> .....	74
3.1.1.2 <i>Validity of Crystal Violet</i> .....	75
3.1.2 Effect of DMSO on SH-SY5Y.....	76
3.1.3 The Effect on Cell Viability of FGAs on SH-SY5Y and COS7 Cell Lines, Using MTT.....	78
3.1.4 The Effect on Cell Viability of FGAs on SH-SY5Y and COS7 Cell Lines Using the Crystal Violet Assay.....	80
3.1.5 The Effect on Cell Viability of SGAs on SH-SY5Y and COS7 Cell Lines Using the MTT Assay.....	82
3.1.6 The Effect on Cell Viability of SGAs on SH-SY5Y and COS7 Cell Lines Using Crystal Violet Assay.....	84
<b>3.1.7 Detecting Apoptosis.....</b>	<b>86</b>
3.1.7.1 <i>Detecting Apoptosis Using Fluorogenic Caspase-3 Substrate</i> .....	86
3.1.7.2 <i>The Effect of Caspase-3 Inhibitor on Cells Treated with FGAs</i> .....	92
3.1.7.3 <i>The Effect of Caspase-3 Inhibitor on Cells Treated with SGAs</i> .....	95
3.1.7.4 <i>The Effect of Caspase-9 Inhibitor on Cell Viability of SH-SY5Y and COS7 Treated with FGAs</i> .....	98
3.1.7.5 <i>The Effect of Caspase-9 Inhibitor on SH-SY5Y and COS7 Treated with SGAs</i> .....	101
3.1.7.6 <i>Cytochrome-C Release from Mitochondria</i> .....	104
3.1.7.7 <i>The Effect of Caspase-8 Inhibitor on SH-SY5Y and COS7 Treated with FGAs</i> .....	107
3.1.7.8 <i>The Effect of Caspase-8 Inhibitor on SH-SY5Y and COS7 treated with SGAs</i> .....	109
<b>3.1.8 Detecting Necrosis by Antipsychotic Drugs.....</b>	<b>112</b>
3.1.8.1 <i>LDH Release</i> .....	112
3.1.8.2 <i>Necrosis Inhibitor</i> .....	115
<b>3.1.9 Detecting Autophagy.....</b>	<b>118</b>
3.1.9.1 <i>Transfection of LC3</i> .....	118
3.1.9.2 <i>LC3B Antibody</i> .....	122

<b>3.2 Discussion</b> .....	<b>125</b>
3.2.1 The Effect of Both FGAs and SGAs on SH-SY5Y and COS7 Cell Lines....	126
3.2.2 The Mechanism of Cell Death Induced by Antipsychotic Drugs on SH-SY5Y and COS7 .....	127
<b>4. The Effects of Antipsychotic Drugs on Cells Overexpressing SERCA and SPCA Ca<sup>2+</sup> Pumps</b> .....	<b>132</b>
<b>4.1 Results</b> .....	<b>134</b>
4.1.1 The Effect of BAPTA-AM.....	134
4.1.2 The Effect of Antipsychotic Drugs on ER Stress .....	138
4.1.3 Transfection.....	140
4.1.4 The Overexpression of SPCA1a-GFP in COS7 .....	142
4.1.5 The Overexpression of SPCA1a-GFP in SH-SY5Y Cells .....	146
4.1.6 The Overexpression of SERCA2b-GFP in COS7 .....	150
4.1.7 The Overexpression of SERCA2b-GFP in SH-SY5Y .....	153
4.1.8 The Effect on Cell Viability of Antipsychotic Drugs on COS7 Transfected with SPCA1a-GFP .....	156
4.1.9 The Effect on Cell Viability of Antipsychotic Drugs on SH-SY5Y Transfected with SPCA1a-GFP .....	158
4.1.10 The Effect on Cell Viability of Antipsychotic Drugs on COS7 Transfected with SERCA2b-GFP .....	163
<b>4.2 Discussion</b> .....	<b>169</b>
4.2.1 The Effect of BAPTA-AM.....	169
4.2.2 ER Stress .....	170
4.2.3. Overexpression of Ca <sup>2+</sup> Pumps .....	170
<b>5. The Effects of Antipsychotic Drugs in Cells Overexpressing Regucalcin</b> <b>173</b>	
<b>5.1 Results</b> .....	<b>174</b>
5.1.1 The Overexpression of RGN-GFP in SH-SY5Y .....	174
5.1.1.2 <i>Analysis of RGN-GFP Transfection in SH-SY5Y Using FACC</i> .....	175
<b>5.1.2 The Overexpression of RGN-GFP in COS7</b> .....	<b>178</b>
5.1.2.1 <i>Analysis of RGN-GFP Expression in COS7 Cells</i> .....	178
5.1.2.2 <i>Analysis of RGN-GFP Expression in COS7 by FACC</i> .....	180
<b>5.1.3 The Effect on Cell Viability of Antipsychotic Drugs in COS7 Cells     Transfected with RGN-GFP</b> .....	<b>182</b>
5.1.3.1 <i>Crystal Violet Cell Viability Assay</i> .....	182
5.1.3.2 <i>Co-localisation of RGN-GFP in COS7 with FGA Drugs</i> .....	184
<b>6. Potency of FGA to Cause Cell Death Decreases upon Differentiation of SH- SY5Y Cells.</b> .....	<b>191</b>
<b>6.1 Results</b> .....	<b>193</b>
6.1.1 Differentiation of SH-SY5Y with Retinoic Acid.....	193
6.1.3 The Effect of FGA on Differentiated SH-SY5Y .....	197
<b>6.2 Discussion</b> .....	<b>200</b>
<b>7. General Discussion and Future Work</b> .....	<b>203</b>
<b>7.1 General Discussion</b> .....	<b>203</b>
<b>7.2 Future Work</b> .....	<b>208</b>
<b>8. References</b> .....	<b>210</b>

## List of Figures

Figure 1-1: Basic neuron structure.....	4
Figure 1-2: Basic chemical synapse structure.....	6
Figure 1-3: Overview of Calcium channels and pumps in different organelles within the cells. ....	10
Figure 1-4: Crystal structure of Ca <sup>2+</sup> ATPase showing the different domains. ....	12
Figure 1-5: General mechanism of Ca <sup>2+</sup> ATPase.....	13
Figure 1-6: The three different splice variants for the human RGN gene. ....	18
Figure 1-7: Crystal structure of human RGN with Ca <sup>2+</sup> bound in the middle. ....	18
Figure 1-8: Three types of cell death and their basic processes.....	25
Figure 1-9: Basic structure of pro-caspase and caspase.....	28
Figure 1-10: General mechanism of apoptosis.....	30
Figure 1-11: Extrinsic and intrinsic cell death-signalling pathways.....	33
Figure 1-12: Chemical structure of chlorpromazine. ....	43
Figure 1-13: Chemical structure of trifluoperazine.....	44
Figure 1-14: Chemical structure of olanzapine.....	45
Figure 1-15: Chemical structure of Quetiapine.....	46
Figure 2-1: View of the haemocytometer square under the microscope. ....	51
Figure 2-2: The OriGene vector with RGN-C tagged Human Variant 1.....	60
Figure 2-3: Proper layering of transfer.....	65
Figure 3-1: The relationship between SH-SY5Y cell number and MTT absorbance.....	75
Figure 3-2: The relationship between SH-SY5Y cell number and crystal violet absorbance.....	76
Figure 3-3: The effect of DMSO on SH-SY5Y cells.....	77
Figure 3-4: Dose-dependent effect on cell viability of different concentrations of FGAs on SH-SY5Y and COS7 cells, using MTT assay.....	79
Figure 3-5: Dose-dependent effect on cell viability of different concentration of FGAs on SH-SY5Y and COS7 using the crystal violet assay. ....	81
Figure 3-6: Dose-dependent effect on cell viability of different concentrations of SGAs on SH-SY5Y and COS7, using the MTT assay. ....	83
Figure 3-7: Dose-dependent effect on cell viability of different concentrations of SGAs on SH-SY5Y and COS7, using the crystal violet assay. ....	85
Figure 3-8: The activation of caspase-3 in SH-SY5Y treated with FGAs.....	87
Figure 3-9: The activation of caspase-3 in COS7 treated with FGAs.....	88
Figure 3-10: The activation of caspase-3 in SH-SY5Y treated with SGAs.....	90
Figure 3-11: The activation of caspase-3 in COS7 treated with SGAs.....	91
Figure 3-12: The effect of caspase-3 inhibitor in SH-SY5Y treated with FGAs..	93
Figure 3-13: The effect of caspase-3 inhibitor in COS7 treated with FGAs. ....	94
Figure 3-14: The effect of caspase-3 inhibitor on SH-SY5Y cells treated with SGAs. ....	96
Figure 3-15: The effect of caspase-3 inhibitor on COS7 cells treated with SGAs. .....	97

Figure 3-16: The effect of caspase-9 inhibitor on SH-SY5Y treated with FGAs.	99
Figure 3-17: The effect of caspase-9 inhibitor on COS7 treated with FGAs.....	100
Figure 3-18: The effect of caspase-9 inhibitor on SH-SY5Y cells treated with SGAs. ....	102
Figure 3-19: The effect of caspase-9 inhibitor on COS7 treated with SGAs.....	103
Figure 3-20: Detection of cytochrome c of mitochondria and cytosol extraction from SH-SY5Y treated with FGAs and SGAs.....	105
Figure 3-21: Detection of cytochrome c of mitochondria and cytosol extraction from COS7 treated with FGAs and SGAs. ....	106
Figure 3-22: The effect of caspase-8 inhibitor on SH-SY5Y treated with FGAs. ....	107
Figure 3-23: The effect of caspase-8 inhibitor on COS7 treated with FGAs.....	108
Figure 3-24: The effect of caspase-8 inhibitor on SH-SY5Y treated with SGAs. ....	110
Figure 3-25: The effect of caspase-8 inhibitor on COS7 treated with SGAs.....	111
Figure 3-26: The effect of FGA on lactate dehydrogenases release. ....	113
Figure 3-27: The effect of SGAs on lactate dehydrogenases release.....	114
Figure 3-28: The effect of necrosis inhibitor on SH-SY5Y and COS7 with FGAs. ....	116
Figure 3-29: The effect of necrosis inhibitor on SH-SY5Y and COS7 with SGAs. ....	117
Figure 3-30: Microscope images of cells transfected with LC3. ....	119
Figure 3-31: Microscope images of SH-SY5Y cells transfected with LC3 and treated with FGAs and SGAs. ....	120
Figure 3-32: Microscope images of COS7 cells transfected with LC3 and treated with FGAs and SGAs. ....	121
Figure 3-33: Detection of LC3B protein in SH-SY5Y treated with FGAs and SGAs. ....	123
Figure 3-34: Detection of LC3 protein in COS7 treated with FGAs and SGAs.	124
Figure 4-1: The effect of BAPTA-AM on SH-SY5Y with FGAs and SGAs.....	135
Figure 4-2: The effect of BAPTA-AM on COS7 with FGAs and SGAs .....	137
Figure 4-3: The detection of CHOP in COS7 cells treated with FGAs and SGAs. ....	138
Figure 4-4: The effect of different transfection reagents with SPCA1a-GFP plasmid on COS7 and SH-SY5Y cells.....	141
Figure 4-5: Microscope image of fluorescent COS7 transfected with 1 µg SPCA1a-GFP/ 2 µL MP after 72 hours. ....	143
Figure 4-6: The ratio of transfected COS7 with SPCA1a-GFP. ....	143
Figure 4-7: Western Blot detection of SPCA on COS7.....	144
Figure 4-8: Flow cytometry measurement of COS7 alone. ....	145
Figure 4-9: Flow cytometry measurement of transfected COS7 with SPCA1a-GFP. ....	145
Figure 4-10: Microscope image of fluorescent SH-SY5Y transfected with 1 µg SPCA1a-GFP/2 µL MP for 72 hours. ....	147

Figure 0-11: The ratio of transfected SH-SY5Y with SPCA1a-GFP. ....	147
Figure 4-12: Western Blot detection of SPCA on SH-SY5Y .....	148
Figure 4-13: Flow cytometry measurement of SH-SY5Y alone.....	149
Figure 4-14: Flow cytometry measurement of transfected SH-SY5Y with SPCA1a-GFP. ....	149
Figure 4-15: Microscope image of transfected COS7 with SERCA2b-GFP.....	150
Figure 4-16: The ratio of transfected COS7 with SERCA2b-GFP.....	151
Figure 4-17: Flow cytometry measurement of transfected COS7 with SERCA2b- GFP. ....	152
Figure 4-18: Microscope image of transfected SH-SY5Y with SERCA2b-GFP. .....	153
Figure 4-19: The ratio of transfected SH-SY5Y with SERCA2b-GFP. ....	154
Figure 4-20: Flow cytometry measurement of transfected SH-SY5Y with SERCA2b-GFP. ....	155
Figure 4-21: The effect on cell viability of FGAs and SGAs on COS7 cells overexpressing SPCA1a-GFP. ....	157
Figure 4-22: The effects of the FGAs and SGAs on cell viability of SH-SY5Y cells in the presence and absence of SPCA1a-GFP. ....	159
Figure 4-23: SH-SY5Y with SPCA1a-GFP control. ....	161
Figure 4-24: SH-SY5Y with SPCA1a-GFP treated with chlorpromazine.....	162
Figure 4-25: The effect of FGAs and SGAs on COS7 cells in the presence and absence of SERCA2b-GFP. ....	165
Figure 4-26: Control COS7 with SERCA2b.....	167
Figure 4-27: COS7 with SERCA2b treated with chlorpromazine.....	168
Figure 5-1: Microscope image of transfected SH-SY5Y with RGN-GFP plasmid. .....	175
Figure 5-2: The ratio of transfected SH-SY5Y with RGN-GFP.....	175
Figure 5-3: Flow cytometry measurement of SH-SY5Y alone.....	176
Figure 5-4: Flow cytometry measurement of transfected SH-SY5Y with RGN- GFP. ....	177
Figure 5-5: Microscope image of fluorescent COS7 transfected with 1 $\mu$ g RGN- GFP/ 2 $\mu$ L MP for 72 hours. ....	179
Figure 5-6: The ratio of transfected COS7 with RGN-GFP. ....	179
Figure 5-7: Flow cytometry analysis of COS7 alone.....	181
Figure 5-8: Flow cytometry measurement of transfected COS7 with RGN-GFP. .....	181
Figure 5-9: The effect on cell viability of FGAs and SGAs on COS7 in the presence and absence of RGN-GFP expression.....	183
Figure 5-10: COS7 RGN-GFP.....	185
Figure 5-11: COS7 RGN-GFP chlorpromazine.....	186
Figure 5-12: RGN-GFP trifluoperazine. ....	187
Figure 6-1: Morphological changes in SH-SY5Y cells upon RA-treatment. ....	194
Figure 6-2: Western Blot showing the neuronal marker GAP43 on differentiated SH-SY5Y cells. ....	196

Figure 6-3: The effect of Chlorpromazine (FGA) on both differentiated and non-differentiated SH-SY5Y.....	198
Figure 6-4: The effect of Trifluoperazine (FGA) on both differentiated and non-differentiated SH-SY5Y cells. ....	199
Figure 7-1: ER stress induced apoptosis (modified from Cano-Gonzales et al., 2018). ....	205

**List of Tables:**

Table 2-1: Transfection Reagents .....	62
Table 2-2: List of primary antibodies for each protein .....	66
Table 2-3: List of the Secondary Antibodies .....	67
Table 3-1: Summary of LC <sub>50</sub> values for all drugs on both cell lines using MTT and crystal violet assay .....	127
Table 3-2: Summary of the mechanism of cell death activated by each generation .....	130
Table 6-1: The LC <sub>50</sub> of FGA on differentiated and undifferentiated SH-SY5Y using crystal violet assay.....	201

## List of Abbreviations

AD	Alzheimer disease
ATP	Adenosine TriPhosphate
Ca <sup>2+</sup>	Calcium Ions
CHOP	C/EBP Homologous Protein
COS7	Fibroblast-Like Monkey Kidney Cell Line
DMEM	Dulbecco's Modified Eagle Media
DMSO	Dimethyl Sulfoxide
ER	Endoplasmic Reticulum
FACS	Flouresence-activated cell counter
FBS	heat-inactivated Foetal Bovine Serum
GFP	Green Fluorescent Protein
HBCD	Hexobromocyclododecane
KDa	kilodalton
LC3	Light Chain 3 Ptoein
LC <sub>50</sub>	Concentration Causing 50% Lethal
LDH	Lactate Dehydrogenase
MTT	3-(4,5-dimethylthiazol-2-yl)-2,5-diphenyltetrazolium bromide
NEAA	Non-Essential Amino Acid
PBS	Phosphate Buffered Saline
PI	Propidium Iodide
RGN	Regucalcin Protein
SDS	Sodium Dodecyl Sulphate
SERCA	Sarco/Endo Plasmic Reticulum Ca <sup>2+</sup> ATPase
SH-SY5Y	Human Brain Neuroblastoma Cell Line
SPCA	secretory pathway Ca <sup>2+</sup> ATPase
TNF	Tumor necrosis factor
TNF- $\alpha$	Tumor necrosis factor- $\alpha$

# **Chapter 1:**

# **Introduction**

## **1.1 Neurons**

The human body consists of various organs and tissues that are composed of different types of cells (Shuster, 2003). Cellular functions and modes of communication determine the role of each organ. The most complex organ in the human body is the brain (Sempere et al., 2004). The nervous system consists of two main types of nerve cells: neurons and non-neuronal cells called glial cells. Neurons sense changes in the environment and then process and transmit information to other cells through electrical and chemical signals. Glial cells support and nourish neurons (Noback et al., 2005). Regardless of type and size, all neurons generally have three morphologically defined regions: the cell body, dendrites, and axons (see figure 1-1).

## **1.2 The Morphologically Defined Regions of a Neuron**

The cell body, also called the soma, is the main part of the neuronal cell and consists of the typical organelles found in other animal cells such as the nucleus, mitochondria, Golgi, and endoplasmic reticulum (ER) (Squire et al., 2008).

Dendrites are short branches extending from the cell body that act as cellular extensions. They receive electrical impulses from other neurons and send the information to the cell body. Since dendrites act as electrical/chemical receivers, they are covered with synapses (Squire, 2008).

Axon are structures that are only found in neurons. Axons begin with an axon hillock and end with axon terminals (see Figure 1-1). At the end of an axon terminal are sites called synapses where the axon sends information to other cells. Axons are able to relay electrical messages across a length ranging from 0.1 mm to 2 mm. The term *action potential* usually refers to the electrical signals generated within neurons (Kandel et al., 2013).

### **1.3 Synapses**

Synapses are the interlinking spaces between any two adjacent neurons, between neurons and gland cells, or between neurons and muscle cells through which the electrical signals are conveyed with the help of chemical transmitters (Berridge, 2008). According to the direction of the information, the sending nerve cell is referred to as the presynaptic neuron, and the receiving nerve cell is referred to as the postsynaptic neuron (Higgins, 2013). Two kinds of synapses exist: electrical synapses and chemical synapses. Signal transmission in electrical synapses happens via gap junctions linking presynaptic neurons' cytoplasm to postsynaptic neurons. Alternately, chemical synapses involve the use of neurotransmitter chemicals to convey signals across the synaptic gap (Lodish et al., 2000).

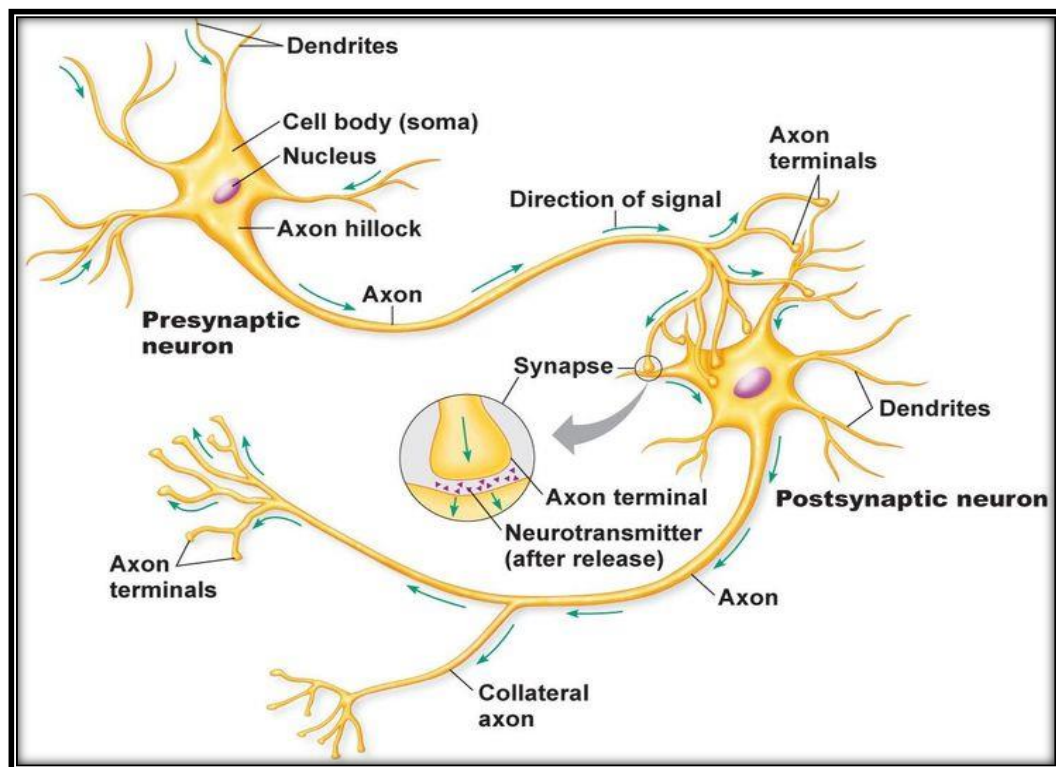


Figure 1-1: Basic neuron structure.

Neurons have the same common organelles as other cells, including a nucleus and mitochondria. However, neurons also contain more specialised structures such as dendrites and axons.

Source: Droualb.faculty.mjc.edu (2015).

## **1.4 Neurotransmitters**

Presynaptic neurons generate the molecules that propagate electrical signals to adjacent neurons; these molecules are known as neurotransmitters (Sugden et al., 2004). Neurotransmitters act as signalling molecules between neurons and between neurones and non-neuronal cells (Grant, 2015). They are released at the chemical end of the synapse into the extracellular environment. These neurotransmitters induce reactions via either inhibition or excitation, depending on the postsynaptic receptor (Lodish et al., 2000). There are three basic categories of neurotransmitter. The first category includes amino acids such as glutamate,  $\gamma$ -aminobutyric acid (GABA), and glycine (Meyres, 2000). The second category includes monoamines such as dopamine, norepinephrine, histamine, and serotonin (Garraway and Hochman, 2001). The third category includes neuropeptides such as somatostatin and neurotensin (Higgins and George, 2007). Neurotransmitter receptors are transmembrane proteins that usually have numerous subunits. The ligands that block receptors' binding sites for other ligands are called antagonists, while the ligands that stimulate the receptors are called agonists (Grant, 2015).

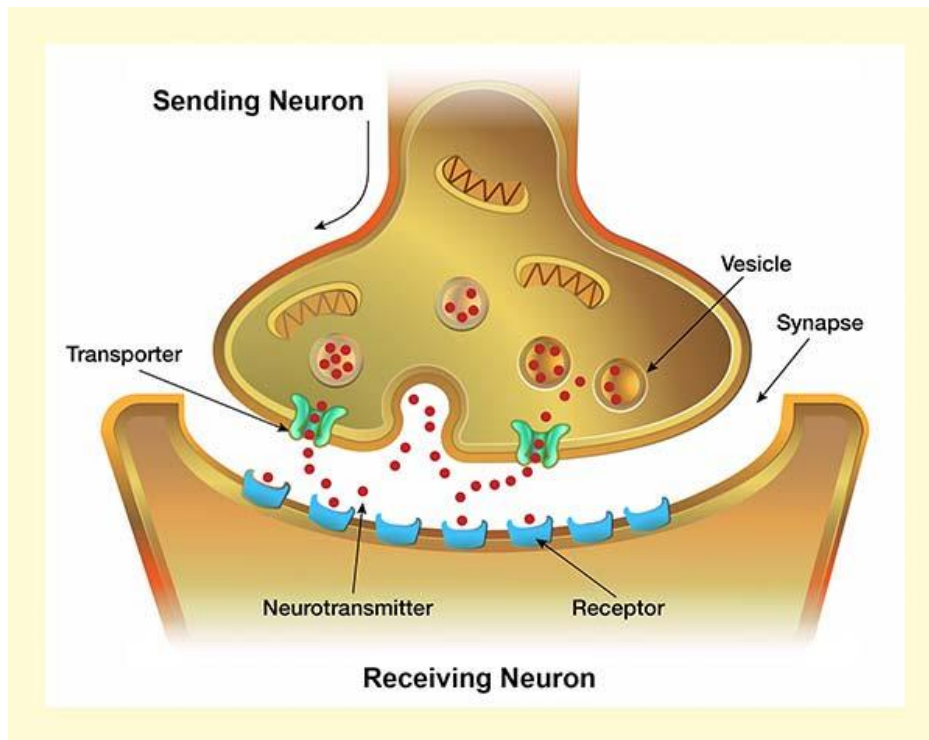


Figure 1-2: Basic chemical synapse structure.

Neurotransmitters are sent and received in chemical synapses via transporters and receptors.

Source: NIDA (2017).

## 1.5 Calcium Ions

Signal transduction generally serves a critical role in the regulation of cellular functions. In synaptic transmission, cytokines, hormones, or neurotransmitters attach to plasma membrane receptors on the extracellular side. This process then induces the intracellular messenger (Sigel et al., 2013).

The calcium ion ( $\text{Ca}^{2+}$ ) serves as the most prominent factor in the transduction of signals within a variety of cells from specialised neurons to bacteria (Clapham, 2007). Cell death is associated with chronic elevated concentrations of  $\text{Ca}^{2+}$  within the cells, despite  $\text{Ca}^{2+}$  at normal concentrations being critical in many cellular processes. This feature makes  $\text{Ca}^{2+}$  unique compared with other ions and molecules in the second messenger category (Duncan et al., 2011).

In addition,  $\text{Ca}^{2+}$  cannot undergo the process of metabolism, as is the case with other second messengers such as cyclic adenosine monophosphate (cAMP). Hence accurate intracellular regulation via various  $\text{Ca}^{2+}$  binding proteins and  $\text{Ca}^{2+}$  transporters is essential. The normal concentration of  $\text{Ca}^{2+}$  within cells is typically 100 nM, which is more than 20,000 times less than the  $\text{Ca}^{2+}$  level commonly found outside the cells (i.e., 2 mM) (Clapham, 1995).  $\text{Ca}^{2+}$  plays an essential role in the physiology and biochemistry of the cells.  $\text{Ca}^{2+}$  enters the cytoplasm through the cell membrane or via the internal calcium stores, such as the ER and mitochondria, or via several other organelles (see Figure 1-3) (Michelangeli et al., 2005).

In vertebrates,  $\text{Ca}^{2+}$  is essential for various physiological processes; therefore, to ensure adequate homeostasis,  $\text{Ca}^{2+}$  concentration has to be maintained within

particular limits. However, different tissues have different concentrations of  $\text{Ca}^{2+}$  inside the extracellular and intracellular fluids. Transport proteins regulate the level of intracellular  $\text{Ca}^{2+}$  in the cells (Sigel et al., 2013). A wide range of stimuli can lead to an increase in cytosolic  $\text{Ca}^{2+}$  concentration, either from intracellular stores or from the extracellular space. Elevated cytosolic  $\text{Ca}^{2+}$  (i.e., the calcium signal) is translated into intracellular responses by different types of calcium-binding proteins (Norman, 1987).  $\text{Ca}^{2+}$  signals affect the regulation of several cell processes, such as neurotransmission, muscle contraction, hormone secretion, growth, metabolism, and cell death (Orrenius and Nicotera, 1994). The effect of  $\text{Ca}^{2+}$  is amplified by many factors, such as protein phosphatases, protein kinases, and calcium-binding proteins (Carafoli, 2003).

### **1.5.1 Neuronal Calcium Ions**

Transiently elevated concentrations of intracellular  $\text{Ca}^{2+}$  provide the impulses for a myriad of processes within the nerve cells. For instance,  $\text{Ca}^{2+}$  serves as the main neurotransmitter secretion inducer (Neher and Sakaba, 2008). Other roles of  $\text{Ca}^{2+}$  in neurons include exciting the nerve cells (Marty and Zimmerberg, 1989), regulating the electrical impulses (Llinas, 1988; Marty and Zimmerberg, 1989), controlling the extent of the plasticity of the synapses (Malenka, 1989), controlling gene expression (Szekelyetal, 1990), regulating neuron metabolism (McCormack and Denton, 1990), and programming the death of cells (Chalfie and Wolinsky, 1990). Many studies have suggested links between dysregulation of  $\text{Ca}^{2+}$  homeostasis and neurodegenerative diseases such as Parkinson's, Alzheimer's, and Huntington's diseases (Cali et al., 2012).

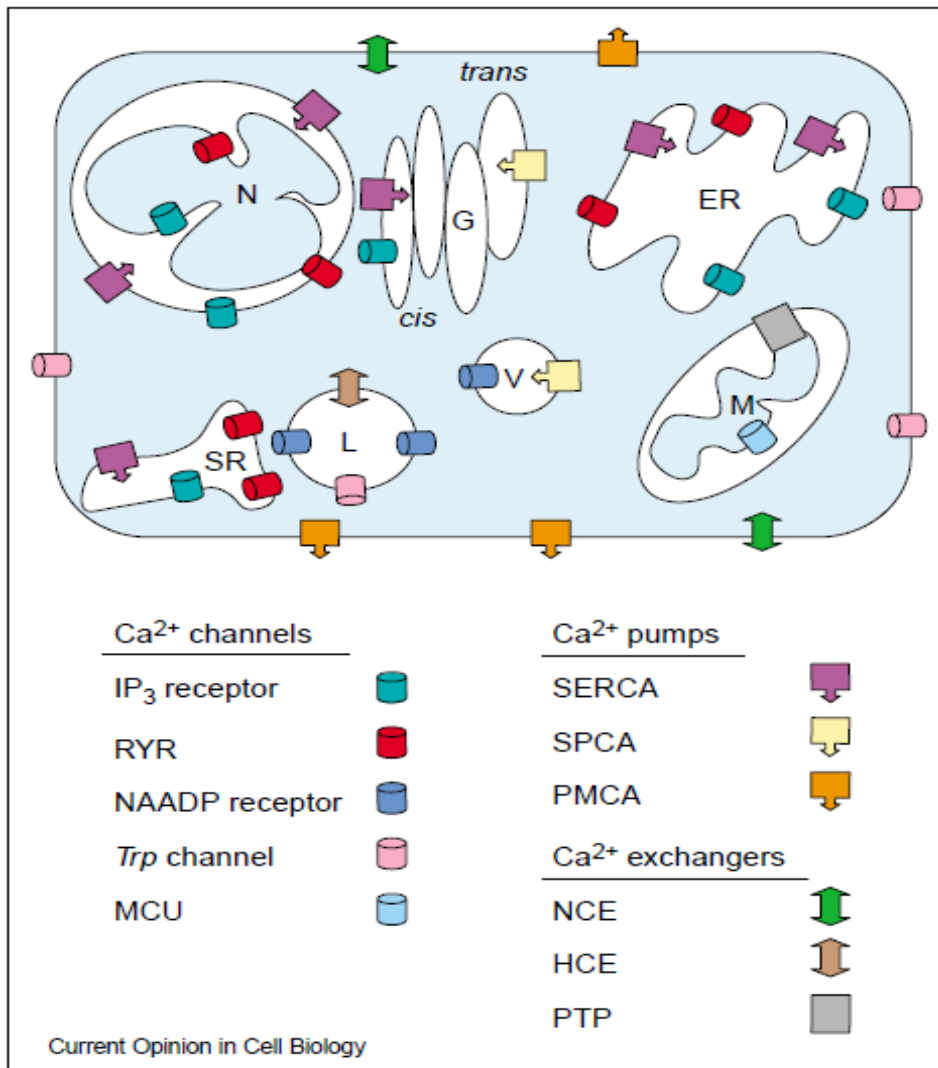


Figure 1-3: Overview of Calcium channels and pumps in different organelles within the cells.

N = Nucleus; G = Golgi body; ER = Endoplasmic Reticulum; SR = Sarcoplasmic Reticulum; L = Lysosome; V = Secretory Vesicles; M= Mitochondria

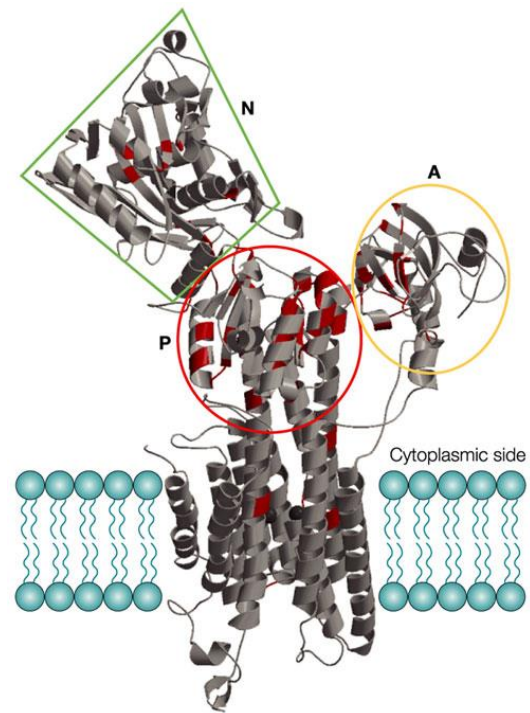
Source: Michelangeli et al. (2005).

## 1.6 Calcium Transporters

### 1.6.1 Calcium Pump

$\text{Ca}^{2+}$  adenosine triphosphatase (ATPase) pumps play a critical role in the control and regulation of  $\text{Ca}^{2+}$  in cell mechanisms and functions (Ogunbayo and Michelangeli, 2007). The pumps possess a high affinity for  $\text{Ca}^{2+}$  and can therefore efficiently control low concentration levels (Carafoli and Brini, 2002). Three  $\text{Ca}^{2+}$  ATPase pumps have been identified in the cells of higher animals. The first pump is located in the membranes of the endo/sarcoplasmic reticulum and is known as the Sarcoplasmic/Endoplasmic Reticulum  $\text{Ca}^{2+}$  ATPase (SERCA) pump. The second pump functions in the Golgi network and is referred to as the Secretory Pathway  $\text{Ca}^{2+}$  ATPase (SPCA) pump. The third pump serves its purpose in the plasma membrane and is known as the Plasma Membrane  $\text{Ca}^{2+}$  ATPase (PMCA) pump (Brini and Carafoli, 2009). All three of these  $\text{Ca}^{2+}$  pumps are characterised as P-type ATPases since they are transiently phosphorylated (Pedersen and Carafoli, 1987). There are four domains in the structure of  $\text{Ca}^{2+}$  ATPase. The three domains on the cytoplasmic side, as shown in (Figure 1-4), are the nucleotide-binding domain (N), the actuator-binding domain (A), and the phosphorylation domain (P) (Toyoshima et al., 2000). (Figure 1-5), shows the mechanism of  $\text{Ca}^{2+}$  ATPase. The mechanism shows that  $\text{Ca}^{2+}$  ATPase can occur in one of two conformations: E1 or E2. In the E1 conformation, the ATPase binds two  $\text{Ca}^{2+}$  ions from the cytoplasmic side of the membrane. In the E2 conformation, those two sites are closed. After the attachment of ATP, the ATPase is phosphorylated on Asp-351 to provide a

phosphorylated intermediate  $E2PCa^{2+}$ . The two  $Ca^{2+}$  binding sites then become low-affinity sites and turn inwards. That causes a loss of  $Ca^{2+}$  to the lumen of the ER/SR, so the ATPase dephosphorylates form an E2 form that returns to E1 (Jencket et al., 1993; Lee and East, 2001).



Nature Reviews | Molecular Cell Biology

Figure 1-4: Crystal structure of  $Ca^{2+}$  ATPase showing the different domains.

Source: Brini and Carafoli (2008).

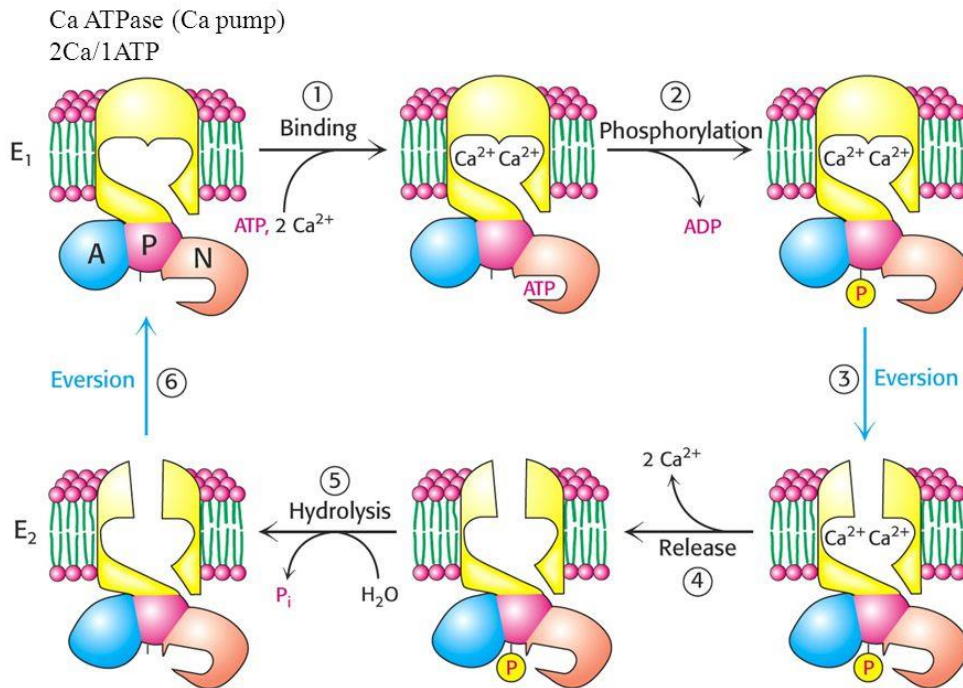


Figure 1-5: General mechanism of Ca<sup>2+</sup> ATPase.

A cartoon illustrating the mechanism of Ca<sup>2+</sup> pumps at different stages through the transport cycle.

Source: Farmer (2006).

### 1.6.1.1 The SERCA Pump

The ER is a very important organelle that has two major roles within the cell: regulation of intracellular Ca<sup>2+</sup> levels and essential role signalling processes (English and Voeltz, 2013). In 1961, the SERCA Ca<sup>2+</sup> pump was initially discovered in skeletal muscle and identified as an adenosine triphosphate (ATP)-

driven  $\text{Ca}^{2+}$  transport system (Ebashi, 1962; Hasselbach and Makinose, 1961). The pump is commonly found in the membrane of the sarcoplasmic reticulum (SR) and ER. It has a molecular weight of 110 KDa and consists of a single chain (MacLennan et al., 1985). Originally the movement processes of the SERCA pump were examined within the SR of both cardiac and skeletal muscles before investigations were expanded to other cells such as brain cells (Michelangeli et al., 1990). The SERCA pump uses energy gained from the hydrolysis of ATP to move  $\text{Ca}^{2+}$  to the luminal portion of the ER and the SR from the cytosol, pumping against the concentration gradient and in the opposite direction as  $3\text{H}^+$  or  $2\text{H}^+$  is returned for every hydrolysed ATP (Carafoli and Brini, 2000). There are three different isoforms of SERCA, known as SERCA1, SERCA2, and SERCA3. The changes in expression pattern that occur during development and tissue differentiation give each isoform specific functions (Brini and Carafoli, 2009). SERCA1a and SERCA1b pumps are expressed in fast-twitch skeletal muscle, while SERCA2b is abundant in neuronal cells (Green et al., 2009). Similarly, SERCA2a is found in the cardiac muscle (Zarain et al., 1990), while SERCA3 is expressed in limited selective non-muscle tissue and cells (Pozzan et al., 1994).

#### *1.6.1.2 The PMCA Pump*

Schatzmann (1966) first discovered the plasma membrane  $\text{Ca}^{2+}$  pump in erythrocytes in 1966. PMCA was then identified and distinguished from other

ATPases by its ability to bind calmodulin (Niggli et al., 1979). The pump functions through a calmodulin regulation mechanism which alters  $\text{Ca}^{2+}$  affinity and transport capacity (Green, 2000; Jarrett and Penniston, 1977). There are four different isoforms of the pump, each one with a different affinity for  $\text{Ca}^{2+}$  and calmodulin. PCMA1 and 4 have very low calmodulin affinity. PCMA2 and 3 have higher calmodulin affinity and can be found in limited tissues (Strehler and Zacharias, 2001). PMCA2 is highly expressed in the nervous cells and has features that distinguish it from the other isoforms (Elwess et al., 1997; Hilfiker et al., 1994).

#### *1.6.1.3 The SPCA Pump*

The  $\text{Ca}^{2+}$  pump of the secretory pathway (SPCA) represents the most recently discovered class of  $\text{Ca}^{2+}$  transporter ATPases. The SPCA pump was initially identified as the plasma membrane-related ATPase in yeast (Rudolph et al., 1989). The SPCA pump was later found to be located in the membrane of Golgi bodies (Antebi and Fink, 1992). In 1992, a related ATPase was identified in rats and other mammals (Gunteski-Hamblin, 1992). However, it was not until the early 2000s that the pump's role was identified in humans and shown to be mutated in Hailey-Hailey disease (Hu et al., 2000; Sudbrak et al., 2000). Hailey-Hailey disease was first discovered by the Hailey brothers in 1939. It is an autosomal dominant skin condition that affects the intertriginous areas (Berger et al., 2007).

Primarily two main isoforms of the SPCA pump have been defined: SPCA1 and SPCA2. SPCA1 has a housekeeping role and is found ubiquitously, with expression in most tissues; however, this isoform is particularly abundant in epidermal cells and keratinocytes (Hu et al., 2000). SPCA2 was identified many years later (Vanoevelen et al., 2005; Xiang et al., 2005). In contrast to SPCA1, the expression of SPCA2 is quite limited in higher-level organisms. Specifically, studies have revealed that the SPCA2 pump is found in the goblet cells of the human colon and in breast cells (Vanoevelen et al., 2005). Conversely, immunofluorescence and fractionation of cells has shown that SPCA1 is located within the Golgi of most mammalian cells (Reinhardt et al., 2004; Van Baelen et al., 2003).

The sub-cellular location of SPCA2 is not fully clear: in some instances it is expressed with the marker of Golgi bodies (Vanoevelen et al., 2005), while in others it is located within markers of the *trans* Golgi network only (Xiang et al., 2005). The SPCA pump transports both  $\text{Ca}^{2+}$  and  $\text{Mn}^{2+}$  into the Golgi and has a high affinity for  $\text{Ca}^{2+}$  (Vanoevelen et al., 2005). The low  $\text{Ca}^{2+}$  concentration in most cytosols at rest thus ensures that the Golgi will be constantly refilled with  $\text{Ca}^{2+}$  (Thomas, 2009).

## 1.7 Regucalcin

The Ca<sup>2+</sup>-binding protein regucalcin (RGN) was discovered in the late 1970s (Yamaguchi and Yamamoto, 1978). It differs from many other Ca<sup>2+</sup>-binding proteins since it does not contain the EF-hand motif (Fujita, 1999). It has been shown that RGN has a multifunctional role in regulating cellular function, an important role in controlling intracellular calcium homeostasis, and a major effect on numerous intracellular signal transduction pathways (Yamaguchi, 2011). RGN is highly expressed in a wide variety of tissues, such as those of the liver, heart, brain, and kidney, as well as in many different cell types (Yamaguchi, 2005). RGN protein and its gene have been identified in many vertebrate and invertebrate species (Yamaguchi, 2011). RGN consists of 299 amino acids with a molecular weight of 33 KDa, and its gene is located on the X chromosome in humans and rats (Fujita et al., 1995). Studies have found three different splice variants for the human RGN gene (see Figure 1-6). Splice variant 1 is the longest, with 299 amino acids. Splice variant 2 has a shorter N-terminus compared to splice variant 1 and 246 amino acids. Finally, splice variant 3 is the shortest, with 227 amino acids, some of which are missing from the middle part of the amino acid sequence compared to both the first and the second splice variants (NCBI, 2013). The 3-dimensional structure of the full-length human regucalcin has also recently been elucidated as shown in (Figure 1-7) (Chakraborti and Bahnson, 2010).

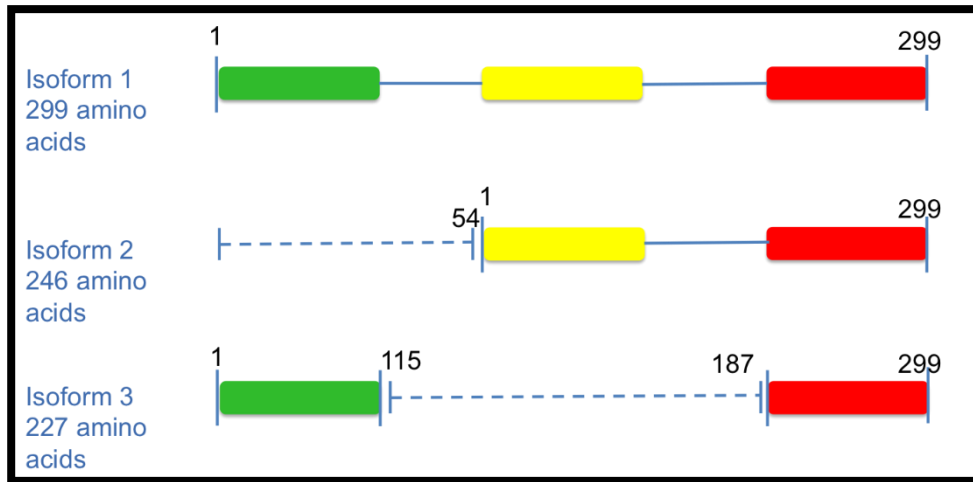


Figure 1-6: The three different splice variants for the human RGN gene.

A description (not to scale) of the three different splice variants for the human regucalcin gene. Although referred to as isoforms, they are in fact splice variants.

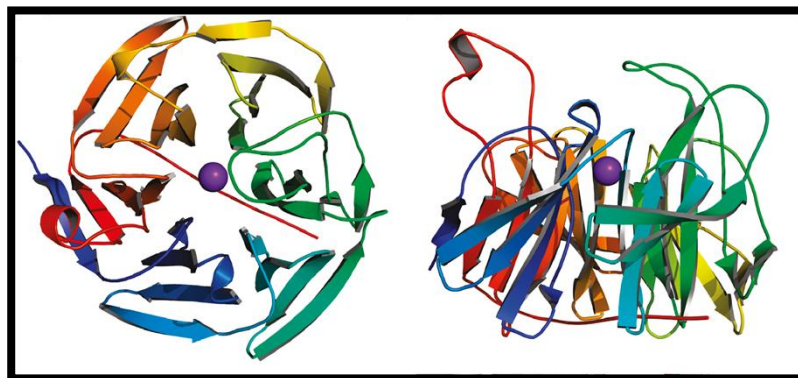


Figure 1-7: Crystal structure of human RGN with Ca<sup>2+</sup> bound in the middle.

Source: Chakraborti and Bahnson (2010).

### 1.7.1 RGN Functions

Many cellular functions are regulated by  $\text{Ca}^{2+}$  signals, including hormone secretion, metabolism, growth, and cell motility (Bootman, 2001). Intracellular  $\text{Ca}^{2+}$  homeostasis is controlled through  $\text{Ca}^{2+}$  pumps and  $\text{Ca}^{2+}$  channels in the plasma membrane, mitochondria, and ER of several cell types (Michelangeli et al., 2005). RGN plays a modulatory role in  $\text{Ca}^{2+}$  pumps, causing increasing activity and expression of several other  $\text{Ca}^{2+}$ -dependent enzymes, such as protein phosphatases, protein kinases, and  $\text{Ca}^{2+}$  calmodulin-dependent nitric oxide synthase (Lai et al., 2011; Omura and Yamaguchi, 1999). In addition, RGN prevents cell proliferation, cell death, and apoptosis caused by different signalling factors (Hukkanen et al., 1995). An investigation using a knockout mouse model indicated that RGN deficiency induces fatty-liver disease (Kondo et al., 2006). Conversely, overexpression of RGN in rats influenced metabolic diseases and the induction of osteoporosis and hyperlipidaemia (Yamaguchi, 2010; Yamaguchi et al., 2004). It has also been demonstrated that overexpression of RGN inhibits cell proliferation as a result of cell cycle regulation (Vaz et al., 2014; Yamaguchi and Daimon, 2005). Moreover, induced by various signalling factors, RGN overexpression suppressed cell death and apoptosis in cloned rat hepatoma cells (Tsurusaki and Yamaguchi, 2002).

### 1.7.2 RGN in the Brain

RGN expression increases during development, peaks in early adulthood, and then declines considerably in old age; as a result, RGN is also known as the senescence marker protein 30 (SMP 30) (Fujita et al., 1996). RGN is expressed in the brain tissue of the cerebral cortex and hippocampus. Enzyme-linked immunosorbent assay (ELISA) has measured the concentration of RGN in brain tissue at  $5 \times 10^{-9}$  M. Similar to its expression, the concentration of RGN in the brain has also been shown to decrease with age (Yamaguchi and Isogai, 1993). Neuronal  $\text{Ca}^{2+}$  homeostasis and  $\text{Ca}^{2+}$  signalling control numerous neuronal functions including plasticity, which is likely to affect learning and memory (Wojda et al., 2008). The concentration of intracellular  $\text{Ca}^{2+}$  in the neuronal cells of the brain is controlled by several transport systems, including  $\text{Na}^+/\text{Ca}^{2+}$  exchanges,  $\text{Ca}^{2+}$  channels, and  $\text{Ca}^{2+}$  ATPase, as well as  $\text{Ca}^{2+}$ -binding proteins (Michelangeli et al., 2005).

$\text{Ca}^{2+}$  homeostasis disruption in brain cells can induce brain diseases (Cheung et al., 2008). Therefore, it has been suggested that RGN may play such a significant role in the maintenance of brain function that if RGN is disturbed, conditions such as Alzheimer's disease (AD) may result or worsen (Yamaguchi, 2012). In addition, the increase of intracellular  $\text{Ca}^{2+}$  in the brain inherent to aging can result in brain toxicity. Therefore, intracellular  $\text{Ca}^{2+}$  signalling is fundamental to neuronal physiology and viability, and the dysregulation of  $\text{Ca}^{2+}$  homeostasis is involved in a diverse range of disease processes (Yamaguchi, 2013). In the rat brain, RGN plays a role in the regulation of intracellular  $\text{Ca}^{2+}$  homeostasis (Yamaguchi et al., 2008).

Additionally, it has been shown that RGN helps to prevent oxidative damage without inducing antioxidant enzymes in the brain (Son et al., 2006).  $\text{Ca}^{2+}$  calmodulin activates nitric oxide (NO) synthase, and the overproduction of NO induces damage in various cells (Schmidt et al., 1992). RGN has an inhibitory effect on NO synthase activity in rat brain tissue, thus minimising the detrimental effect of NO (Tobisawa and Yamaguchi, 2003). One of the main factors contributing to AD pathogenesis is neuronal  $\text{Ca}^{2+}$  dysregulation (Demuro et al., 2010). Recent studies have demonstrated functional associations between dense-core plaques (amyloid plaques) and  $\text{Ca}^{2+}$  signalling alterations in an AD mouse model (Kumar-Singh et al., 2005). Interactions between intracellular  $\text{Ca}^{2+}$  and  $\beta$ -amyloid are related to AD pathogenesis, and  $\text{Ca}^{2+}$  perturbations are a fundamental aspect of excitotoxicity, synaptic degeneration, and cell death (Frandsen and Schousboe, 1991).

## 1.8 Alzheimer's Disease

Alzheimer's disease is a genetically complex, slowly progressive, and irreversible neurodegenerative disease of the brain (Hampel, 2011). It is the most common form of dementia and is characterised by memory loss or other cognitive skills. It develops when nerve cells in the brain die or no longer function normally, which eventually impairs an individual's ability to carry out daily activities (Weiner et al., 2012). Several researchers have reported that energy failure and accumulative intracellular waste play fundamental roles in the process of neurodegenerative diseases such as Alzheimer's disease (Godoy et al., 2014). The aggregation of insoluble forms of amyloid $\beta$  (A $\beta$ ) in extracellular spaces and the accumulation of the microtubule protein tau in neurofibrillary tangles in neurons are both associated with Alzheimer's disease. A $\beta$  is derived by the proteolytic cleavage of amyloid precursor protein (APP) by the enzymes families  $\gamma$ -secretase and  $\beta$ -secretase, which both include presenilin 1 (PS1) and PS2 (Masters et al., 2015). Alzheimer's disease is categorised by cognitive decline, loss of ability to perform daily activities, and many other behavioural symptoms (McKhann et al., 1984). Alzheimer's patients develop neuropsychiatric symptoms like delusion, aggressiveness, and agitation. These symptoms eventually lead to functional decline (Lopez et al., 1999) and the need for institutionalisation (Steele et al., 1990), and they also contribute to caregiver stress and depression (Clyburn et al., 2000; Coen et al., 1997). In the past few years, studies have been focused on the treatment of these neuropsychiatric symptoms by the interventions with agents such as anticholinesterases,

benzodiazepines antidepressants, and antipsychotics (Szulik, 2007). Antipsychotics are considered one of the medications most often prescribed to control the symptoms associated with Alzheimer's disease (Schneider et al., 1990; Silva et al., 2011).

## 1.9 Cell Death

Cell death in its various forms and different mechanisms shapes the essence of life (Chaabane et al., 2013). It is now known that there are at least three individual types of cell death processes, each with different mechanisms: apoptosis (i.e., programmed cell death), necrosis, and autophagy (see Figure 1-8) (Green, 2011). The major difference between these three predominant types of cell death is that necrosis is a pathological process leading to tissue inflammation, while apoptosis may take place as a physiological phenomenon that is essential for life (Messner, 2012). Autophagy, in turn, is a highly controlled process that regulates the degradation of cellular components (Mizushima and Komatsu, 2011). The term *autophagy* is based on the Greek phrase meaning “the eating of self” (Deter, 1967). Autophagy has always been described as a different form of non-apoptotic death that is also distinct from necrosis (Levine and Yuan, 2005). The mechanism of autophagy is a highly protective degradation mechanism (El-Khattouti et al., 2013). Three categories of autophagy have been described: macroautophagy, microautophagy, and chaperone-mediated autophagy (Mijaljica et al., 2011). Macroautophagy is believed to be the main category of autophagy (Mizushima and Komatsu, 2011).

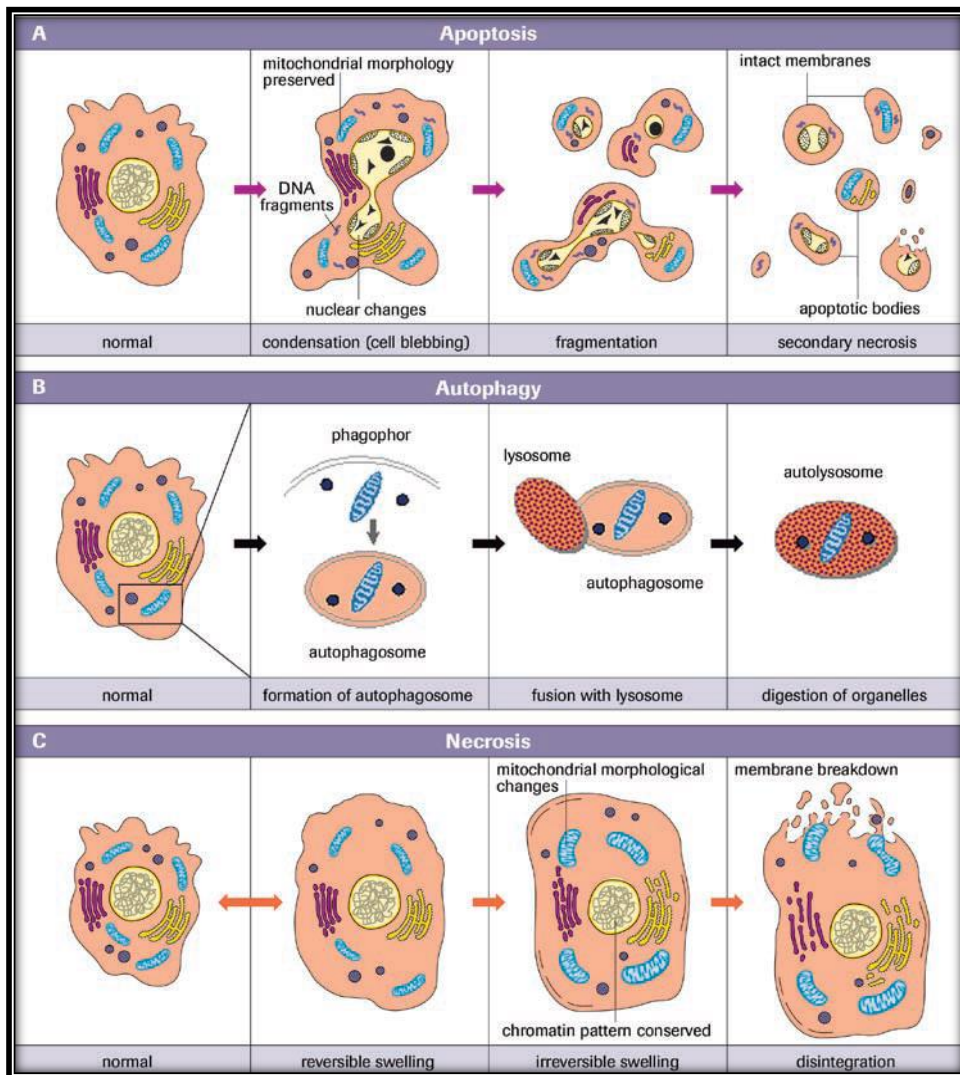


Figure 1-8: Three types of cell death and their basic processes.

(A). Apoptosis is characterised by the typical cellular shrinkage and the formation of apoptotic bodies without the leakage of cell contents.

(B). Autophagy involves the appearance of the autophagosomes and their fusion with lysosomes.

(C). Necrosis occurs when the cell swells until the plasma membrane ruptures, causing leakage of cellular contents.

Source: GmbH (2008).

### **1.9.1 Apoptosis**

The term *apoptosis* was first used to define a morphologically distinct form of cell death (Kerr, 1972). Apoptosis is an essential cellular process that is important for protecting normal organism function. It is a natural process that usually occurs during aging and development, as well as a homeostatic mechanism that maintains the cell population in tissues. Additionally, apoptosis occurs as a protection mechanism when cells are damaged by diseases or immune reactions (Norbury and Hickson, 2001). Cells will enter apoptosis in the event of DNA damage in order to protect other cells and thereby prevent abnormalities from developing in the tissue. Therefore, apoptosis failure can cause various pathological conditions, such as cancer, developmental abnormalities, and neurodegenerative diseases including Alzheimer's disease, stroke, and Parkinson's disease (Earnshaw et al., 1999). Apoptosis is a rigorously controlled biological mechanism involving the removal of injured cells without causing inflammation or destruction of the surrounding tissue.

The process of apoptosis involves DNA fragmentation, cell shrinkage, membrane blebbing, and disassembly into membrane-enclosed vesicles called apoptotic bodies (Figure 1-7) (Zhang and Ming, 2000). The process of apoptosis is crucial and needs to be controlled very carefully, because the death of the wrong cell, or the death of the right cell but at the wrong time, can affect entire organ systems and even result in the organism's death (Wallach and Kovalenko, 2014). Conversely,

the absence of apoptosis can be detrimental too, and over-proliferation of cells without regulation can result in malignancies (Nikoletopulou et al., 2013)

A variety of cell signalling pathways are involved in the regulation of both cell death and survival. Apoptosis alone is stimulated by two main pathways and controlled by multiple extrinsic and intrinsic ligands. Some of these regulators include the Bcl-2 family proteins and proteins released from the mitochondria and caspases. In addition, an overload of  $\text{Ca}^{2+}$  in neuronal cells can play an important role in apoptosis (Nikoletopulou et al., 2013).

#### *1.9.1.1 Caspases*

The fundamental enzymes in the mechanism of apoptosis are called caspases, which are a family of the cysteine proteases. The term *caspase* is derived from the fact that these proteases are classified as Cysteine-dependent, **AS**partate-specific prote**ASE**s (Alnemri et al., 1996; Shi, 2004). Pro-caspase is the inactive form that causes no harm (Shi, 2004). Up to 14 caspases have been discovered, with 11 of them expressed in humans (Li, 2008).

Caspases are cysteine proteases, as they have a cysteine residue in the active site. They all share the same peptide sequence: -Glu-Ala-Cys-X-Gly-, with X being any amino acid. There are three domains in the pro-caspases. At the N-terminal end is a pro-domain, in the middle is a large subunit domain, and at the C-terminal is a small subunit domain (Chang et al., 2000; Fuentes-Prior and Salvesen, 2004).

In the process of activation, as shown in (Figure 1-9), cleavage takes place between the large subunit and small subunit domains, concluding with a separate protein. To generate the active enzyme, the two small subunits and the large subunits are joined together to form the active complex (Fuentes-Prior, 2004).

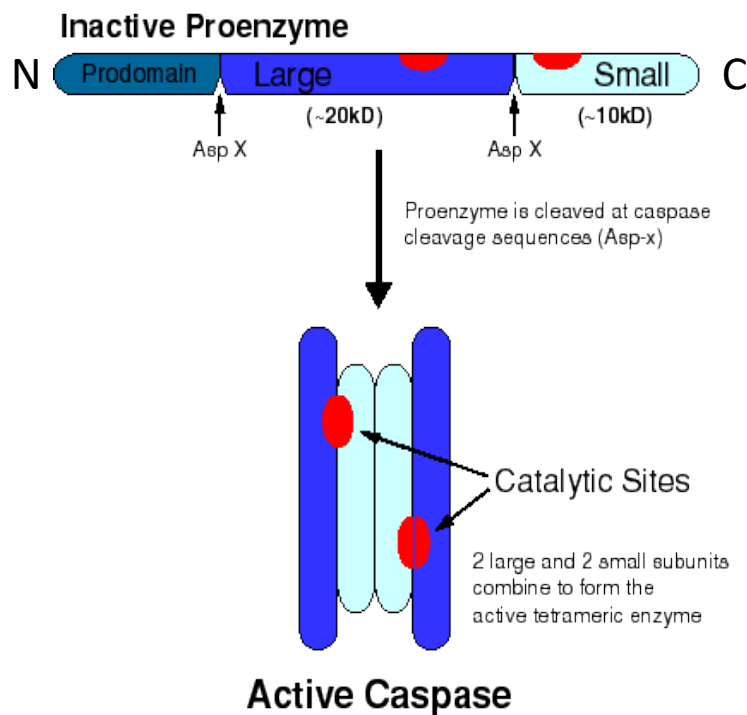


Figure 1-9: Basic structure of pro-caspase and caspase.

The inactive structure of pro-caspase contains three parts: a pro-domain, a large subunit, and a small subunit. The length of the pro-domain differs among caspases, and the pro-enzyme is activated when two large and two small subunits combine to form an active tetrameric enzyme.

Source: Hui et al. (2004).

### **1.9.2 The Apoptosis Pathway**

Studies have shown that two pathways can induce apoptosis: the extrinsic (death receptor) pathway and the intrinsic (mitochondrial) pathway. However, new evidence has shown that the two pathways are linked, and the mediators in one pathway can stimulate the other pathway (Igney and Krammer, 2002). An additional pathway is the granzyme pathway, which can also induce apoptosis through either granzyme A or granzyme B. The three pathways—intrinsic, extrinsic, and granzyme B—all converge on the same point: the cleavage of caspase-3 by caspase 8, 9, or 10 see (Figure 1-10). Alternately, the granzyme A pathway stimulates a similar, caspase-independent pathway through single-stranded DNA cleavage (Martinvalet et al., 2005). Studies have shown that both the activation of caspase-3 and the mitochondrial pathway are critical for granzyme B-induced killing (Goping et al., 2003). Reports have also shown that granzyme A is important in cytotoxic T cell-induced apoptosis and activates caspase-independent pathways by causing DNA nicking via DNase, which has an essential role in immune surveillance to inhibit cancer throughout the induction of tumour cell apoptosis (Fan, 2003).

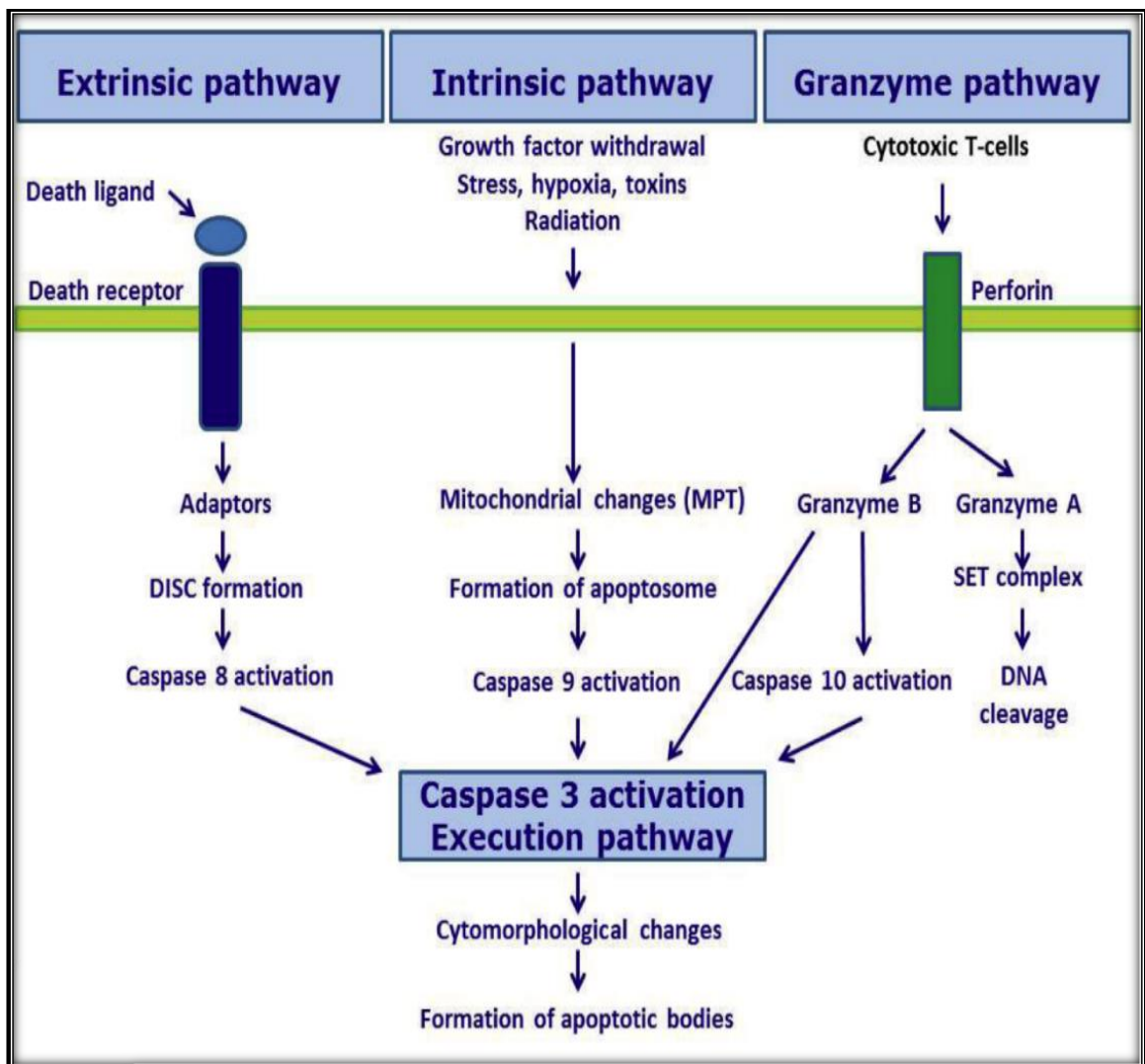


Figure 1-10: General mechanism of apoptosis.

An overview of the three different pathways of apoptosis, i.e., the extrinsic, intrinsic, and granzyme pathways, and the caspases that activate cell death.

Source: Boucher et al. (2010).

### *1.9.2.1 The Intrinsic Pathway*

The intrinsic pathway is also known as the mitochondrial pathway or the BCL-2-regulated pathway (Pradelli et al., 2010). This pathway is highly controlled by the BCL-2 family of proteins (Hakem, 1998). It is activated by several intracellular signals such as DNA damage, cytotoxic stress, and the absence of some hormones or cytokines. All of these stimuli bring about changes in the mitochondrial membrane (Saelens et al., 2004). Mitochondrial membrane depolarisation leads to the opening of the permeability transition pore (PTP), which results in the release of two main groups of pro-apoptotic proteins into the cytosol (Saelens et al., 2004). The first group contains cytochrome *c* (cyt *c*), which activates procaspases-9 and Apaf-1 to form apoptosome, which in turn activates caspase-9 itself (Hill et al., 2004; Riedl, 2007). The second group includes apoptosis-inducing factor (AIF), which causes DNA fragmentation (Susin et al., 2000). The regulation of the intrinsic apoptotic events occurs through the Bcl-2 protein family. The Bcl-2 protein family is classified into two groups according to their action: either anti-apoptotic, such as Bcl-2 and Bcl-x, or pro-apoptotic, such as Bax and Bak (Chipuk et al., 2008). The activation of caspase-9 induces and stimulates the activation of apoptotic cell death through activation of caspase-3 see (Figure 1-11) (Duprez et al., 2009).

### *1.9.2.2 The Extrinsic Pathway*

The extrinsic pathway, also known as the death-receptor pathway, is activated when the death ligand binds to cell surface receptors (Saikumar and Venkatachalam, 2009). The death receptors are members of the tumour necrosis factor (TNF) family, which also includes FasL/FasR or TNF-  $\alpha$ /TNFr1 (Locksley et al., 2001). The signalling by these receptors induces a variety of cellular responses including cell death (Youle, 2008).

Binding the Fas ligand to Fas receptors results in the formation of the Fas-associated death domain (FADD). This induces a death-inducing signalling complex (DISC), resulting in the activation of procaspase-8 (Kischkel et al., 1995; Wajaut et al., 2002). Caspase-8, when activated, in turn leads to the formation of downstream executioner caspases such as caspase 3 see (Figure 1-11) (Ashkenazi, 2008).

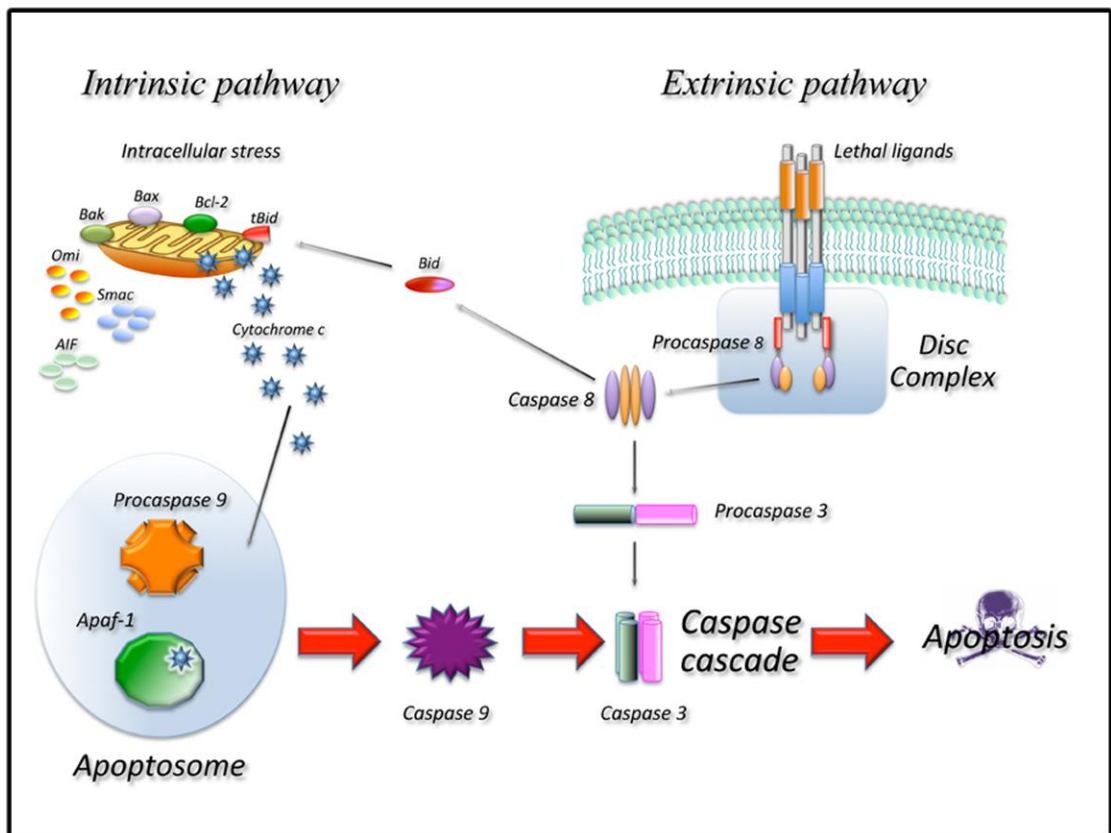


Figure 1-11: Extrinsic and intrinsic cell death-signalling pathways.

Through the intrinsic pathway, the release of cytochrome c from the mitochondria causes the formation of the apoptosome and activation of caspase 9. In the extrinsic pathway, upon ligand binding to specific receptors, a DISC is formed, and caspase 8 is activated. Caspases 8 and 9 then activate downstream caspases such as caspase 3, resulting in apoptotic cell death.

Source: AGING (2012).

### 1.9.3 Necrosis

Necrosis is a type of cell death that for many years was considered to be an uncontrolled mechanism of cell death (Golstein and Kroemer, 2006). However, recent studies have shown that necrosis could be a result of various signal transduction pathways (Festjens et al., 2006). Research has demonstrated that necrosis occurs as a response to physico-chemical stress (Nicotera et al., 1999; Proskuryakov et al., 2003), changes that take place during development (Roach and Clarke, 2000), and neurodegeneration and pathogen infection (Vanlangenakker et al., 2008).

Generally, necrotic cell death begins with the swelling of the cytoplasm and organelles, followed by damage to the cell membrane, which in turn results in the release of the cellular contents to the surrounding extracellular area, causing inflammation (Saikumar and Venkatachalam, 2009). It has been established that stimulation of the death receptor  $\text{TNF}\alpha$  can activate apoptosis as well as necrosis (Grooten et al., 1993; Vercaemmen et al., 1997). Studies have also demonstrated that when the caspase-dependent pathway is blocked, necrosis may occur (Festjens et al., 2006). In addition, several factors, such as reactive oxygen species (ROS),  $\text{Ca}^{2+}$ , and phospholipases, may also be involved in necrosis (Golstein, 2007). Furthermore, DNA damage by oxidative stress can result in hyperactivation of poly (ADP-ribose) polymerase-1 (PARP-1) that then leads to necrosis (Jagtap and Szabo, 2005; Vanlangenakker et al., 2008). Necrosis occurs by both physiological

and pathophysiological mechanisms and can free the body from cancer cells that have developed during tumorigenesis (Festjes et al., 2006).

#### **1.9.4 Regulated Necrosis**

Regulated necrosis, which also called necroptosis, is a type of cell death that shares features of both apoptosis and necrosis (Hirsova and Gores, 2015). As described previously, apoptosis occurs through the engagement of several pathways causing the activation of caspase protease, which in turn leads to cell death through formation of apoptotic bodies. At first, regulated necrosis was believed to be a caspase-independent form of cell death only activated by treatment of TNF in the presence of pan-caspase inhibitors (Vercammen et al., 1998). However, it is now understood that the activation of necroptosis also requires the inhibition of caspase-8 (Linkermann and Green, 2014). In addition to TNFR1-regulated necrosis, necrosis can also be initiated by various death receptors such as FAS (Vercammen et al., 1998) and in some cell types by TNFR2, TRAILR1, and TRAILR2 (Chan et al., 2003; Holler et al., 2005; Jouan-Lanhouet et al., 2012). This usually occurs when apoptosis is blocked by the inhibition of some caspases as approved for T cells (Scheller et al., 2006) or due to low levels of ATP (Los et al., 2002; Skulacher, 2006). The downstream of signalling cascade (TNF $\alpha$  and TNFR1) can also initiate regulated necrosis (Zhang et al., 2009) in addition to receptor-interacting protein kinase 1 (RIPK1) (Degterev et al., 2008; Degterev et al., 2005; Kalai et al., 2002)

and (RIPK3) (Zhang et al., 2009; Cho et al., 2009; Feng et al., 2007; He et al., 2009). Both (RIPK1) and (RIPK3) play fundamental roles in the induction of regulated necrosis (Holler et al., 2000). Necrostatin is a Trp-based molecule (5-(1H-indol-3-ylmethyl) 3-methyl-2-thioxo-4-imidazolidinone) that was first recognised as an inhibitor of regulated necrosis by blocking the kinase activity of RIP1 (Degterev et al., 2005).

### **1.9.5 Autophagy**

The word *autophagy* is a Greek word which means self-eating. The process was first described over 40 years ago by Christian de Duve. The focus was on the observed degradation of intra-cellular structures such as mitochondria in rat liver perfused with glucagon (Deter et al., 1967). Autophagy plays an important role in balancing sources of energy during critical times in development and during fasting, and it also has a housekeeping role by removing damaged organelles and aggregated proteins (Glick et al., 2010). Autophagy is initiated by stress-related conditions such as starvation, oxidative stress, and protein aggregation (Dikic and Elazar, 2018). Autophagy also has a protective effect against some diseases. It degrades the aggregate-prone intracytoplasmic proteins that cause many neurodegenerative diseases (Sarkar et al., 2009), and it can protect against infectious diseases caused by pathogenic agents (Rubinsztein et al., 2015). The activation of autophagy is driven by a large number of proteins, such as Autophagy-

Related Genes (ATGs) phosphatidylinositol 3-kinase (PI3K), and microtubule-associated protein 1 Light Chain3 (LC3) (Mizushima et al., 2011; Axe et al., 2008; Shimizu et al., 2014). These proteins are responsible for the formation of autophagosome via two major steps: elongation and nucleation of membrane isolation (Shimizu et al., 2014). The LC3 microtubule-associated protein is known to exist in autophagosomes, and it is considered to be a marker for autophagy (Kabeya et al., 2000; Mizushima et al., 2004).

Once an autophagosome has enveloped the proteins/organelles desired for degradation, it then fuses with lysosomes/autolysosomes. As this organelle contains a digestive enzyme, the contents are therefore degraded, and the components reutilised by the cell (Mizushima et al., 2010).

## 1.10 Antipsychotic Drugs

The term *antipsychotic drug* is applied to medications that are primarily used to manage several psychiatric disorders, including schizophrenia and bipolar mania, and to control psychiatric symptoms, such as delusion, hallucination, agitation, and psychomotor excitement, in different mental illnesses (Sommer et al., 2012). More than 40 drugs described as antipsychotics are available for clinical use. These are commonly classified into two classes: first-generation antipsychotics (FGAs) and second-generation antipsychotics (SGAs) (Seida et al., 2012). According to their chemical structure, they are further classified into five subgroups: phenothiazines (FGA), thioanthenes (FGA), diphenylbutylpiperidines (FGA and SGA), butyrophenones (FGA), and benzodiazepines (SGA) (Foster, 2001). Reports have shown that, during the last 20 years, the use of antipsychotic drugs has increased markedly, particularly in children and teenagers (Zito et al., 2000). These drugs are also commonly used in agitated/aggressive patients with a neurodegenerative disease such as Alzheimer's (Corbett et al., 2014). A number of clinical studies have suggested that patients with Alzheimer disease shouldn't be given antipsychotic drugs for several of reasons, including the observation that they speed up the progression of these types of neurodegenerative diseases (Oscar et al., 2013).

### **1.10.1 First-Generation Antipsychotics (FGAs)**

The FGA drugs are also known as “typical” antipsychotics, “classic” antipsychotics, “neuroleptics”, and dopamine antagonists. FGAs were initially established in the early 1950s, when chlorpromazine was being investigated by Courvoisier et al. (1953) in animal studies (Pichot, 1996). The results obtained in rodents showed that chlorpromazine extends sleep induced by barbiturates. Chlorpromazine also demonstrated inhibition of apomorphine-induced vomiting in dogs. Furthermore, in mice, chlorpromazine prevented the automatic avoidance-escape response. In 1951, Huguenard and Laborit administered chlorpromazine to patients for its potential anaesthetic effects during surgery (Shen, 1999). In 1952, Hamon et al. (1952) and Delay et al. (1952) extended the usage of chlorpromazine to psychiatric patients, where the researchers discovered the drug’s antipsychotic effects (Ban, 2007).

After the first 2 years of chlorpromazine prescription, the main side effect identified was acute extrapyramidal symptoms (Steck, 1954). Extrapyramidal symptoms are classified in general into two groups of signs and related disorders: hypokinetic symptoms, such as found in Parkinson’s disease, and hyperkinetic symptoms, such as found in Huntington’s disease. Both groups of symptoms appear after using drugs that act to block dopamine. Mostly, extrapyramidal symptoms are recognised by observation, or by a brief examination (Sanders and Gillig, 2012). In 1959, the first reports of tardive dyskinesia were recognised as cause for concern (Hippius, 1989). In addition, although the positive symptoms, such as delusions,

hallucinations, and disorders of thought, became more controlled by the drugs, a noteworthy drawback of chlorpromazine was low efficacy in the avoidance of negative symptoms, such as societal isolation and the flattening of emotions (Rang et al., 2016). More recently, the FGAs have been succeeded by the SGAs, which are characterised by fewer or no severe adverse events such as dyskinesia and dystonia compared with FGAs. However, FGAs are still in use today in developed countries such as the UK (Dibben et al., 2016).

### **1.10.2 Second-Generation Antipsychotics (SGAs)**

Many newer antipsychotic drugs, such as risperidone, olanzapine, and quetiapine, were developed and approved by various governing bodies in the 1980s. These novel antipsychotics are known as SGAs or “atypical” antipsychotic drugs. These antipsychotics possess fewer adverse effects compared with FGAs due to their ability to specifically target the 5HT<sub>2A</sub> receptors of serotonin (Hill et al., 2010). The development of SGAs was considered to be a major breakthrough in treating mental illness because SGAs produced antipsychotic effects with minimal extrapyramidal symptoms (Divac et al., 2014). To distinguish between the two generations of antipsychotics, the term *atypical* was used to define these newer drugs. Clozapine, the first SGA, was introduced in the early 1960s after a group of pharmaceutical researchers in Switzerland were able to refute the theory that extrapyramidal symptoms and antipsychotics were related (Hippius, 1996).

Clozapine's early use proved that it was suitable for treating both positive symptoms, such as disorganised behaviour and hallucination, and negative symptoms such as severe social withdrawal (American Psychiatric Association, 1994). After the success of clozapine, other atypical antipsychotic drugs were developed, such as risperidone in 1994 and olanzapine in 1996 (Beasley et al., 1996).

SGAs have been shown to result in lower extrapyramidal symptoms compared to FGAs, although dose-related extrapyramidal symptoms do occur with certain SGAs (Owens, 1994; Peuskens, 1995; Daniel et al., 1999). However, these newer antipsychotics carry a much greater risk of developing obesity, hyperlipidaemia, and type II diabetes (Ross et al., 2006).

Some studies have reported that the use of FGAs has reduced in recent years, generally due to the increase in prescriptions of SGAs (Rosenheck et al., 2006). Nevertheless, because FGAs are significantly less costly than SGAs, they continue to be used regularly in clinical practice (Falzer et al., 2008). For this reason, both FGAs and SGAs were evaluated in this research.

### **1.10.3 Mechanism of Action**

During the 1960s, it became clear that the neuronal function occurred through the secretion of neurotransmitters. Today, up to 100 different neurotransmitters are known. In the target cell, most antipsychotic drugs block or enhance the action of neurotransmitters by binding to the receptors (Healy, 2009). All antipsychotic drugs share the same mechanism of action, namely blocking dopamine receptors in the brain (Gelder, 2006). There are five different isoforms of dopamine receptors in humans (Seeman, 1992). Types 1 and 5 are receptors, known as the D1 group of receptors, and share a similar structure and degree of drug sensitivity. Dopamine receptors 2, 3, and 4 share a very similar structure, but have different sensitivities to antipsychotic drugs and are classified as the D2 group (Seeman, 2004). Antipsychotic drugs act to block the D2 receptors in the dopamine pathways of the brain (Nandra and Agius, 2012). According to this terminology, SGAs are recognised as dopamine-serotonin antagonists, since they generally have a high affinity for 5HT<sub>2A</sub> receptors (Sadock et al., 2009). This has established the view that SGAs have atypical properties and a low risk of extrapyramidal symptoms.

### 1.10.4 Chlorpromazine

Molecular Formula:  $C_{17}H_{19}ClN_2S$

3-(2-chloro-10*H*-phenothiazin-10-yl)-*N,N*-dimethyl-propan-1-amine



Figure 1-12: Chemical structure of chlorpromazine.

Source: Chempider website.

Chlorpromazine is a dopamine antagonist in the FGA antipsychotic class. It was first used in 1952 and belongs to the phenothiazine family (Wisner and Schaefer 2015). Chlorpromazine was more effective than other drugs used for the treatment of psychoses at the time it was introduced, such as morphine (Haavik, 1977). Because it primarily reduces the symptoms of psychosis, it is generally used to treat schizophrenia. This drug is also used in the management of severe behavioural disorders accompanied by aggression, combativeness, or excessive excitability. Chlorpromazine can also be used in non-mentally ill patients as a sedative for excessive anxiety and agitation (Charpentier et al., 1952). The pharmacokinetics range of chlorpromazine is between 100-300ng/mL (Grunder et al., 2009). Chlorpromazine acts as an aminoalkyl antagonist on  $\alpha_1$ -adrenoceptors, histamine

H<sub>1</sub> receptors, and muscarinic cholinergic receptors. By blocking the α<sub>1</sub>-adrenoceptor and H<sub>1</sub> receptor, chlorpromazine induces sedation and hypotensive effects (Gelder, 2006).

### 1.10.5 Trifluoperazine

Molecular Formula: C<sub>21</sub>H<sub>24</sub>F<sub>3</sub>N<sub>3</sub>S

10-[3-(4-Methyl-1-piperazinyl)propyl]-2-(trifluoromethyl)-10H-phenothiazine

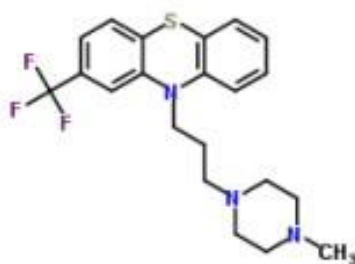


Figure 1-13: Chemical structure of trifluoperazine

Source: Chempider website.

Trifluoperazine is an FGA that also belongs to the phenothiazine family. It was first used in 1958 (Goddard, 1959). Trifluoperazine is prescribed to treat the signs of schizophrenia, and on a short-term basis, it is also used to treat anxiety and depression (Cowdry and Gardner, 1988). The pharmacokinetics range of trifluoperazine is between 200-800ng/mL (Grunder et al., 2009). Trifluoperazine is the most selective dopamine receptor antagonist (Potter and Hollister, 2004). It is

considered to have mild sedation effects and the greatest extrapyramidal symptoms (Gelder, 2006).

### 1.10.6 Olanzapine

Molecular Formula:  $C_{17}H_{20}N_4S$

2-Methyl-4-(4-methyl-1-piperazinyl)-10H-thieno[2,3-b][1,5]benzodiazepine

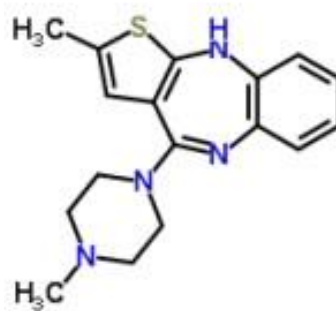


Figure 1-14: Chemical structure of olanzapine.

Source: Chempider website.

First used in 1996 (Taylor et al., 1999), olanzapine is an SGA that belongs to the thienobenzodiazepine class. Studies have shown that olanzapine is effective and may be safely used in patients with psychotic depression (Rothschild et al., 1999). The average daily use of olanzapine is 5-30mg/day, the mean plasma concentration range from 10 to 54ng/mL (Fellows et al., 2003). The affinity of olanzapine for other receptors, such as the H<sub>1</sub> receptor, is stronger than its affinity for the D<sub>2</sub> receptor. This feature makes olanzapine a superior SGA in influencing sedation (Gelder et al., 2004).

### 1.10.7 Quetiapine

Molecular Formula: C<sub>21</sub>H<sub>25</sub>N<sub>3</sub>O<sub>2</sub>S

11-[4-[2-(2-hydroxyethoxy)ethyl]-1 piperazinyl]dibenzo[b,f][1,4] thiazepine

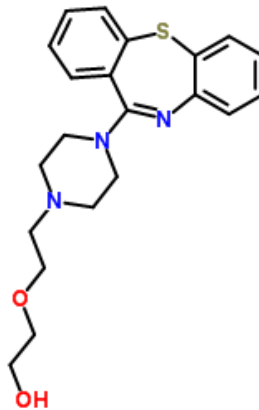


Figure 1-15: Chemical structure of Quetiapine.

Source: Chempider website.

Quetiapine is a dibenzothiazepine SGA drug (Nemeroff et al., 2002) that was first developed in 1985 and approved by the US Food and Drug Administration in 1997 (Riedel et al., 2007). It is usually prescribed to manage moderate to severe acute manic episodes and the positive and negative symptoms of schizophrenia (Riede et al., 2007). The suggested therapeutic dosage in the plasma is 70-170ng/mL (Baunmann et al., 2004). (Quetiapine has a higher affinity for serotonergic (5HT<sub>02A</sub>) than for dopaminergic D<sub>1</sub> and D<sub>2</sub> receptors (Bandelow et al., 2000).

### **Aim of this project:**

The contra-indication of using antipsychotic drugs in patient with neurodegenerative diseases has been highlighted in terms of disease progression and patient life spans. In this study our aim is to investigate the neurotoxicity of these drugs and to identify their mechanisms of cell death.

### **Objectives:**

- To investigate the toxic effects of the first and second generations of antipsychotic drugs on both SH-SY5Y brain cells and COS7 kidney-like cells.
  
- To identify the mechanisms of cell death (apoptosis, necrosis, or autophagy) caused by FGAs and SGAs.
  
- To investigate in both generations of antipsychotic drugs the protective role of Ca<sup>+2</sup> pumps SERCA2b and SPCA1a against toxicity after their overexpression in SH-SY5Y and COS7 cells.
  
- To overexpress RGN in both SH-SY5Y and COS7 and then investigate the effect of antipsychotic drugs on transfected cells.
  
- To differentiate SH-SY5Y Human Neuroblastoma Cells with Retinoic Acid (RA) and then investigate the cytotoxic effect of FGAs on these cells.

## **Chapter 2:**

# **Materials and Methods**

## **2. Materials and Methods**

### **2.1 Cell culture**

The human neuroblastoma cell line SH-SY5Y (ATCC® CRL-2266™) and the fibroblast-like monkey kidney cell line COS7 (ATCC® CRL-1651™) cells were grown in Dulbecco's Modified Eagle Media (DMEM) with phenol red and L-glutamine (Life Technologies). The highest passage number of SH-SY5Y used in this project was 20, and 30 for COS7. The media was supplemented with 10% heat-inactivated Foetal Bovine Serum (FBS) (Life Technologies), 1% penicillin/streptomycin (Sigma-Aldrich), and 1% Non-Essential Amino Acid (NEAA) (Sigma-Aldrich). Cells were transferred into 25 cm<sup>3</sup> or 75 cm<sup>3</sup> vented cell culture falcon flasks inside a vertical laminar hood. The hood and all materials used were either cleaned with a 70% ethanol solution or autoclaved. All cells were incubated in a CO<sub>2</sub> incubator (LEEC) at 37 °C and 5% CO<sub>2</sub>.

### **2.2 Subculture**

The cells were routinely sub-cultured when they reached a confluency of 70–80% in the flasks, which was determined by viewing them under a microscope. Cells were diluted at a rate of 1:5 to 1:10 for SH-SY5Y or 1:3 to 1:10 for COS7 for subculture. When the cells reached the desired confluency, the media was removed, the cells were washed with Phosphate Buffered Saline (PBS) (Lonza),

and 2–3 ml of 0.05% Trypsin/EDTA (Life Technologies) was added. The cells were then incubated for 3–5 minutes in the CO<sub>2</sub> incubator until the cells became detached. Then fresh media was added to stop the reaction, and the cells were transferred to a new flask with an appropriate amount of fresh media.

### **2.3 Cell Counting**

10 µL of cell suspension was placed in a micro tube, and then 10 µL of trypan blue (Sigma-Aldrich) was added in order to distinguish between living and dead cells. 20 µL of cell suspension was added to the haemocytometer to quantify the population of the cells under the microscope. The number of cells inside the grid reflected the number of cells in 0.1 µL. The method used to count the cells was as follows (Figure 2-1), each chamber was divided into a pattern of nine large squares; the cells touching the top and left lines were counted; however, the cells touching the bottom and right lines were not.

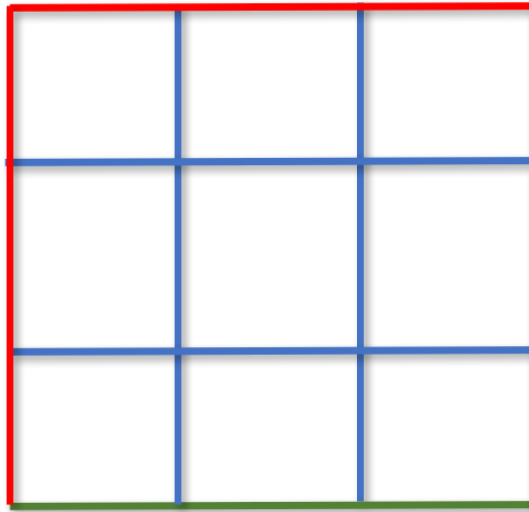


Figure 2-1: View of the haemocytometer square under the microscope.

Cells within the full square were counted by including the cells touching the red lines (top and left) and excluding the cells touching the green lines (right and bottom).

## 2.4 Cryopreservation of Cells

When the cells reached the maximum confluency of 70–80% and were not in use, they were frozen and stored in liquid nitrogen. Cells were trypsinised into a suspension, then centrifuged at 1,000 rpm at 4°C for 5 minutes. The media was removed from the cells, and 10% of Dimethyl Sulfoxide (DMSO) (Sigma-Aldrich) in complete DMEM media was added. 1 mL of the solution was transferred to cryovials, and each vial was labelled according to the cell type, passage number, and date and then stored in an isopropanol jacket at -80°C for 24 hours. The vials were then transferred to liquid nitrogen.

## **2.5 MTT (3-(4,5-Dimethylthiazol-2-yl)-2,5-**

### **Diphenyltetrazolium Bromide) Cell Viability Assay**

Cells (typically  $40 \times 10^4$ ) were seeded in 24 well cell culture plates and incubated overnight. On the second day, the old media was removed, and fresh DMEM media, but without phenol red or FBS, was added to each well. A stock solution of the drug was prepared by dissolving it in DMSO, and different concentrations of the drug were incubated with the cells for a 24-hour period (the DMSO was  $<0.2\%$  v/v). After 24 hours, the MTT cell viability assay was conducted by removing the drugs containing media and adding 0.5 mL of 0.5 mg/ml 3-(4,5-Dimethylthiazol-2-yl)-2,5-diphenyl tetrazolium bromide (MTT reagent) (Sigma-Aldrich), dissolved in PBS, to each well and incubating for about 1–4 hours in a CO<sub>2</sub> incubator. The MTT solution was removed, and 0.5 mL DMSO was added to each well to dissolve the cells. Viable cells formed a formazan product within active mitochondria, which was dissolved in the DMSO (Riss et al., 2004). The solution from each well was then transferred to a 96-well plate and read using a colorimetric plate reader (Biotek) at 590 nm.

## **2.6 Crystal Violet**

Cells were plated at  $40 \times 10^4$  per well in a 24-well plate and incubated overnight. The next day, the wells were washed with PBS, and then 4% paraformaldehyde in PBS (Affymetrix) was added to the cells and incubated in the CO<sub>2</sub> incubator for 20 minutes. The cells were then washed with PBS and stained with 1% crystal violet (dissolved in 5% ethanol in dH<sub>2</sub>O) for 30 minutes at room temperature. To assess viability the cells were then washed three times with dH<sub>2</sub>O to remove non-adherent cells and left to air dry for 1 hour. 10% acetic acid was added to each well and incubated at room temperature for 20 minutes with shaking. The absorbance of the samples was measured by a plate reader at 570 nm, and acetic acid was used as the blank.

## **2.7 Sample Preparation**

### **2.7.1 Stock Solutions**

The stock solutions were prepared by dissolving each drug in DMSO. Because of its known toxicity, the cells were incubated with DMSO alone to determine the correct concentration to use in order to minimise DMSO-induced cell death. The concentrations of the stock solutions were 15 mM Chlorpromazine (Sigma-Aldrich), 15 mM Trifluoperazine (Sigma-Aldrich), 100 mM Olanzapine (Sigma-Aldrich), and 100 mM Quetiapine (Cayman Chemical).

### **2.7.2 Positive Control Solution**

Hexabromocyclododecane (HBCD) is a brominated flame retardant found worldwide in wildlife and the environment (Arnot et al., 2009). Previous studies have investigated the cytotoxicity of HBCD in SH-SY-5Y cells and determined the LC<sub>50</sub> to be 2.7  $\mu$ M (Al-Mousa, 2010). It was found that HBCD induced cell death by apoptosis by activating caspase and increasing the concentration of intracellular Ca<sup>2+</sup> (Al-Mousa and Michelangeli, 2012). In addition, it was found that HBCD induced autophagy (Michelangeli personal communications). For these reasons, HBCD (Sigma-Aldrich) was used as a positive control for apoptosis and autophagy. The stock solution used was 3 mM.

## **2.8 Mechanism of Cell Death**

### **2.8.1 Apoptosis**

#### *2.8.1.1 Caspase Inhibitors*

Cells were seeded in cell culture plates and incubated overnight. On the second day, the old media was removed, and fresh media, but without phenol red or FBS, was added. Caspase-3 inhibitor (Ac-DEVD-CMK, Sigma-Aldrich), Caspase-8 inhibitor (N-Acetyl-Ile-Glu-Thr-Asp-al, Sigma-Aldrich), and Caspase-9 inhibitor (Z-LEHD-FMK G-Bioscience) were dissolved in DMSO with final concentration 50  $\mu$ M and added to the cells for 4 hours before adding the drugs. Then the LC<sub>50</sub> concentration

for each drug was added to the cells and incubated in a CO<sub>2</sub> incubator for 24 hours. After 24 hours, MTT and crystal violet assay were performed.

#### *2.8.1.2 Caspase substrates*

Cells were seeded in sterilised 35-mm glass bottom dishes and incubated until they reached 70% confluency. The cells were treated for 24 hours with the LC<sub>50</sub> for each drug in media without FBS and with phenol red and then incubated for 24 hours. After 24 hours, 2 µM of Nuc View 488 Caspase-3 substrate (Biotium) was added and left for 1 hour, then examined under the fluorescence microscope using a 40x lens under brightfield and fluorescence channels GFP  $\lambda_{exc} = 488$  nm and  $\lambda_{em} = 502$  nm.

#### *2.8.1.3 Cytochrome-c release*

Cells were seeded in 6-well plates with complete growth media for 24 hours to reach 70% confluency. After 24 hours, cells were treated with the LC<sub>50</sub> for each drug and incubated for 24 hours. After treatment, cells were trypsinised and centrifuged at 1500 rpm for 5 minutes. Cells were re-suspended in 150 µL lysis buffer (20 mM HEPES, 1.5 mM MgCl<sub>2</sub>, 10m MKCl, 1 mM EGTA, 1 mM EDTA, 1 mM DTT, and 1 mM PMSF; PH 7.5) and incubated in ice for 30 minutes. Then cells were disrupted with a sonicating homogeniser and centrifuged at 14000 rpm

for 10 minutes at 4°C to collect the mitochondria pellet fraction, which was then re-suspended in lysis buffer. The solution was then transferred to a fresh ultra-centrifuge tube and centrifuged again at 100,000 g for 30 minutes to collect the supernatant (cytosolic fraction). The amount of protein in the mitochondrial and cytosolic fractions were determined by the Bio-Rad DC assay, then analysed by Western blots using an anti-cytochrome c antibody (Sigma-Aldrich).

## **2.8.2 Necrosis**

### *2.8.2.1 Lactate Dehydrogenase (LDH) Release*

Cells were seeded in 6-well cell culture plates and incubated overnight. The next day, the old media was removed, and fresh media, without FBS or phenol red, was added. The cells were treated with drugs for different time periods from 5 to 24 hours, and the control was treated with 10% Triton X-100 (Sigma-Aldrich) for 1 hour. The solution from each well was centrifuged at 1500 rpm for 10 minutes. In a cuvette, 500µL of each supernatant was added to 500 µL of the cocktail buffer (0.66mM Sodium pyruvate, 100mM Potassium phosphate, 0.23mM β-Nicotinamide adenine dinucleotide NADH; pH 7), and the absorbance change was measured by a spectrophotometer (Ultrospec 1000) at 340 nm. % LDH release was calculated as the experimental rate divided by the rate observed for the Triton X-100 treated cells.

### *2.8.2.2 Necrosis Inhibitor*

Cells were seeded in 24-well cell culture plates and incubated overnight. On the second day, the old media was removed, and fresh media, without phenol red or FBS, was added. Necrosis inhibitor IM-54 (Alfa Aesar), with a final concentration of 5  $\mu$ M, was added to the cells for 4 hours before adding the drugs. After the drugs were added, MTT and crystal violet assay, were performed after 2, 4, 6, and 24 hours.

## **2.8.3 Autophagy**

### *2.8.3.1 GFP-LC3 Transfection as Autophagosome Marker*

Cells were seeded in a sterilised 35-mm glass bottom dish and incubated until they reached 50% confluency. The next day, cells were transfected with LC3-GFP plasmid (Prof. Vincent Wong, Macau University) using TurboFectin 8.0 transfection reagent (OriGene), following the manufacturer's instructions, and left for 48 hours. Cells were then treated with the LC<sub>50</sub> concentration for each drug and incubated for 24 hours. For a positive control, cells were incubated with Hanks buffer (starvation media) for 30 minutes. The next day, cells were washed with PBS and fixed with 4% paraformaldehyde. Then fluorescence images were taken by Nikon A1R Inverted Confocal/TIRF microscopy at  $\lambda_{\text{exc}} = 488 \text{ nm}$ ,  $\lambda_{\text{em}} = 502 \text{ nm}$ .

### *2.8.3.2 LC3B Antibody*

Cells were seeded in 6-well plates with complete growth media and incubated in a CO<sub>2</sub> incubator until they reached 70% confluency. The next day, cells were treated with the LC<sub>50</sub> concentration for each drug and left for 24 hours. After 24 hours, cells were trypsinised and centrifuged at 1500 rpm for 10 minutes. Cells were then re-suspended in 100 µL of RIPA buffer (1% Triton X100, 0.5% w/v Sodium Deoxycholate, 10% SDS; pH 7.2) with protease inhibitor and incubated on ice for 30 minutes. Then cells were then disrupted with homogeniser and centrifuged at 14000 rpm for 10 minutes at 4°C. The amount of protein in the solution was determined by a Bio Rad DC protein assay kit and then analysed by Western blot (using the LC3B Antibody (Cell Signalling)).

## **2.9 Preparation of Agar Plates and LB Broth Medium**

Sterilised 2% LB broth media was prepared by dissolving 20 g of LB broth in 1 L dH<sub>2</sub>O, and 1.5% of LB agar was made by dissolving 1.5 g of agar powder in 100 mL of LB broth. Both solutions were autoclaved. After LB broth solution cooled down, it was mixed with ampicillin antibiotic (Sigma-Aldrich) at 0.1 mg/ml final concentration. The agar mixture was then poured into 10-cm-diameter petri dishes and left to set. For selecting and growing bacteria containing the LC3-GFP plasmid, kanamycin (0.025 mg/ml) was used as the antibiotic.

## **2.10 RGN-GFP Plasmid Preparation**

To transform the RGN plasmid (Figure 2-2) into DH5 $\alpha$  bacterial cells, the RGN plasmid was heat shocked. First, a tube of 50  $\mu$ L cells were thawed on ice. Then 1  $\mu$ L of RGN plasmid (0.1  $\mu$ g/ $\mu$ l Human cDNA clone with GFP at the C-terminal pCMV6 AC-GFP-RGN; OriGene), as shown in (Figure 2-2), was added, and the tube was placed on ice for another 30 minutes. The cells were heat shocked at 42°C for 30 seconds then placed on ice for 5 minutes. After the heat shock, 950  $\mu$ l of LB media was added to the tube, and the tube was incubated at 37°C for 1 hour. The cells were mixed by flicking the tube, and different dilutions of the solution were spread on the ampicillin agar plates and incubated overnight at 37°C. After incubating the agar plates for 24 hours, a single colony was transferred to a tube containing LB media with antibiotic and placed in a shaking incubator at 24 hours at 37°C for 18 hours. After 18 hours, a glycerol stock from the bacteria was stored at -80°C.

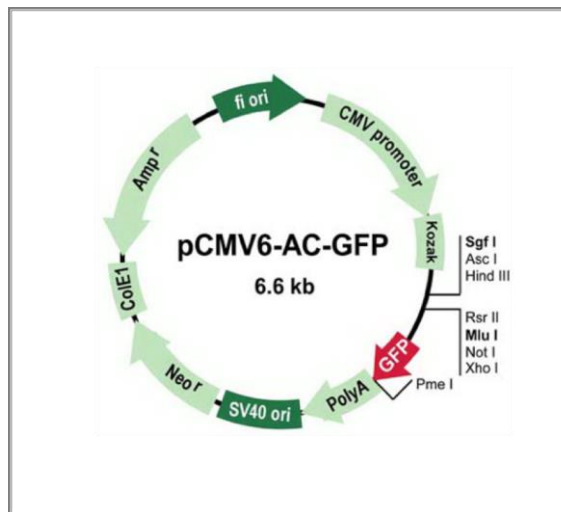


Figure 2-2: The OriGene vector with RGN-C tagged Human Variant 1.

## 2.11 Bacteria Recovery

From previous work in our group, a bacteria glycerol stock of SERCA2b-GFP, SPCA1a-GFP, and LC3-GFP were stored at  $-80^{\circ}\text{C}$ . Without thawing the stock, a small amount of the bacteria was scraped by a sterilised pipette tip and placed into 5 ml of LB broth with 0.025 mg/ml of kanamycin for LC3-GFP or 0.1 mg/ml ampicillin for both SERCA2b-GFP and SPCA1a-GFP. The tubes were incubated at  $37^{\circ}\text{C}$  with shaking. The next day, different dilutions of the solutions were spread on agar plates and incubated overnight at  $37^{\circ}\text{C}$ . After incubating the agar plates for 24 hours, a single colony was transferred to a tube containing LB media with the relevant antibiotic and placed in a shaking incubator at  $37^{\circ}\text{C}$  for 18 hours. After 18 hours, a glycerol stock from the bacteria was stored at  $-80^{\circ}\text{C}$ .

## **2.12 Plasmid Maxi-Prep**

An Invitrogen HiPure Plasmid Filter Maxiprep Kit was used for plasmid purification. The DNA was extracted following the manufacturer's instructions. The amount of DNA purified was measured by NanoDrop spectrophotometer (ND-1000).

## **2.13 Transient Transfection**

Cells were seeded at a density of  $2 \times 10^4$  for COS7 and  $1 \times 10^4$  for SH-SY5Y per well in 24-well cell culture plates and incubated inside a CO<sub>2</sub> incubator at 37°C and 5% CO<sub>2</sub> for 24 hours. Three transfection conditions were examined at ratios of 1:2, 2:4, and 1:3 µg/µL of each DNA plasmid (SERCA2b-GFP, SPCA1a-GFP, RGN-GFP, RGN-GFP, and PcDNA), again per the manufacturer's instructions for each of the transfection reagents see Table 2-1. Briefly free serum media was mixed with transfection reagent. Then the DNA plasmid was added and left for 20 minutes. The mixture was then added to the cells (each condition in triplicate) and incubated in a CO<sub>2</sub> incubator for 24 hours. After 24 hours, the old media was removed, and fresh growth media was added. The cells were then visualised under light and fluorescence microscopy every 24 hours for three days, to determine the level of GFP-expressing cells to record optimal results.

Table 2-1: Transfection Reagents

Transfection Reagent	Company	Catalogue No.	Ratio Range DNA µg: TR µL
TurboFect	Thermo scientific	00244342	1:2 – 2:6
TurboFectin 8.0 (Used for LC3-GFP)	OriGene	TF81001	1:3, 2:3, and 1:6
Effectene	Qiagen	301425	0.1:2 – 1:8
Metafectene	Biontex	T020-1.0	1:2 – 1:7
Metafectene Pro (Used for SERCA2b- GFP, SPCA1a-GFP and RGN-GFP)	Biontex	T040-1.0	1:2 – 1:7

## 2.14 Protein Extraction

The cells were grown in 6-well plates and incubated until they reached 70% confluency. The control and treated cells were trypsinised by adding 0.5 ml of trypsin-EDTA to each well and incubated for 2 minutes. Then 1 ml of full media was added to stop the reaction. The solution was then centrifuged for 5 minutes at 1500 rpm. The cell pellets were re-suspended with RIPA buffer (1% Triton X100, 0.5% w/v Sodium Deoxycholate, 10% SDS; pH 7.2) with protease inhibitor cocktail tablets (Roche) and incubated on ice for 30 minutes with flicking every 10 minutes. The cells were disrupted and homogenised then centrifuged at 14000 rpm for 15 minutes at 4°C.

## **2.15 Protein Estimation**

The concentration of proteins was determined using the Bio Rad DC protein assay kit (BIO-RAD) following the manufacturer's guidelines. To generate a standard calibration curve, 2  $\mu$ L of each concentration of standard bovine serum albumin (BSA) (0, 0.625, 1.25, 2.5, 5, and 10 mg/mL) was added in duplicate wells in a 96-well plate. 2  $\mu$ L of each sample was added to the plate in triplicate. For all wells, 25  $\mu$ L of reagent SA (20  $\mu$ L reagent S to each 1 ml reagent A) and 200  $\mu$ L of reagent B were added. The plate was left for 15 minutes in the dark at room temperature, and the absorbance was measured by a plate reader at 645 nm.

## **2.16 Protein Separation by SDS Page**

A protein sample of 20–40  $\mu$ g from the cells was prepared by adding the loading buffer (62.5 mM Tris pH 6.8 with HCl, 2.3% v/v SDS, 25% w/v Glycerol, 5% v/v  $\beta$ -mercaptoethanol, Bromophenol Blue) at a ratio of 1:3. The samples were heated at 80°C for 10 minutes. The prepared samples and protein ladder molecular weight marker (Thermo Scientific) were loaded into the stacking gel (4% Acrylamide, 125 mM Tris-HCl pH 6.8, 0.1% SDS, 10  $\mu$ l/10ml TEMD, 10%w/v APS, 7.35 ml dH<sub>2</sub>O). The resolving gel (12.5% Acrylamide, 375 mM Tris-HCl pH 8.8, 0.1 SDS, 15  $\mu$ l/10ml TEMD, 10% w/v APS, 7 ml dH<sub>2</sub>O) and the positions were labelled. The gel was placed in the tank, and the running buffer (25 mM tris, 192 mM glycine, and 0.1% SDS) was added. The samples were electrophoresed at 125 volts and 400

mA for 60 minutes, or when the bromophenol blue dye front reached the bottom of the gel.

### **2.17 Western Blot Protein Transfer**

After running the gel, the protein was transferred from the gel to the nitrocellulose membranes using the Trans-Blot Turbo system from BIO RAD. After placing the gel and the membrane in the right order, with the filter paper, the transfer took about 7 minutes see (Figure 2-3). The membrane was marked by pencil at the position of the protein marker. It was then blocked in 5% dried skimmed milk powder dissolved in TBS-T (20 mM Tris, 137 mM NaCl, 0.1% Tween pH 7.6) for 1 hour with gentle agitation. Table 2-2, shows a list of the antibodies used. The primary antibodies were diluted as described in Table 2-2, with 3% albumin bovine BSA in TBS-T, which was added to the membrane and incubated overnight with gentle agitating at 4°C. The next day, the membrane was washed three times with TBS-T for at least 5 minutes each time. The secondary antibodies, according to the proteins seen in Table 2-3, were diluted with 3% albumin bovine BSA in TBS-T, added to the washed membrane, foiled, and incubated for 1 hour with gentle agitation. The membrane was then washed five times with TBS-T for 10 minutes each time. The last wash for the membrane was with TBS (20 mM tris, 137 mM NaCl pH 7.6), and the membrane was dried with filter paper. The membranes were then imaged using a Li-Cor Odyssey Scanner. Using Image Studio Lite software for the analysis,

bands that give a saturated intensity appear green. In all results presented, gels with saturated levels were not included

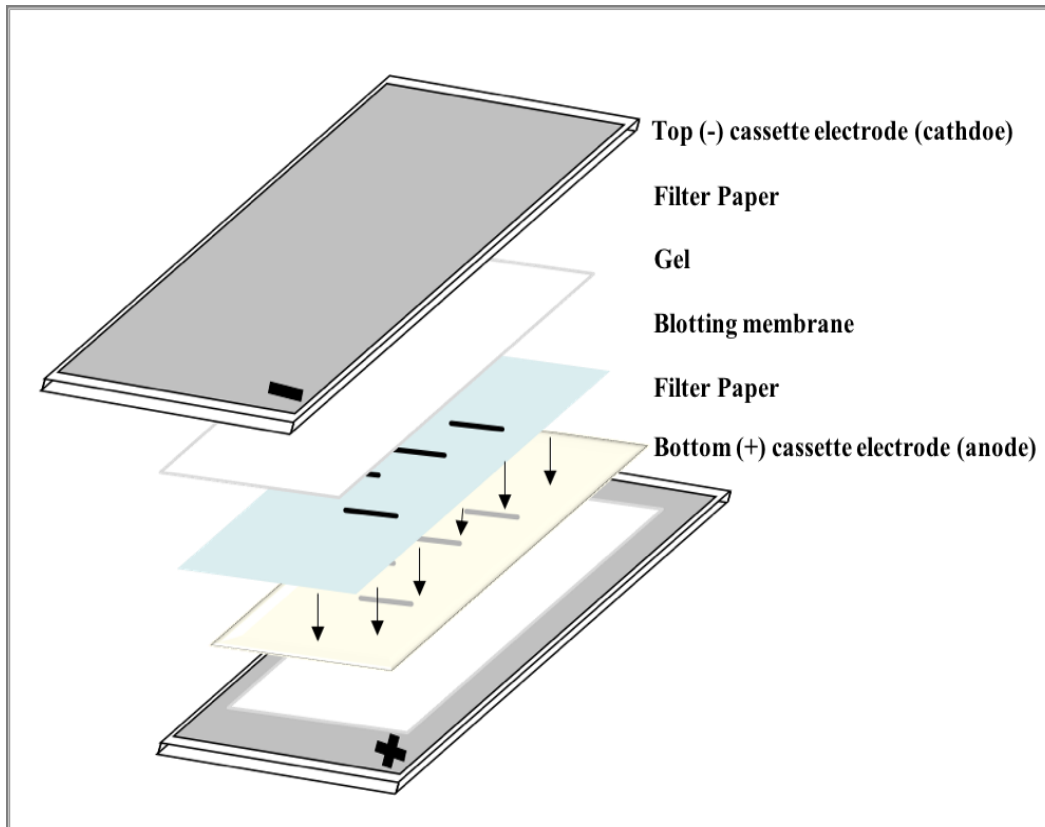


Figure 2-3: Proper layering of transfer.

Table 2-2: List of primary antibodies for each protein

Primary Antibody	Size	Host	Company	Catalogue No.	Dilution
Cytochrome-c Anti-cytochrome c	15 kDa	Sheep	Sigma- Aldrich	C9616	1:500
	27 kDa	Rabbit	Novus Biologicals	NBP2-13172	1:1000
LC3B	1416 kDa	Rabbit	Cell Signalling	2775	1:1000
SERCA Y1F4	100 kDa	Mouse	Gift from Prof. J.M. East, the University of Southampton		1:500
SPCA LTQQ	100 kDa	Rabbit	Prof. F. Michelangeli group, the University of Birmingham		1:100
RGN SMP3- (FL-299)	35 kDa	Rabbit	Santa Cruz	Sc-292770	1:200
Differentiation GAP 43	43 kDa	Rabbit	GeneTex	Ab16053	1:1000
Anti $\beta$ -actin	42 kDa	Mouse	Sigma- Aldrich	A2228	1:5000

Table 2-3: List of the Secondary Antibodies

Secondary Antibody	Source	Company	Catalogue No.	Dilution
Cytochrome-c	Donkey	Novus Biologicals	NBP1-73006	1:10000
SERCA2b	Anti-Mouse	Licor	IR-dye 680	1:10000
LC3IIB	Anti-Rabbit	Licor	IR-dye 800	1:10000
CHOP	Anti-Rabbit			1:10000
SPCA1a	Anti-Rabbit	Licor	IR-dye 800	1:10000
RGN	Anti-Rabbit			1:10000
Differentiation	Anti-Rabbit			1:10000

## **2.18 Flow Cytometry**

To evaluate the percentage of transfection efficiency and dead cells by fluorescence-activated cell counter (FACC), the FACSCalibur (BD Biosciences, CA) was used. Cells were seeded in a 6-well plate and incubated to reach the appropriate confluency. After transfecting the cells with SERCA2b-GFP, SPCA1a-GFP, and RGN-GFP, the cells were trypsinised by adding 0.5 mL of 0.05% trypsin-EDTA to each well and then 1 mL of full media. Cells were then centrifuged at 1000 rpm for 2 minutes. The pellet was carefully washed with PBS then re-suspended in PBS containing 3  $\mu$ M Propidium Iodide (PI) (Invitrogen, USA) and 2% FBS. The cells were transferred to FACC tubes and incubated on ice for 30 minutes. To excite both GFP and PI channels, the machine was set to 488 nm of an argon laser. The samples run through the machine, and data were analysed using FlowJo software.

## **2.19 Co-Localisation**

Sterilised cover slips were placed in 6-well plates, and cells were added and incubated overnight. Then the cells were transfected with SERCA-GFP, SPCA-GFP, and RGN-GFP. After 48 hours, cells were treated with LC<sub>50</sub> concentration of each drug for 24 hours. The next day, the cells were washed with PBS, and 5  $\mu$ M of MitoTracker Deep Red FM (Cell Signalling) was added to the cells and incubated

for 30 minutes. The cells were then washed twice with PBS and fixed with 4% paraformaldehyde for 20 minutes. After washing the cells with PBS, the cover slip was removed from the plate, one drop of Fluoroshield™ with DAPI histology mounting medium (Sigma-Aldrich) was added, and the cover slip was then placed upside down on a slide. The slides were left to dry in the dark before being examined using the Nikon A1R Inverted Confocal/TIRF microscope.

## 2.20 Confocal Microscopy

The Nikon A1R Inverted Confocal/TIRF microscope was used to observe the transfected fixed cells using the oil immersion lens 100x under brightfield and fluorescence channels:

GFP  $\lambda_{exc} = 488 \text{ nm}$ ,  $\lambda_{em} = 502 \text{ nm}$

MitoTracker Deep Red FM  $\lambda_{exc} = 644 \text{ nm}$ ,  $\lambda_{em} = 665 \text{ nm}$

Fluoroshield™ with DAPI  $\lambda_{exc} = 360 \text{ nm}$ ,  $\lambda_{em} = 460 \text{ nm}$

Colocalization was analysed using JACoP toolbox following Bolte and Cordelieres (2006) guide. Images were analysed by Fiji software.

## 2.21 Differentiation of Sh-SY5Y Cells with Retinoic Acid

Low passage number SH-SY5Y cells (less than 20) were washed with PBS and trypsinised with 2 ml of trypsin/EDTA from a confluent 75 cm<sup>3</sup> flask. 10 ml of

complete growth media was added to the flask. The solution was then transferred to a 15-ml centrifuge tube and centrifuged at 1000 g for 2 minutes. Cells were then plated in 6-well plates with 100,000 cells per well and incubated overnight. The next day, the old complete growth media was removed, and 2 ml of the differentiation media with 2.5% FBS, 1% Pen/strep, 2 mM Glutamine, and 10  $\mu$ M All-trans retinoic acid was added and changed thereafter every two days. Cells were examined on the third, fifth, and seventh days under the microscope. Western blotting using Anti-GAP43 antibody, a differentiation neuronal marker, was used to determine differentiation.

## **2.22 Statistics**

The collected data were analysed using Graph Pad Prism software version 7. All data were normally distributed, and the percentage data (that is not normally distributed) were transformed using logit transformation before t-testing. A two-tailed Student's t-test was applied for unpaired data, and the P values were considered significant at  $\leq 0.05$  (mean  $\pm$  SD and n = 3 and each experiment had typically 6 technical replicates) ie mean of 3 experiments ,6 repeats per experiment. (P value statistical significance started at \*P $\leq$ 0.05, \*\*P $\leq$ 0.01, \*\*\*P $\leq$ 0.001, \*\*\*\*P $<$  0.0001 using unpaired two-tailed t-tests.) For flow cytometry data, FlowJo software was used, and for analysing the bands on the blots gels, Image Studio Lite software was used.

## **Chapter 3:**

# **A Systematic Investigation of the Mechanisms of Cell Death Induced by Antipsychotic Drugs**

### **3. A Systematic Investigation of the Mechanisms of Cell Death Induced by Antipsychotic Drugs**

#### **Introduction**

Antipsychotic drugs are types of medication used to manage many psychotic symptoms such as delusion and hallucination (Iris et al., 2012). They can also be prescribed to elderly people with dementia disorders such as Alzheimer's disease in order to reduce agitation (Martinez et al., 2013). However, these drugs have been linked to increase in the progression of the disease and reduced life expectancy (Oscar et al., 2013). These drugs are mainly classified into first-generation antipsychotics (FGAs) and second-generation antipsychotics (SGAs), according to their mechanism of action. Although it is known that the side effects of the first generation of the drugs are associated with extrapyramidal symptoms such as acute dyskinesia, dystonic reactions, and akathisia (Blair and Dauner, 1992), the drugs are still extensively used in the UK (Marston et al., 2014).

This chapter reports on a comparison of the effect of FGAs and SGAs and investigates their mechanism of cell death on both a neuronal (SH-SY5Y) and a non-neuronal kidney (COS7) cell line. The drugs used in this study are reported to be the most commonly prescribed antipsychotic drugs in the UK: chlorpromazine and trifluoperazine from the first generation, and olanzapine and quetiapine from the second generation (Vallianatou, 2016). The neurotoxicity and cytotoxicity of both generations of the antipsychotic drugs were measured by two different cell viability methods: MTT and crystal violet assays. After determining the lethal

concentration 50 (LC<sub>50</sub>) of each drug, several experiments were undertaken to elucidate their mechanisms of cell death, whether via apoptosis, necrosis, or autophagy.

## **3.1 Results**

### **3.1.1 Cell Viability**

#### *3.1.1.1 Validity of MTT*

MTT is a sensitive colorimetric assay which assesses cell viability through monitoring functional mitochondria in living cells (Meerlii et al., 2011). This assay was used to evaluate the viability of SH-SY5Y and COS7 cells following treatment by some antipsychotic drugs.

To test the validity of this method, a control experiment was performed. Different numbers of SH-SY5Y cells, which were determined by using cell-counting methods, were plated and incubated in a CO<sub>2</sub> incubator at 37 °C for 24 hours. However, this method assesses mitochondrial activity and we assume that dead cells have little or no mitochondrial reductase activity. The MTT assay was performed, and the absorbance values were recorded. Increases in cell numbers caused increases in absorbance values, as shown in (Figure 3-1). A strong linear correlation between the absorbance and cell number was confirmed by the R<sup>2</sup> value of 0.98, which reflects the validity of the MTT assay.

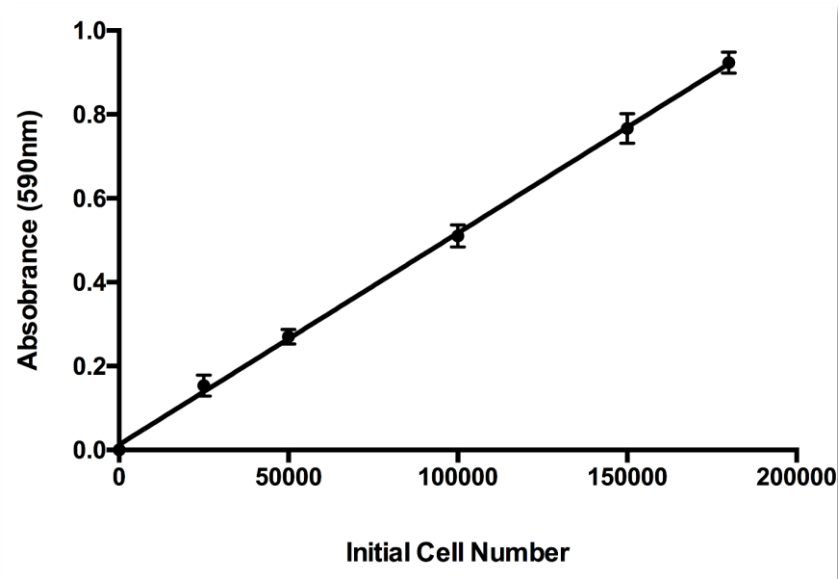


Figure 3-1: The relationship between SH-SY5Y cell number and MTT absorbance.

Cells were plated at a density of 0–200,000 cells per well in a 24-well plate and incubated for 24 hours at 37°C. After 24 hours, cell viability was measured using MTT assay. The data represented the mean ± SD, n = 6.

#### 3.1.1.2 Validity of Crystal Violet

Crystal violet assay is a quantitative colorimetric method of detecting cell viability by staining protein and DNA in viable adherent cells (Feoktistova, 2016). For validating the method, different numbers of cells were incubated for 24 hours prior to staining. As seen in (Figure 3-2), there is a strong linear correlation between the absorbance and cell number when was confirmed by the  $R^2$  value of 0.98, and this reflects the validity of the assay.

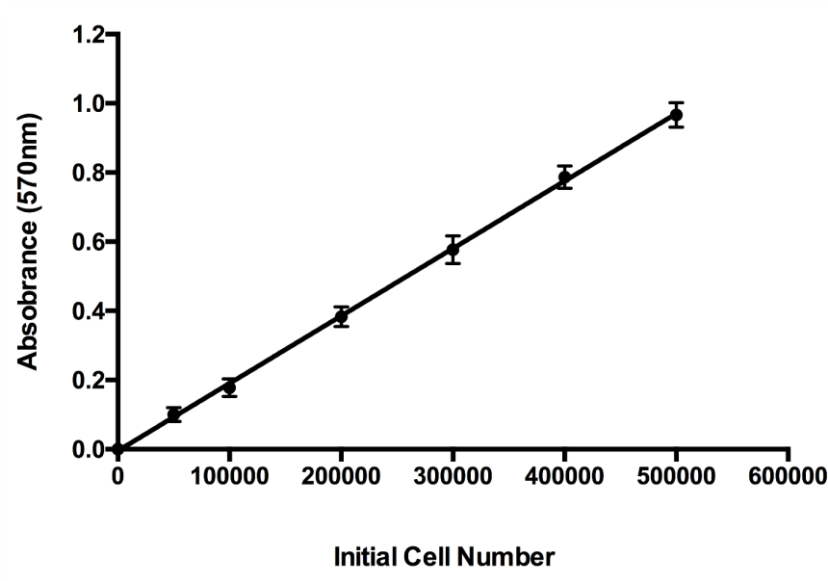


Figure 3-1: The relationship between SH-SY5Y cell number and crystal violet absorbance.

Cells were plated at a density of 0–600,000 cells per well in a 24-well plate and incubated for 24 hours at 37°C. After 24 hours, crystal violet cell viability assay was used. The data represented the mean  $\pm$  SD, n = 6.

### 3.1.2 Effect of DMSO on SH-SY5Y

Dimethyl Sulfoxide (DMSO) solution was used to dissolve drugs and inhibitors. To assess the effect of DMSO on the SH-SY5Y cells, an investigation of different concentrations of DMSO was performed. The cells were plated and incubated in a CO<sub>2</sub> incubator at 37°C, and a different concentration of DMSO was added to the cells and incubated for 24 hours. After 24 hours, MTT cell viability assays and crystal violet assays were undertaken, and the cells were incubated in a CO<sub>2</sub>

incubator at 37 °C with the 0.5 mg/ml MTT solutions for 40 minutes. Following solubilisation, the absorbance values were then recorded. The curve of the relationship between DMSO concentrations and SH-SY5Y cell viability (%) is shown in (Figure 3-3). From these results, the total concentration of DMSO in all further experiments was kept at less than 0.2% v/v to minimise the effects of DMSO-induced cell death.

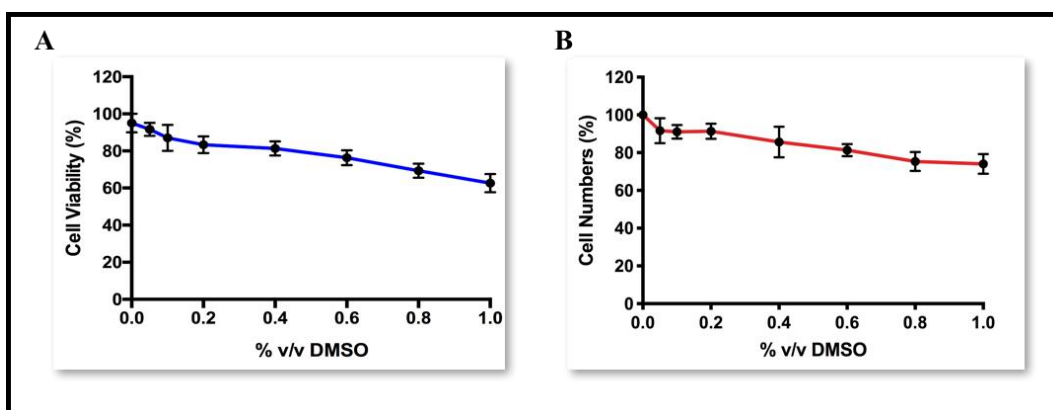


Figure 3-2: The effect of DMSO on SH-SY5Y cells.

Cells were plated in 6-well plates at a density of  $4 \times 10^4$  per well for 24 hours. Then different amounts of DMSO 0-1% were added to 1 ml of cells per well and incubated for 24 hours at 37°C. (A) Cell viability was measured by using MTT assay. The data represented the mean  $\pm$  SD, n = 6, repeated 3 times. (B) After 24 hours, crystal violet cell viability assay was used. The data represented the mean  $\pm$  SD, n = 6.

### **3.1.3 The Effect on Cell Viability of FGAs on SH-SY5Y and COS7 Cell Lines, Using MTT**

The effect of FGAs on SH-SY5Y and COS7 cells was investigated by using different concentrations of the drugs dissolved in DMSO. The cells were plated and incubated at 37°C in a CO<sub>2</sub> incubator for 24 hours. After 24 hours, cells were treated with a range of different concentrations of the drugs for 24 hours. MTT assays were performed, and absorbance values were recorded. The relationships between drug concentration (µM) and cell viability (%) are shown in (Figure 3-4). Chlorpromazine and trifluoperazine have similar LC<sub>50</sub> values for both SH-SY5Y cells and COS7 cells. In addition, it appears that SH-SY5Y cells are more sensitive to cell death by FGAs than are COS7 cells by MTT assay.

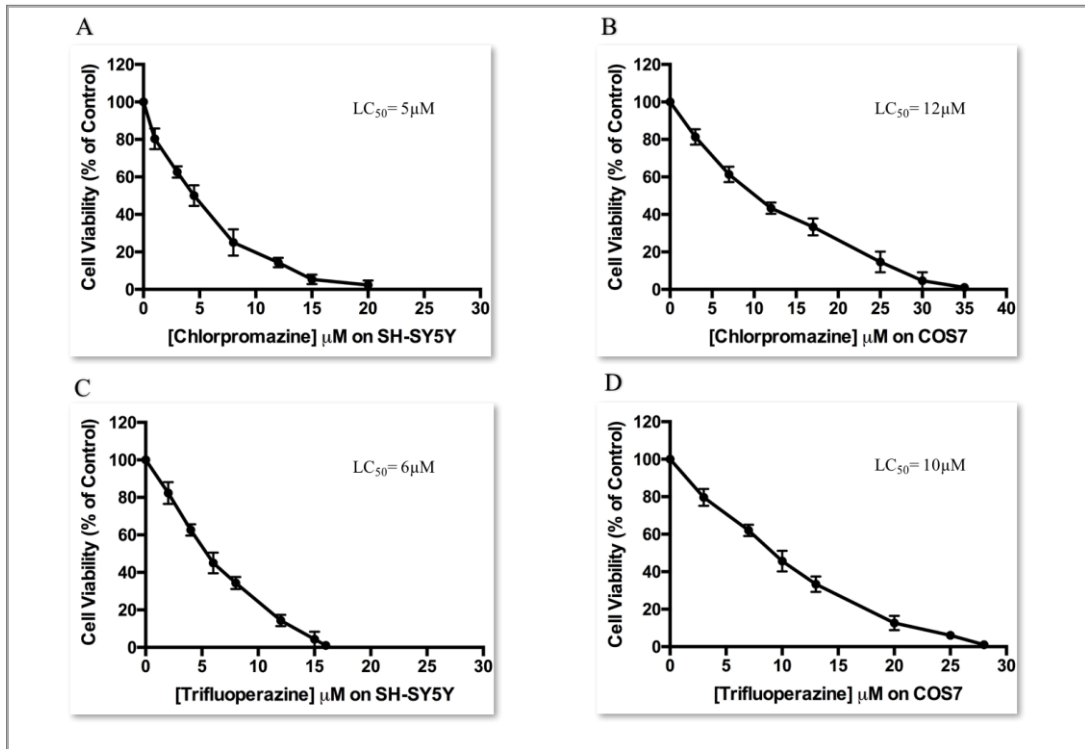


Figure 3-3: Dose-dependent effect on cell viability of different concentrations of FGAs on SH-SY5Y and COS7 cells, using MTT assay.

Cells were plated at a density of  $4 \times 10^4$  cells per well for SH-SY5Y and  $2 \times 10^5$  cells per well for COS7 and incubated for 24 hours at 37°C. Cells were then treated with different concentrations of the FGAs (chlorpromazine and trifluoperazine) for 24 hours at 37°C. After 24 hours, cell viability was measured using the MTT assay. The data represented the mean  $\pm$  SD, n = 6, repeated 3 times.

### **3.1.4 The Effect on Cell Viability of FGAs on SH-SY5Y and COS7 Cell Lines Using the Crystal Violet Assay**

The effect of FGAs on SH-SY5Y and COS7 cells was investigated using different concentrations of the drugs dissolved in DMSO. The cells were plated and incubated at 37°C in a CO<sub>2</sub> incubator with different concentrations of the drugs. Crystal violet assay was applied, and the absorbance values were recorded. The relationships between drug concentration (µM) and cell viability (%) are shown in (Figure 3-5). The crystal violet results showed very similar LC<sub>50</sub> value for these drugs are to the results gained by the MTT method. This method also indicated that SH-SY5Y cells are more sensitive than COS7 cells to FGAs.

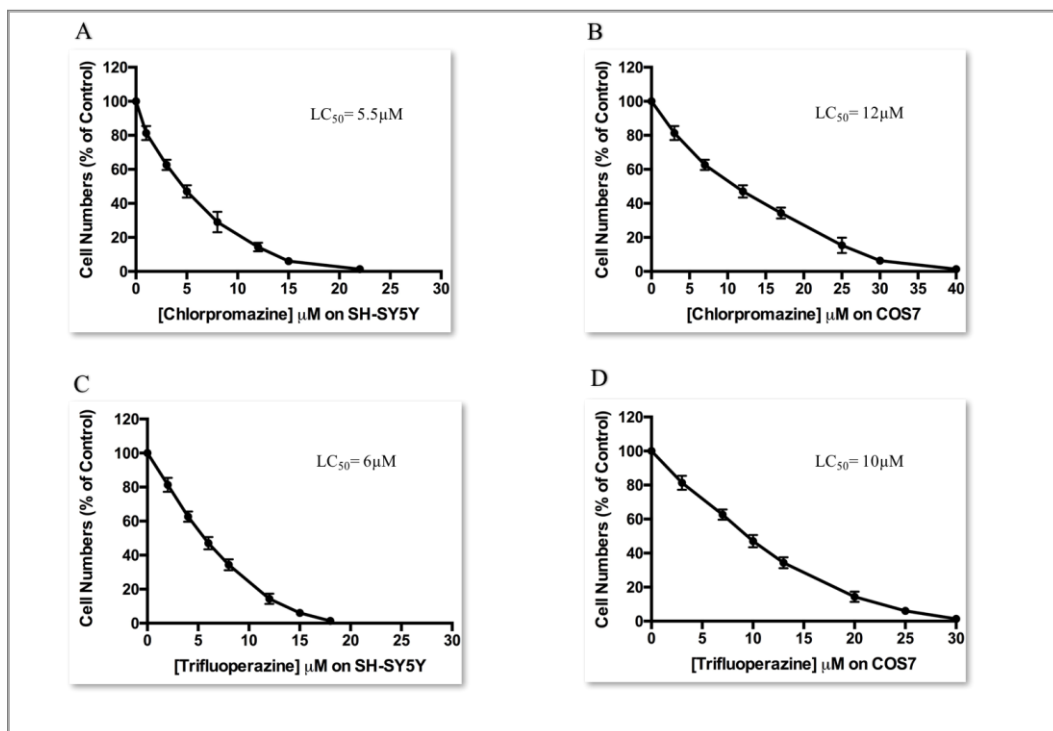


Figure 3-4: Dose-dependent effect on cell viability of different concentration of FGAs on SH-SY5Y and COS7 using the crystal violet assay.

Cells were plated at a density of  $4 \times 10^4$  cells per well for SH-SY5Y and  $2 \times 10^5$  cells per well for COS7 and incubated for 24 hours at  $37^\circ\text{C}$ . Cells were then treated with different concentrations of the FGAs (chlorpromazine and trifluoperazine) for 24 hours at  $37^\circ\text{C}$ . After 24 hours, cell viability was measured using the crystal violet assay. The data represented the mean  $\pm$  SD,  $n = 6$ , repeated 3 times.

### **3.1.5 The Effect on Cell Viability of SGAs on SH-SY5Y and COS7 Cell**

#### **Lines Using the MTT Assay**

The effect of SGAs on SH-SY5Y and COS7 cells was investigated by using different concentrations of the drugs dissolved in DMSO. The cells were plated and incubated at 37°C in a CO<sub>2</sub> incubator with different concentrations of the drugs. MTT assay was used, and the absorbance values were recorded. The relationships between drug concentration (µM) and cell viability (%) are shown in (Figure 3-6). SGAs are less toxic and cause less cell death than FGAs. However, the LC<sub>50</sub> values for SH-SY5Y cells were lower than for COS7 for the MTT method. This result again indicates that neuronal cells are more sensitive to antipsychotic drugs compared to non-neuronal cells.

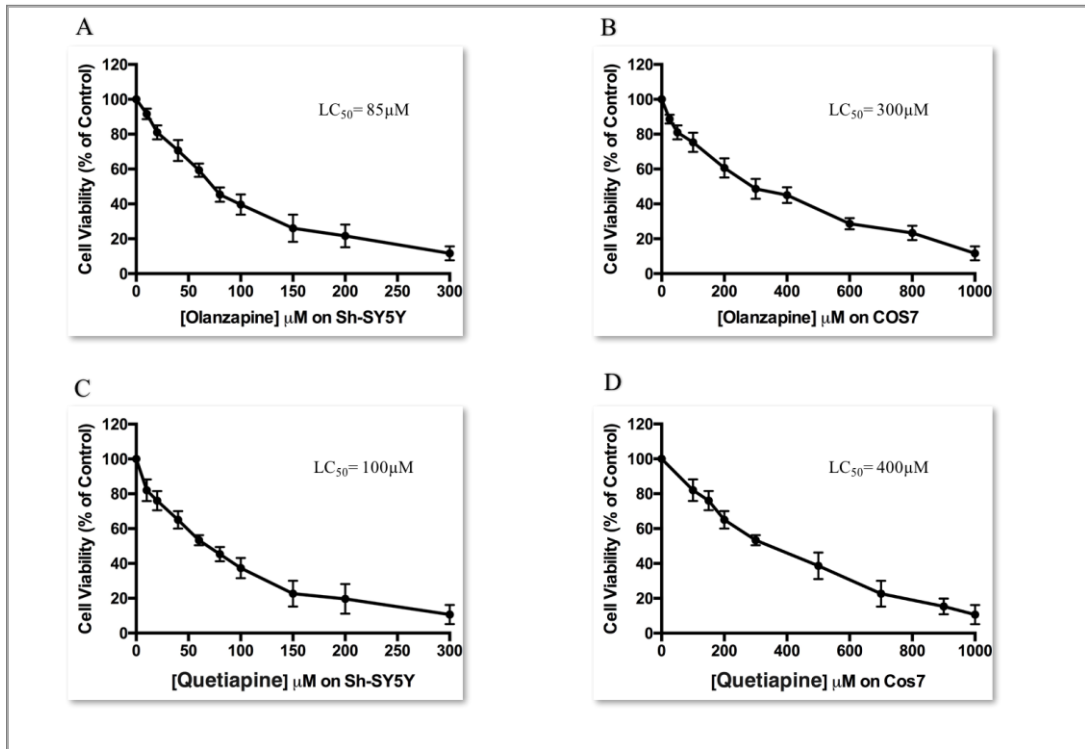


Figure 3-5: Dose-dependent effect on cell viability of different concentrations of SGAs on SH-SY5Y and COS7, using the MTT assay.

Cells were plated at a density of  $4 \times 10^4$  cells per well for SH-SY5Y and  $2 \times 10^5$  cells per well for COS7 and incubated for 24 hours at 37°C. Cells were then treated with different concentrations of the SGAs (olanzapine and quetiapine) for 24 hours at 37°C. After 24 hours, cell viability was measured using MTT assay. The data represented the mean  $\pm$  SD, n = 6, repeated 3 times.

### **3.1.6 The Effect on Cell Viability of SGAs on SH-SY5Y and COS7 Cell**

#### **Lines Using Crystal Violet Assay**

The effect of SGAs on SH-SY5Y and COS7 cells was investigated by using different concentrations of the drugs dissolved in DMSO. The cells were plated and incubated at 37°C in a CO<sub>2</sub> incubator with different concentrations of the drugs. Crystal violet assays were undertaken, and the absorbance values were recorded. The relationships between drug concentration (µM) and cell viability (%) are shown in (Figure 3-7). Similar results for LC<sub>50</sub> values were determined using crystal violet assay and to those from MTT assay.

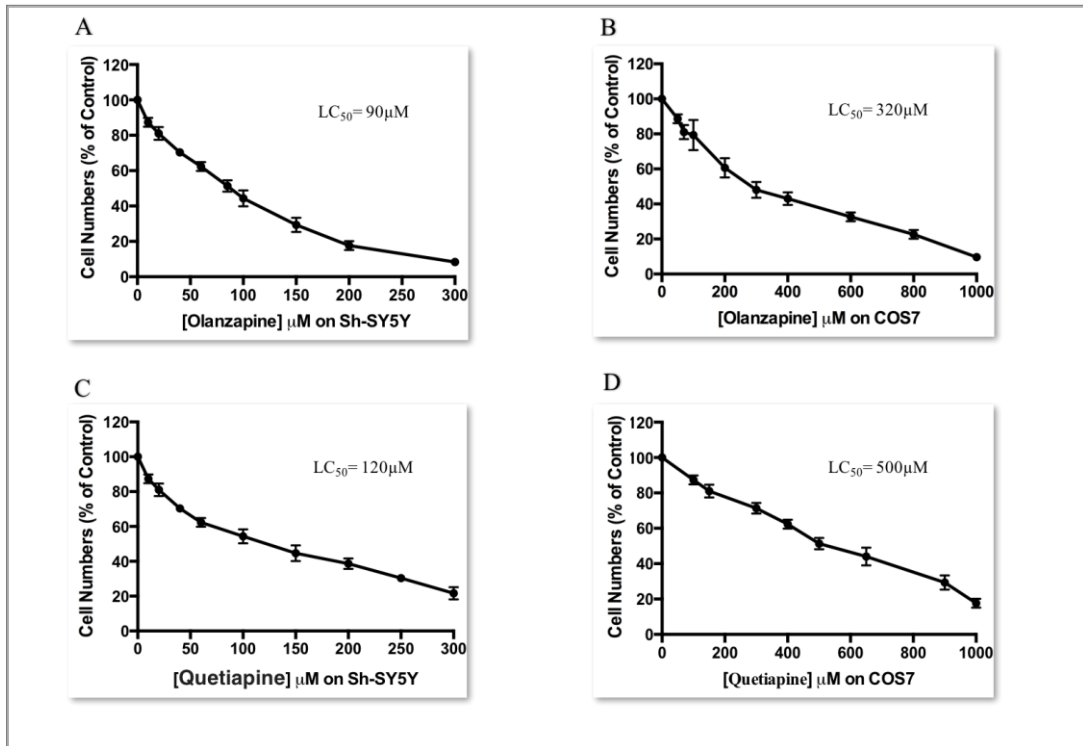


Figure 3-6: Dose-dependent effect on cell viability of different concentrations of SGAs on SH-SY5Y and COS7, using the crystal violet assay.

Cells were plated at density of  $4 \times 10^4$  cells per well for SH-SY5Y and  $2 \times 10^5$  cells per well for COS7 and incubated for 24 hours at 37°C. Cells were then treated with different concentrations of the SGAs (olanzapine and quetiapine) for 24 hours at 37°C. After 24 hours, cell viability was measured using the crystal violet assay. The data represented the mean  $\pm$  SD, n = 6, repeated 3 times.

### **3.1.7 Detecting Apoptosis**

#### *3.1.7.1 Detecting Apoptosis Using Fluorogenic Caspase-3 Substrate*

To determine whether cell death induced by both FGAs and SGAs occurs through caspase-dependent mechanisms and is therefore apoptosis, caspase-3 fluorogenic substrate (Nuc View 488 caspase-3 substrate) was used. Cells were incubated in a CO<sub>2</sub> incubator at 37°C alone as a control and with the LC<sub>50</sub> for each drug for 24 hours. The next day, before examining the cells under the microscope, 2 μM of caspase-3 substrate was added to the cells and incubated for 2 hours. (Figures 3-8 to Figure 3-11), show the images from the microscope for the control and treated cells under brightfield and fluorescent illumination. Cells were counted, and the percentages of fluorescent cells (i.e. apoptotic cells) were plotted. The results show a significant difference in treated cells compared to control cells. FGAs showed a greater than 60% level of apoptotic cells in both SH-SY5Y cells and COS7 cells at the LC<sub>50</sub> concentration values. However, for the SGAs, only 20–30% of the cells exhibited apoptosis when treated at the LC<sub>50</sub> concentration values. These results would suggest that both FGAs and SGAs induce cell death predominantly by apoptosis, but FGAs to a greater extent than SGAs.

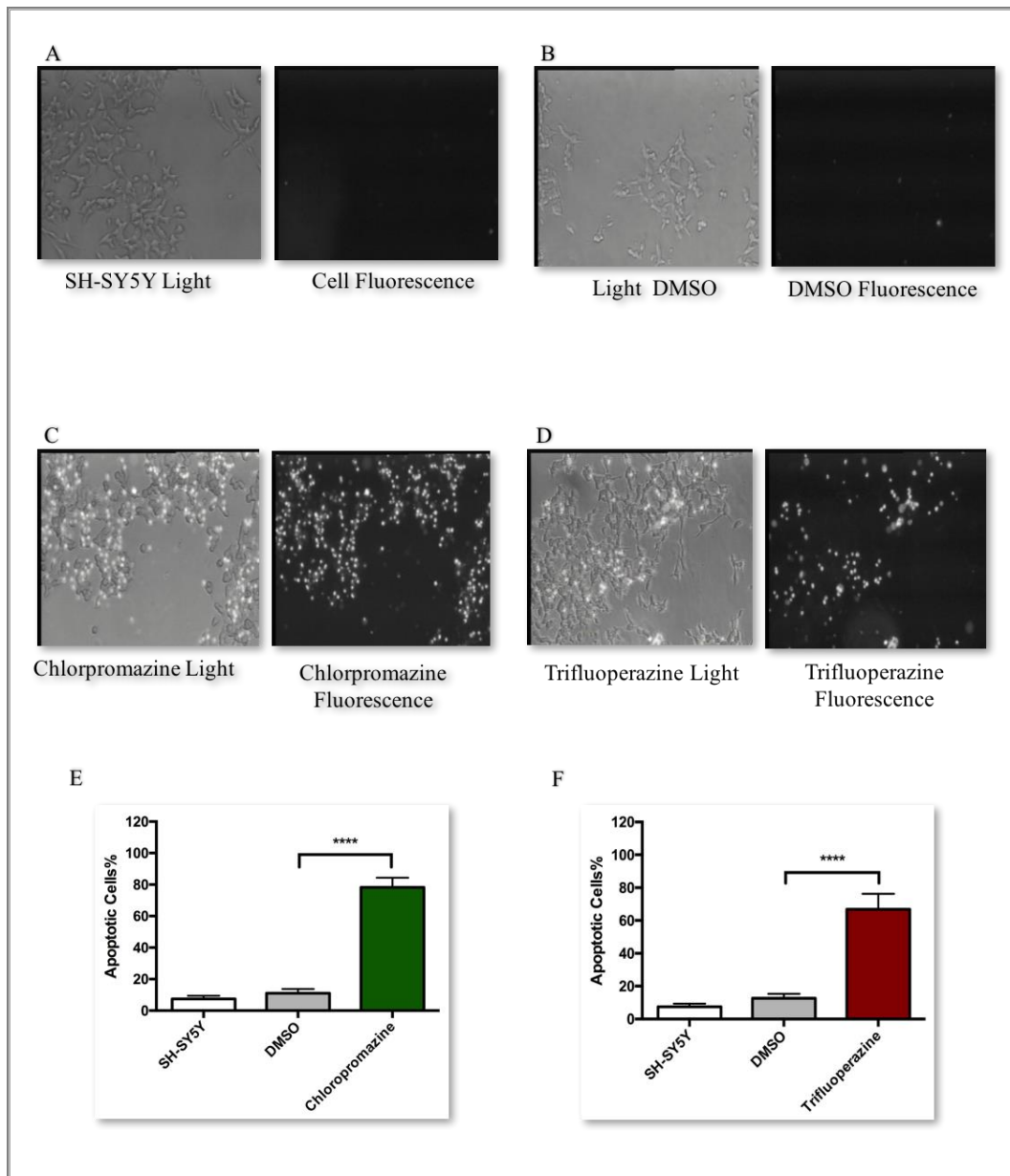


Figure 3-7: The activation of caspase-3 in SH-SY5Y treated with FGAs.

Cells were seeded in sterilised glass bottom dishes and incubated for 24 hours. After 24 hours, cells were treated with the  $LC_{50}$  of the FGAs (chlorpromazine and trifluoperazine) and incubated for 24 hours. Before examination, cells were treated with 2  $\mu$ M of caspase-3 fluorogenic substrate for 1 hour. The figure shows (A) light and fluorescence images for cells alone; (B) light and fluorescence images for cells incubated with DMSO alone; (C)

light and fluorescence images for cells treated with 5  $\mu$ M chlorpromazine; (D) light and fluorescence images for cells treated with 6  $\mu$ M trifluoperazine; (E) the percentage of apoptotic cells when treated with chlorpromazine; (F) the percentage of apoptotic cells when treated with trifluoperazine. The data represented the mean  $\pm$  SD, repeated 3 times. (P value statistically significant at \*\*\*\*P < 0.0001 using two-tailed unpaired t-tests.)

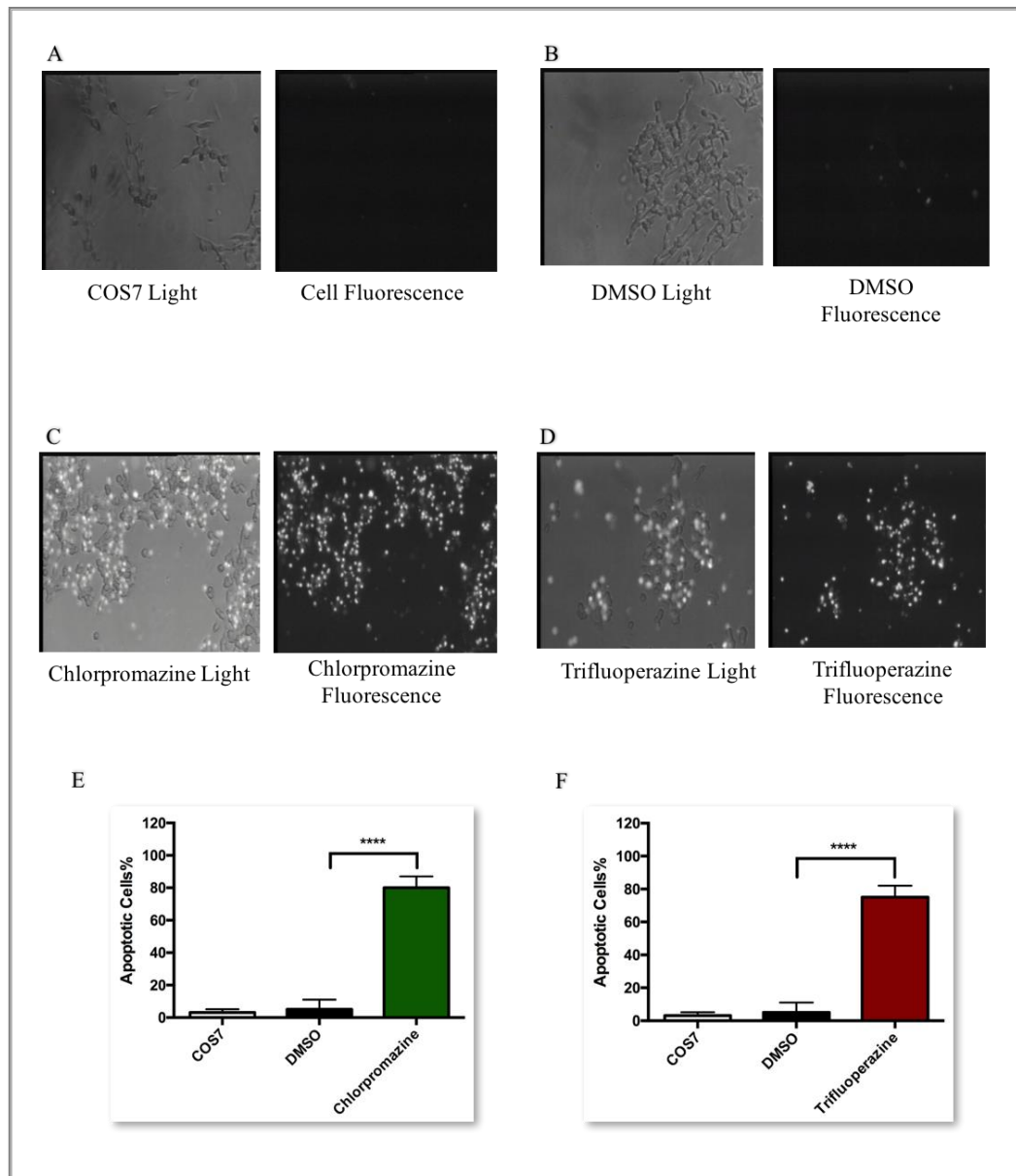


Figure 3-8: The activation of caspase-3 in COS7 treated with FGAs.

Cells were seeded in sterilised glass bottom dishes and incubated for 24 hours. After 24 hours, cells were treated with the LC<sub>50</sub> of each drug and incubated for 24 hours. Before examination, cells were treated with 2 µM of caspase-3 fluorogenic substrate for 1 hour. The figure shows (A) light and fluorescence images for cells alone; (B) light and fluorescence images for cells incubated with DMSO alone; (C) light and fluorescence images for cells treated with 12 µM chlorpromazine; (D) light and fluorescence images for cells treated with 10 µM trifluoperazine; (E) the percentage of apoptotic cells when treated with chlorpromazine; (F) the percentage of apoptotic cells when treated with trifluoperazine. The data represented the mean ± SD, repeated 3 times. (P value statistically significant at \*\*\*\*P < 0.0001 using two-tailed unpaired t-tests.)

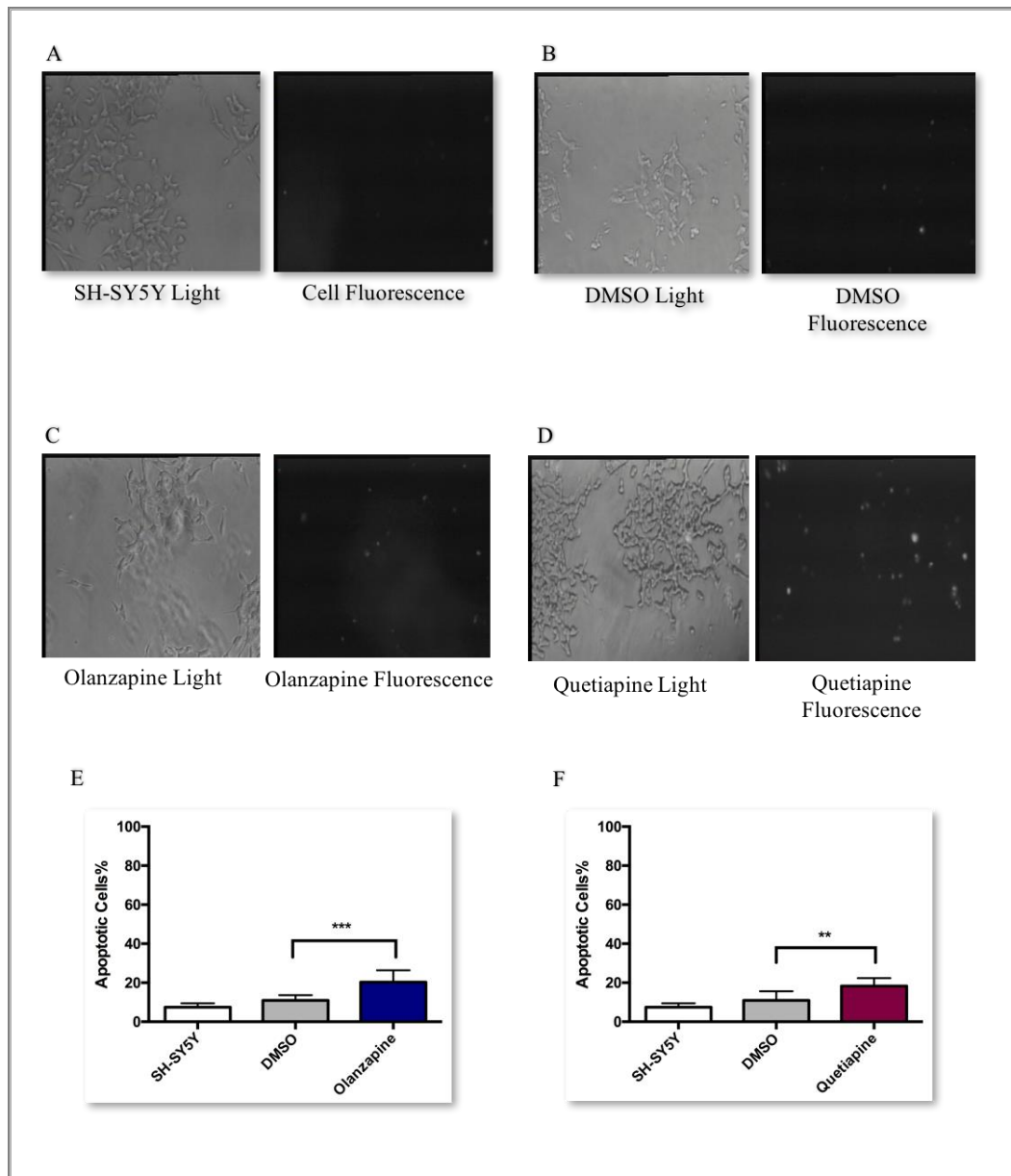


Figure 3-9: The activation of caspase-3 in SH-SY5Y treated with SGAs.

Cells were seeded in sterilised glass bottom dishes and incubated for 24 hours. After 24 hours cells, were treated with the  $LC_{50}$  of each drug and incubated for 24 hours. Before examination, cells were treated with  $2 \mu\text{M}$  of caspase-3 fluorogenic substrate for 1 hour. The figure shows (A) light and fluorescence images for cells alone; (B) light and fluorescence images for cells incubated with DMSO alone; (C) light and fluorescence images for cells treated with  $85 \mu\text{M}$  olanzapine; (D) light and fluorescence images for cells

treated with 100  $\mu$ M quetiapine; (E) the percentage of apoptotic cells when treated with olanzapine; (F) the percentage of apoptotic cells when treated with quetiapine. The data represented the mean  $\pm$  SD, repeated 3 times. (P value statistically significant at \*\* $P \leq 0.01$  and \*\*\*  $P \leq 0.001$  using two-tailed unpaired t-tests.)

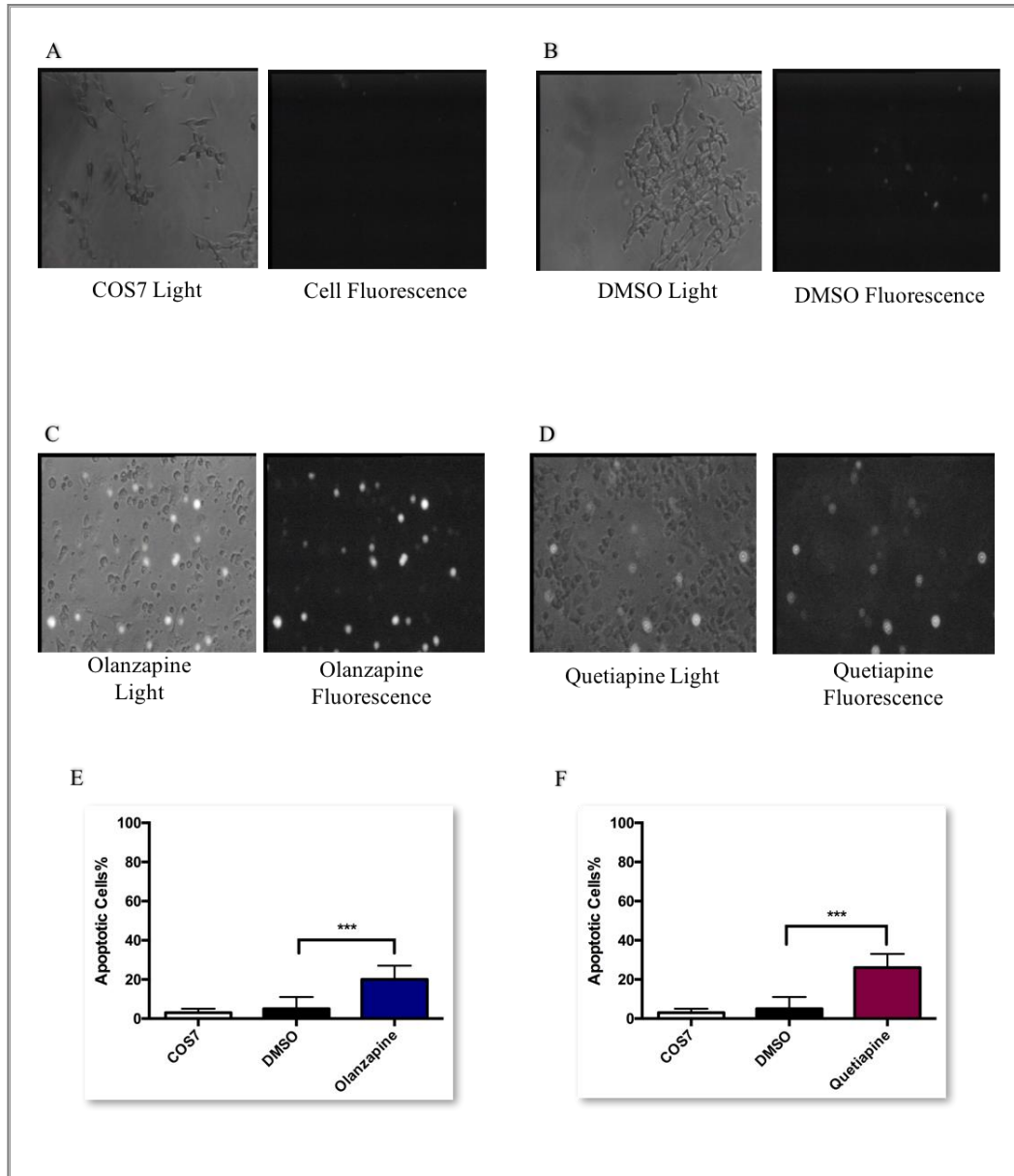


Figure 3-10: The activation of caspase-3 in COS7 treated with SGAs.

Cells were seeded in sterilised glass bottom dishes and incubated for 24 hours. After 24 hours, cells were treated with the  $LC_{50}$  of each drug and incubated for 24 hours. Before

examination, cells were treated with 2  $\mu$ M of caspase-3 fluorogenic substrate for 1 hour. The figure shows (A) light and fluorescence images for cells alone; (B) light and fluorescence images for cells incubated with DMSO alone; (C) light and fluorescence images for cells treated with 300  $\mu$ M olanzapine; (D) light and fluorescence images for cells treated with 400  $\mu$ M quetiapine; (E) the percentage of apoptotic cells when treated with olanzapine; (F) the percentage of apoptotic cells when treated with quetiapine. The data represent the mean  $\pm$  SD repeated 3 times. (P value statistically significant at \*\*\* $P \leq 0.001$  using two-tailed unpaired t-tests).

### *3.1.7.2 The Effect of Caspase-3 Inhibitor on Cells Treated with FGAs*

To investigate further whether cell death induced by FGAs occurred through a caspase-dependent mechanism, caspase-3 inhibitor was also used to see if the inhibitor could protect against drug-induced cell death. (Figure 3-12) shows cell viability assays using MTT and crystal violet on SH-SY5Y cells incubated with 50  $\mu$ M of caspase-3 inhibitor for 4 hours then treated with the  $LC_{50}$  for the FGAs for 24 hours. The results showed that the inhibition of caspase-3 significantly increased the cell viability of SH-SY5Y compared to cells treated with drugs alone. (Figure 3-13) shows the cell viability using both MTT and crystal violet on COS7 cells incubated with 50  $\mu$ M of caspase-3 inhibitor [the concentration was used according to the previous study by Al-Mousa et al., (2012)] for 4 hours then treated with the  $LC_{50}$  for the FGAs for 24 hours. The results also showed a significant increase in cell viability in samples treated with the drugs after the inhibition of caspase-3.

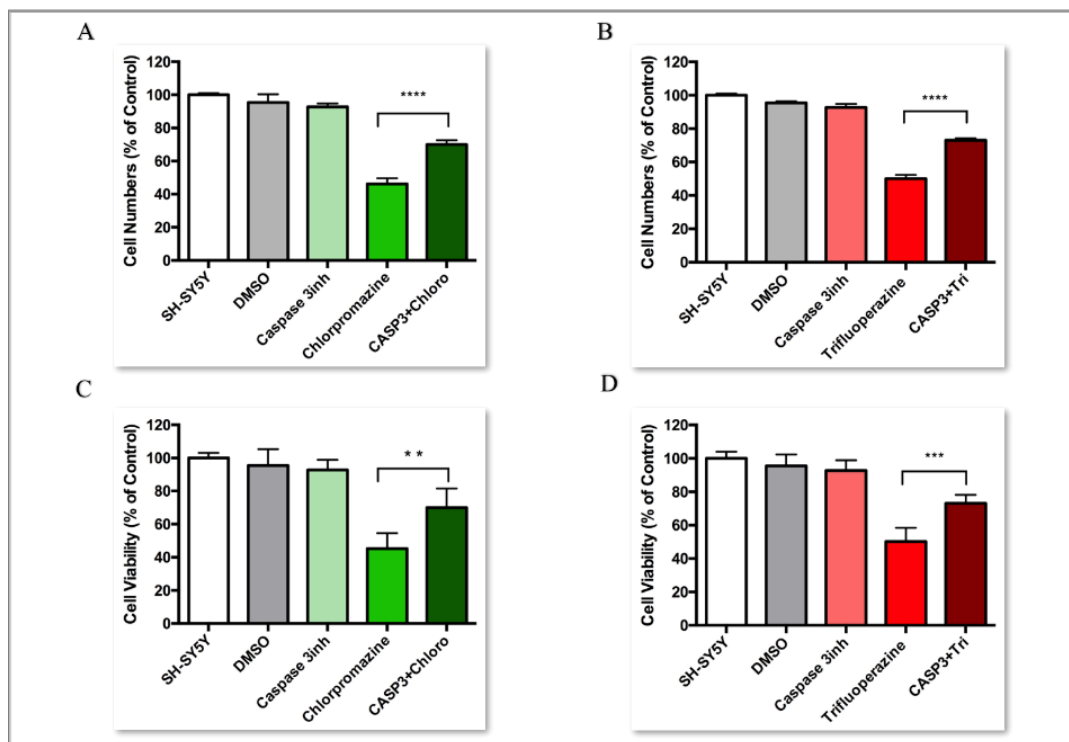


Figure 3-11: The effect of caspase-3 inhibitor in SH-SY5Y treated with FGAs.

SH-SY5Y cells were plated in a 24-well cell culture plate at a density of  $4 \times 10^4$  per well for 24 hours. After 24 hours, cells were incubated with 50  $\mu\text{M}$  caspase-3 inhibitor for 4 hours inside the incubator at  $37^\circ\text{C}$ , then treated with the  $\text{LC}_{50}$  of the FGAs for 24 hours. After 24 hours, cell viability was measured by using MTT and crystal violet assays. The figure shows (A) crystal violet assay of SH-SY5Y with 5  $\mu\text{M}$  chlorpromazine; (B) crystal violet assay of SH-SY5Y with 6  $\mu\text{M}$  trifluoperazine; (C) MTT assay of SH-SY5Y with 5  $\mu\text{M}$  chlorpromazine; (D) MTT assay of SH-SY5Y with 6  $\mu\text{M}$  trifluoperazine. The results are presented as % to the control (non-treated SH-SY5Y cells) of mean  $\pm$  SD and  $n = 6$ , repeated 3 times. (P value statistically significant at  $*P \leq 0.05$ ,  $**P \leq 0.01$ ,  $***P \leq 0.001$ ,  $****P < 0.0001$  using two-tailed unpaired t-tests).

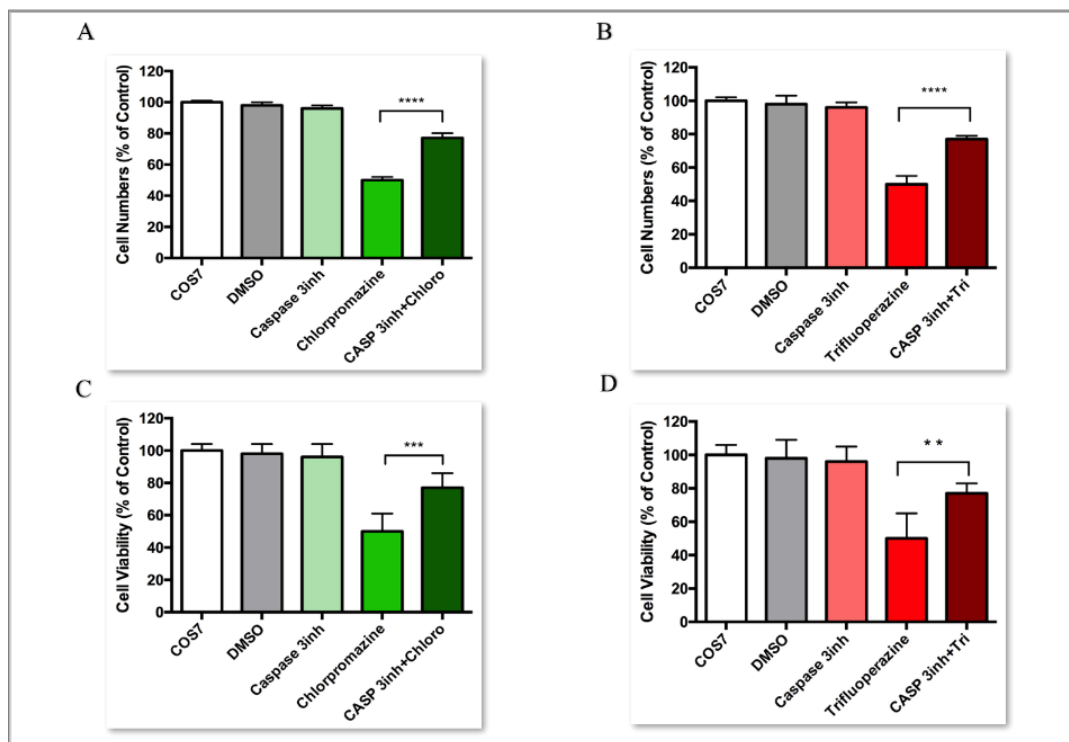


Figure 3-12: The effect of caspase-3 inhibitor in COS7 treated with FGAs.

COS7 cells were plated in a 24-well cell culture plate at a density of  $2 \times 10^5$  per well for 24 hours. After 24 hours, cells were incubated with 50  $\mu\text{M}$  caspase-3 inhibitor for 4 hours inside the incubator at  $37^\circ\text{C}$  then treated with the  $\text{LC}_{50}$  of the FGAs for 24 hours. After 24 hours, cell viability was measured using MTT and crystal violet assays. The figure shows (A) crystal violet assay of COS7 with 12  $\mu\text{M}$  chlorpromazine; (B) crystal violet assay of SH-SY5Y with 10  $\mu\text{M}$  trifluoperazine; (C) MTT assay of COS7 with 12  $\mu\text{M}$  chlorpromazine; (D) MTT assay of SH-SY5Y with 10  $\mu\text{M}$  trifluoperazine. The results are presented as % to the control (non-treated COS7 cells) of mean  $\pm$  SD and  $n = 6$ , repeated 3 times. P value statistically significant at \*\* $P \leq 0.01$ , \*\*\* $P \leq 0.001$ , \*\*\*\* $P < 0.0001$  using two-tailed unpaired t-tests.

### *3.1.7.3 The Effect of Caspase-3 Inhibitor on Cells Treated with SGAs*

These experiments used the caspase-3 inhibitor to confirm whether cell death induced by SGAs is through apoptosis. (Figure-14) shows the results of the MTT and crystal violet absorbance of SH-SY5Y cells incubated with 50  $\mu$ M of caspase-3 inhibitor for 4 hours then treated with the  $LC_{50}$  for the SGAs for 24 hours. The results showed that the inhibition of caspase-3 modestly but significantly increased the cell viability of SH-SY5Y compared to cells treated with drugs alone. (Figure-15) shows the MTT and crystal violet absorbance results of COS7 cells incubated with 50  $\mu$ M caspase-3 inhibitor for 4 hours then treated with the  $LC_{50}$  for the SGAs for 24 hours. These results also showed a small but significant increase in cell viability in samples treated with the drugs after the inhibition of caspase-3. These small increases in the presence of caspase-3 inhibitor correspond well with the fact that only 20–30% of the cells treated with the SGAs showed apoptosis.

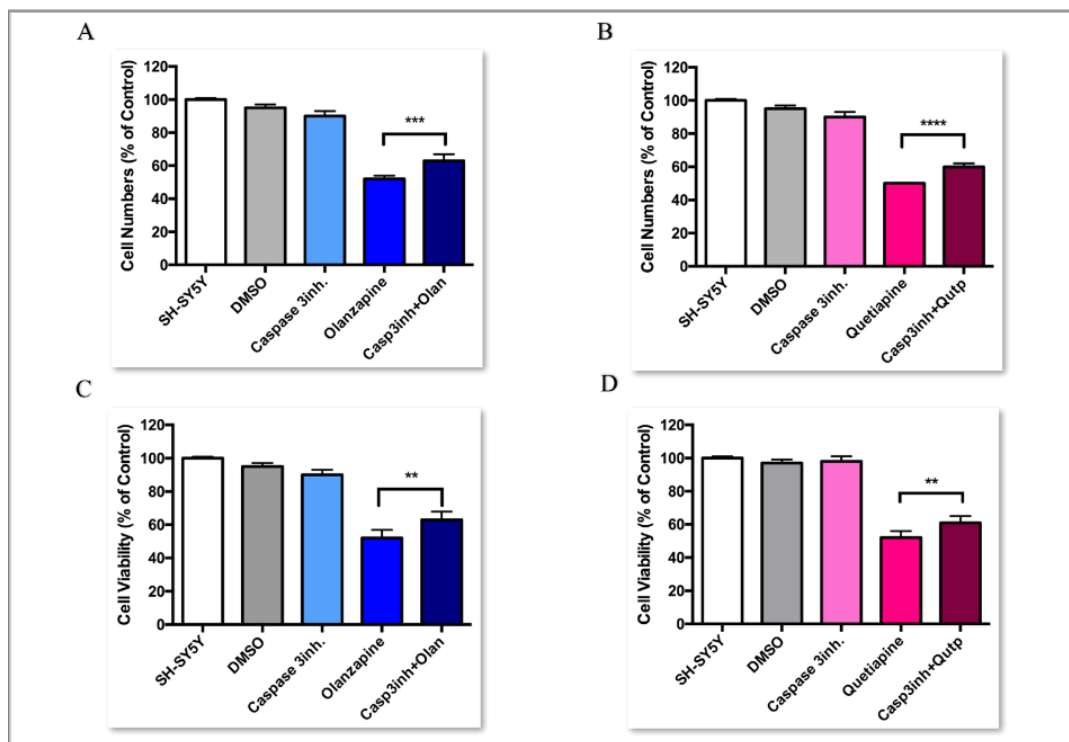


Figure 3-13: The effect of caspase-3 inhibitor on SH-SY5Y cells treated with SGAs.

SH-SY5Y cells were plated in a 24-well cell culture plate at a density of  $4 \times 10^4$  per well for 24 hours. After 24 hours, cells were incubated with 50  $\mu\text{M}$  caspase-3 inhibitor for 4 hours inside the incubator at  $37^\circ\text{C}$  then treated with the  $\text{LC}_{50}$  of the SGAs for 24 hours. After 24 hours, cell viability was measured using MTT and crystal violet assays. The figure shows (A) crystal violet assay of SH-SY5Y with 85  $\mu\text{M}$  olanzapine; (B) crystal violet assay of SH-SY5Y with 120  $\mu\text{M}$  quetiapine; (C) MTT assay of SH-SY5Y with 85  $\mu\text{M}$  olanzapine; (D) MTT assay of SH-SY5Y with 100  $\mu\text{M}$  quetiapine. The results are presented as % to the control (non-treated SH-SY5Y cells) of mean  $\pm$  SD and  $n = 6$ , repeated 3 times. P value statistically significant at  $**P \leq 0.01$ ,  $***P \leq 0.001$ ,  $****P < 0.0001$  using two-tailed unpaired t-tests.

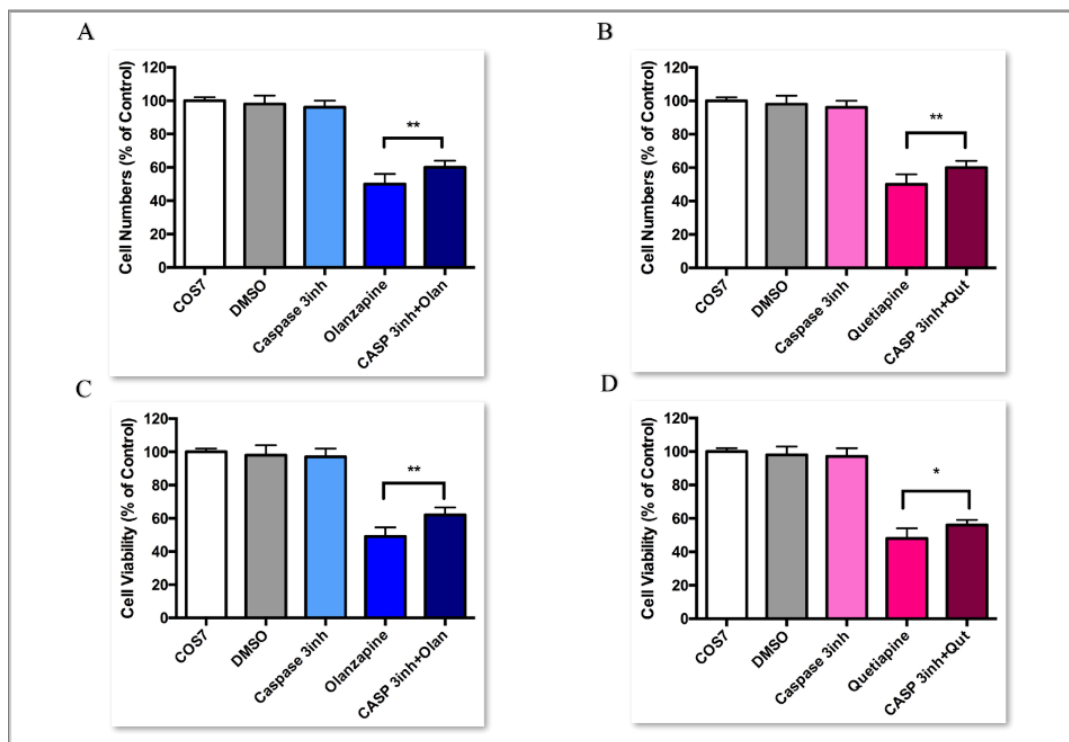


Figure 3-14: The effect of caspase-3 inhibitor on COS7 cells treated with SGAs.

COS7 cells were plated in a 24-well cell culture plate at a density of  $2 \times 10^5$  per well for 24 hours. After 24 hours, cells were incubated with 50  $\mu\text{M}$  caspase-3 inhibitor for 4 hours inside the incubator at  $37^\circ\text{C}$  then treated with the  $\text{LC}_{50}$  of the SGAs for 24 hours. After 24 hours, cell viability was measured using MTT and crystal violet assays. The figure shows (A) crystal violet assay of COS7 cells with 320  $\mu\text{M}$  olanzapine; (B) crystal violet assay of COS7 cells with 500  $\mu\text{M}$  quetiapine; (C) MTT assay of COS7 cells with 300  $\mu\text{M}$  olanzapine; (D) MTT assay of COS7 cells with 4000  $\mu\text{M}$  quetiapine. The results are presented as % to the control (non-treated COS7 cells) of mean  $\pm$  SD and  $n = 6$ , repeated 3 times. P value statistically significant at  $*P \leq 0.05$ ,  $**P \leq 0.01$  using two-tailed unpaired t-tests.

#### *3.1.7.4 The Effect of Caspase-9 Inhibitor on Cell Viability of SH-SY5Y and COS7 Treated with FGAs*

After confirming the involvement of apoptosis and caspase-3, this study was performed to determine which pathway (intrinsic or extrinsic) of the mechanism of apoptosis is involved. For the intrinsic pathway, caspase-9 inhibitor was used. Cells were pre-treated for 4 hours with 50  $\mu$ M of caspase-9 inhibitor then with the LC<sub>50</sub> for each drug for 24 hours. As shown in (Figure 3-16) and (Figure 3-17), the inhibition of caspase-9 produced no significant protection for the cells treated with the FGAs.

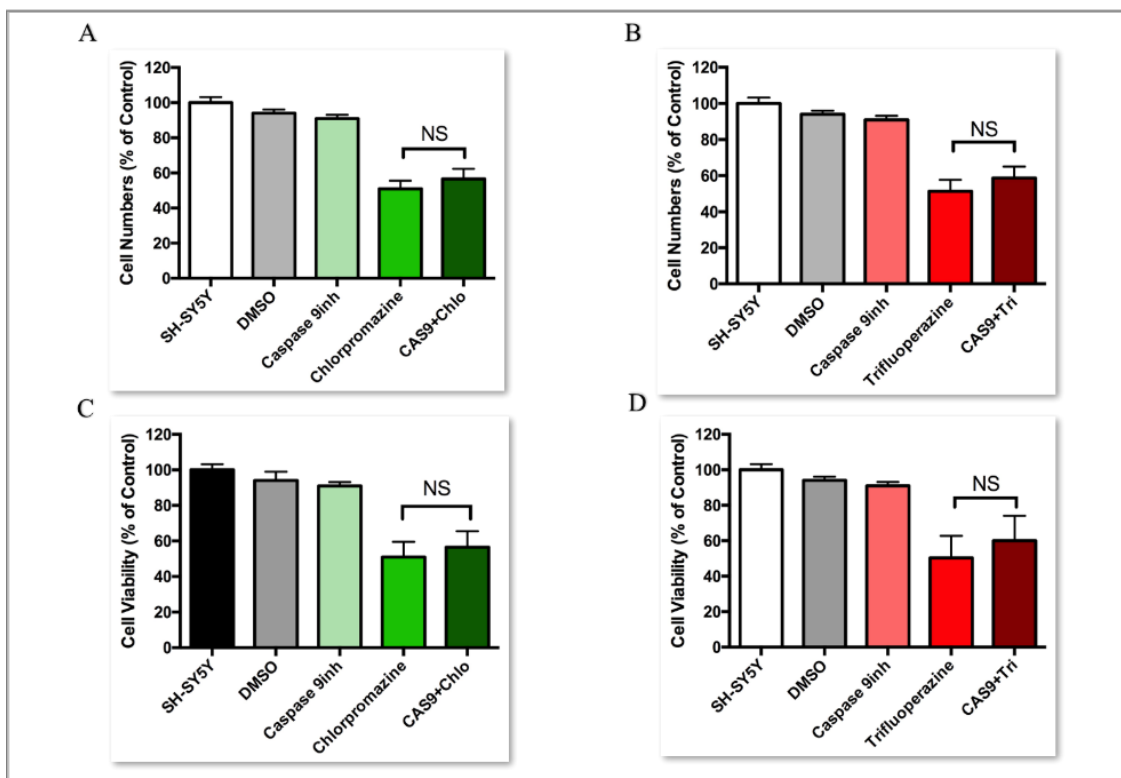


Figure 3-15: The effect of caspase-9 inhibitor on SH-SY5Y treated with FGAs.

SH-SY5Y cells were plated in a 24-well cell culture plate at a density of  $4 \times 10^4$  per well for 24 hours. After 24 hours, cells were incubated with 50  $\mu\text{M}$  caspase-9 inhibitor for 4 hours inside the incubator at  $37^\circ\text{C}$  then treated with the  $\text{LC}_{50}$  of the FGAs for 24 hours. After 24 hours, cell viability was measured using both MTT and crystal violet assays. The figure shows (A) crystal violet assay of SH-SY5Y with 5  $\mu\text{M}$  chlorpromazine; (B) crystal violet assay of SH-SY5Y with 6  $\mu\text{M}$  trifluoperazine; (C) MTT assay of SH-SY5Y with 5  $\mu\text{M}$  chlorpromazine; (D) MTT assay of SH-SY5Y with 6  $\mu\text{M}$  trifluoperazine. The results are presented as % to the control (non-treated SH-SY5Y cells) of mean  $\pm$  SD and  $n = 6$ , repeated 3 times. T-testing showed no significant protection.

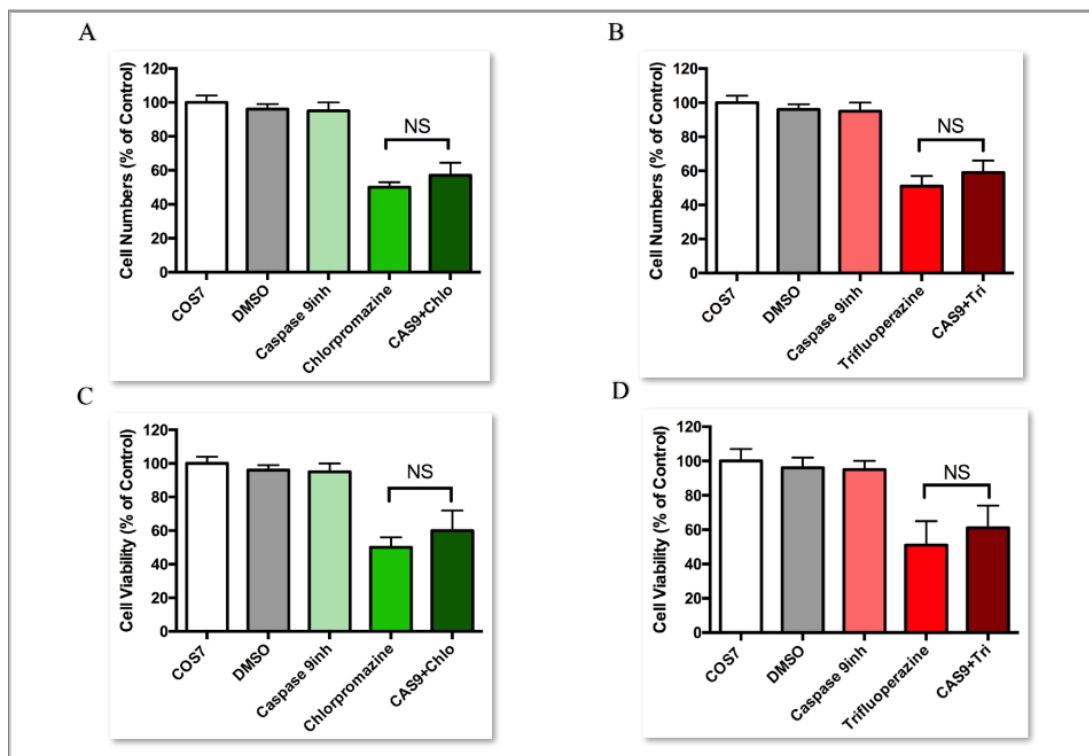


Figure 3-16: The effect of caspase-9 inhibitor on COS7 treated with FGAs.

COS7 cells were plated in a 24-well cell culture plate at a density of  $2 \times 10^5$  per well for 24 hours. After 24 hours, cells were incubated with 50  $\mu\text{M}$  caspase-9 inhibitor for 4 hours inside a  $\text{CO}_2$  incubator at  $37^\circ\text{C}$  then treated with the  $\text{LC}_{50}$  of the FGAs for 24 hours. After 24 hours, cell viability was measured by using MTT and crystal violet assays. The figure shows (A) crystal violet assay of COS7 with 12  $\mu\text{M}$  chlorpromazine; (B) crystal violet assay of SH-SY5Y with 10  $\mu\text{M}$  trifluoperazine; (C) MTT assay of COS7 with 12  $\mu\text{M}$  chlorpromazine; (D) MTT assay of SH-SY5Y with 10  $\mu\text{M}$  trifluoperazine. The results are presented as % to the control (non-treated COS7 cells) of mean  $\pm$  SD and  $n = 6$ , repeated 3 times. T-testing showed no significant protection.

*3.1.7.5 The Effect of Caspase-9 Inhibitor on SH-SY5Y and COS7 Treated with SGAs*

After confirming the modest involvement of caspase-3 in cells treated with SGAs, this study inhibited caspase-9 before treating the cells with drugs to determine if apoptosis had occurred through the extrinsic pathway. Cells were pre-treated for 4 hours with 50  $\mu$ M of caspase-9 inhibitor then incubated with the LC<sub>50</sub> for each drug for 24 hours before cell viability was measured. As shown in (Figure 3-18) (SH-SY5Y) and (Figure 3-19), (COS7), there was a small but significant protection for both cell lines after the inhibition of caspase-9 compared to cells treated with the SGAs alone.

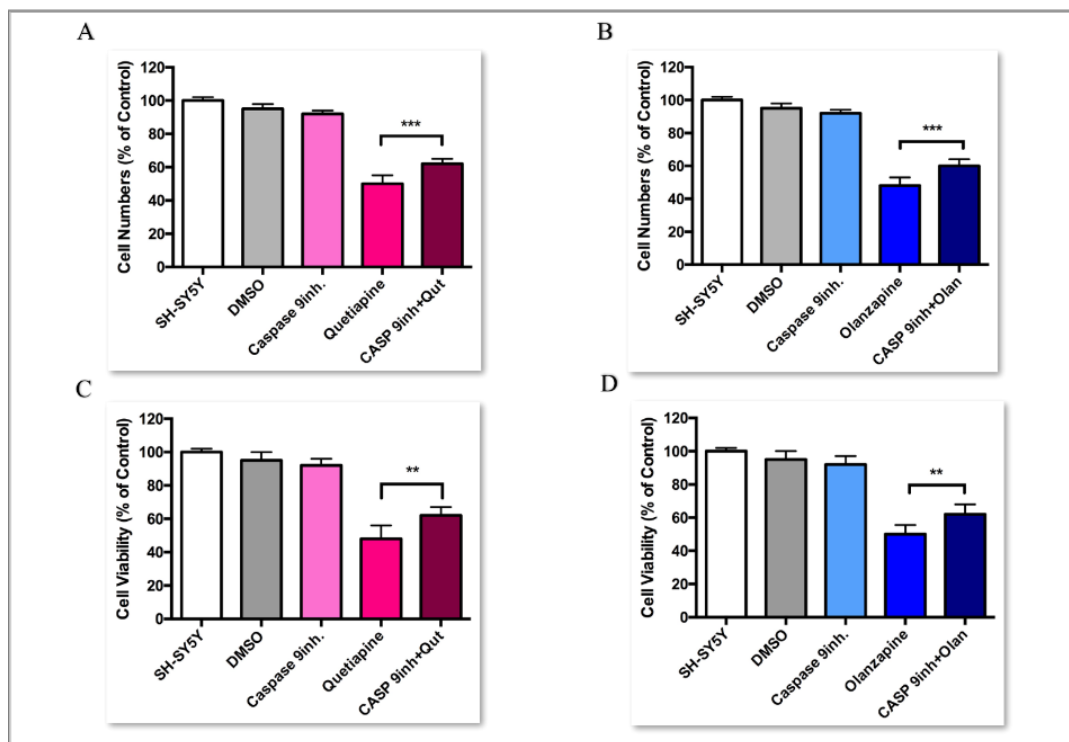


Figure 3-17: The effect of caspase-9 inhibitor on SH-SY5Y cells treated with SGAs.

SH-SY5Y cells were plated in a 24-well cell culture plate at a density of  $4 \times 10^4$  per well for 24 hours. After 24 hours, cells were incubated with 50  $\mu\text{M}$  of caspase-9 inhibitor for 4 hours inside the incubator at  $37^\circ\text{C}$  then treated with the  $\text{LC}_{50}$  of the SGAs for 24 hours. After 24 hours, cell viability was measured using MTT and crystal violet assays. The figure shows (A) crystal violet assay of SH-SY5Y with 120  $\mu\text{M}$  quetiapine; (B) crystal violet assay of SH-SY5Y with 85  $\mu\text{M}$  olanzapine; (C) MTT assay of SH-SY5Y with 100  $\mu\text{M}$  quetiapine; (D) MTT assay of SH-SY5Y with 85  $\mu\text{M}$  olanzapine. The results are presented as % to the control (non-treated SH-SY5Y cells) of mean  $\pm$  SD and  $n = 6$ , repeated 3 times. P value statistically significant at  $**P \leq 0.01$ ,  $***P \leq 0.001$  using two-tailed unpaired t-tests.

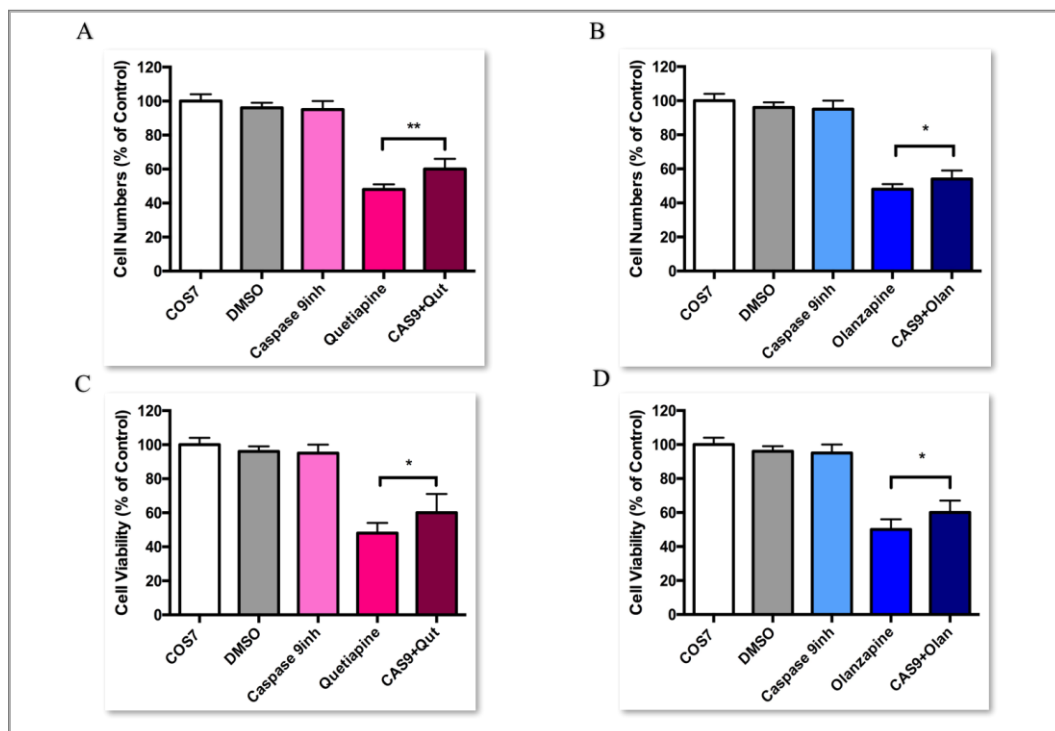


Figure 3-18: The effect of caspase-9 inhibitor on COS7 treated with SGAs.

COS7 cells were plated in a 24-well cell culture plate at a density of  $2 \times 10^5$  per well for 24 hours. After 24 hours, cells were incubated with  $50 \mu\text{M}$  of caspase-9 inhibitor for 4 hours inside the incubator at  $37^\circ\text{C}$  then treated with the  $\text{LC}_{50}$  of the SGAs for 24 hours. After 24 hours, cell viability was measured using MTT and crystal violet assays. The figure shows (A) crystal violet absorbance of COS7 with  $500 \mu\text{M}$  quetiapine; (B) crystal violet absorbance of COS7 with  $320 \mu\text{M}$  olanzapine; (C) MTT absorbance of COS7 with  $4000 \mu\text{M}$  quetiapine; (D) MTT absorbance of COS7 with  $300 \mu\text{M}$  olanzapine. The results are presented as % to the control (non-treated COS7 cells) of mean  $\pm$  SD and  $n = 6$ , repeated 3 times. P value statistically significant at  $*P \leq 0.05$ ,  $**P \leq 0.01$  using two-tailed unpaired t-tests.

### *3.1.7.6 Cytochrome-C Release from Mitochondria*

To confirm the results of the involvement of the activation of caspase-9 during cell death induced by some of the FGAs and SGAs, cytochrome c release from the mitochondria was detected by immunoblotting analysis. Cytochrome c is a pro-apoptotic factor which is released from the mitochondria in the intrinsic pathway (Wang and Youle, 2009). After treating the cells with the LC<sub>50</sub> for each drug for 24 hours, protein extraction from the mitochondrial pellet and cytosol was measured for the presence of cytochrome c, with  $\beta$ -actin as the loading marker. The same amount of protein from each sample was loaded onto the gel followed by immunoblotting analysis with anti-cytochrome C antibody. As seen in (Figure 3-20), and (Figure 3-21), (A) is the membrane image from a Li-Cor Odyssey scanner, and (B) is an analysis of each band (ratio of the band intensity of the sample/the intensity of  $\beta$ -actin). From both cell lines, a high level of cytochrome c was detected in the cytosol after treating the cells with SGAs, but little cytochrome C in the cytosol was detected in the cytosol fraction with FGAs.

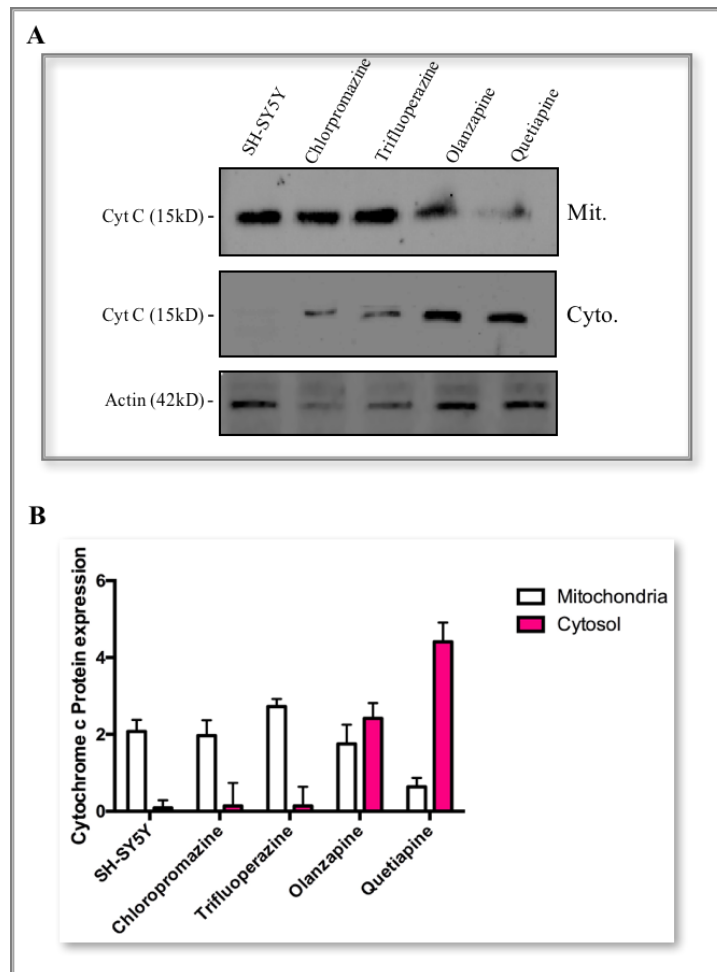


Figure 3-19: Detection of cytochrome c of mitochondria and cytosol extraction from SH-SY5Y treated with FGAs and SGAs.

SH-SY5Y cells were plated in a 6-well plate for 24 hours. After 24 hours, cells were treated with the  $LC_{50}$  for each drug for 24 hours. After trypsinising and homogenising the cells and separating the mitochondrial pellet (Mito) and cytosolic fraction (Cyto), protein concentration was measured. 30  $\mu$ g of each protein sample was loaded onto the gel and run for 1 hour. The gel was then transferred with the membrane and incubated in anti-cytochrome c primary antibody. After incubating the membrane with the secondary antibody, the membrane was imaged using a Li-Cor Odyssey scanner as seen in (A). Bands were normalised to  $\beta$ -actin, and the amount of cytochrome c expression was plotted in graph (B). Experiments were repeated 3 times. Values are mean  $\pm$  SD.

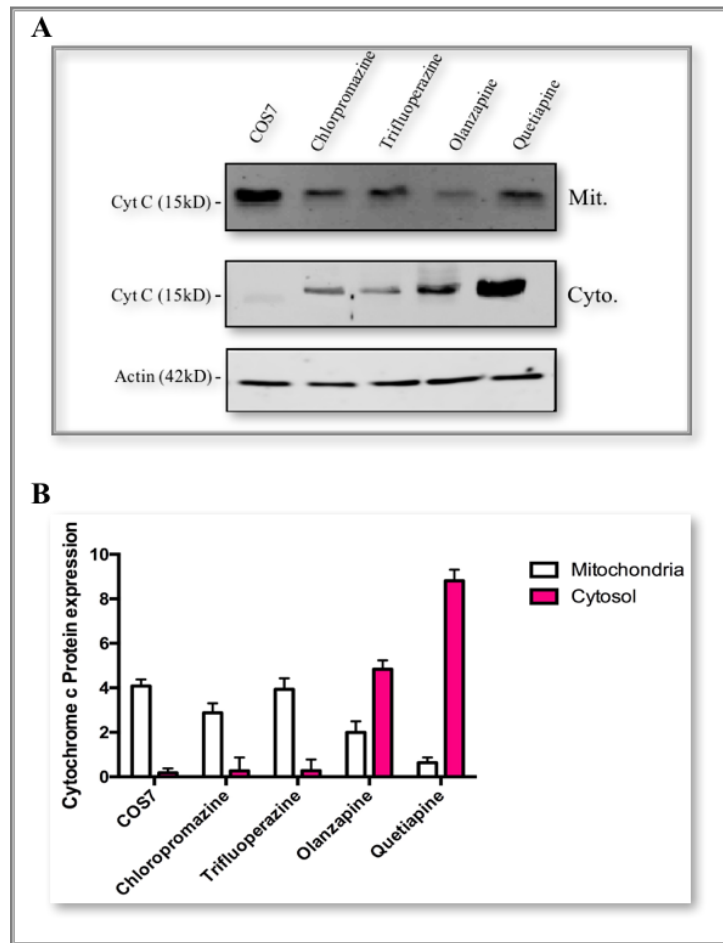


Figure 3-20: Detection of cytochrome c of mitochondria and cytosol extraction from COS7 treated with FGAs and SGAs.

COS7 cells were plated in a 6-well plate for 24 hours. After 24 hours, cells were treated with the  $LC_{50}$  for each drug for 24 hours. After trypsinising the cells and separating the mitochondrial pellet (Mito) and cytosolic fraction (Cyto), protein concentration was measured. 30  $\mu$ g of each protein sample was uploaded to the gel and run for 1 hour. The gel was then transferred to the membrane and incubated in anti-cytochrome c primary antibody. After incubating the membrane with the secondary antibody, it was imaged using a Li-Cor Odyssey scanner as seen in (A). Bands were normalised to  $\beta$ -actin, and the amount of cytochrome c expression was plotted in graph (B). Experiments were repeated 3 times. Values are mean  $\pm$  SD.

### 3.1.7.7 The Effect of Caspase-8 Inhibitor on SH-SY5Y and COS7 Treated with FGAs

After confirming that cell death induced by the FGAs has not occurred via the intrinsic pathway, caspase-8 inhibitor was used, since caspase-8 is activated during the extrinsic pathway of apoptosis. Cells were pre-treated for 4 hours with 50  $\mu$ M of caspase-8 inhibitor, then incubated with the LC<sub>50</sub> for each drug for 24 hours before cell viability assays were performed. As shown in (Figure 3-22) and (Figure 3-23), there was significant protection in both cell lines after inhibition of caspase-8 compared to cells treated with the FGAs alone. The protection in most cases was approaching the cell viability levels seen in the absence of the FGAs, thus indicating that cell death was largely reduced by caspase-8 inhibitor.

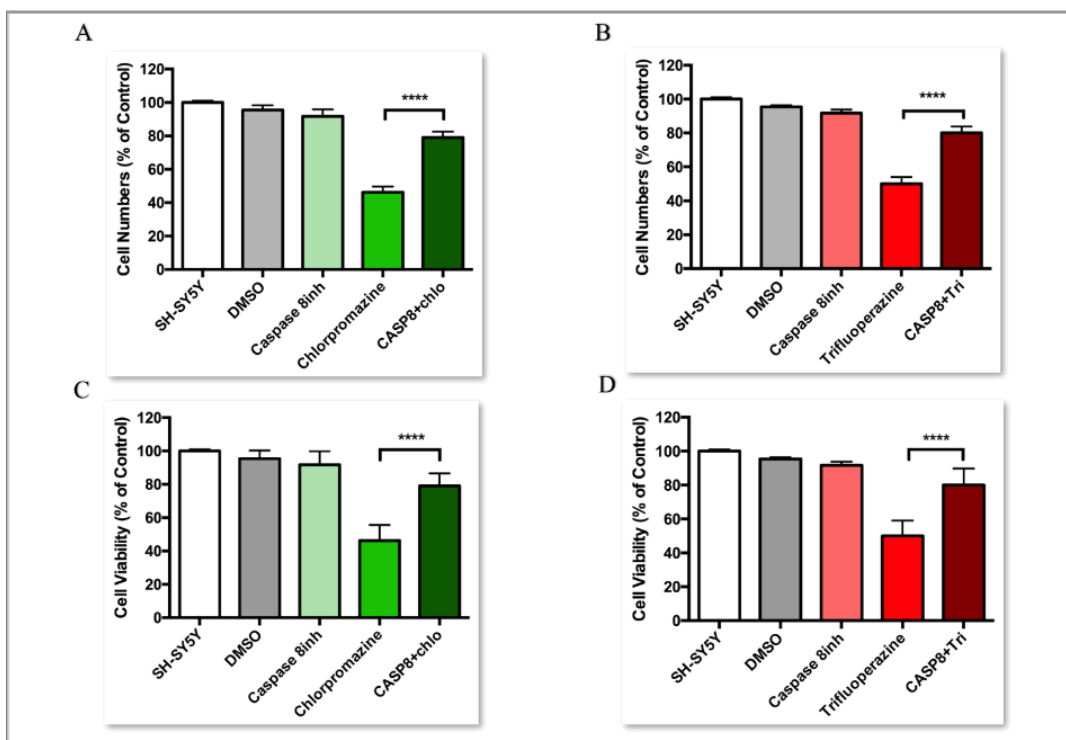


Figure 3-21: The effect of caspase-8 inhibitor on SH-SY5Y treated with FGAs.

SH-SY5Y cells were plated in a 24-well cell culture plate at a density of  $4 \times 10^4$  per well for 24 hours. After 24 hours, cells were incubated with  $50 \mu\text{M}$  of caspase-8 inhibitor for 4 hours inside the incubator at  $37^\circ\text{C}$ , then treated with the  $\text{LC}_{50}$  for the FGAs for 24 hours. After 24 hours, cell viability was measured by using MTT and crystal violet assays. The figure shows (A) crystal violet assay of SH-SY5Y with  $5 \mu\text{M}$  chlorpromazine; (B) crystal violet assay of SH-SY5Y with  $6 \mu\text{M}$  trifluoperazine; (C) MTT assay of SH-SY5Y with  $5 \mu\text{M}$  chlorpromazine; (D) MTT assay of SH-SY5Y with  $6 \mu\text{M}$  trifluoperazine. The results are presented as % of the control (non-treated SH-SY5Y cells) of mean  $\pm$  SD and  $n = 6$ , repeated 3 times. P value statistically significant \*\*\*\* $P < 0.0001$  using two-tailed unpaired t-tests.

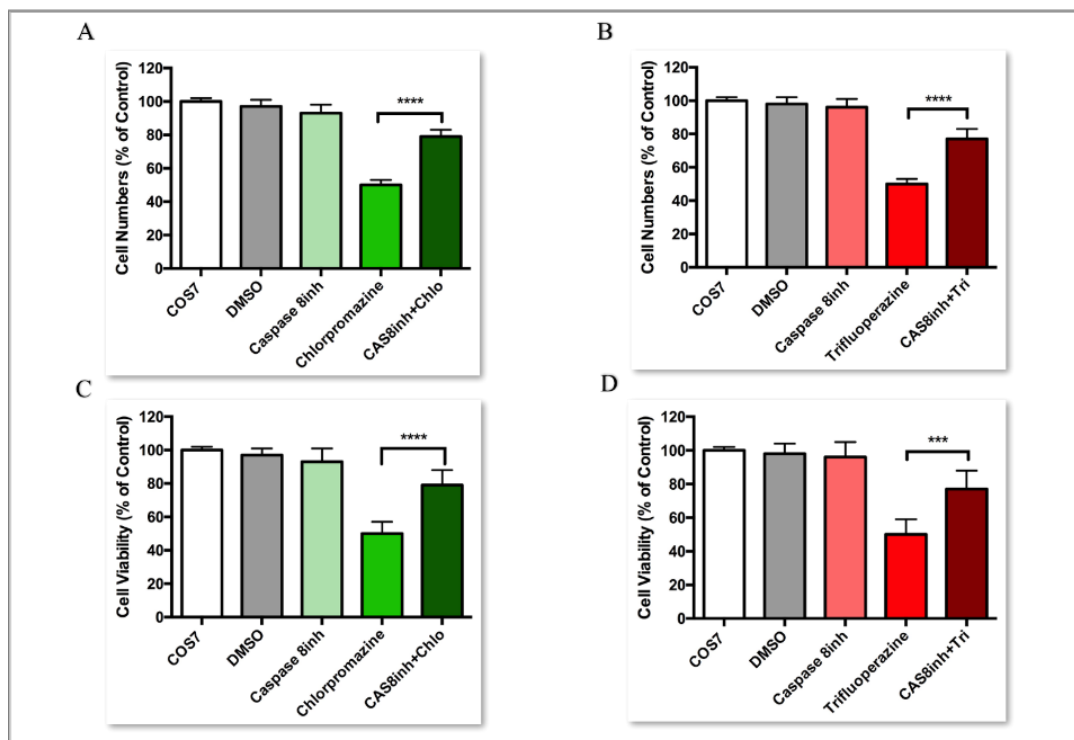


Figure 3-22: The effect of caspase-8 inhibitor on COS7 treated with FGAs.

COS7 cells were plated in a 24-well cell culture plate at a density of  $2 \times 10^5$  per well for 24 hours. After 24 hours, cells were incubated with  $50 \mu\text{M}$  of caspase-8 inhibitor for 4 hours inside the  $\text{CO}_2$  incubator at  $37^\circ\text{C}$ , then treated with the  $\text{LC}_{50}$  for the FGAs for 24 hours. After 24 hours, cell viability was measured using MTT and crystal violet assays. The figure

shows (A) crystal violet assay of COS7 with 12  $\mu$ M chlorpromazine; (B) crystal violet assay of SH-SY5Y with 10  $\mu$ M trifluoperazine; (C) MTT assay of COS7 with 12  $\mu$ M chlorpromazine; (D) MTT assay of SH-SY5Y with 10  $\mu$ M trifluoperazine. The results presented as % of the control (non-treated COS7 cells) of mean  $\pm$  SD and n = 6, repeated 3 times. P value statistically significant \*\*\*P $\leq$ 0.001, \*\*\*\*P < 0.0001 using two-tailed unpaired t-test.

#### *3.1.7.8 The Effect of Caspase-8 Inhibitor on SH-SY5Y and COS7 treated with SGAs*

The previous experiments confirmed that the SGAs induced cell death through the intrinsic pathway as there was some protection against cell death when caspase-9 was inhibited. The following experiments were performed to investigate if there is also an activation of the extrinsic pathway by SGAs through caspase-8. Cells were pre-treated for 4 hours with 50  $\mu$ M of caspase-8 inhibitor and then with the LC<sub>50</sub> for each drug for 24 hours before cell viability was measured. As shown in (Figure 3-24) and (Figure 3-25), the inhibition of caspase-8 produced no significant protection of cells treated with SGAs.

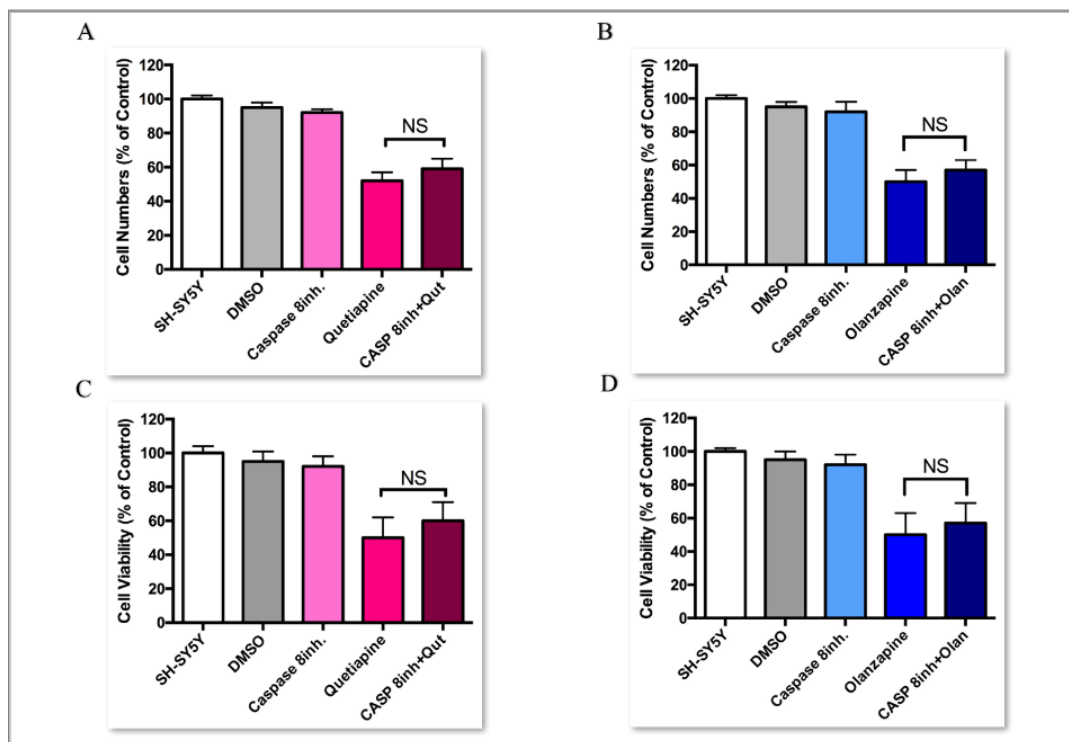


Figure 3-23: The effect of caspase-8 inhibitor on SH-SY5Y treated with SGAs.

SH-SY5Y cells were plated in a 24-well cell culture plate at a density of  $4 \times 10^4$  per well for 24 hours. After 24 hours, cells were incubated with 50  $\mu\text{M}$  of caspase-8 inhibitor for 4 hours inside the  $\text{CO}_2$  incubator at  $37^\circ\text{C}$  then treated with the  $\text{LC}_{50}$  of SGAs for 24 hours. After 24 hours, cell viability was measured using MTT and crystal violet assays. The figure shows (A) crystal violet assay of SH-SY5Y with 120  $\mu\text{M}$  quetiapine; (B) crystal violet assay of SH-SY5Y with 85  $\mu\text{M}$  olanzapine; (C) MTT assay of SH-SY5Y with 100  $\mu\text{M}$  quetiapine; (D) MTT assay of SH-SY5Y with 85  $\mu\text{M}$  olanzapine. The results are presented as % to the control (non-treated SH-SY5Y cells) of mean  $\pm$  SD and  $n = 6$ , repeated 3 times. T-testing showed no significant protection.

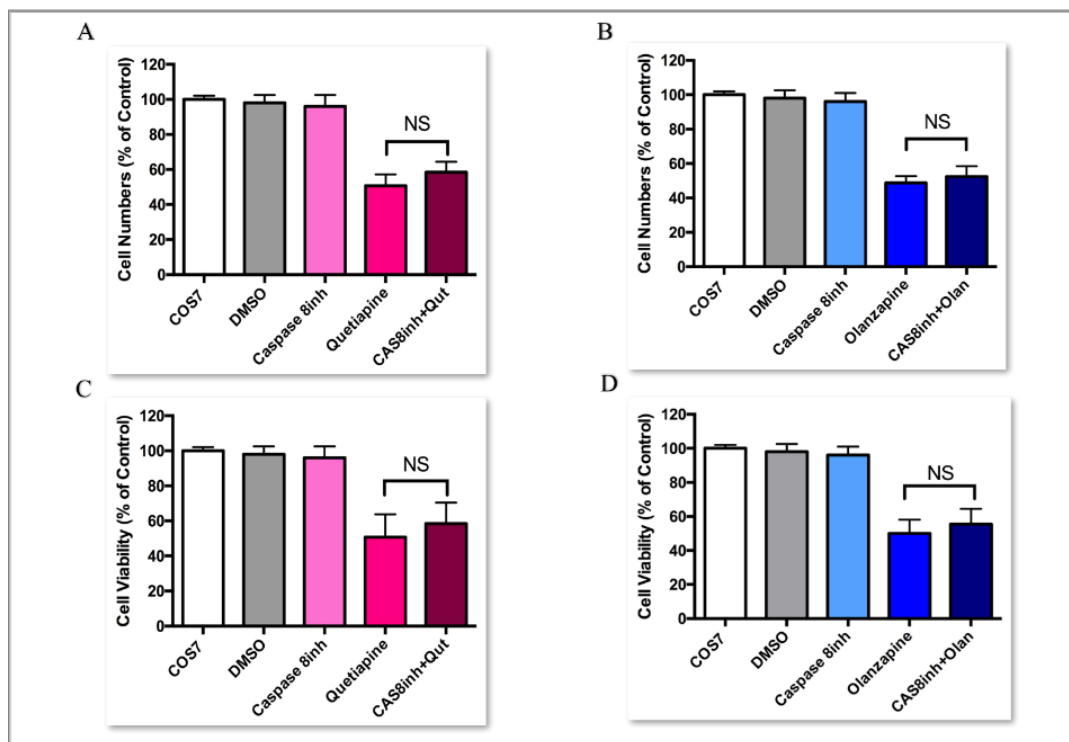


Figure 3-24: The effect of caspase-8 inhibitor on COS7 treated with SGAs.

COS7 cells were plated in a 24-well cell culture plate at a density of  $2 \times 10^5$  per well for 24 hours. After 24 hours, cells were incubated with  $50 \mu\text{M}$  of caspase-8 inhibitor for 4 hours inside the  $\text{CO}_2$  incubator at  $37^\circ\text{C}$  then treated with the  $\text{LC}_{50}$  of the SGAs for 24 hours. After 24 hours, cell viability was measured using MTT and crystal violet assays. The figure shows (A) crystal violet assay of COS7 with  $500 \mu\text{M}$  quetiapine; (B) crystal violet assay of COS7 with  $320 \mu\text{M}$  olanzapine; (C) MTT assay of COS7 with  $400 \mu\text{M}$  quetiapine; (D) MTT assay of COS7 with  $300 \mu\text{M}$  olanzapine. The results are presented as % of the control (non-treated COS7 cells) of mean  $\pm$  SD and  $n = 6$ , repeated 3 times. T-testing showed no significant difference.

### **3.1.8 Detecting Necrosis by Antipsychotic Drugs**

To determine whether cell death was occurring through necrosis, two experimental approaches were undertaken. The first was to measure the leakage of lactate dehydrogenase (LDH) from the cells (Chan et al., 2013), and the second was to assess the effects of a necrosis inhibitor on cell viability (Dodo et al., 2005).

#### *3.1.8.1 LDH Release*

During necrosis, the main feature is the damage of the plasma membrane resulting in the leakage of the intracellular fluid (Maes et al., 2015). Therefore, the experiments to determine necrosis involved measurement of lactate dehydrogenase (LDH) release from the cells. Cells were incubated in a 6-well plate and treated with the LC<sub>50</sub> for each drug for 24 hours. For a positive control, cells were treated with 1% Triton X-100, and non-treated cells were considered as a negative control. DMSO alone was also included as a solvent control. Both cell lines, SH-SY5Y and COS7, after treatment with the FGAs showed no significant increase in LDH release compared to the negative control see (Figure 3-26). As shown in (Figure 3-27), cells treated with SGAs also showed no significant differences.

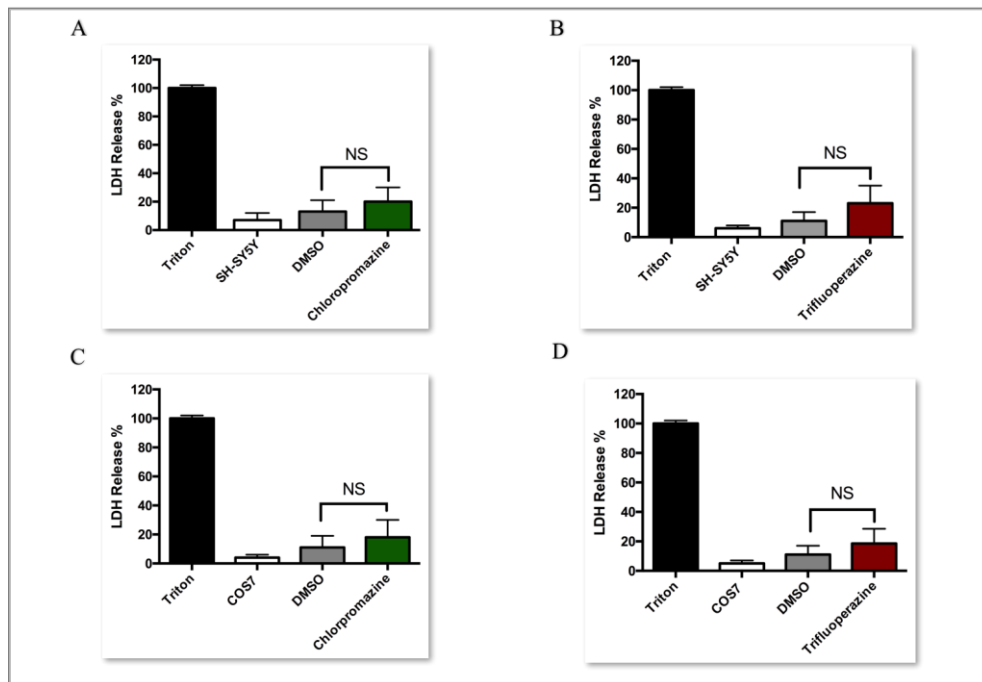


Figure 3-25: The effect of FGA on lactate dehydrogenases release.

Cells were seeded in a 6-well plate for 24 hours. After 24 hours, cells were treated with the  $LC_{50}$  for each drug for 24 hours. Positive control was treated with triton for 1 hour. Then the solution from each well was analysed to measure the LDH activity in each sample. The results are presented as % to the control (cells treated with triton) of mean  $\pm$  SD and  $n = 6$ , repeated 3 times. P value obtained using two-tailed unpaired t-testing showed no significance difference.

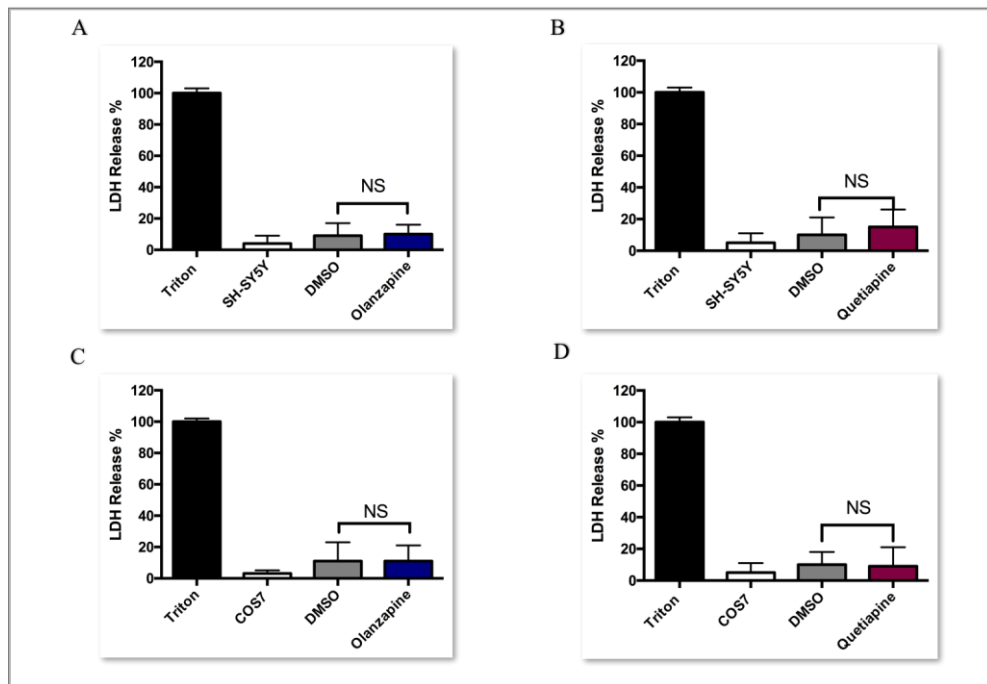


Figure 3-26: The effect of SGAs on lactate dehydrogenases release.

Cells were seeded in a 6-well plate for 24 hours. After 24 hours, cells were treated with the  $LC_{50}$  for each drug for 24 hours. Positive control was treated with triton for 1 hour. Then the solution from each well was analysed to measure the LDH released in each sample. The results are presented as % to the control (cells treated with triton) of mean  $\pm$  SD and  $n = 6$ , repeated 3 times. T-testing showed no significant difference.

### *3.1.8.2 Necrosis Inhibitor*

To confirm the involvement of regulated necrosis (necroptosis) in cell death induced by these antipsychotic drugs, necrosis inhibitor reagent, namely a RIP kinase inhibitor (i.e. Necrosis Inhibitor, IM-54), was used. Cells were pre-treated for 4 hours with 5  $\mu$ M of necrosis inhibitor then with the LC<sub>50</sub> for each drug for 24 hours. Cell viability assays were then performed. As (Figure 3-28) shows, the results showed a small but significant increase in cell numbers for both SH-SY5Y and COS7 cells treated with the FGAs after the inhibition of regulated necrosis compared to cells treated with the drugs alone. The small increases may reflect a minor role for regulated necrosis in cell death by FGAs. However, there was no significant protection after the inhibition of regulated necrosis of cells treated with the SGAs (see Figure 3-29).

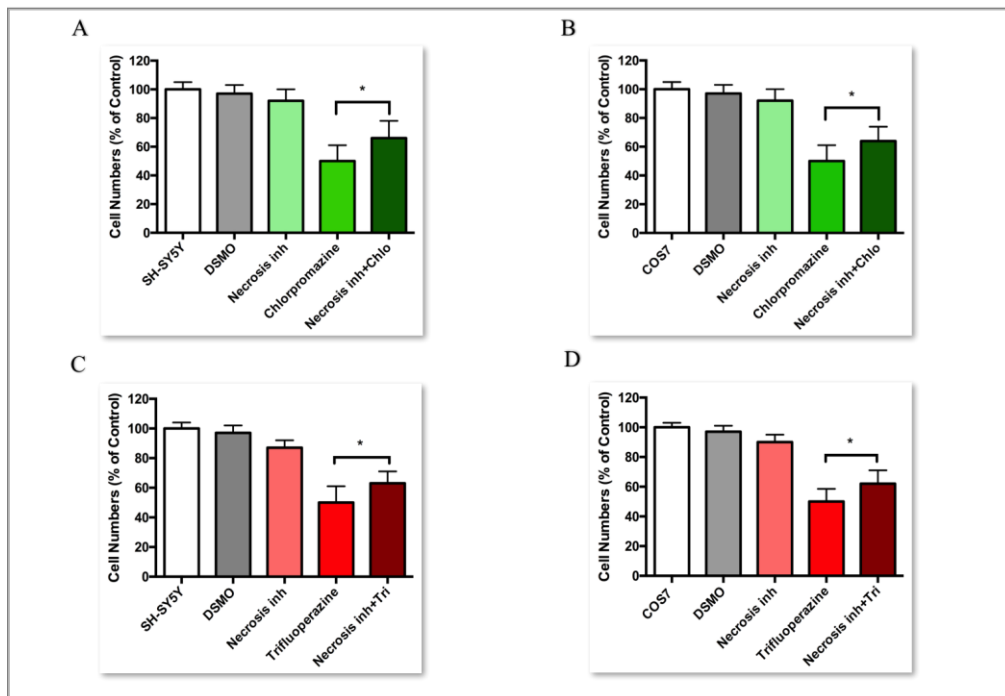


Figure 3-27: The effect of necrosis inhibitor on SH-SY5Y and COS7 with FGAs.

Cells were plated in a 24-well cell culture plate for 24 hours. After 24 hours, cells were incubated with 5  $\mu$ M of necrosis inhibitor for 4 hours inside the incubator at 37°C then treated with the LC<sub>50</sub> of the FGAs for 24 hours. After 24 hours, cell viability was measured by using crystal violet assays. The figure shows (A) crystal violet assay of SH-SY5Y with 5  $\mu$ M chlorpromazine; (B) crystal violet assay of COS7 with 12  $\mu$ M chlorpromazine; (C) crystal violet assay of SH-SY5Y with 6  $\mu$ M trifluoperazine; (D) crystal violet assay of COS7 with 10  $\mu$ M trifluoperazine. The results are presented as % to the control (non-treated cells) of mean  $\pm$  SD, repeated 3 times. P value statistically significant at \*P $\leq$ 0.05 using two-tailed unpaired t-tests.

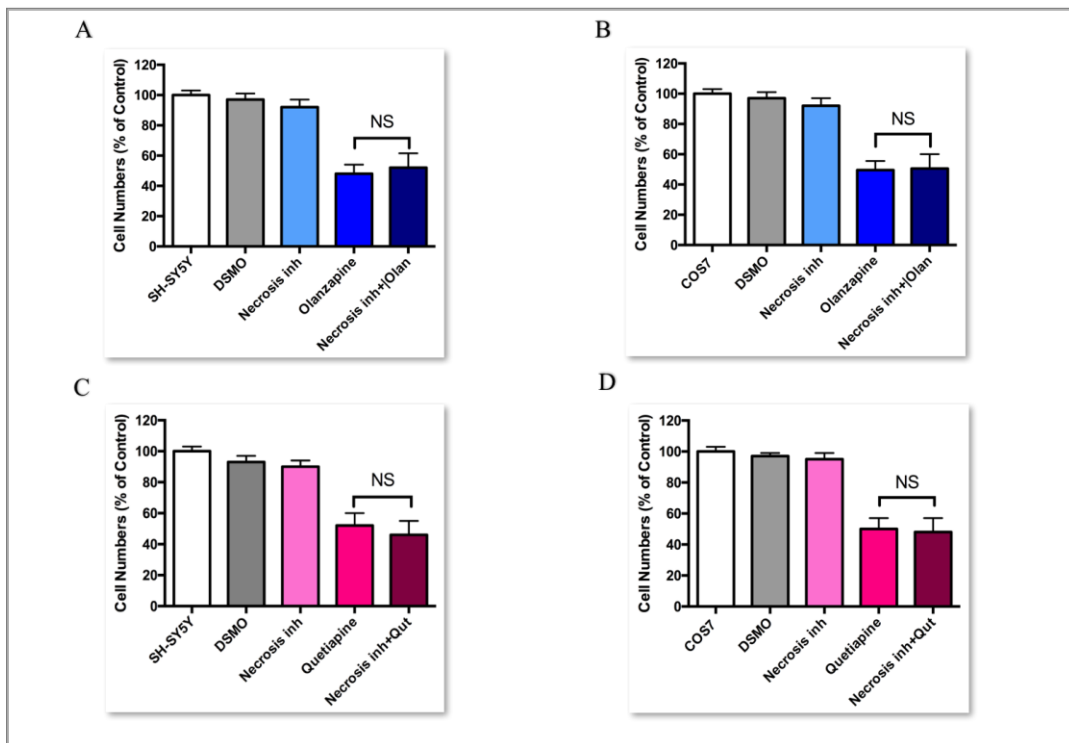


Figure 3-28: The effect of necrosis inhibitor on SH-SY5Y and COS7 with SGAs.

Cells were plated in a 24-well cell culture plate for 24 hours. After 24 hours, cells were incubated with 5  $\mu\text{M}$  necrosis inhibitor for 4 hours inside the incubator at 37°C then treated with the  $\text{LC}_{50}$  of FGAs for 24 hours. After 24 hours, cell viability was measured by crystal violet assays. The figure shows (A) crystal violet assay of SH-SY5Y with 85  $\mu\text{M}$  olanzapine; (B) crystal violet assay of COS7 with 300  $\mu\text{M}$  olanzapine; (C) crystal violet assay of SH-SY5Y with 300  $\mu\text{M}$  quetiapine; (D) crystal violet assay of COS7 with 500  $\mu\text{M}$  quetiapine. The results are presented as % to the control (non-treated cells) of mean  $\pm$  SD, repeated 3 times. T-test showed no significant difference.

### **3.1.9 Detecting Autophagy**

#### *3.1.9.1 Transfection of LC3*

Cell death can also occur through autophagy (Tsujiimoto and Shimizu, 2005). A primary method of detecting autophagy is to locate LC3-GFP via fluorescence microscopy to quantify the presence of autophagosomes. Cells were transfected with LC3-GFP plasmid for 72 hours then treated with LC<sub>50</sub> for each drug for 24 hours. After the 24 hours, cells were fixed and examined under a fluorescence microscope. (Figure 3-30 A and B) shows the negative control of SH-SY5Y and COS7 cells transfected with only LC3-GFP plasmid. Only diffuse staining was observed. (Figure 3-30) (C and D) shows the formation of puncta after transfecting the cells with LC3-GFP and incubating the cells with starvation medium to induce autophagy. (Figure 3-31) and (Figure 3-32) show the microscope images of both cell lines treated with the FGAs and SGAs. Cells treated with these drugs showed no significant formation of puncta compared to the control, an indication that cell death is not induced by autophagy.

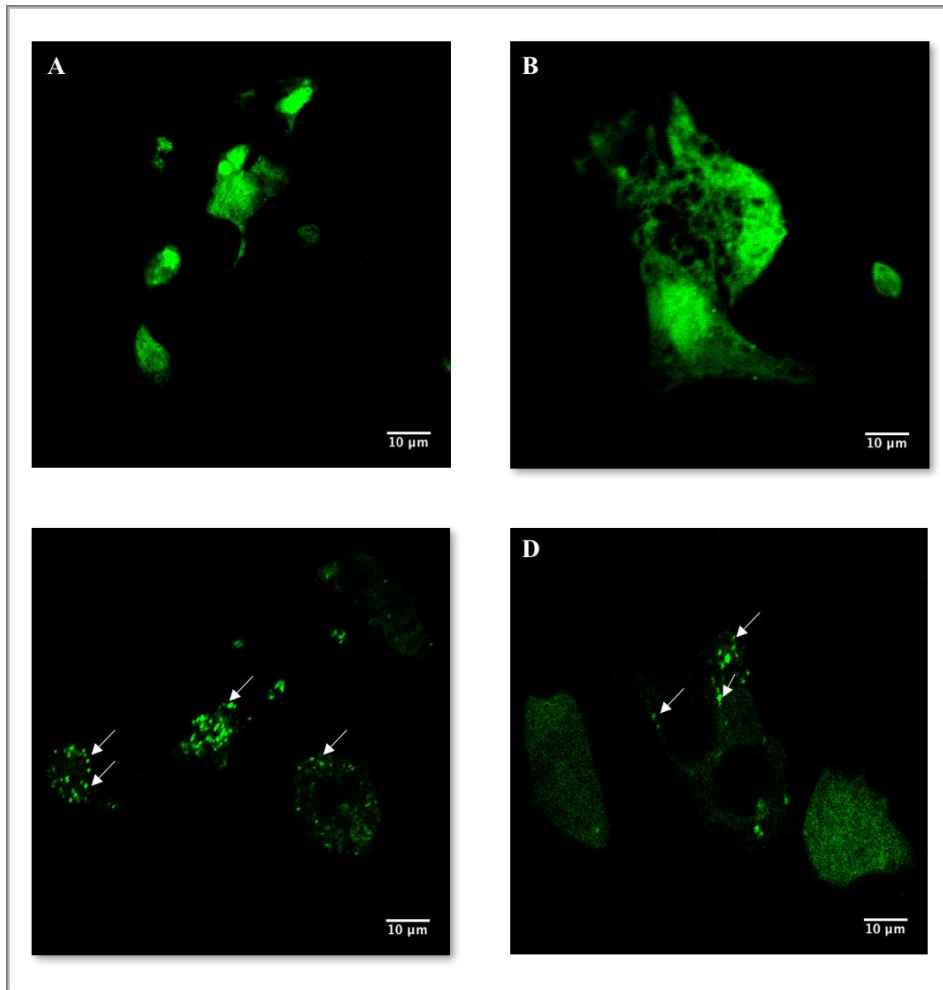


Figure 3-29: Microscope images of cells transfected with LC3.

Cells were plated in a sterilised glass bottom dish and transfected with LC3-GFP plasmid for 72 hours. Positive and negative controls were fixed with 4% PFA, and images were taken by Nikon A1R inverted confocal microscopy at  $\lambda_{exc} = 488 \text{ nm}$ ,  $\lambda_{em} = 502 \text{ nm}$ . (Green channels for GFP)

- (A) Negative control of SH-SY5Y transfected with LC3 alone
- (B) Negative control of COS7 transfected with LC3 alone
- (C) Positive control of SH-SY5Y transfected with LC3 and incubated in starvation medium
- (D) Positive control of COS7 transfected with LC3 and incubated in starvation medium

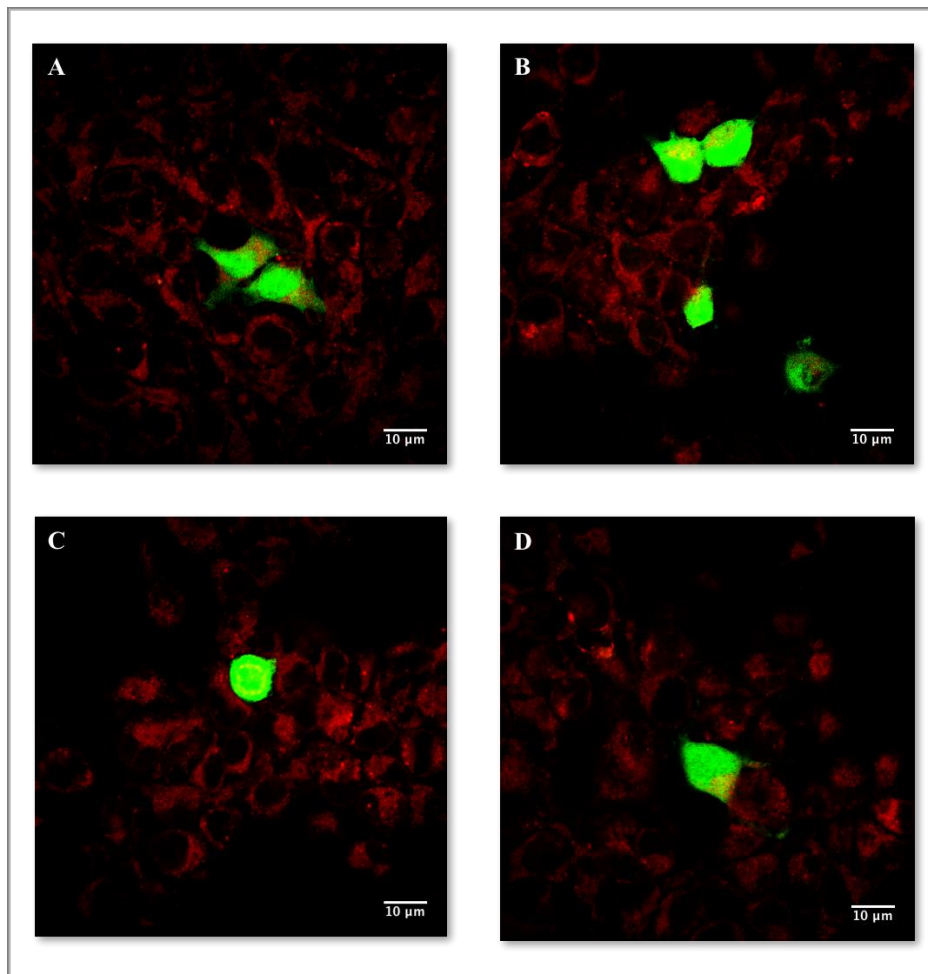


Figure 3-30: Microscope images of SH-SY5Y cells transfected with LC3 and treated with FGAs and SGAs.

SH-SY5Y were plated in a sterilised glass bottom dish and transfected with LC3-GFP plasmid for 72 hours then treated with FGAs and SGAs for 24 hours. After the 24 hours, cells were fixed with 4% PFA, and images were taken by Nikon A1R inverted confocal microscopy at  $\lambda_{exc} = 488 \text{ nm}$ ,  $\lambda_{em} = 502 \text{ nm}$ . (Green channels for GFP and Red channels for Mitotracker)

- (A) SH-SY5Y cells transfected with LC3 and treated with chlorpromazine  $5 \mu\text{M}$
- (B) SH-SY5Y cells transfected with LC3 and treated with trifluoperazine  $6 \mu\text{M}$
- (C) SH-SY5Y cells transfected with LC3 and treated with olanzapine  $85 \mu\text{M}$
- (D) SH-SY5Y cells transfected with LC3 and treated with quetiapine  $100 \mu\text{M}$

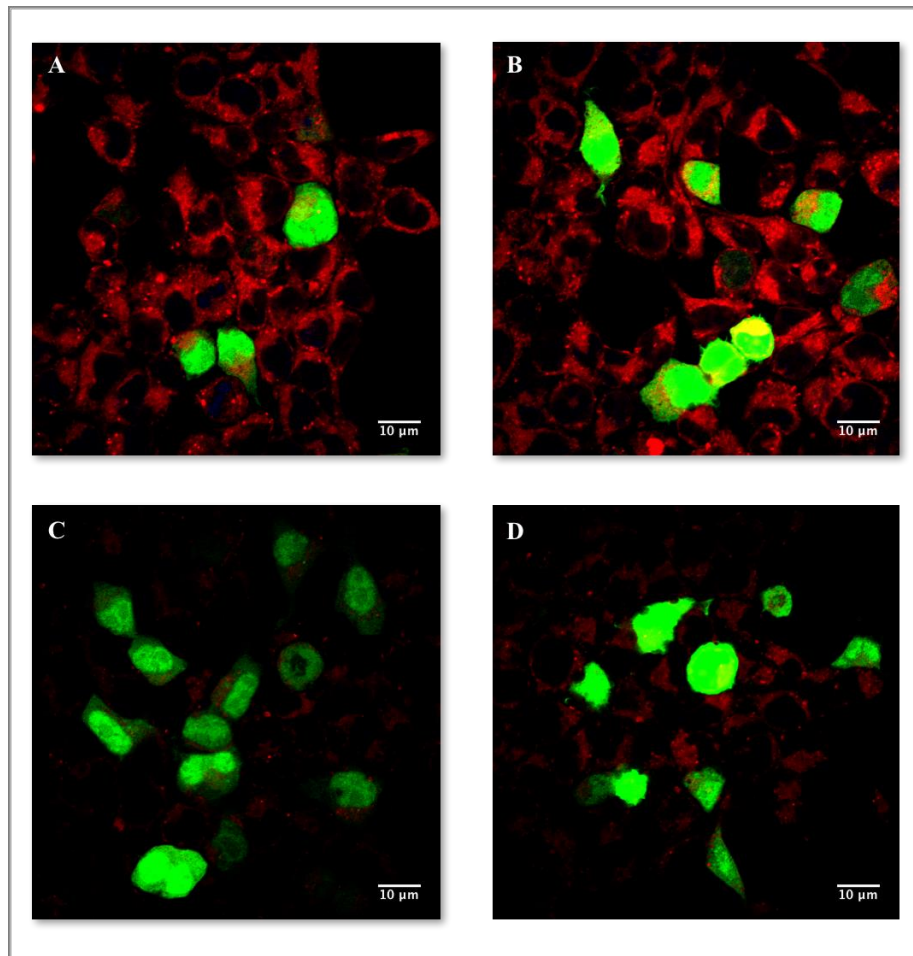


Figure 3-31: Microscope images of COS7 cells transfected with LC3 and treated with FGAs and SGAs.

COS7 cells were plated in a sterilised glass bottom dish and transfected with LC3-GFP for 72 hours then treated with FGAs and SGAs for 24 hours. After the 24 hours, cells were fixed with 4% PFA, and images were taken by Nikon A1R inverted confocal microscopy at  $\lambda_{exc}=488\text{nm}$ ,  $\lambda_{em}=502\text{nm}$ . (Green channels for GFP and Red channels for Mitotracker)

(A) COS7 cells transfected with LC3 and treated with chlorpromazine 12  $\mu\text{M}$

(B) COS7 cells transfected with LC3 and treated with trifluoperazine 10  $\mu\text{M}$

(C) COS7 cells transfected with LC3 and treated with olanzapine 200  $\mu\text{M}$

(D) COS7 cells transfected with LC3 and treated with quetiapine 400  $\mu\text{M}$

### *3.1.9.2 LC3B Antibody*

A second experiment was used to determine whether autophagy was involved in cell death by these antipsychotic drugs. LC3 is a widely used protein marker for autophagy (Tanida et al., 2008). LC3BI is truncated into the smaller protein LC3BII upon induction of autophagy (Mizushima and Yoshimori, 2005). Therefore, the ratio of LC3BI to LC3BII was used as an indication of autophagy, and western blotting was used to determine these levels. After plating the cells in a 6-well plate and treating them with the  $LC_{50}$  for each drug for 24 hours, the cells were trypsinised and solubilised for protein estimation. The amount of LC3B and  $\beta$ -actin from each sample was detected via western blotting using appropriate primary and secondary antibody.

(Figure 3-33) and (Figure 3-34), show an increase in the amount of LC3BII compared to LC3BI for SH-SY5Y cells incubated with starvation medium. The SH-SY5Y cells were treated with HBCD, a known autophagic inducer (Michelangeli personal communications). On the other hand, there was little difference in the ratio of LC3BI and LC3II in cells treated with either FGAs or SGAs for both cell lines. From the membrane, it appears the total of LC3B goes up when inducing autophagy, this could be a slight issue with loading. However, when considering the ratio of the bands with respect with the marker ( $\beta$ -actin), little effects were seen with antipsychotic drugs.

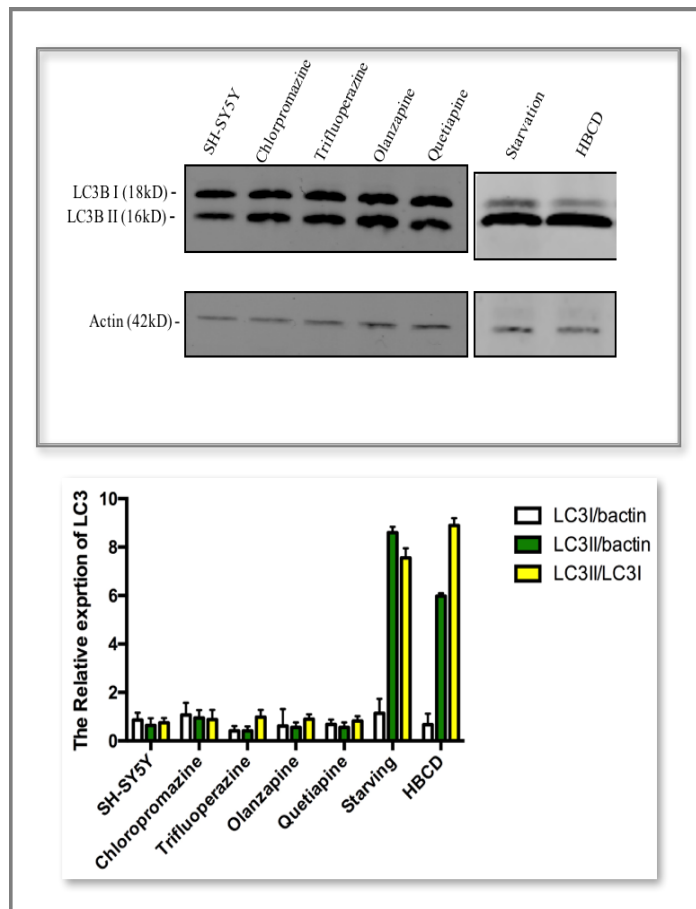


Figure 3-32: Detection of LC3B protein in SH-SY5Y treated with FGAs and SGAs.

SH-SY5Y cells were plated in a 6-well plate for 24 hours. Cells were then treated with the  $LC_{50}$  for each drug for another 24 hours. Cells were solubilised, and protein concentration of each sample was measured. 30  $\mu$ g of each protein sample was loaded onto the gel and run for 1 hour. The gel was then transferred onto membrane and incubated in LC3B primary antibody raised in rabbit. After incubating the membrane with the secondary antibody, it was imaged using a Li-Cor Odyssey scanner. Bands were normalised to  $\beta$ -actin, and the amount and ratio of LC3BI and LC3BII was plotted. Experiment was repeated 3 times.

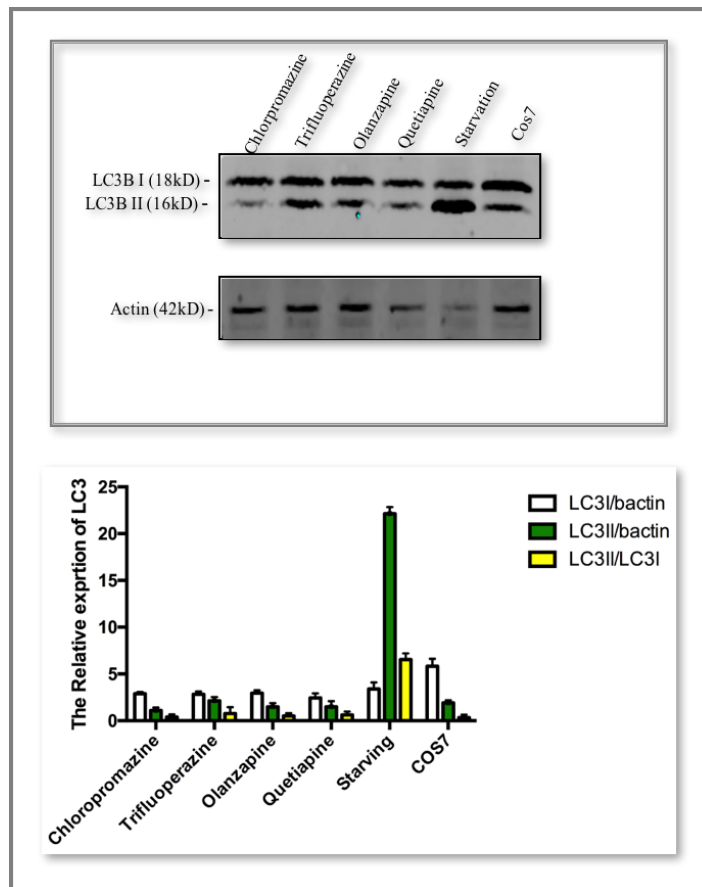


Figure 3-33: Detection of LC3 protein in COS7 treated with FGAs and SGAs.

COS7 cells were plated in a 6-well plate for 24 hours. Cells were then treated with the LC<sub>50</sub> for each drug for another 24 hours. Cells were solubilised, and protein concentration of each sample was measured. 30 µg of each protein sample was loaded onto the gel and run for 1 hour. The proteins on the gel were then transferred to a membrane and incubated in LC3B primary antibody raised in rabbit. After incubating the membrane with the secondary antibody, the membrane was imaged using a Li-Cor Odyssey scanner. Bands were normalised to β-actin, and the amount and ratio of LC3BI and LC3BII was plotted. Experiment was repeated 3 times.

## **3.2 Discussion**

Antipsychotic drugs were first developed to treat psychiatric disorders such as schizophrenia and bipolar disorder (Seida et al., 2012), and sometimes they are used as treatment for depression (Wright et al., 2013). They are widely used for patients with Alzheimer's disease to reduce and manage the aggression and agitation caused by the disease (Schneider et al., 2006). Antipsychotic drugs are classified into first-generation antipsychotics (FGAs) and second-generation antipsychotics (SGA), or typical and atypical drugs (He et al., 2009). Previous research has suggested limiting the use of FGAs in elderly patients because of these drugs' various side effects (Raphael et al., 2005).

The first objective of this chapter is to compare the effect of the FGAs chlorpromazine and trifluoperazine to the effect of the SGAs olanzapine and quetiapine on both the SH-SY5Y neuronal cell line and the COS7 kidney-like cell line. The second objective was to determine the mechanism of cell death induced by these drugs.

### **3.2.1 The Effect of Both FGAs and SGAs on SH-SY5Y and COS7 Cell Lines**

The concentration dependence of the effect of antipsychotic drugs on neuronal and non-neuronal cell lines was investigated. The toxicity of FGAs and SGAs was tested in both the SH-SY5Y neuronal cell line and the COS7 kidney-like cell line. The results indicate that the FGAs are more toxic compared to the SGAs on both cell lines. This finding is supported by the previous studies of Gassó et al. (2012) and Dwyer et al. (2003), which showed that the FGA haloperidol had a more toxic effect on SK-N-SH than did two SGAs (risperidone and paliperidone). Secondly, the LC<sub>50</sub> values for chlorpromazine, trifluoperazine, olanzapine, and quetiapine in the neuronal cell line were at less than half of that in the COS7 kidney-like cell line. This study confirmed that the neurotoxicity of the two generations of antipsychotics exceeded their cytotoxicity effect, and therefore indicates that neuronal cells are at greater risk of cell death with low concentrations of antipsychotics than other cell types. Wiklund et al. (2010) reported a similar observation, namely that LC<sub>50</sub> values are different according to the cell lines. In fact, another study by Raphael et al. (2005) also confirmed that both generations have a high neurotoxic effect and decreased the viability of cells in a neuronal cell culture. Table 3-1, summarises the LC<sub>50</sub> values for each drug to each cell line for this study.

Table 3-1: Summary of LC<sub>50</sub> values for all drugs on both cell lines using MTT and crystal violet assay

Drug	LC <sub>50</sub> SH-SY5Y MTT	LC <sub>50</sub> COS7 MTT	LC <sub>50</sub> SH-SY5Y Crystal Violet	LC <sub>50</sub> COS7 Crystal Violet
Chlorpromazine (FGA)	5±2.8 µM	12±4.1 µM	5.5±1.4 µM	12±1 µM
Trifluoperazine (FGA)	6±3.1 µM	10±2.3 µM	6± µM	10±0.9 µM
Olanzapine (SGA)	85±2.8 µM	300±3 µM	90±1.9 µM	320>±2 µM
Quetiapine (SGA)	100±2.3 µM	>400±4.1 µM	120±1.2 µM	500±3.2 µM

### 3.2.2 The Mechanism of Cell Death Induced by Antipsychotic Drugs on SH-SY5Y and COS7

The three mechanisms of cell death (apoptosis, necrosis, and autophagy) were investigated in this chapter. For apoptosis, the first step was studying the effect of caspase-3 inhibitor and caspase-3 substrate on both cell lines. Caspase-3 is an executioner caspase which directly initiates apoptosis (Slee et al., 2000). As a first step in investigating the involvement of apoptosis, caspase-3 substrate was used. As seen in the results in (Figure 3-8, Figure 3-9, Figure 3-10 and Figure 3-11) all treated cells with both generations of drugs showed the involvement of caspase-3. This study also showed that after inhibiting caspase-3, there was an increase in cell viability compared to cells treated with the drugs alone. These experiments thus

confirmed the involvement of apoptosis in general, a finding supported by previous studies that have also reported cell death induced by some antipsychotics to be caspase-dependent apoptosis (Gil-Ad et al., 2004; Ukai et al., 2004).

Since apoptosis has two main pathways, extrinsic and intrinsic, other caspase reagents were used in this study to determine which pathway is activated by these drugs. In the intrinsic pathway, cytochrome c is released from the mitochondria, which results in the activation of caspase-9 (Riedl and Salvesen, 2007). The extrinsic pathway, in contrast, is activated by the death receptors, which leads to the activation of caspase-8 (Kominami et al., 2012).

To examine whether cell death induced by antipsychotic drugs occurs through the intrinsic pathway, two methods were used. First, cell viability was measured after inhibiting caspase-9. Second, the cytochrome c release from the mitochondria into the cytosol was measured. As seen in the results, both cell lines showed no protection or increase in cell viability after the treatment with the FGAs in the presence and absence of caspase-9 inhibitor. However, in cells treated with the SGAs, there was an increase both in cell viability after the inhibition of caspase-9 and in the amount of cytochrome c in the cytosol.

Caspase-8 inhibitor was used to indicate if the apoptosis induced by these drugs occurs through the extrinsic pathway. As seen in the results, both cell lines showed a significant increase in cell viability after the treatment with the FGAs in the presence of caspase-8 inhibitor, which suggested the involvement of the extrinsic

pathway. However, caspase-8 inhibitor did not have any protection effect against the SGAs.

In general, various groups have reported that antipsychotic drugs, both typical and atypical, activate caspase-3, -8, and -9. However, the concentration of the drugs and the time of incubation could have a great effect on which cell death pathway will be activated. Most of the studies that have reported an increase of cytochrome c release or damage to the mitochondria by FGAs, especially chlorpromazine, have used a higher concentration of the drug of  $\sim 35 \mu\text{M}$  (Modica-Napolitano et al., 2003).

Necrosis was also investigated in this chapter by using two different methods. First, the amount of LDH released from the cells after treatment with the drugs was measured. Second, the cell viability of treated cells with and without necrosis inhibitor reagent was compared. The results in this study suggested that regulated necrosis is induced, albeit at a low level, after treatment with the FGAs, but not with the SGAs. Such findings are in agreement with the results of studies by Andreassen and Jorgensen (2000), Galili et al. (2000), and Post et al. (2002), which found that cell death induced by antipsychotics occurs through apoptosis rather than necrosis.

The last mechanism of cell death investigated in this study was autophagy. From the results of both experiments, (detecting the LC3B and the formation of autophagosomes) it was concluded that autophagy is not involved. It has been proposed in a study by Vucicevic et al., (2014), that chlorpromazine induced

autophagy in SH-SY5Y. the difference they used a higher concentration more than 100 $\mu$ M for more that 24 hours.

Thus, in summary, the study in this chapter has revealed that cell death induced by antipsychotic drugs occur through apoptosis with both FGAs and SGAs and regulated necrosis in FGA-treated cells. (no significant induction of necrosis was seen with SGAs). There was no evidence for induction of autophagy. In this study, we showed that the effect of antipsychotic drugs in vitro were highly neurotoxic causing mainly apoptosis and the first generation was far more toxic than the second.

Table 3-2: Summary of the mechanism of cell death activated by each generation

Cells	FGA							SGA						
	Apoptosis			Necrosis		Autophagy		Apoptosis			Necrosis		Autophagy	
	Casp.3	Casp.9	Casp.8	LDH	Nec.inh	LC3	LC3IB	Casp.3	Casp.9	Casp.8	LDH	Nec.inh	LC3	LC3IB
SH-SY5Y	✓	✗	✓	✗	✓	✗	✗	✓	✓	✗	✗	✗	✗	✗
COS7	✓	✗	✓	✗	✓	✗	✗	✓	✓	✗	✗	✗	✗	✗

## **Chapter 4:**

# **The Effects of Antipsychotic Drugs on Cells Overexpressing SERCA and SPCA Ca<sup>2+</sup> Pumps**

## **4. The Effects of Antipsychotic Drugs on Cells Overexpressing SERCA and SPCA Ca<sup>2+</sup> Pumps**

### **Introduction**

Ca<sup>2+</sup> plays an essential role in most of the activities of eukaryotic cells. Therefore, it is very important for Ca<sup>2+</sup> levels to be regulated in the cells in both time and space (Brini et al., 2013; Carafoli, 2007). There are two main mechanisms that regulate Ca<sup>2+</sup> within the cell: The first is soluble proteins such as calmodulin reversibly binding to it. The second is numerous proteins mediating its transport across the cellular and organellar membranes (Michelangeli et al., 2005). If there is an abnormality or regulation failure in Ca<sup>2+</sup> homeostasis within the cell, numerous diseases or even cell death can result (Carafoli, 2007). Ca<sup>2+</sup> pumps play an important role in Ca<sup>2+</sup> homeostasis, as their malfunction is associated with a number of diseases such as cancer and cardiovascular disease (Pua et al., 2016). Neurons are also directly affected by the regulation of Ca<sup>2+</sup> homeostasis (Brini et al., 2014). Therefore, incorrect functioning of Ca<sup>2+</sup> homeostasis may result in a number of neurodegenerative diseases such as Alzheimer's disease and Parkinson's disease (Brini and Carafoli, 2009; Popugaeva et al., 2015).

There are several isoforms of SERCA and SPCA Ca<sup>2+</sup> pumps that are located respectively in the membranes of the endoplasmic reticulum and the secretory pathway- Golgi body. Of these, SERCA2b and SPCA1a are the most common isoforms found in non-muscle cells and as such represent the housekeeping

isoforms (Vandecaetsbeek et al., 2011). The function of these pumps is to maintain the high concentration of  $\text{Ca}^{2+}$  in the lumen of the ER and the Golgi that is required for normal cell function and to bring the cytosolic free  $\text{Ca}^{2+}$  concentration back to its resting level after cell activation (Wuytack et al., 2002).

Earlier studies by the Michelangeli group have reported that certain first-generation antipsychotics have the ability to inhibit  $\text{Ca}^{2+}$  pumps and  $\text{Ca}^{2+}$  channels and therefore could be involved in disrupting intracellular  $\text{Ca}^{2+}$  homeostasis (Khan et al., 2000; Khan et al., 2001).

From the previous chapter, we showed that cell death was via apoptosis and regulated necrosis. In this chapter we investigate whether this cell death is also via a calcium dependent process.

We know that  $\text{Ca}^{2+}$  can play a role in a variety of cell death mechanisms, in this study we want to indicate whether  $\text{Ca}^{2+}$  has a role to play in cell death induced by antipsychotic drugs, by investigating the effect of BAPTA (a calcium chelator) and the effects of increasing the level of  $\text{Ca}^{2+}$  transporting ATPases in the ER and in the Golgi. Therefore, SERCA2b and SPCA1a were overexpressed in cells to investigate their potential protective role against antipsychotic drugs toxicity in both SH-SY5Y and COS7 cells.

## 4.1 Results

### 4.1.1 The Effect of BAPTA-AM

#### 4.1.1.1 *The Effect of BAPTA-AM on SH-SY5Y Cells*

BAPTA-AM is a well-known cell-permeant chelator that binds  $\text{Ca}^{2+}$  (Alberdi et al., 2001). In this study, BAPTA-AM was used to determine if excessive elevation of intracellular  $\text{Ca}^{2+}$  concentration is involved in the cell death caused by the antipsychotic drugs tested on both SH-SY5Y and COS7 cells. Cells were plated in 24-well cell culture plates for 24 hours. After 24 hours, 10  $\mu\text{M}$  of BAPTA-AM was added to the cells and incubated for 4 hours at 37°C. Cells with and without BAPTA-AM were then treated with the  $\text{LC}_{50}$  of each drug for 24 hours. (Figure 4-1), shows the crystal violet cell viability results of the effect of BAPTA-AM on the control and on the SH-SY5Y cells treated with the first-generation antipsychotics (FGAs) and second-generation antipsychotics (SGAs). Cells incubated with BAPTA-AM alone (10  $\mu\text{M}$ ) showed no cytotoxic effect. Cells treated with BAPTA-AM and an FGA (chlorpromazine and trifluoperazine) showed a statistically significant 20% increase in viable cell numbers compared to cells treated with the drugs alone ( $P = 0.0002$  and  $0.0007$ , respectively). Cells treated with an SGA (olanzapine and quetiapine) also showed a statistically significant 10% increase in viable cell numbers compared to cells treated with the drugs alone ( $P = 0.0217$  and  $0.0369$ , respectively).

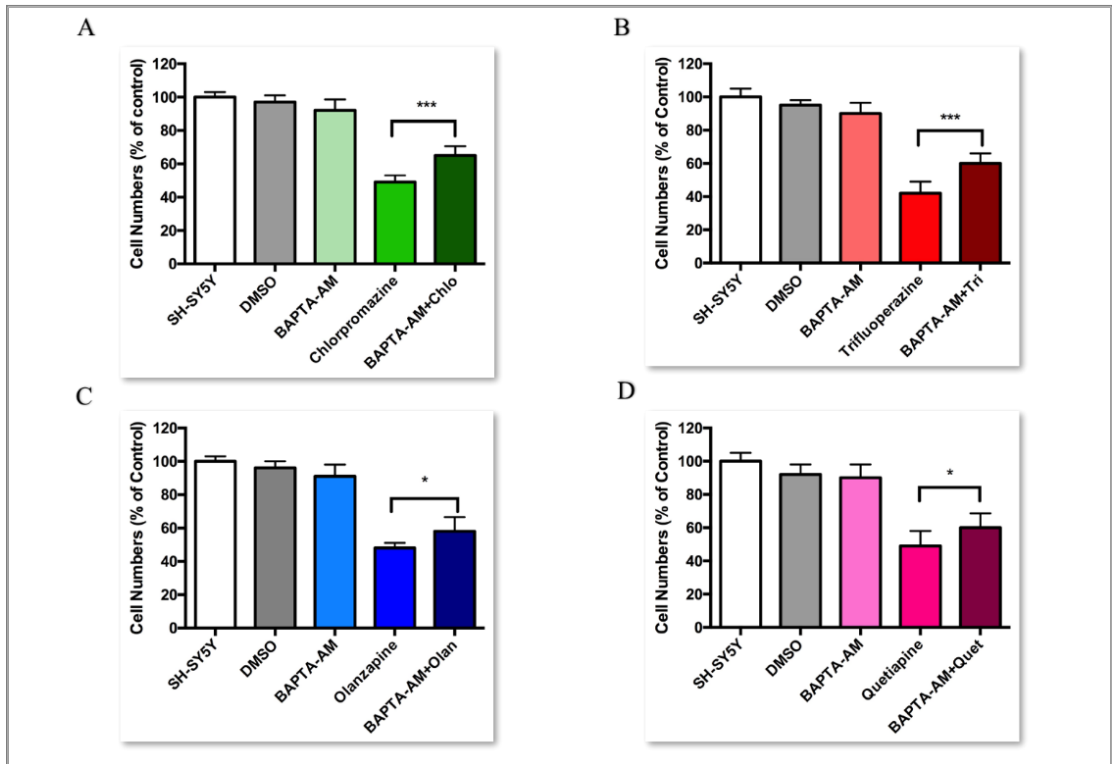


Figure 4-1: The effect of BAPTA-AM on SH-SY5Y with FGAs and SGAs

SH-SY5Y cells were plated in 24-well cell culture plates at a density of  $4 \times 10^4$  per well for 24 hours. After the 24 hours, cells were incubated with  $10 \mu\text{M}$  BAPTA-AM for 4 hours inside the  $\text{CO}_2$  incubator at  $37^\circ\text{C}$  then treated with the  $\text{LC}_{50}$  of each drug. The figure shows the results after 24 hours for (A) chlorpromazine  $5 \mu\text{M}$ , (B) trifluoperazine  $6 \mu\text{M}$ , (C) olanzapine  $85 \mu\text{M}$ , and (D) quetiapine  $100 \mu\text{M}$ . After 24 hours, cell viability was measured using crystal violet assay, and the absorbance was read at  $590 \text{ nm}$ . The results are presented as % to the control (non-treated SH-SY5Y cells) of mean  $\pm$  SD, repeated 3 times. P value statistically significant at  $*P \leq 0.05$ ,  $*** P \leq 0.001$  using two-tailed unpaired t-tests.

#### *4.1.1.2 The Effect of BAPTA-AM on COS7 Cells*

Cells were plated in 24-well cell culture plates for 24 hours. After the 24 hours, 10  $\mu$ M of BAPTA-AM was added to the cells and incubated for 4 hours at 37°C. Cells with and without BAPTA-AM were then treated with the LC<sub>50</sub> of each drug for 24 hours. (Figure 4-2), shows the cell viability crystal violet assay results of the effect of BAPTA-AM on the control and on the COS7 cells treated with the FGAs and SGAs. Again, cells incubated with BAPTA-AM alone showed no toxic effect on viability. Cells treated with BAPTA-AM and an FGA (chlorpromazine and trifluoperazine) showed a statistically significant 20% increase in viable cell numbers compared to cells with the drugs alone (P = 0.0009 and 0.0008, respectively). When treated with an SGA (olanzapine and quetiapine) the cells also showed a statistically significant 10% increase in viability compared to cells with the drugs alone (P = 0.0317 and 0.0419, respectively). Taken together, these results would indicate that the cytotoxicity caused by these drugs is due, at least in part, to Ca<sup>2+</sup>-dependent cell death mechanisms.

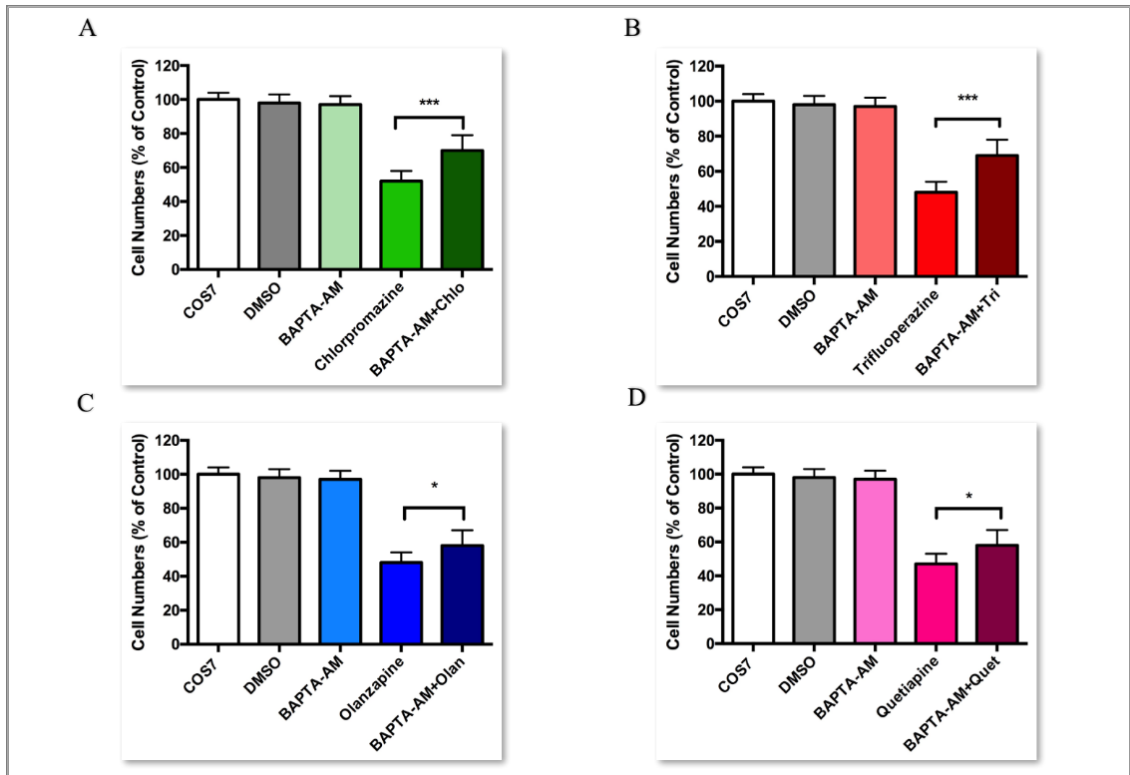


Figure 4-2: The effect of BAPTA-AM on COS7 with FGAs and SGAs

COS7 cells were plated in a 24-well cell culture plate at a density of  $2 \times 10^5$  per well for 24 hours. After the 24 hours, cells were incubated with  $10 \mu\text{M}$  of BAPTA-AM for 4 hours at  $37^\circ\text{C}$  then treated with the  $\text{LC}_{50}$  of each drug. The figure shows the results after 24 hours for (A) chlorpromazine  $12 \mu\text{M}$ , (B) trifluoperazine  $10 \mu\text{M}$ , (C) olanzapine  $300 \mu\text{M}$ , and (D) quetiapine  $400 \mu\text{M}$ . After 24 hours, cells were assessed for viability with crystal violet assay, and the absorbance was read at  $590 \text{ nm}$ . The results are presented as % to the control (non-treated COS7 cells) of mean  $\pm$  SD, repeated 3 times. P value statistically significant at  $*P \leq 0.05$ ,  $*** P \leq 0.001$  using two-tailed unpaired t-tests.

#### 4.1.2 The Effect of Antipsychotic Drugs on ER Stress

To investigate the effects of the antipsychotic drugs on ER stress, the level of expression of the ER stress response protein CHOP (GADD 153) (Oyadomar and Mori, 2004) was measured using a CHOP-specific antibody. Previous studies have shown a link between disruption of Ca<sup>2+</sup> homeostasis, apoptosis, and the ER stress response in different cell lines, with many studies using CHOP expression as the ER stress marker (Martin-Perez et al., 2014; Yamaguchi et al., 2004; Lu et al., 2014). After plating the cells in a 6-well plate and treating them with the LC<sub>50</sub> for each drug, and with thapsigargin (TG) as a positive control, the cells were then trypsinised and solubilised for protein estimation followed by western blotting. As seen from the immunoblot in (Figure 4-3), CHOP was elevated significantly in samples treated with all the drugs except olanzapine.

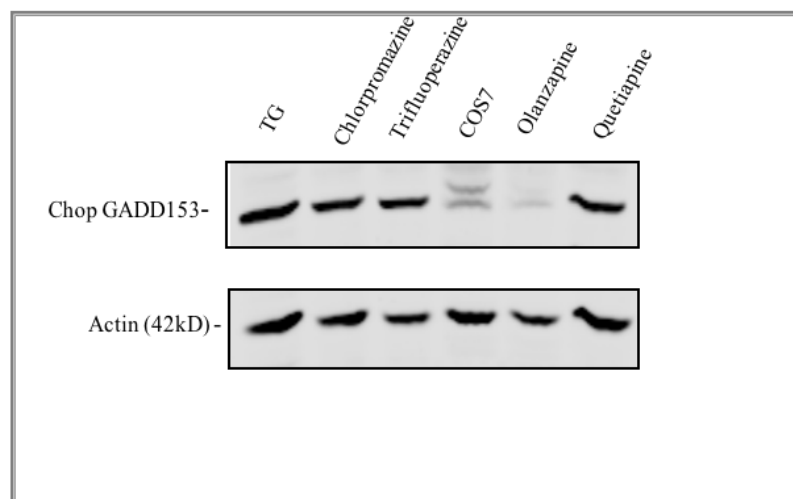


Figure 4-3: The detection of CHOP in COS7 cells treated with FGAs and SGAs.

COS7 cells were plated in 6-well plates for 24 hours. Cells were then treated with the LC<sub>50</sub> for each drug for another 24 hours or with thapsigargin (TG) as a positive control. Cells were solubilised, and the protein concentration of each sample was measured. 30 µg of each protein sample was loaded onto the gel and run for 1 hour. The proteins on the gel were then transferred to a membrane and incubated in CHOP/GADD153 primary antibody raised in rabbit. After incubating the membrane with the secondary antibody, the membrane was imaged using a Li-Cor Odyssey scanner.

### **4.1.3 Transfection**

#### *4.1.3.1 The Effect of Different Transfection Reagents on Cells*

To achieve maximum transfection efficiency, five different reagents were tested in this study. The first reagent was TurboFect, a polymer-based reagent purchased from Thermo Scientific. Following the manufacturer's instructions for each reagent, cells were plated in 24-well cell culture plates at a density of  $2 \times 10^4$  for COS7 and  $2 \times 10^4$  for SH-SY5Y in 1 ml of growth media per well for 24 hours. Before the transfection, three different conditions of DNA and transfection reagents were prepared (1  $\mu\text{g}$  DNA/2  $\mu\text{L}$  transfection reagent, 1  $\mu\text{g}$  DNA/3  $\mu\text{L}$  transfection reagent, and 1  $\mu\text{g}$  DNA/4  $\mu\text{L}$  transfection reagent) by diluting the DNA in 100  $\mu\text{L}$  of serum-free growth media. After vortex, the right amount of transfection reagent was added to each diluted DNA sample, mixed immediately, and then incubated at room temperature for 20 minutes. Then 100  $\mu\text{L}$  of the solution was added to each well. After 24 hours, the media was changed, and crystal violet cell viability assay was undertaken to test the effect of these reagents on the cells. (Figure 4-4), shows the effect of these transfection reagents on cell numbers after 24 hours of incubation and images under fluorescence microscopy after 72 hours of adding the SPCA1a-GFP plasmid DNA. (Figure 4-4 A) shows the effect of TurboFect on both cell lines, revealing a toxic effect on SH-SY5Y cells. The other transfection reagents, namely (B) Effectene, (C) TurboFectin 8.0, (D) Metafectene Pro, and (E) Metafectene, have no toxic on either cell line. The best transfection efficiency was determined to be with Metafectene Pro.

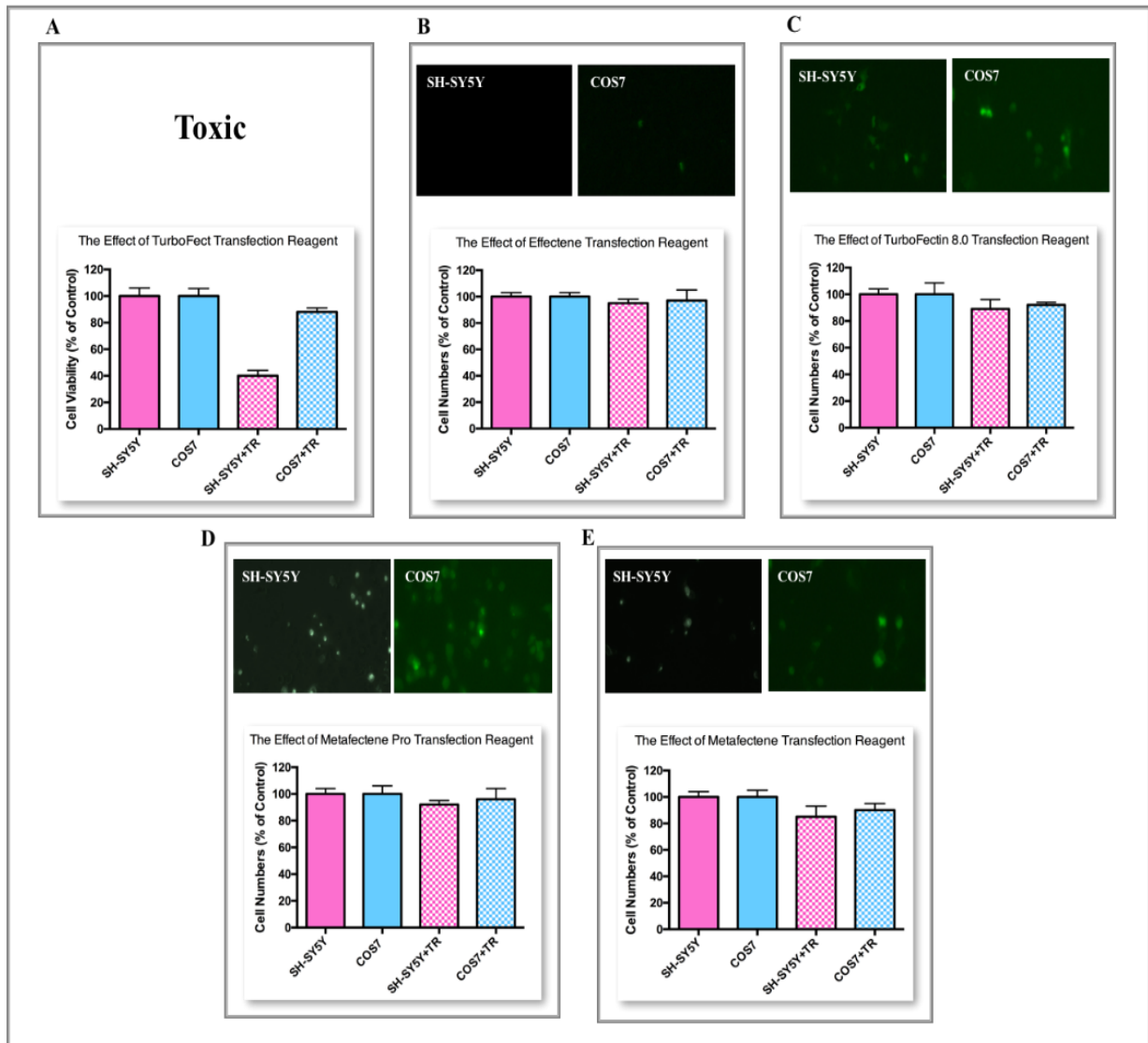


Figure 4-4: The effect of different transfection reagents with SPCA1a-GFP plasmid on COS7 and SH-SY5Y cells

Cells were plated in a 24-cell culture plate incubated for 24 hours. Before transfection, SPCA1a-GFP plasmid DNA was diluted in free serum media. Then the transfection reagents were added according to the manufacturer's instructions. After 24 hours, crystal violet assay was applied. The figure shows the effect of transfection reagents on both cell lines of (A) TurboFect, (B) Effectene, (C) TurboFectin 8.0, (D) Metafectene Pro, and (E) Metafectene.

#### **4.1.4 The Overexpression of SPCA1a-GFP in COS7**

##### *4.1.4.1 Analysis of SPCA1a-GFP Expression in COS7 Cells*

Metafectene Pro (MP) transfection reagent was used due to its lowest toxicity on the cells and its high level of transfection efficiency. Three different conditions were used to determine the best results for SPCA1a-GFP 1  $\mu\text{g}$  DNA/2  $\mu\text{L}$  MP, 1  $\mu\text{g}$  DNA /3  $\mu\text{L}$  MP, and 1  $\mu\text{g}$  DNA /4  $\mu\text{L}$  MP. Following the instructions for transfection, cells were transfected and examined under the microscope every 24 hours. (Figure 4-5) shows an image of transfected COS7 with SPCA1a-GFP after 72 hours under the fluorescence microscopy. (Figures 4-6) shows the percentage of fluorescence cells after 24, 48, and 72 hours for each condition. The best condition was 1  $\mu\text{g}$  DNA/2  $\mu\text{L}$  MP for 72 hours, which gave about 40% transfection efficiency confirmed after the use of western blot (Figure 4-7). Accordingly, that is what was used for the rest of the experiments presented in this chapter.

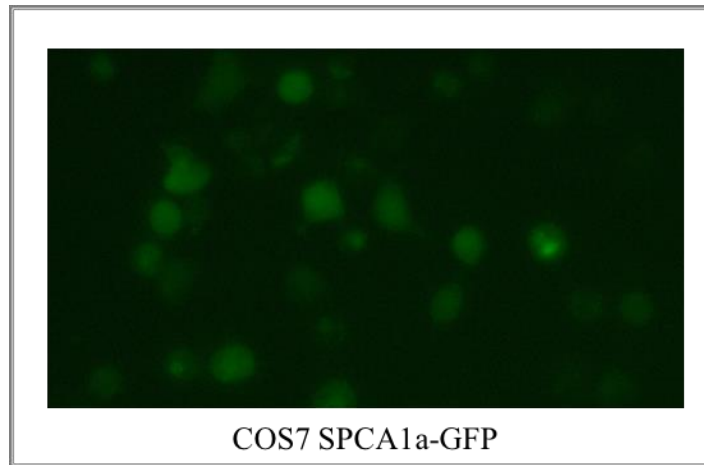


Figure 4-5: Microscope image of fluorescent COS7 transfected with 1  $\mu\text{g}$  SPCA1a-GFP/ 2  $\mu\text{L}$  MP after 72 hours.

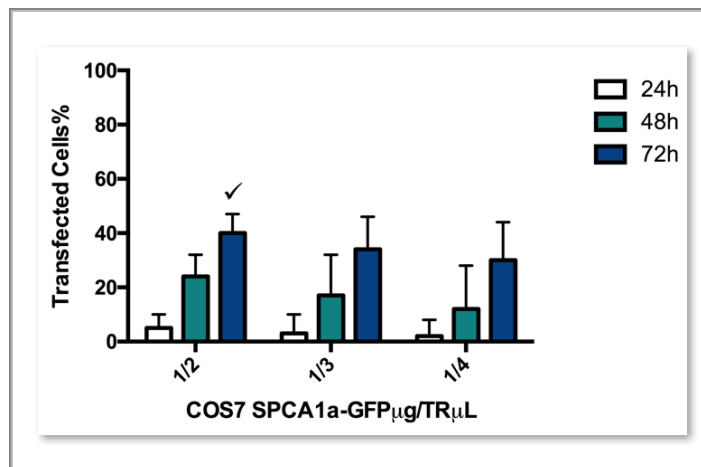


Figure 4-6: The ratio of transfected COS7 with SPCA1a-GFP.

COS7 cells were plated in a 24-well plate at a density of  $2 \times 10^4$ /well. Cells were transfected with SPCA1a-GFP plasmid at three conditions. Every 24 hours, cells were examined under the fluorescence microscope, and the ratio was calculated by counting the fluorescent cells against all cells counted under brightfield. Cells transfected for 72 hours with 1  $\mu\text{g}$

SPCA1a-GFP with 2  $\mu$ L MP had the best efficiency. The data represents the mean  $\pm$  SD, n= 3.

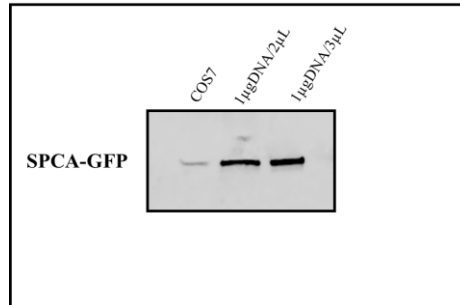


Figure 4-7: Western Blot detection of SPCA on COS7

COS7 cells were plated in a 6-well plate for 24 hours. Cells were then transfected with the SPCA-GFP for 72 hours. Cells were solubilised, and protein concentration of each sample was measured. 30  $\mu$ g of each protein sample was loaded onto the gel and run for 1 hour. The gel was then transferred onto membrane and incubated in LTQQ primary antibody raised in rabbit. After incubating the membrane with the secondary antibody, it was imaged using a Li-Cor Odyssey scanner.

#### 4.1.4.2 Analysis of SPCA1a-GFP Expression in COS7 Cells

A Fluorescence-Activated Cell Counter (FACC) was used as another method to count the fluorescent cells and determine transfection efficiency. Following the same procedure for transfection, cells were seeded in a 6-well cell culture plate and transfected with SPCA1aGFP for 72 hours. Cells were then trypsinised with 0.05% trypsin-EDTA and centrifuged at 1000 rpm for 2 minutes. The pellet was re-suspended with PBS containing 2% FBS and 3  $\mu$ M PI and transferred to FACC tubes. (Figure 4-8), shows the result of flow cytometry for COS7 alone as a control that was considered to be 100% live cells. (Figure 4-9), represents the result of COS7 transfected with SPCA1a-GFP at condition 1  $\mu$ g DNA/2  $\mu$ L MP. The results

show that virtually all cells were live, with 62% of cells being deemed non-fluorescent and 36% transfected.

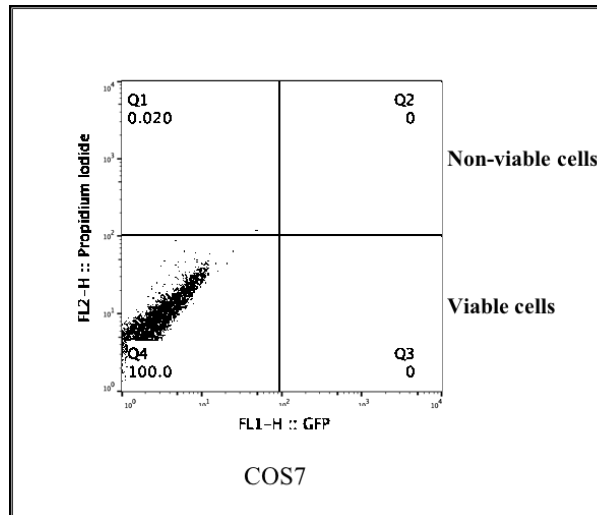


Figure 4-8: Flow cytometry measurement of COS7 alone.

Cells were plated in a 6-well cell culture plate alone and used in FACC as a control.

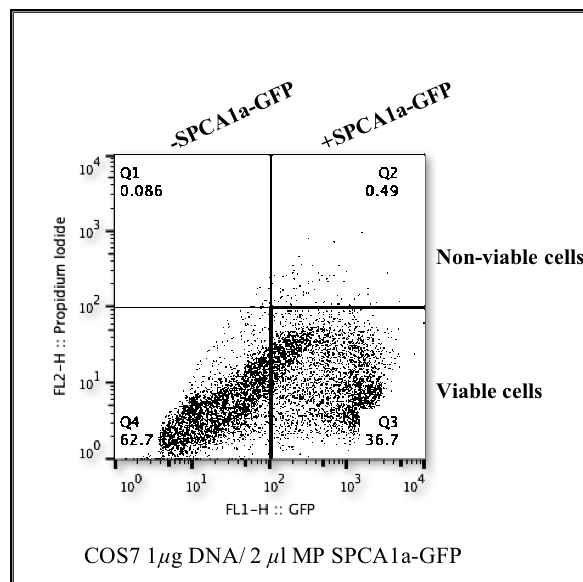


Figure 4-9: Flow cytometry measurement of transfected COS7 with SPCA1a-GFP.

Cells were plated in a 6-well cell culture plate for 24 hours. The cells were then transfected with SPCA1a-GFP for 72 hours. The number of transfected cells was measured by FACC.

As shown in the figure, 62% of the cells were viable without transfection, 36.7% of the total number of cells were viable and transfected with SPCA1a-GFP, and only 0.5% of the cells were transfected and non-viable.

#### **4.1.5 The Overexpression of SPCA1a-GFP in SH-SY5Y Cells**

##### *4.1.5.1 Analysis of SPCA1a-GFP Expression in SH-SY5Y Cells*

To determine the best transfection efficiency for the SPCA1a-GFP plasmid in SH-SY5Y cells, the Metafectene Pro (MP) transfection reagent was used with three different conditions: 1  $\mu$ g DNA/2  $\mu$ L MP, 1  $\mu$ g DNA/3  $\mu$ L MP, and 1  $\mu$ g DNA/4  $\mu$ L MP of the plasmid/MP. Following the same instructions, SH-SY5Y cells were transfected and examined under the microscope for three days. (Figure 4-10) represents the fluorescence microscopy image of transfected cells with 1  $\mu$ g SPCA1a-GFP/2  $\mu$ L MP after 72 hours. (Figure 4-11) shows the percentage of fluorescence cells after 24, 48, and 72 hours for each condition. The best condition was 1  $\mu$ g DNA/2  $\mu$ L MP for 72 hours, which gave about 25% transfection, confirmed after the use of western blot (Figure 4-12). Accordingly, that is what was used for the rest of the experiments.

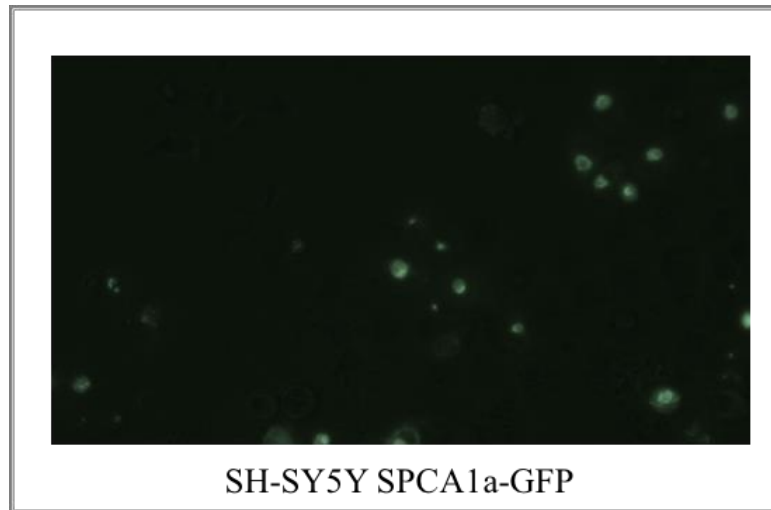


Figure 4-10: Microscope image of fluorescent SH-SY5Y transfected with 1  $\mu\text{g}$  SPCA1a-GFP/2  $\mu\text{L}$  MP for 72 hours.

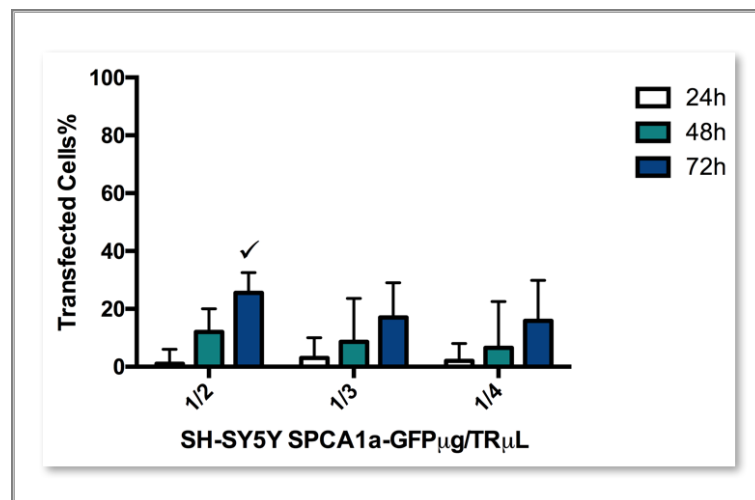


Figure 4-11: The ratio of transfected SH-SY5Y with SPCA1a-GFP.

SH-SY5Y cells were plated in a 24-well plate at a density of  $1 \times 10^4$ /well. Cells were transfected with SPCA1a-GFP using the three conditions. Every 24 hours, cells were examined under the fluorescence microscope, and percentage of fluorescent cells was determined. Cells were transfected for 72 hours with 1  $\mu\text{g}$  SPCA1a-GFP and with 2  $\mu\text{L}$  MP, which had the best efficiency. The data represents the mean  $\pm$  SD, n = 3.

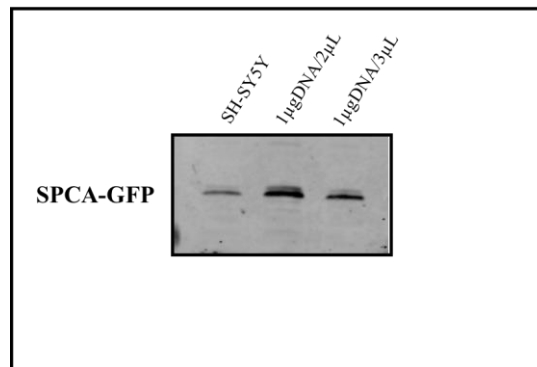


Figure 4-12: Western Blot detection of SPCA on SH-SY5Y

SH-SY5Y cells were plated in a 6-well plate for 24 hours. Cells were then transfected with the SPCA-GFP for 72 hours. Cells were solubilised, and protein concentration of each sample was measured. 30 µg of each protein sample was loaded onto the gel and run for 1 hour. The gel was then transferred onto membrane and incubated in LTQQ primary antibody raised in rabbit. After incubating the membrane with the secondary antibody, it was imaged using a Li-Cor Odyssey scanner.

#### 4.1.5.2 Analysis of SPCA1a-GFP Expression in SH-SY5Y by FACC

To confirm the transfection efficiency, cells were also analysed by FACC. (Figure 4-13) represents the control sample of SH-SY5Y cells, which showed 99% live cells and 1% non-viable cells. (Figure 4-14) shows that the amount of viable SH-SY5Y cells transfected with SPCA1a-GFP was 21%, while 76% were non-transfected. It also shows very low levels of non-viable cells in each population of transfected and un-transfected cells.

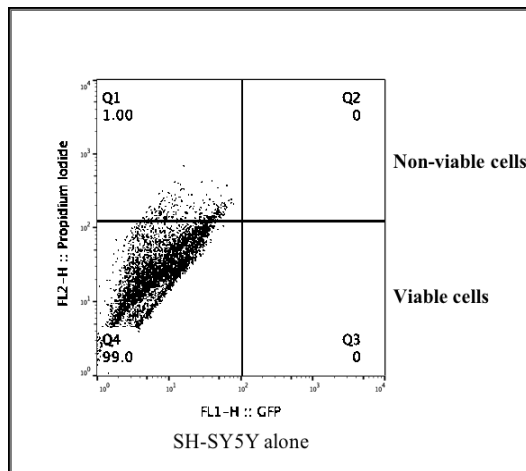


Figure 4-13: Flow cytometry measurement of SH-SY5Y alone.

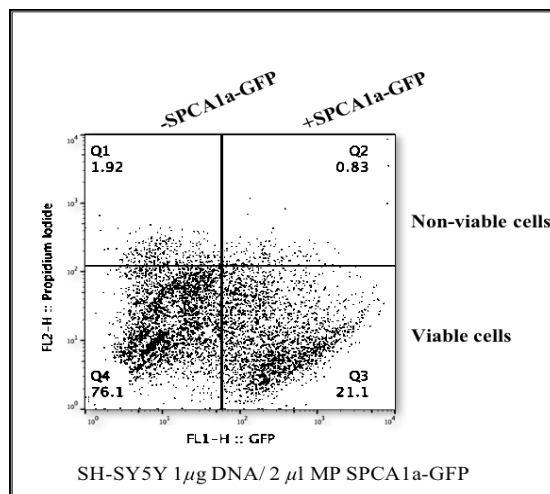


Figure 4-14: Flow cytometry measurement of transfected SH-SY5Y with SPCA1a-GFP.

SH-SY5Y cells were plated in a 6-well cell culture plate for 24 hours. The cells were then transfected with SPCA1a-GFP for 72 hours. The number of transfected cells was measured by FACC. As shown in the figure, 76.1% of the cells were viable without transfection, 21.1% of the total number of the cells were viable and transfected with SPCA1a-GFP, and only 0.83% of the cells were transfected and non-viable.

## 4.1.6 The Overexpression of SERCA2b-GFP in COS7

### 4.1.6.1 Analysis of SERCA2b-GFP Expression in COS7 Cells

COS7 cells were plated in a 24-well cell culture plate and transfected with SERCA2b-GFP following the same methods used in this study (see section 4.1.4). The three different conditions were examined by fluorescence microscopy for three consecutive days. (Figure 4-15) shows the best results of the transfection after 72 hours at the condition of 1  $\mu\text{g}$  SERCA2b-GFP plasmid and 4  $\mu\text{L}$  MP. (Figure 4-16) represents the percentage transfection efficiency for each condition during the three days. It can be seen that the best condition was 1  $\mu\text{g}$  DNA/4  $\mu\text{L}$  MP for 72 hours, which gave a transfection efficiency of 32%.

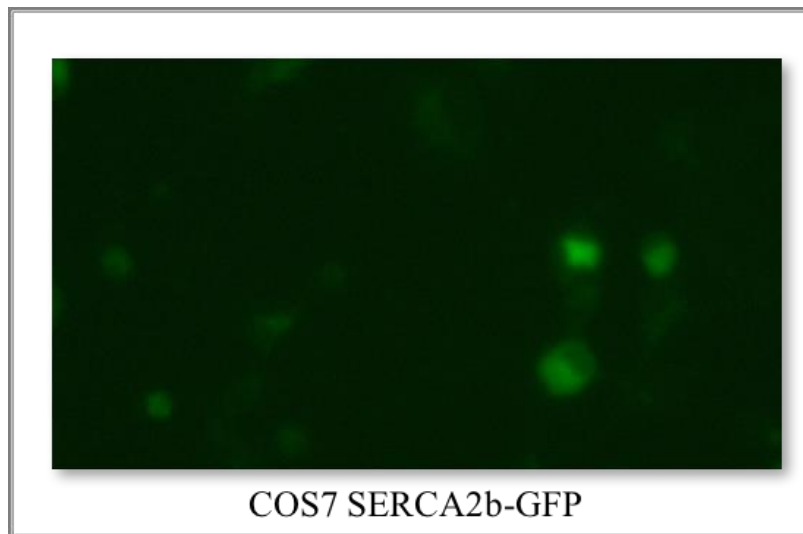


Figure 4-15: Microscope image of transfected COS7 with SERCA2b-GFP.

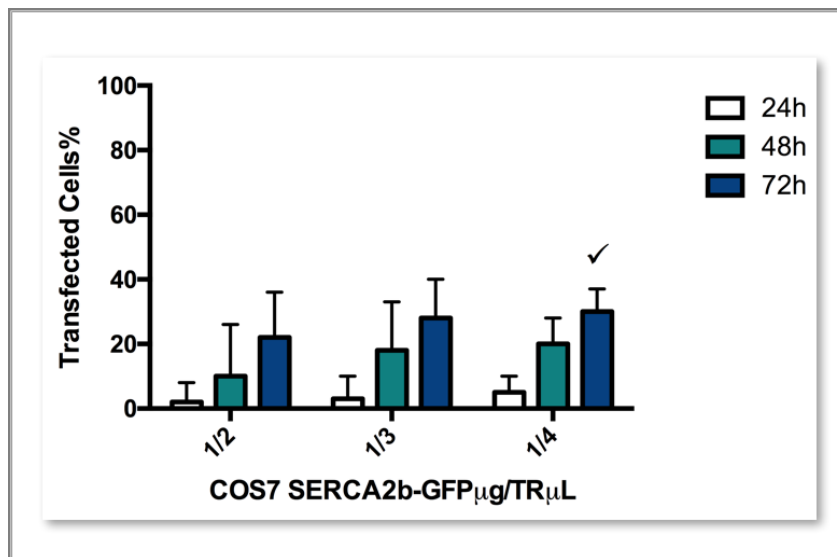


Figure 4-16: The ratio of transfected COS7 with SERCA2b-GFP.

COS7 cells were plated in a 24-well plate at a density of  $2 \times 10^4$  per well. Cells were transfected with SERCA2b-GFP at three conditions: 1  $\mu$ g DNA/2  $\mu$ L MP, 1  $\mu$ g DNA/3  $\mu$ L MP, and 1  $\mu$ g DNA/4  $\mu$ L MP. Every 24 hours, cells were examined under the fluorescence microscope, and the percentage of fluorescent cells was determined. Cells were transfected for 72 hours with 1  $\mu$ g SPCA1a-GFP plasmid and with 4  $\mu$ L MP, which had the best efficiency. The data are the mean  $\pm$  SD, n=3

#### 4.1.6.2 Analysis of SERCA2b-GFP Expression in COS7 by FACC

For confirmation of the transfection efficiency, cells were also analysed by FACC. (Figure 4-17) shows the amount of viable, transfected COS7 cells with SERCA2b-GFP was 27% compared to 71% viable non-transfected cells. It also shows about 1% non-viable transfected cells. Therefore, overexpressing SERCA2b has little effect on cell viability.

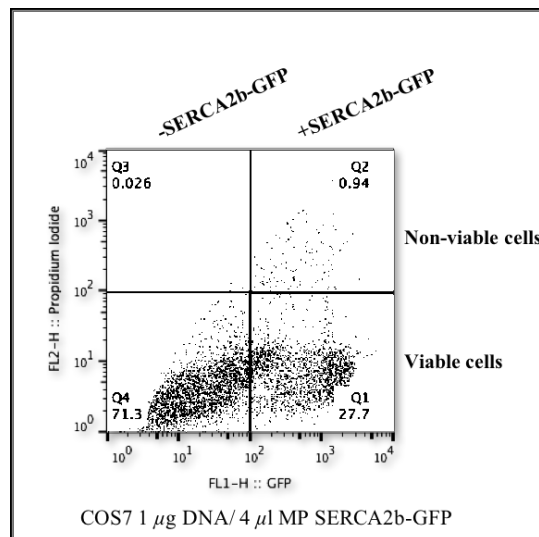


Figure 4-17: Flow cytometry measurement of transfected COS7 with SERCA2b-GFP.

COS7 cells were plated in 6-well cell culture plates for 24 hours. The cells were then transfected with SERCA2b-GFP for 72 hours. The number of transfected cells was measured by FACC. As shown in the figure, 71.3% of the cells were viable but not transfected, while 27.7% of the total number of the cells were viable and transfected with SERCA2b-GFP. Only < 1% of the cells were deemed to be non-viable.

#### **4.1.7 The Overexpression of SERCA2b-GFP in SH-SY5Y**

##### *4.1.7.1 Analysis of SERCA2b-GFP Expression in SH-SY5Y Cells*

To determine the best condition for transfecting SH-SY5Y with SERCA2b-GFP, the instructions for transfection were repeated for the four non-toxic transfection reagents. Cells were incubated with the plasmid for three days and examined by fluorescence microscopy every 24 hours. As shown in (Figure 4-18) and (Figure 4-19), very few cells were transfected with Metafectene Pro (MP).

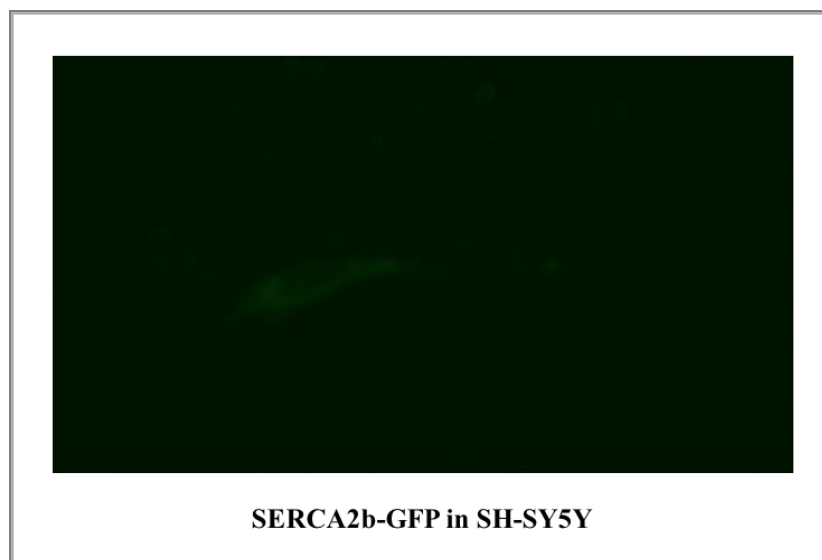


Figure 4-18: Microscope image of transfected SH-SY5Y with SERCA2b-GFP.

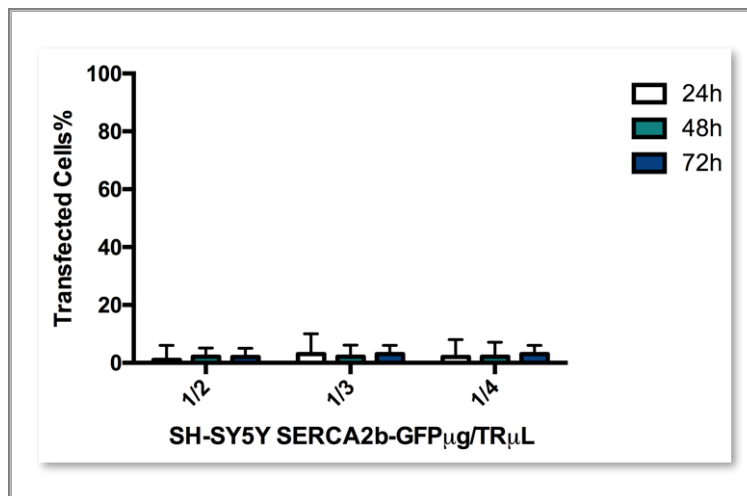


Figure 4-19: The ratio of transfected SH-SY5Y with SERCA2b-GFP.

SH-SY5Y cells were plated in a 24-well plate at a density of  $1 \times 10^4$  per well. Cells were transfected with SERCA2b-GFP and MP under three conditions: 1  $\mu\text{g}$  DNA/2  $\mu\text{L}$  MP, 1  $\mu\text{g}$  DNA/3  $\mu\text{L}$  MP, and 1  $\mu\text{g}$  DNA/4  $\mu\text{L}$  MP ( $\mu\text{g}$  plasmid /  $\mu\text{L}$  Metafectene Pro). Every 24 hours, the cells were examined under the fluorescence microscope, but few to no fluorescent cells were observed.

#### 4.1.7.2 Analysis of SERCA2b-GFP Expression in SH-SY5Y Cells by FACC

For further investigation as to whether SH-SY5Y cells were transfected with SERCA2b-GFP, cells were counted using FACC. As presented in (Figure 4-20), none of the cells were transfected.

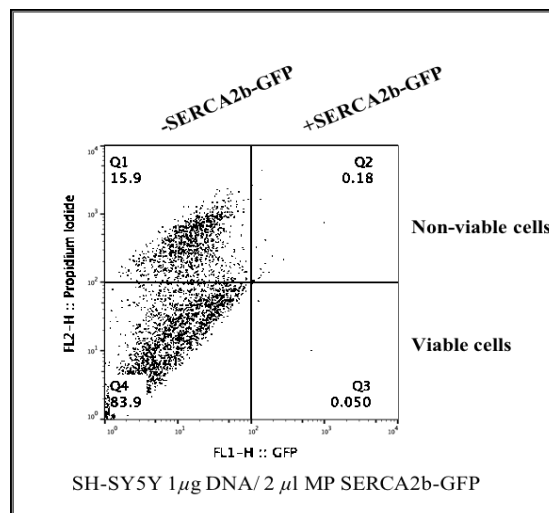


Figure 4-20: Flow cytometry measurement of transfected SH-SY5Y with SERCA2b-GFP.

SH-SY5Y cells were plated in 6-well cell culture plates for 24 hours. The cells were then transfected with SERCA2b-GFP for 72 hours. The number of transfected cells was measured by FACC. As shown in the figure, 83.9% of the cells were viable without transfection, and around 16% of the total number of the cells were non-viable and non-transfected with SERCA2b-GFP. Very few cells were transfected with SERCA2b-GFP.

## **4.1.8 The Effect on Cell Viability of Antipsychotic Drugs on COS7 Transfected with SPCA1a-GFP**

### *4.1.8.1 Crystal Violet Cell Viability Assay*

After determining the best condition for transfection with SPCA1a-GFP, the cells were treated with the antipsychotic drugs to study if overexpression of this Ca<sup>2+</sup> pump gives any protection against cell death. Following the instructions for transfection, cells were plated in 24-well cell culture plates and transfected with the SPCA1a-GFP plasmid or the empty plasmid pcDNA (used as a control for the transfection) for 72 hours. After examining the cells under the microscope to ensure that transfection had taken place, cells were treated with the LC<sub>50</sub> for each drug and left for 24 hours. Then crystal violet cell viability assays were undertaken. (Figure 4-21) shows the results of the four different drugs. (A) shows the effect of chlorpromazine on COS7 alone, on COS7 with pcDNA, and on transfected COS7 with SPCA1a-GFP. (B) shows the effect of trifluoperazine on COS7 alone, on COS7 with pcDNA, and on transfected COS7 with SPCA1a-GFP. (C) shows the effect of olanzapine on COS7 alone, on COS7 with pcDNA, and on transfected COS7 with SPCA1a-GFP. Finally, (D) shows the effect of quetiapine on COS7 alone, on COS7 with pcDNA, and on transfected COS7 with SPCA1a-GFP. None of the results showed significant protection against cell toxicity due to these drugs upon overexpression of SPCA1a-GFP.

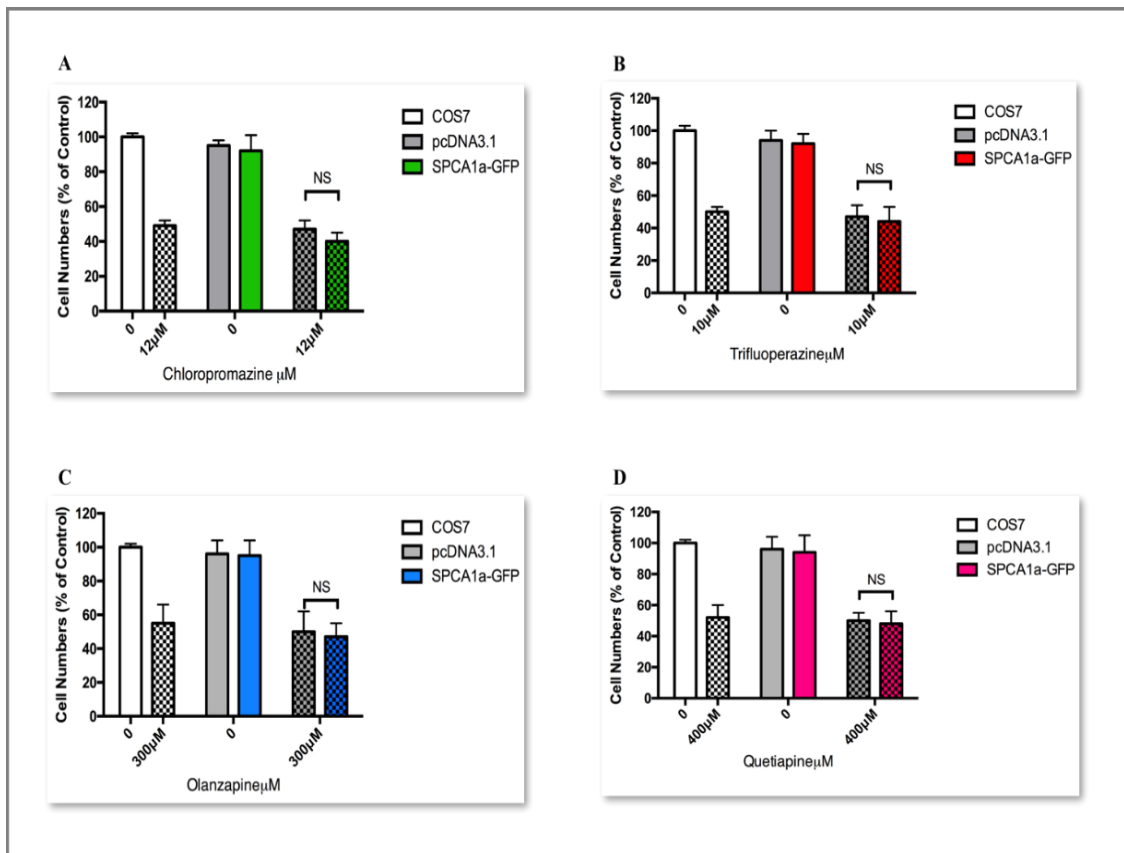


Figure 4-21: The effect on cell viability of FGAs and SGAs on COS7 cells overexpressing SPCA1a-GFP.

COS7 cells were plated in 24-well cell culture plates at a density of  $2 \times 10^4$  per well for 24 hours. After the 24 hours, cells were transfected with SPCA1a-GFP plasmid and incubated at  $37^\circ\text{C}$  for 72 hours. Cells were then treated for 24 hours with the  $\text{LC}_{50}$  of each drug, namely (A) chlorpromazine  $12 \mu\text{M}$ , (B) trifluoperazine  $10 \mu\text{M}$ , (C) olanzapine  $300 \mu\text{M}$ , and (D) quetiapine  $400 \mu\text{M}$ . Cells were then stained with crystal violet, and the absorbance was read at  $590 \text{ nm}$ . The results are presented as % to the control (non-treated, non-transfected COS7 cells) of mean  $\pm$  SD, repeated 3 times. (cross-hatching indicates cells treated with drugs, coloured are transfected)

## **4.1.9 The Effect on Cell Viability of Antipsychotic Drugs on SH-SY5Y Transfected with SPCA1a-GFP**

### *4.1.9.1 Crystal Violet Assay*

After determining the best condition for transfection with SPCA1a-GFP, the transfected cells were treated with the drugs to study whether protection against cell death was present. Following the instructions for transfection, cells were plated in 24-well cell culture plates and transfected with SPCA1a-GFP plasmid and empty pcDNA plasmid (used as a control for the transfection) for 72 hours. After examining the cells under the microscope to ensure transfection had taken place, cells were treated with the  $LC_{50}$  for each drug and left for 24 hours. The crystal violet cell viability assay was then undertaken. (Figure 4-22) shows the results of the four different drugs. (A) shows the effect of chlorpromazine on SH-SY5Y alone, when transfected with empty plasmid (pcDNA), and when transfected with SPCA1a-GFP. (B) shows the effect of trifluoperazine on SH-SY5Y alone, when transfected with pcDNA, and when transfected with SPCA1a-GFP. (C) shows the effect of olanzapine on SH-SY5Y alone, when transfected with pcDNA, and when transfected with SPCA1a-GFP. Finally, (D) shows the effect of quetiapine on SH-SY5Y alone, when transfected with pcDNA, and when transfected with SPCA1a-GFP. Again, as with the COS7 cells, none of the results showed significant protection against cell death by these drugs in SH-SY5Y cells overexpressing SPCA1a-GFP.

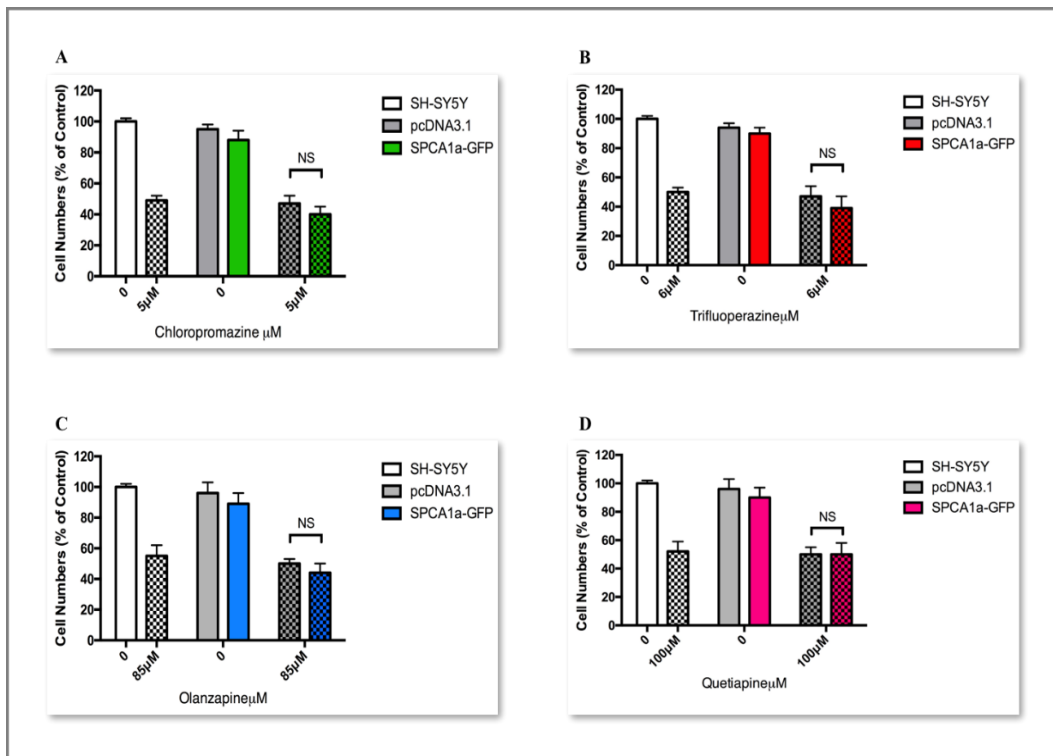


Figure 4-22: The effects of the FGAs and SGAs on cell viability of SH-SY5Y cells in the presence and absence of SPCA1a-GFP.

SH-SY5Y cells were plated in 24-well cell culture plates at a density of  $1 \times 10^4$  per well for 24 hours. After the 24 hours, cells were transfected with SPCA1a-GFP and incubated at 37°C for 72 hours. Cells were then treated for 24 hours with the  $LC_{50}$  of each drug, namely with (A) chlorpromazine 5 μM, (B) trifluoperazine 5 μM, (C) olanzapine 85 μM, and (D) quetiapine 100 μM. After 24 hours, cells were stained with crystal violet, and the absorbance was read at 590 nm. The results are presented as % compared to the control (non-treated, non-transfected SH-SY5Y cells) of mean  $\pm$  SD, repeated 3 times. (cross-hatching indicates cells treated with drugs, coloured are transfected)

#### *4.1.9.2 Co-localisation of SPCA1a-GFP in SH-SY5Y with Antipsychotic Drugs*

To investigate whether the localisation of SPCA1a-GFP was altered in SH-SY5Y cells following treatment with these drugs, SPCA1a-GFP-transfected cells were also labelled with both MitoTracker Red (to identify mitochondria) and DAPI (a blue fluorescent stain to identify nuclei). After labelling, the cells were fixed and imaged under the fluorescence microscope to detect any co-localisation (Figure 4-23). In SPCA1a-GFP-transfected control SH-SY5Y cells, there was little co-localisation between the SPCA1 (green) and either the mitochondria (red) or nuclei (blue), as determined by Pearson's coefficient values for pixel colour overlap using the Fiji and JACops plug-ins. These values, with  $r$  values of between  $<0.1$  and  $0.3$ , are indicative of little co-localisation occurring. However, what was clear from (Figure 4-23), was that SPCA1a did appear to localise around the edges of the nuclei, which is consistent with the findings of Wootton et al. (2004) and Baron et al. (2010), who also showed that SPCA1 tended to localise close to the nuclear membrane, a site where the Golgi body is typically found (Wootton et al., 2004). Next the SPCA1a-GFP-transfected SH-SY5Y cells were treated with the FGA chlorpromazine to investigate whether this altered its localisation. Following 24-hour treatment with this drug, the transfected cells were stained with MitoTracker and DAPI. (Figure 4-24), shows again little overlap (co-localisation) with SPCA1a and the mitochondria and nuclei as determined by the Pearson's coefficient values.

The location of SPCA1a-GFP was again noted to be mostly around the exterior of the nucleus.

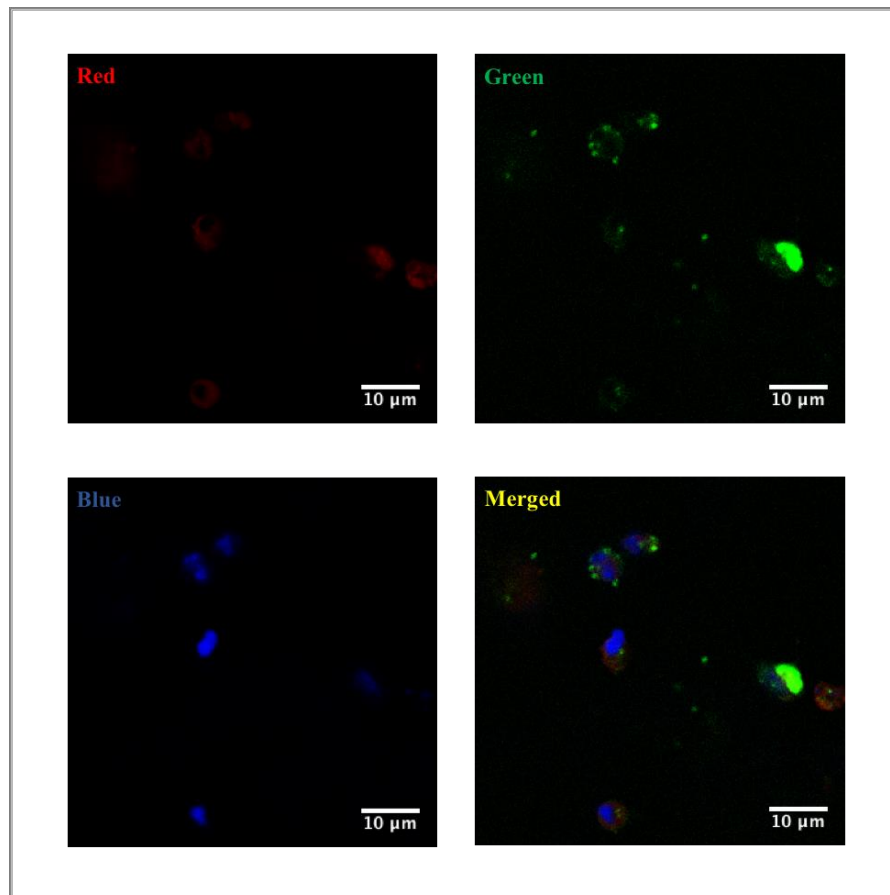


Figure 4-23: SH-SY5Y with SPCA1a-GFP control.

SH-SY5Y cells were plated on a cover slip placed on 6-well plate for 24 hours then transfected with SPC1a-GFP for 72 hours. Cells were then stained with 5 μM of MitoTracker for 30 minutes. After fixing the cells, a drop of DAPI mounting media was added, and cells were visualised with 100 oil magnification. 20 cells of each sample were used to calculate the  $r$ , experiment repeated 3 times.

GFP green channel  $\lambda_{exc} = 488 \text{ nm}$ ,  $\lambda_{em} = 502 \text{ nm}$

MitoTracker deep red FM channel  $\lambda_{exc} = 644 \text{ nm}$ ,  $\lambda_{em} = 665 \text{ nm}$

Fluoroshield with DAPI blue channel  $\lambda_{exc} = 360 \text{ nm}$ ,  $\lambda_{em} = 460 \text{ nm}$

Merged image of Red and Green; Pearson's Coefficient:  $r = 0.25$ .

Merged image of Blue and Green; Pearson's Coefficient:  $r = 0.10$

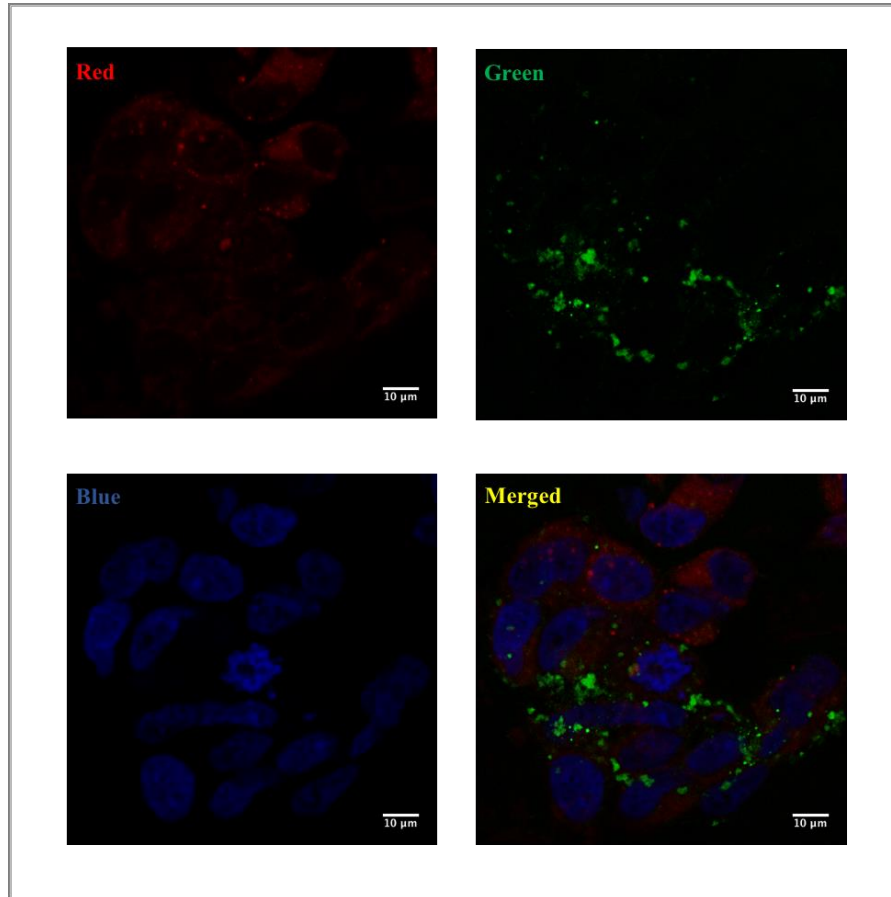


Figure 4-24: SH-SY5Y with SPCA1a-GFP treated with chlorpromazine.

SH-SY5Y cells were plated on a cover slip placed on a 6-well plate for 24 hours then transfected with SPCA1a-GFP for 72 hours. Cells were treated with  $LC_{50}$  for chlorpromazine for 24 hours then stained with  $5 \mu\text{M}$  of MitoTracker for 30 minutes. After fixing the cells, a drop of DAPI mounting media was added, and cells were visualised with 100 oil magnification. 20 cells of each sample were used to calculate the  $r$ , experiment repeated 3 times.

GFP green channel  $\lambda_{exc} = 488 \text{ nm}$ ,  $\lambda_{em} = 502 \text{ nm}$

MitoTracker deep red FM channel  $\lambda_{exc} = 644 \text{ nm}$ ,  $\lambda_{em} = 665 \text{ nm}$

Fluoroshield with DAPI blue channel  $\lambda_{exc} = 360 \text{ nm}$ ,  $\lambda_{em} = 460 \text{ nm}$

Merged image of Red and Green; Pearson's Coefficient:  $r=0.22$

Merged image of Blue and Green; Pearson's Coefficient:  $r=0.036$

#### **4.1.10 The Effect on Cell Viability of Antipsychotic Drugs on COS7 Transfected with SERCA2b-GFP**

##### *4.1.10.1 Effects of SERCA2b-GFP transfection on Cell Viability in the Presence of FGAs and SGAs*

As SH-SY5Y cells could not be transfected with SERCA2b-GFP, for the subsequent studies presented below, only COS7 cells were used.

After determining the best condition for transfection with SERCA2b-GFP, the transfected cells were treated with the drugs to study if protection against cell death was present. Following the instructions for transfection, cells were plated in 24-well cell culture plates and transfected with SERCA2b-GFP and pcDNA (used as a control for the transfection) for 72 hours. After examining the cells under the fluorescence microscope to ensure transfection took place, cells were treated with the  $LC_{50}$  for each drug and left for 24 hours. Then crystal violet cell viability assays were undertaken. (Figure 4-25), shows the results of the four different drugs. (A) shows the effect of chlorpromazine on COS7 cells alone, on COS7 transfected with pcDNA, and on COS7 cells transfected with SERCA2b-GFP. There was a significant increase in cell numbers (22%) with SERCA2b-GFP expressing cells compared to the effect of the drug on cells transfected with pcDNA (\*\* $P=0.002$ ). (Figure 4-25 B) shows the effect of trifluoperazine in COS7 cells transfected with SERCA2b-GFP. Again, the results show a significant increase in cell numbers of about 20% in SERCA2b-GFP-transfected cells compared to pcDNA-transfected

cells treated with trifluoperazine (\*\*P=0.0064). For the SGA, similar results indicative of SERCA2b protection were also observed. (Figure 4-25 C) shows a statistically significant increase of 12% on cell viability of the effect of olanzapine on COS7 cells transfected with SERCA2b-GFP compared to pcDNA-transfected cells (\*P = 0.0412). In (Figure 4-25 D), a similar increase (15%) in cell viability with quetiapine was observed (\*P= 0.0183).

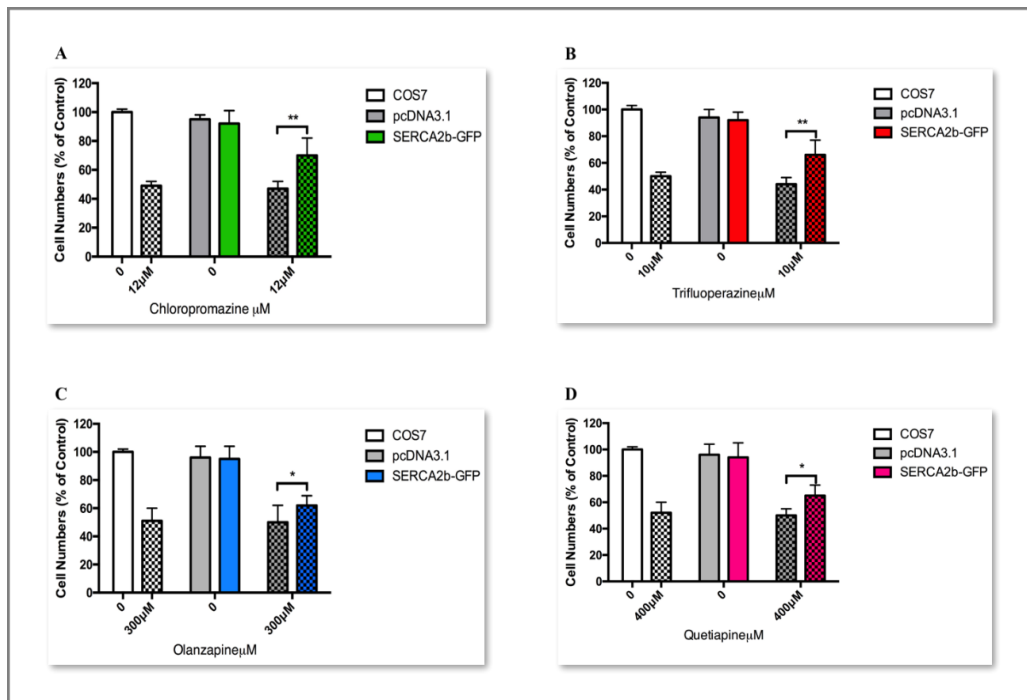


Figure 4-25: The effect of FGAs and SGAs on COS7 cells in the presence and absence of SERCA2b-GFP.

COS7 cells were plated in 24-well cell culture plates at a density of  $2 \times 10^4$  per well for 24 hours. After the 24 hours, cells were transfected with either SERCA2b-GFP plasmid or empty plasmid (pcDNA) and incubated at  $37^\circ\text{C}$  for 72 hours. Cells were then treated for 24 hours with the  $\text{LC}_{50}$  of each drug, namely with (A) chlorpromazine 12  $\mu\text{M}$ , (B) trifluoperazine 10  $\mu\text{M}$ , (C) olanzapine 300  $\mu\text{M}$ , and (D) quetiapine 400  $\mu\text{M}$ . After 24 hours, cells were stained with crystal violet, and the absorbance was read at 590 nm. The results are presented as % to the control (non-treated, non-transfected COS7 cells) of the mean  $\pm$  SD, repeated 3 times. Results shows a significant increase in cell number  $**P \leq 0.01$ ,  $*P \leq 0.05$ . Cross-hatching indicates cells treated with drugs, coloured are transfected.

#### *4.1.10.2 Co-localisation of SERCA2b-GFP in COS7 with Antipsychotic Drugs*

After transfecting the cells with SERCA2b-GFP, cells were treated with the LC<sub>50</sub> for chlorpromazine for 24 hours. Cells were stained with 0.5 µM of MitoTracker for 30 minutes and then with DAPI containing histology mounting media. (Figure 4-26), shows control images from confocal microscopy of COS7 transfected with SERCA2b-GFP alone. As shown in the figure, SERCA2b-GFP gave a diffuse reticulate type distribution inside the cells consistent with its localisation being around the endoplasmic reticulum. This type of distribution has also been observed for SERCA-GFP in other studies (Newton et al., 2003; Baron et al., 2010). Again, consistent with this observation, a co-localisation analysis of SERCA2b (green) with either mitochondria (red) or nuclei (blue) showed little overlap as determined by the Pearson's coefficient values ( $r$ ) of around 0.3 for each.

(Figure 4-27), shows COS7 cells transfected with SERCA2b-GFP and then treated with chlorpromazine (12 µM) for 24 hours. As can be seen, SERCA2b-GFP still displays a reticulate diffuse distribution throughout the body of the cell. However, co-localisation analysis indicates that there is a greater degree of overlap between SERCA and mitochondria as compared to control cells (Pearson's coefficient  $r = 0.69$  in drug-treated cells, compared to untreated cells where the coefficient  $r = 0.30$ ).

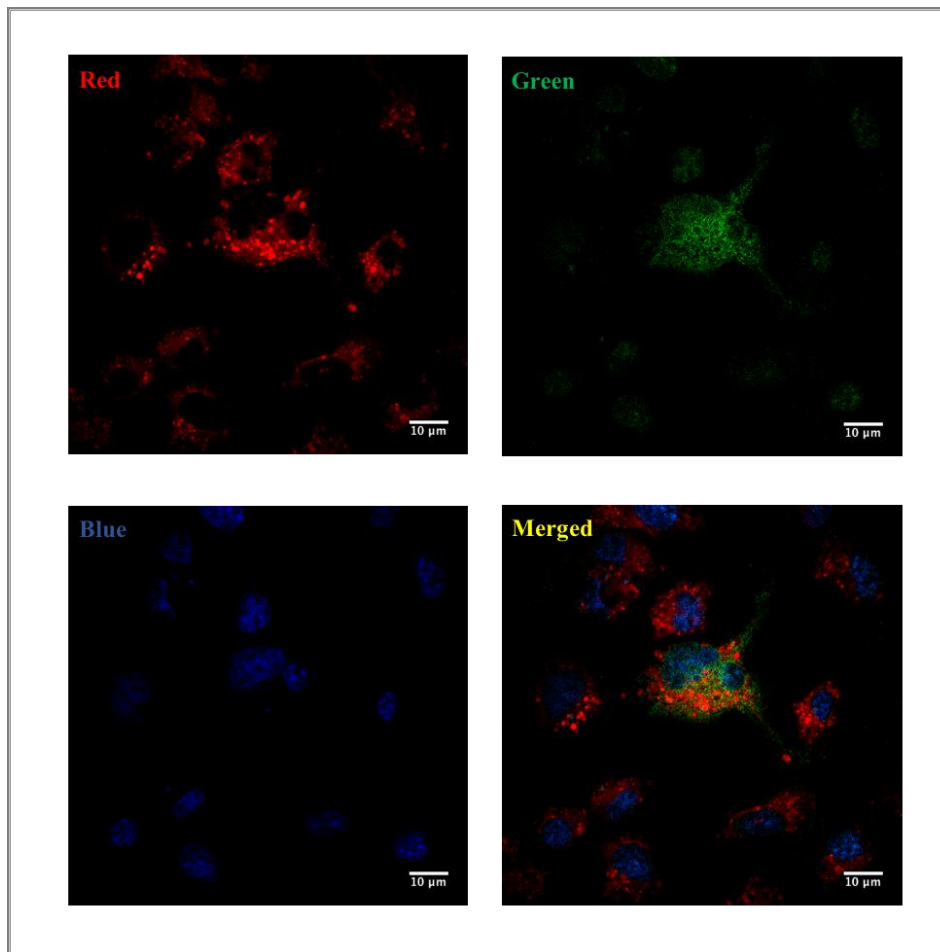


Figure 4-26: Control COS7 with SERCA2b.

COS7 cells were plated on cover slips and placed into 6-well plates for 24 hours then transfected with SERCA2b-GFP for 72 hours. Cells were then stained with 5  $\mu$ M of MitoTracker for 30 minutes after fixing with DAPI mounting media and visualised with x100 oil magnification. 20 cells of each sample were used to calculate the  $r$ , experiment repeated 3 times.

GFP green channel  $\lambda_{exc} = 488$  nm,  $\lambda_{em} = 502$  nm

MitoTracker deep red FM channel  $\lambda_{exc} = 644$  nm,  $\lambda_{em} = 665$  nm

Fluoroshield with DAPI blue channel  $\lambda_{exc} = 360$  nm,  $\lambda_{em} = 460$  nm

Merged image of Red and Green; Pearson's Coefficient:  $r = 0.30$ .

Merged image of Blue and Green; Pearson's Coefficient:  $r = 0.35$

Images are representative of three experiments.

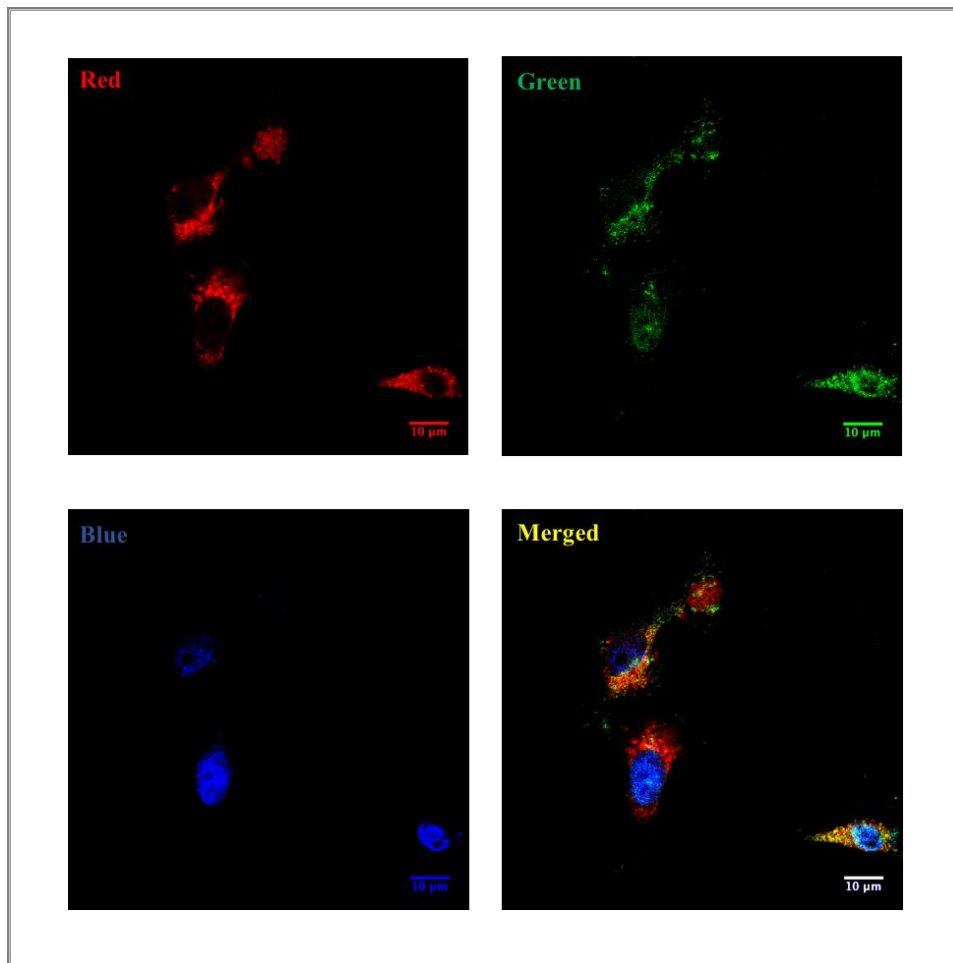


Figure 4-27: COS7 with SERCA2b treated with chlorpromazine.

COS7 cells were plated on a cover slip placed on 6-well plate for 24 hours then transfected with SERCA2b-GFP for 72 hours. Cells were treated with  $LC_{50}$  for chlorpromazine for 24 hours then stained with 5  $\mu$ M of MitoTracker for 30 minutes. After fixing the cells, a drop of DAPI mounting media was added, and cells were visualised with 100 oil magnification. 20 cells of each sample were used to calculate the  $r$ , experiment repeated 3 times.

GFP green channel  $\lambda_{exc} = 488$  nm,  $\lambda_{em} = 502$  nm

MitoTracker deep red FM channel  $\lambda_{exc} = 644$  nm,  $\lambda_{em} = 665$  nm

Fluoroshield with DAPI blue channel  $\lambda_{exc} = 360$  nm,  $\lambda_{em} = 460$  nm

Merged image of Red and Green; Pearson's Coefficient:  $r = 0.69$

Merged image of Blue and Green; Pearson's Coefficient:  $r = 0.41$

## **4.2 Discussion**

Previous studies have suggested that a failure in the regulation of neuronal  $\text{Ca}^{2+}$  homeostasis plays a role in Alzheimer's disease and other neurodegenerative diseases (Mattson, 2007; Bezprovanny and Mattson, 2008). To date, both FGAs and SGAs are commonly used to reduce agitation and aggression in some patients that have these neurodegenerative conditions (Ostinelli et al., 2017). The aim of this chapter was to investigate the involvement of  $\text{Ca}^{2+}$  and particularly  $\text{Ca}^{2+}$  pumps in cell death induced by antipsychotic drugs, since earlier studies have indicated that some FGAs were able to specifically inhibit SERCA  $\text{Ca}^{2+}$  pumps (Khan et al., 2000).

### **4.2.1 The Effect of BAPTA-AM**

The results presented in this study as seen in (Figure 4-1) and (Figure 4-2) clearly demonstrated that there was a significant protection against both generations of antipsychotic drugs in the presence of BAPTA-AM. This result therefore indicates the involvement of  $\text{Ca}^{2+}$  in cell death induced by the antipsychotic drugs, which could possibly be due to the drugs' effects upon dys-regulation of  $\text{Ca}^{2+}$  homeostasis (Kodavanti et al., 1993). Other studies have also shown that the neurotoxic effects of some of these drugs could possibly be by inhibiting  $\text{Ca}^{2+}$  pumps (Kodavanti et al., 1993; Bhattacharyya and Sen 1999; Khan et al., 2000).

### **4.2.2 ER Stress**

To assess whether excessive depletion of  $\text{Ca}^{2+}$  from the ER by inhibiting  $\text{Ca}^{2+}$  pumps, and hence ER stress, was a major factor in the cytotoxicity of these drugs, a marker for the ER stress response was measured. The data presented in this chapter demonstrated that FGAs induced ER stress by the activation of the CHOP pathway. The results were mixed for the SGAs. Other previous studies have similarly reported the involvement of ER stress in the presence of antipsychotic drugs (Ozasa et al., 2013; Laressergues et al., 2012). Recent studies have suggested that ER stress, which leads to increased expression of CHOP, can elevate the Trail-R2 (or other death receptors), which in turn can lead to activation of caspase-8 and apoptosis, independent of this receptor binding its death ligand (Cano-Gonzales et al., 2018; Yamaguchi and Wang 2004; Lu et al., 2014). This process could well explain the results seen in Chapter 3, where the FGAs caused apoptosis through the caspase-8 pathway.

### **4.2.3. Overexpression of $\text{Ca}^{2+}$ Pumps**

After ascertaining that these drugs caused cell death by a  $\text{Ca}^{2+}$  mediated process that also induced ER stress, the next step was to determine whether the effects on cell viability of these drugs was a consequence of the general elevation of cytosolic  $\text{Ca}^{2+}$  or more specifically a consequence of the depletion of  $\text{Ca}^{2+}$  from the ER  $\text{Ca}^{2+}$  store that initiated the ER stress response. To address this question, the cells were

transfected to overexpress either SERCA2b-GFP, which specifically reduced the cytosolic  $\text{Ca}^{2+}$  level by refilling the ER (and therefore reducing ER stress), or by overexpressing SPCA1a-GFP, which reduced the cytosolic  $\text{Ca}^{2+}$  by filling the Golgi body  $\text{Ca}^{2+}$  store. The results presented in this chapter clearly showed that only overexpression of SERCA was able to improve cell viability upon subsequent treatment with these drugs. This finding would therefore lead to the conclusion that these antipsychotic drugs cause cell death, at least in part, by the activation of the ER stress response.

#### **4.2.4 Co-localisation studies**

The major finding from the co-localisation experiments was that there was some potential for SERCA to partially co-localise with the mitochondria upon treatment with the FGA chlorpromazine. There is no evidence within the scientific literature to indicate that under any conditions SERCA can be found in the mitochondria. However, several reports have described a re-arrangement of organelles within the cytoplasm of the cell, such that the ER membrane and the mitochondrial membrane come into very close proximity, especially under stress conditions, in order to allow for efficient  $\text{Ca}^{2+}$  and protein transfer between the two organelles (Szabadkai and Rizzuto, 2004; Michelangeli et al., 2005; Iacqua et al., 2017). The increased “co-localisation” between SERCA and the mitochondria could well be due to these mitochondria-ER contacts

## **Chapter 5:**

# **The Effects of Antipsychotic Drugs in Cells Overexpressing Regucalcin**

## **5. The Effects of Antipsychotic Drugs in Cells Overexpressing Regucalcin**

### **Introduction**

Regucalcin (RGN) is a  $\text{Ca}^{2+}$  binding protein that plays an important role in regulating signal transduction pathways and intracellular  $\text{Ca}^{2+}$  homeostasis (Yamaguchi, 2014). Studies have shown that deficiency of RGN is linked to dysregulation of oxidative stress and the induction of apoptosis (Yamaguchi, 2012a). RGN is identified to have numerous controlling functions in mammalian cells; specifically, intracellular  $\text{Ca}^{2+}$  homeostasis is controlled by RGN through effects on several types of  $\text{Ca}^{2+}$  ATPase pumps, such as the plasma membrane  $\text{Ca}^{2+}$  ATPase (PMCA) and the sarco-/endoplasmic reticulum  $\text{Ca}^{2+}$  ATPase (SERCA), which are ubiquitous in many cell types (Yamaguchi, 2000). Several studies have suggested that RGN also plays an essential role in neuronal cells (Yamaguchi, 2012). It is expressed in the neuronal cells of rat brains, and its expression decreases with age (Yamaguchi et al., 1999; Yamaguchi, 2012). RGN is also found in the kidney cortex of rats (Shimokawa and Yamaguchi, 1992; Yamaguchi and Isogai, 1993). Previous studies have shown that RGN is highly expressed in kidney and particularly kidney proximal tubular cells (Yamaguchi, 2012b), and it has been shown to play a role in the protection of kidney cells against cell death (Nakagawa and Yamaguchi, 2005). The aim of this chapter is to investigate whether the toxicity caused by first-generation antipsychotics (FGAs) and second-generation antipsychotics (SGAs)

can be protected against by overexpressing RGN in neuronal cells (SH-SY5Y) and kidney cells (COS7).

## **5.1 Results**

### **5.1.1 The Overexpression of RGN-GFP in SH-SY5Y**

#### *5.1.1.1 Analysis of RGN-GFP Expression in SH-SY5Y*

To determine the best condition for transfecting SH-SY5Y cells with a plasmid containing the RGN-GFP gene, the instructions for transfection, were repeated for the four non-toxic transfection reagents. Cells were incubated with the RGN-GFP plasmid for three days and examined under the fluorescence microscope every 24 hours. First, any toxic effects of the transfection reagents on the cells were determined. Then the efficiency of the transfection was investigated. The best transfection reagent with the lowest toxic effect is Metafectene Pro (MP), which was therefore used for transfection. As shown in (Figure 5-1) and (Figure 5-2), none of the cells were transfected, even after trying to optimise the conditions.

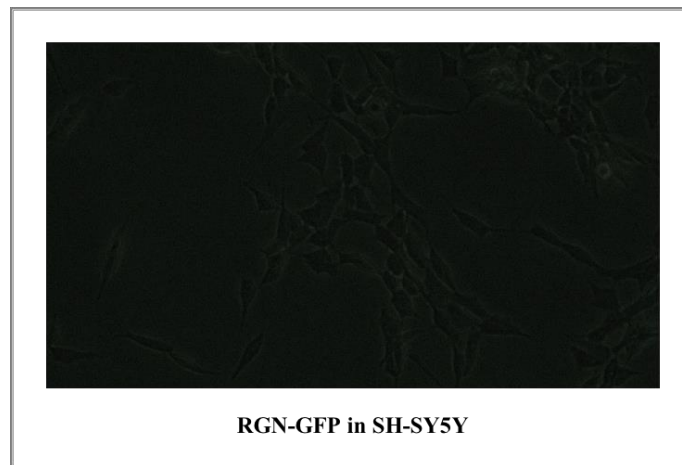


Figure 5-1: Microscope image of transfected SH-SY5Y with RGN-GFP plasmid.

After transfecting SH-SY5Y with RGN-GFP for three days, none of the cells were transfected.

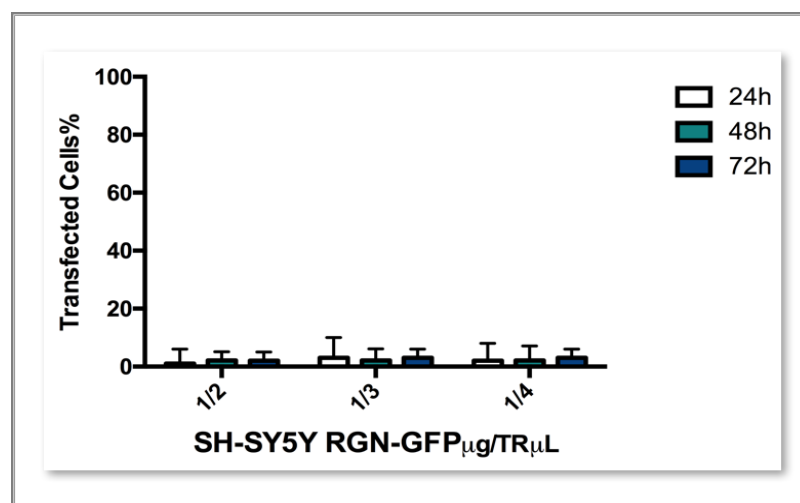


Figure 5-2: The ratio of transfected SH-SY5Y with RGN-GFP.

SH-SY5Y cells were plated in a 24-well plate at a density of  $1 \times 10^4$  per well. Cells were transfected with RGN-GFP at three conditions: 1  $\mu\text{g}$  DNA/2  $\mu\text{L}$  MP, 1  $\mu\text{g}$  DNA/3  $\mu\text{L}$  MP, and 1  $\mu\text{g}$  DNA/4  $\mu\text{L}$  MP. Every 24 hours, cells were examined under the fluorescence microscope for three days. There were very few fluorescent cells.

#### 5.1.1.2 Analysis of RGN-GFP Transfection in SH-SY5Y Using FACC

To further investigate whether SH-SY5Y cells were transfected with RGN-GFP, cells were analysed using FACS. Un-transfected cells were stained with propidium iodide (PI) and analysed as the control see (Figure 5-3). 99% of the cells were deemed to be viable. Cells transfected with RGN-GFP were then analysed. As shown in (Figure 5-4), again less than 0.2% of the cells were transfected, even though about 96% were deemed to be alive. Therefore, from these results, it was clear that SH-SY5Y cells proved difficult to transfect with the RGN-GFP plasmid. As such, no further experiments to investigate the effect of RGN on antipsychotic drugs were undertaken with these cells.

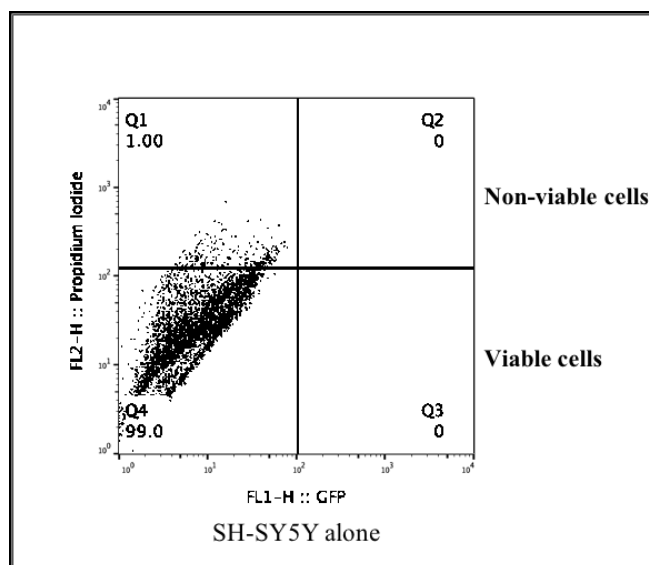


Figure 5-3: Flow cytometry measurement of SH-SY5Y alone.

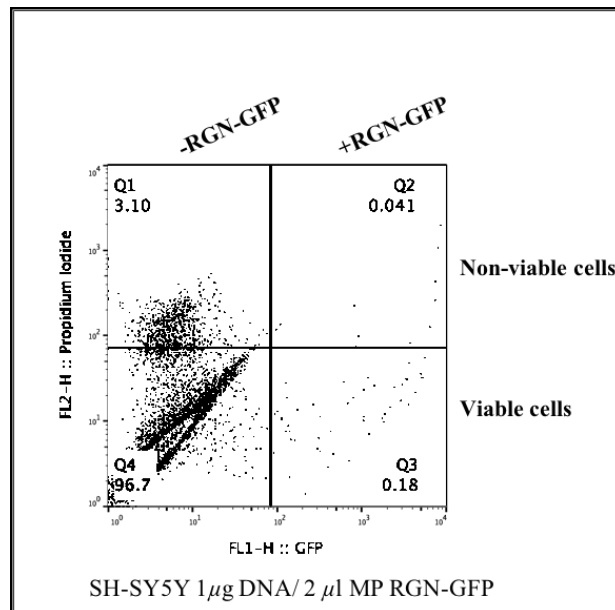


Figure 5-4: Flow cytometry measurement of transfected SH-SY5Y with RGN-GFP.

SH-SY5Y cells were plated in a 6-well cell culture plate for 24 hours. The cells were then transfected with RGN-GFP for 72 hours. The number of transfected cells was measured by FACC. As shown in Figure 5-4, 96.7% of the cells were viable without transfection, 3% of the total number of the cells were non-viable and non-transfected with RGN-GFP, and  $\leq 0.2\%$  of the viable cells were transfected with RGN-GFP. The scatter plots are representative of three experiments.

## **5.1.2 The Overexpression of RGN-GFP in COS7**

### *5.1.2.1 Analysis of RGN-GFP Expression in COS7 Cells*

Examination of all the transfection reagents showed that Metafectene Pro (MP) has the lowest toxic effect and highest transfection efficiency. It was therefore used in this study. COS7 cells were plated in a 24-well cell culture plate for 24 hours then transfected with RGN-GFP following the instructions. Transfection took place under three different conditions: 1 µg DNA/2 µL MP, 1 µg DNA/3 µL MP, and 1 µg DNA/4 µL MP. The cells were examined using the fluorescence microscope for three days to assess levels of transfection. (Figure 5-5) shows the best results of the transfection after 72 hours under the condition of 1 µg RGN-GFP plasmid and 2 µL MP. (Figure 5-6) represents the percentage of transfected cells for each condition during the three days. The highest efficiency was with 1 µg DNA/2 µL MP, which gave about 30–40% transfection efficiency.

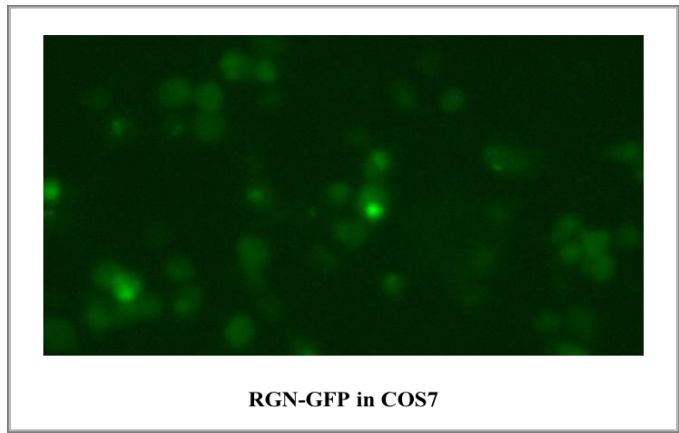


Figure 5-5: Microscope image of fluorescent COS7 transfected with 1  $\mu\text{g}$  RGN-GFP/ 2  $\mu\text{L}$  MP for 72 hours.

Under these conditions, 30–40% of the cells were transfected.

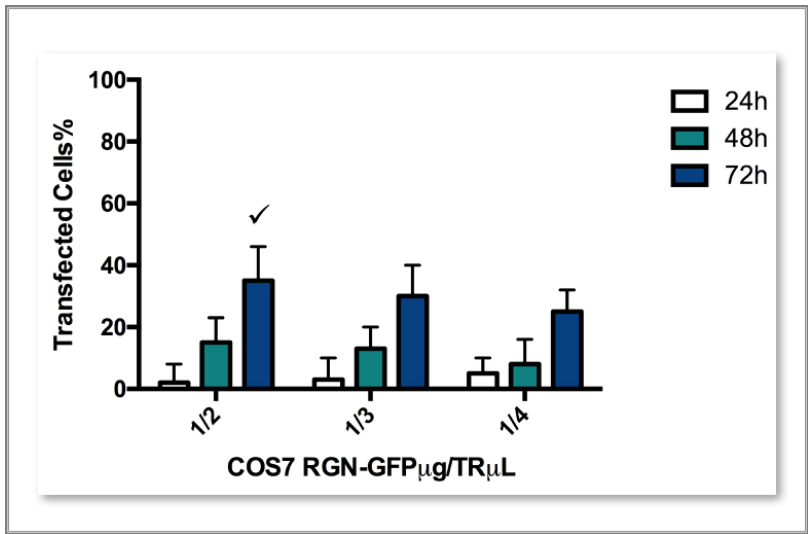


Figure 5-6: The ratio of transfected COS7 with RGN-GFP.

COS7 cells were plated in a 24-well plate at a density of  $2 \times 10^4$  per well. Cells were transfected with RGN-GFP using three conditions 1  $\mu\text{g}$  DNA/2  $\mu\text{L}$  MP, 1  $\mu\text{g}$  DNA/3  $\mu\text{L}$  MP and 1  $\mu\text{g}$  DNA/4  $\mu\text{L}$  MP. Every 24 hours, cells were examined under fluorescence microscopy, and the percentage was calculated by counting the numbers of fluorescent cells against all cells under brightfield. Cells transfected for 72 hours with 1  $\mu\text{g}$  RGN-GFP with 2  $\mu\text{L}$  MP showed the best transfection efficiency.

#### *5.1.2.2 Analysis of RGN-GFP Expression in COS7 by FACC*

FACC was used to determine the number of fluorescent cells following transfection. Following the same procedure for transfection, cells were seeded in a 6-well cell culture plate and transfected with RGN-GFP for 72 hours. Cells were then trypsinised with 0.05% trypsin-EDTA and centrifuged at 1000 rpm for 2 minutes. The cell pellet was re-suspended with PBS containing 2% FBS and 3  $\mu$ M PI and transferred to a FACC tube. (Figure 5-7) shows the result of FACC analysis for COS7 alone (as a control), which showed 100% live cells. (Figure 5-8), represents the result of COS7 transfected with RGN-GFP under the optimal condition (1  $\mu$ g DNA/2  $\mu$ L MP). The results showed that 66.3% were viable and un-transfected cells, and 33.1% were viable and transfected cells, with about 0.5% of all cells non-viable.

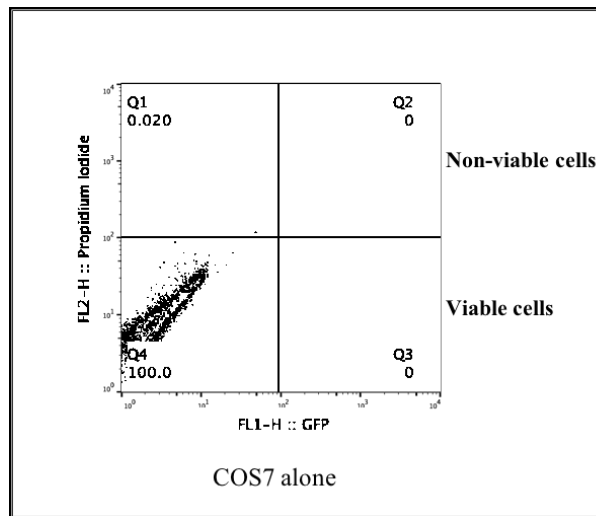


Figure 5-7: Flow cytometry analysis of COS7 alone.

Cells were treated with PI to determine non-viable cells.

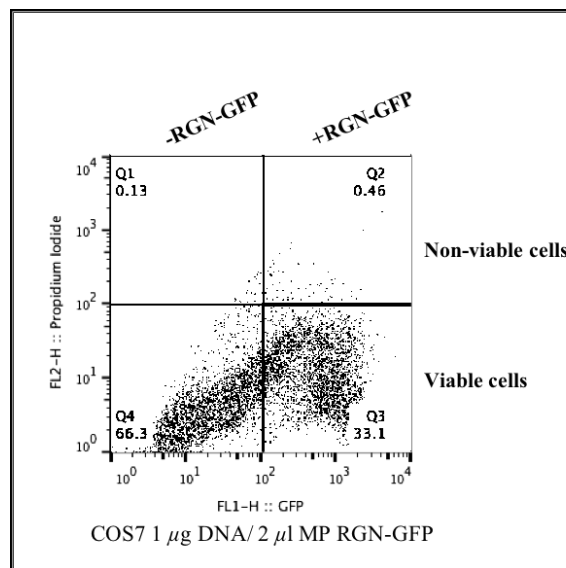


Figure 5-8: Flow cytometry measurement of transfected COS7 with RGN-GFP.

COS7 cells were plated in a 6-well cell culture plate for 24 hours. The cells were then transfected with RGN-GFP for 72 hours. The number of transfected cells was measured by FACC. As shown in the figure, 66.3% of the cells were viable but not transfected, 33.1% of the total number of the cells were viable and transfected with RGN-GFP, and only 0.46% of the cells were transfected and non-viable.

### **5.1.3 The Effect on Cell Viability of Antipsychotic Drugs in COS7**

#### **Cells Transfected with RGN-GFP**

##### *5.1.3.1 Crystal Violet Cell Viability Assay*

After determining the best conditions for transfection with RGN-GFP, transfected cells were treated with the FGAs and SGAs to study whether RGN gives some protection against cell death. Following the instructions for transfection, cells were plated in 24-well cell culture plates and transfected with RGN-GFP plasmid and empty plasmid pcDNA (used as a control for the transfection) for 72 hours. After examining the cells under fluorescence microscopy to ensure transfection had occurred, the cells were treated with the LC<sub>50</sub> for each drug and left for 24 hours. Then cell viability was measured using crystal violet assay. (Figure 5-9), shows the results of the effect of RGN-GFP on COS7 with the four different drugs. (A) shows the effect of chlorpromazine on COS7 alone, on COS7 with empty vector pcDNA, and on COS7 transfected with RGN-GFP plasmid alone and treated with chlorpromazine. (B) shows the effect of trifluoperazine on COS7 alone, on COS7 with pcDNA empty plasmid, and on transfected COS7 with RGN-GFP plasmid alone and treated with trifluoperazine. (C) shows the effect of olanzapine on COS7 alone, on COS7 with pcDNA empty plasmid, and on transfected COS7 with RGN-GFP plasmid alone and treated with the drug. Finally, (D) shows the effect of quetiapine on COS7 alone, on COS7 with pcDNA empty plasmid, and on transfected COS7 with RGN-GFP plasmid and treated with quetiapine. It is known that increased expression of RGN causes a reduction in cell proliferation

(Yamaguchi, 2012), which would account for a lower cell number post-transfection with RGN. In addition, overexpression of RGN-GFP also increased the number of viable cells following treatment with FGA, but had no effect on cell viability with SGA drugs.

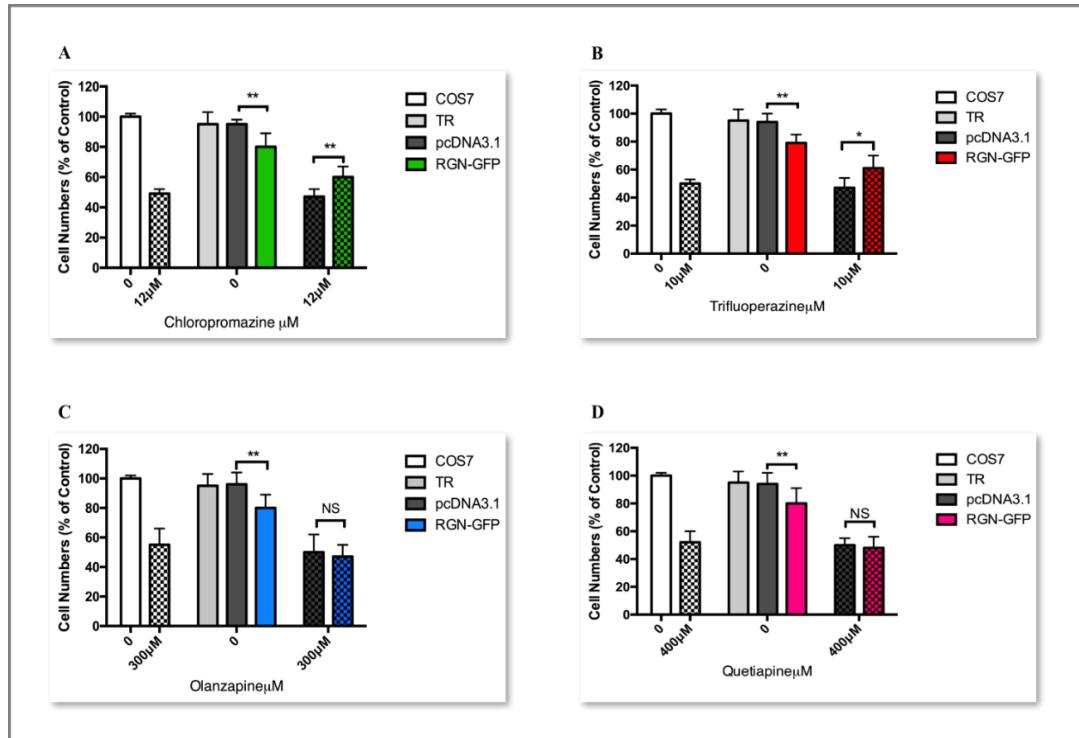


Figure 5-9: The effect on cell viability of FGAs and SGAs on COS7 in the presence and absence of RGN-GFP expression.

COS7 cells were plated in a 24-well cell culture plate at a density of  $2 \times 10^4$  per well for 24 hours. After 24 hours, cells were transfected with RGN-GFP plasmid under the condition 1 µg DNA/2 µL MP and incubated at 37°C for 72 hours. Cells were then treated for 24 hours with the  $LC_{50}$  of each drug, namely with (A) chlorpromazine 12 µM, (B) trifluoperazine 10 µM, (C) olanzapine 300 µM, and (D) quetiapine 400 µM. After 24 hours, cells were stained with crystal violet, and the absorbance was read at 590 nm. The results are presented as % compared to the control (non-treated, non-transfected COS7 cells). The data represented the mean  $\pm$  SD, repeated 3 times. P value statistically significant at \* $P \leq 0.05$  and \*\* $P \leq 0.01$  using two-tailed unpaired t-tests.

### *5.1.3.2 Co-localisation of RGN-GFP in COS7 with FGA Drugs*

Previous studies have shown that RGN can localise to a variety of cellular locations (Pillai et al., 2017). An investigation was undertaken to assess its localisation in COS7 cells and whether this localisation altered upon exposure to FGAs due to the induction of cell stress. In this study, localisation of RGN was monitored by assessing the green fluorescence of RGN-GFP. To identify other organelles, red fluorescence was monitored in order to distinguish mitochondria using MitoTracker Red, and blue fluorescence was used to identify the nucleus using DAPI. After transfecting the cells with RGN-GFP, cells were treated with the LC<sub>50</sub> for both chlorpromazine and trifluoperazine for 24 hours. Cells were stained with 0.5 µM of MitoTracker for 30 minutes then treated with DAPI histology mounting media. (Figure 5-10) shows control images from confocal microscopy of COS7 transfected with RGN-GFP alone. RGN-GFP showed little overlap with mitochondria (Pearson's Coefficient = 0.03). In (Figure 5-11), transfected COS7 with RGN-GFP treated with chlorpromazine showed for greater overlap with mitochondria (Pearson's Coefficient = 0.828). (Figure 5-12) shows the images for COS7 transfected with RGN-GFP and treated with trifluoperazine. The results indicate that there was again very strong overlap between RGN and mitochondria (Pearson's Coefficient = 0.75).

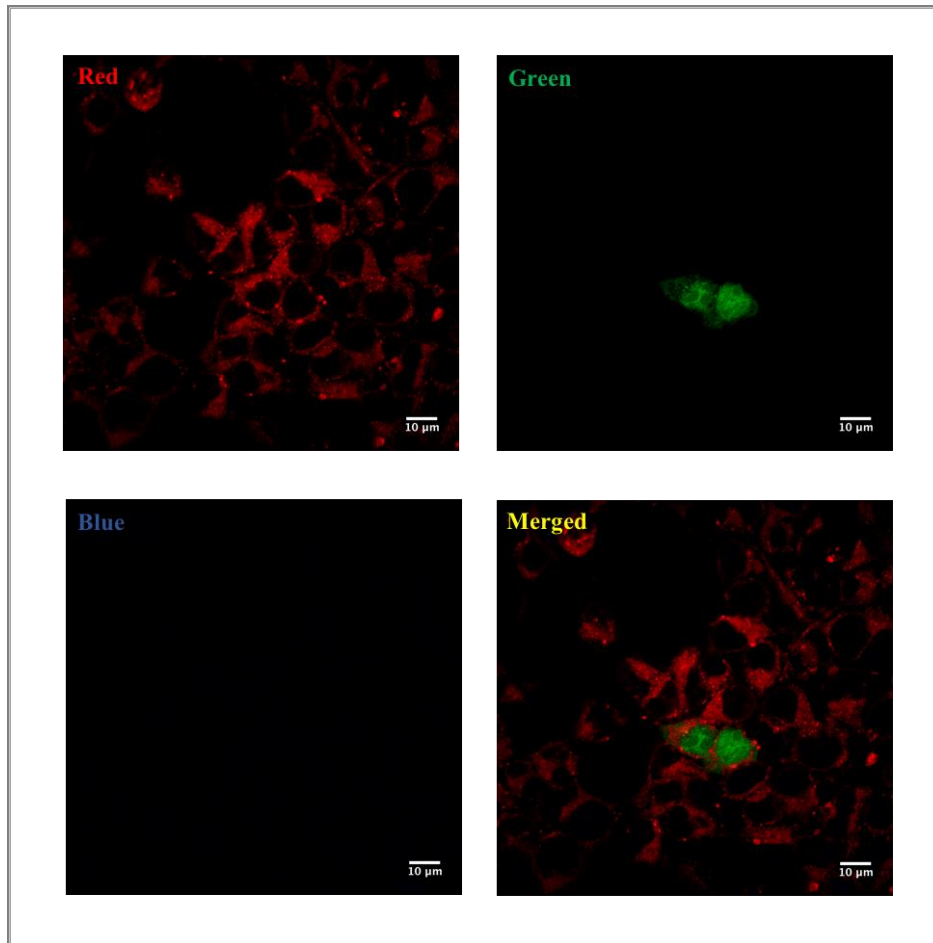


Figure 5-10: COS7 RGN-GFP.

COS7 cells were plated on a cover slip and placed in a 6-well plate for 24 hours then transfected with RGN-GFP for 72 hours. Cells were stained with 5 µM MitoTracker for 30 minutes. After fixing the cells with DAPI mounting media, the cells were visualised with x100 oil magnification.

GFP green channel  $\lambda_{exc} = 488 \text{ nm}$ ,  $\lambda_{em} = 502 \text{ nm}$

MitoTracker deep Red FM channel  $\lambda_{exc} = 644 \text{ nm}$ ,  $\lambda_{em} = 665 \text{ nm}$

Fluoroshield with DAPI blue channel  $\lambda_{exc} = 360 \text{ nm}$ ,  $\lambda_{em} = 460 \text{ nm}$

Merged image of Red and Green; Pearson's Coefficient:  $r = 0.026$ .

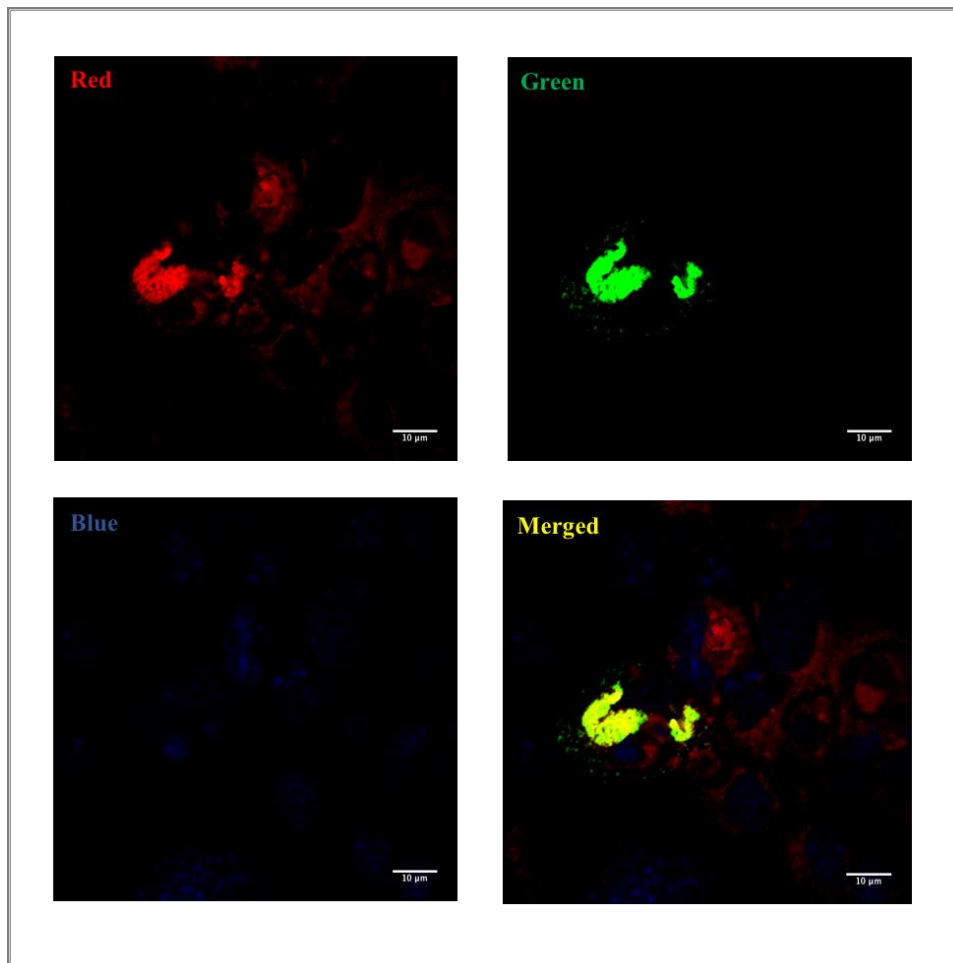


Figure 5-11: COS7 RGN-GFP chlorpromazine.

COS7 cells were plated on a cover slip and placed in a 6-well plate for 24 hours then transfected with RGN-GFP for 72 hours. Cells were treated with  $LC_{50}$  for chlorpromazine for 24 hours then stained with 5  $\mu$ M of MitoTracker for 30 minutes. After fixing the cells with DAPI mounting media, the cells were visualised with x100 oil magnification. 20 cells of each sample were used to calculate the  $r$ , experiment repeated 3 times.

GFP green channel  $\lambda_{exc} = 488$  nm,  $\lambda_{em} = 502$  nm

MitoTracker deep red FM channel  $\lambda_{exc} = 644$  nm,  $\lambda_{em} = 665$  nm

Fluoroshield with DAPI blue channel  $\lambda_{exc} = 360$  nm,  $\lambda_{em} = 460$  nm

Merged image of Red and Green; Pearson's Coefficient:  $r = 0.828$ .

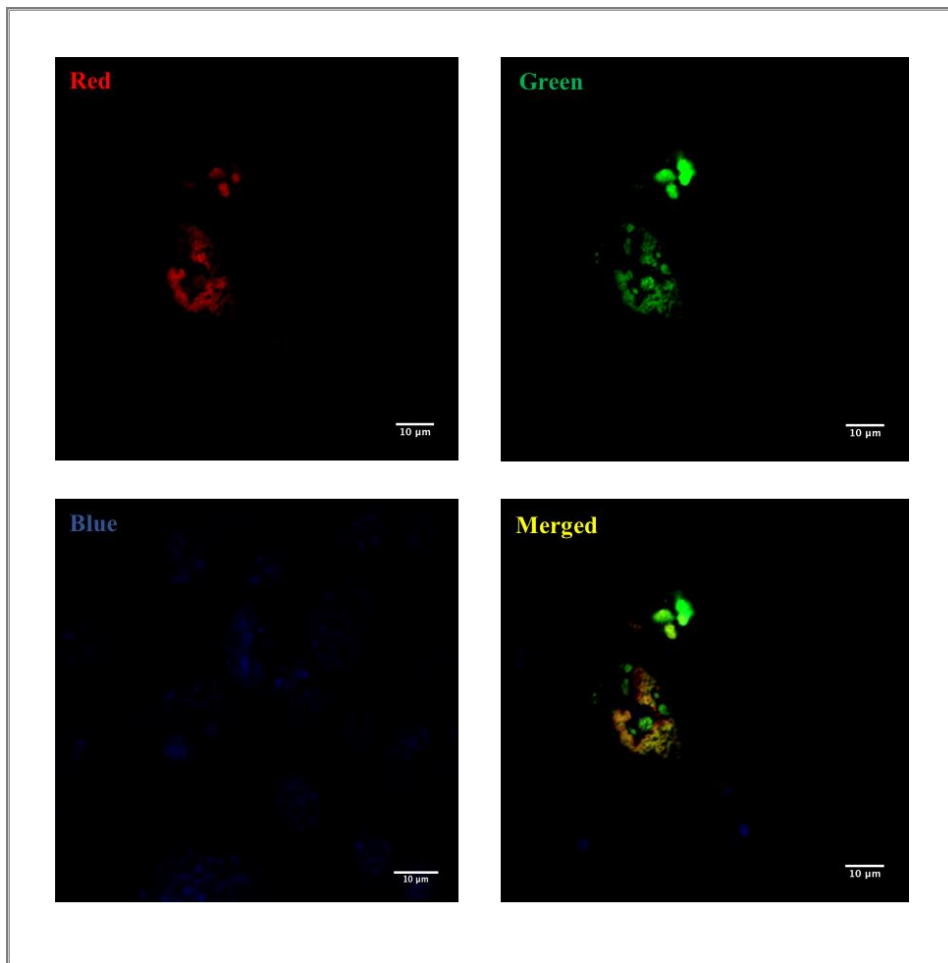


Figure 5-12: RGN-GFP trifluoperazine.

COS7 cells were plated on a cover slip and placed on 6-well plate for 24 hours then transfected with RGN-GFP for 72 hours. Cells were treated with  $LC_{50}$  for trifluoperazine for 24 hours then stained with  $5 \mu\text{M}$  of MitoTracker for 30 minutes. After fixing the cells with DAPI mounting media, the cells were visualised with x100 oil magnification. 20 cells of each sample were used to calculate the  $r$ , experiment repeated 3 times.

GFP green channel  $\lambda_{\text{exc}} = 488 \text{ nm}$ ,  $\lambda_{\text{em}} = 502 \text{ nm}$

MitoTracker deep red FM channel  $\lambda_{\text{exc}} = 644 \text{ nm}$ ,  $\lambda_{\text{em}} = 665 \text{ nm}$

Fluoroshield with DAPI blue channel  $\lambda_{\text{exc}} = 360 \text{ nm}$ ,  $\lambda_{\text{em}} = 460 \text{ nm}$

Merged image of Red and Green; Pearson's Coefficient:  $r = 0.754$ .

## 5.2 Discussion

The main objective of this chapter was to investigate the effect of RGN on the SH-SY5Y neuroblastoma cell line and COS7 kidney-like cell line in the presence of both generations of antipsychotic drugs. After trying many transfection reagents to transfect SH-SY5Y with RGN-GFP, none of the cells showed any appreciable level of transfection. On the other hand, more than 30% of the COS7 cells were transfected with RGN-GFP using the transfection agent Metafectene Pro (MP). From this study and the data presented in (Figure 5-9), cells transfected with RGN-GFP show a significant decrease in cell number compared to cells transfected with pcDNA alone. This finding is in agreement with other studies that have showed that RGN decreases cell proliferation (Yamaguchi, 2012). The results from FACC see (Figure 5-8) indicates that cells are not killed by RGN or the transfection reagent. Our data also confirm previous observations that RGN can decrease cell proliferation by slowing the cell cycle at the G1 and G1/M phase (Nakagawa et al., 2005). As seen from the results shown in (Figure 5-9), the cytotoxic effect of the FGAs is reduced in the presence of RGN. It has been proposed that numerous stimulatory causes of apoptosis cell death, namely TNF- $\alpha$ , LPS, thapsigargin, and Bay K 8644 in cloned normal rat kidney proximal epithelial and other cell types, are reduced in the case of the overexpression of RGN (Nakagawa et al., 2005; Izumi and Yamaguchi, 2004). The reduction of cell death may link to the suggestion that RGN inhibits the activity of caspase-3 (Yamaguchi et al., 2016). As discussed in Chapter 3, cell death induced by FGAs occurs mainly through apoptosis. A study

published by Yamaguchi (2013) suggested that RGN plays a role in decreasing the apoptotic cell death that can occur through various signalling factors that reduce both intrinsic and extrinsic apoptosis pathways.

## **Chapter 6:**

# **Potency of FGA to Cause Cell Death Decreases upon Differentiation of SH-SY5Y Cells.**

## **6. Potency of FGA to Cause Cell Death Decreases upon Differentiation of SH-SY5Y Cells.**

### **Introduction**

Neuroblastoma is a common extracranial solid cancer that commonly occurs in children under the age of 5 years, with the average age of diagnosis being around 18 months (Brodeur et al., 2016). Neuroblastomas mostly develop from the adrenal gland, but they can also form in sympathetic nervous tissue, including in the paraspinal sympathetic ganglia in the abdomen and chest (Angstman et al., 1990; Brisse et al., 2011; Brodeur et al., 2016). Although there has been some improvement in prognosis of patients over the past few years, patients with this type of cancer still have poor long-term survival rates (Mullassery and Losty, 2015).

SH-SY5Y cells are derived from human neuroblastoma cells and are the in vitro model for neuronal cells used in this study. This cell line is a subline of SK-N-SH cells that was found in 1970 in cultures from a bone marrow biopsy of a metastatic neuroblastoma of a 4-year-old female (Xicoy et al., 2017). By their nature, cancer-derived cell lines are undifferentiated and typically proliferative. SH-SY5Y neuroblastoma cells have the ability to be differentiated into cells possessing a more mature, neuron-like phenotype through manipulation of the culture medium (Ross et al., 1983; Encinas et al., 2000). In neurotoxicity research, differentiated neuronal SH-SY5Y cells have been used by treating cells with retinoic acid (Kovalevich and Langford, 2013).

Previous studies have suggested that patients with schizophrenia have a lower risk of cancer compared to other populations (Mortensen, 1989; Castts and Castts, 2000). Many researches have been investigating the possible link between the reduction of cancer and schizophrenia (Jablensky and Lawrence, 2001; Dalton et al., 2005). Genetic factors (Catts and Catts, 2008) and antipsychotic drugs have both been considered as possibilities for the reduced cancer levels in these patients (Mortensen, 1987; Mortensen, 1992).

The aim of the study in this chapter is to differentiate the neuroblastoma cell line SH-SY5Y to more neuronal-like cells with retinoic acid (RA) in order to investigate and compare the toxicity of the first generation of antipsychotic drugs on these differentiated cells.

## 6.1 Results

### 6.1.1 Differentiation of SH-SY5Y with Retinoic Acid

All-trans retinoic acid (RA) is the most common reagent used for differentiating SH-SY5Y cells using a concentration range from 5 to 100  $\mu\text{M}$  for different periods (Lotan, 1996; Melino et al., 1997; Xicoy et al., 2017). In this study, 10  $\mu\text{M}$  of RA was used with a lower concentration of FBS (2.5% v/v). Cells were plated in a 6-well cell culture plate at a density of  $1 \times 10^5$  cells/well with complete growth media for 24 hours. After 24 hours, 2 ml of fresh differentiated media containing 2.5% v/v FBS, 1% NEAA, 1% Pen/strep, 2 mM Glutamine, and 10  $\mu\text{M}$  RA was added to each well and changed every two days for up to 7 days.

### 6.1.2 *Confirming the Differentiation of SH-SY5Y*

#### 6.1.2.1 *Microscopy*

Bright field microscopy was used to determine the morphological changes of SH-SY5Y cells treated with 10  $\mu\text{M}$  RA for 7 days following the procedure outlined in (Section 6.1.1). The results presented in (Figure 6-1), show micrographs of control cells and SH-SY5Y cells treated with 10  $\mu\text{M}$  of RA at different times (day 0 control, day 3, day 5, and day 7). There were obvious changes in cell appearance both in the numbers and length of neurites on each cell. In control cells, some cells showed a few neurites of relatively short length (Figure 6-1-A). However, upon RA treatment for 7 days (Figure 6-1-D), it was clear that most cells had longer and more neurites compared to control cells. This result was also indicated to some extent after 5 days

(Figure 6-1-C), and to a much lesser extent after 3 days of RA treatment (Figure 6-1-B).

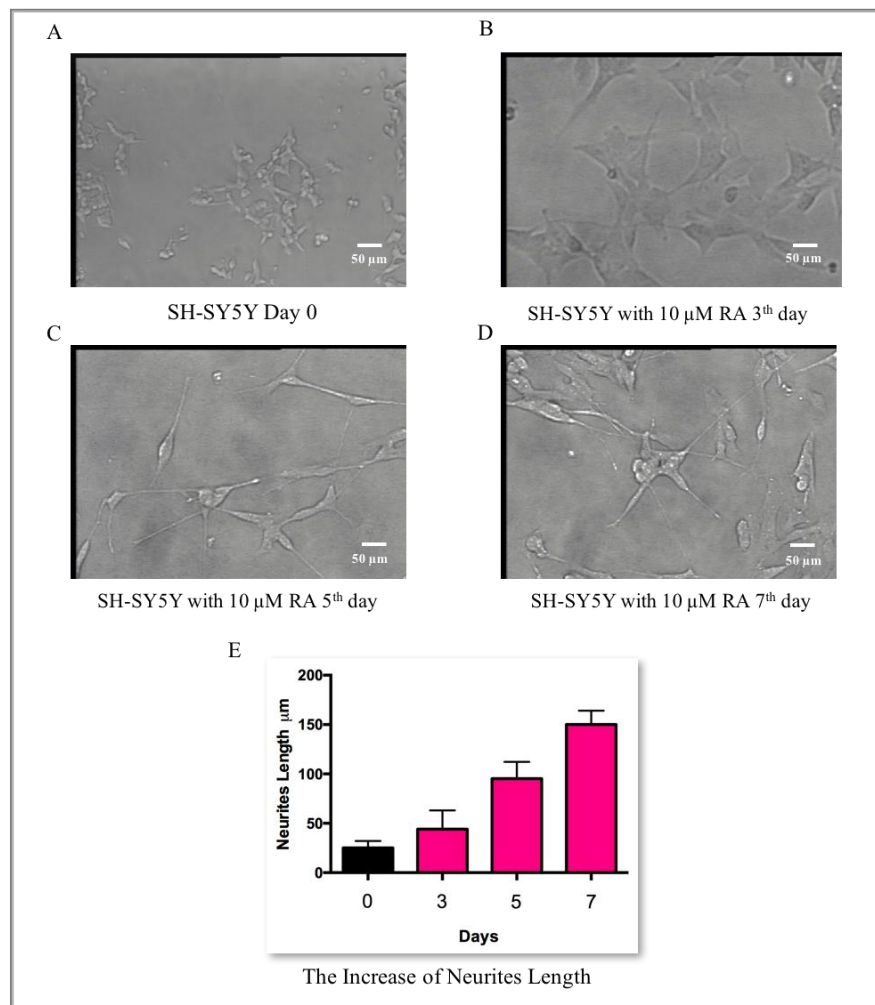


Figure 6-1: Morphological changes in SH-SY5Y cells upon RA-treatment.

SH-SY5Y cells were plated in a 6-well plate at a density of 100,000 cells per well. After 24 hours, cells were incubated with differentiation media. Images were taken under the light microscope 20x on days 0, 3, 5, and 7. (A) Undifferentiated SH-SY5Y in complete media. (B) SH-SY5Y treated with 10  $\mu$ M RA for 3 days. (C) SH-SY5Y treated with 10

$\mu\text{M}$  RA for 5 days. (D) SH-SY5Y treated with 10  $\mu\text{M}$  RA for 7 days. (E) The average increase of neurite length. These results were typical of three separate experiments.

#### *6.1.2.2 Expression of GAP43 in RA-Treated SH-SY5Y cells*

To further confirm that the cells were becoming differentiated upon RA treatment, a differentiation marker was monitored in the RA-treated cells. The expression of GAP43 as a neuronal marker was used to determine neuron-like differentiation using Western blotting (Kovalevich and Langford, 2016). Cells were differentiated following the procedure outlined in Section 6.1.1 for up to 7 days. Protein concentration from the control cells and RA-treated cells was determined, and the same amount of each sample was run on the gel. Membrane transfer and immunostaining with GAP43 antibody and  $\beta$ -actin antibody normalised the protein expression of each sample. The results in (Figure 6-2), show the increased expression of GAP43 as a differentiated neuronal marker over the time period following treatment with 10  $\mu\text{M}$  RA, compared with non-treated cells.

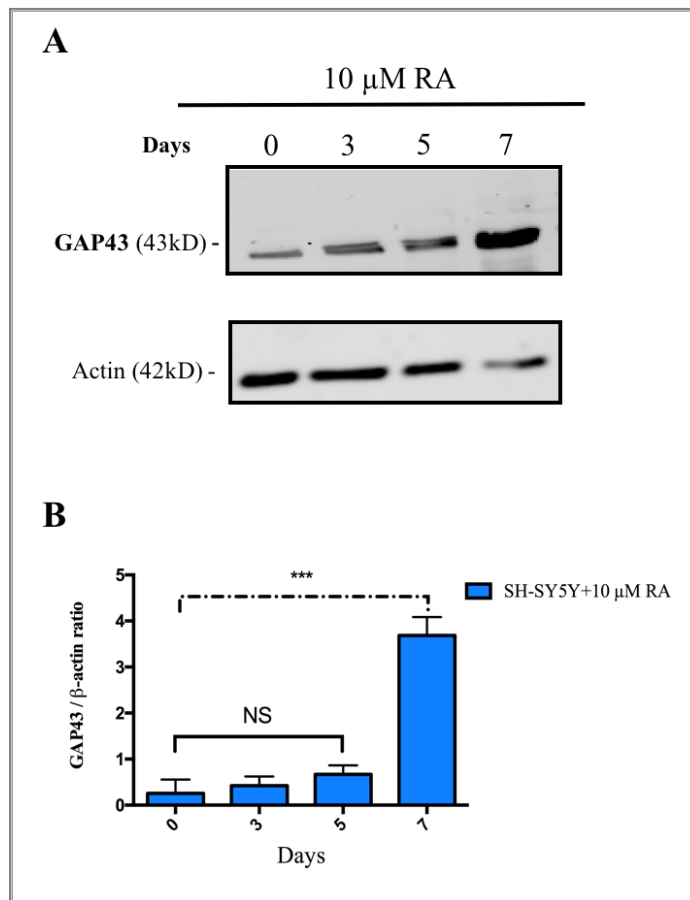


Figure 6-2: Western Blot showing the neuronal marker GAP43 on differentiated SH-SY5Y cells.

SH-SY5Y cells were plated in a 6-well plate at a density of 100,000 cells per well. After 24 hours, cells were incubated with differentiation media for 3, 5, and 7 days. Proteins of each sample were collected, separated by gel electrophoreses, and then immunoblot by Western blotting was performed. Figure 6-2, (A) shows the expression of GAP43 for each sample. (B) shows the expression level of GAP43 during the 7 days of treatment. On the 7<sup>th</sup> day, there was a 3-fold increase compared to the control (non-treated SH-SY5Y cells). The data represent the mean  $\pm$ SD, repeated 3 times. (P value statistical significance at \*\*\* $P \leq 0.001$  using unpaired two-tailed t-tests.)

### **6.1.3 The Effect of FGA on Differentiated SH-SY5Y**

After the confirmation of cell differentiation, when the SH-SY5Y cells had become more neuronal-like, the effects of the FGA drugs were tested on these cells. Cells were differentiated. On the 7<sup>th</sup> day, the differentiated media was replaced with clear media (no FBS), and SH-SY5Y cells were treated with the LC<sub>50</sub> (6 μM chlorpromazine and 5 μM trifluoperazine) for each drug for a period of 24 hours. Cell viability was then determined by the crystal violet assays. The results in (Figure 6-2-A) and (Figure 6-3-A) show a significant difference in the toxic effect of these FGA drugs between differentiated and non-differentiated SH-SY5Y cells. To determine the LC<sub>50</sub> for chlorpromazine and trifluoperazine for the differentiated cells, the control and differentiated cells were treated with different concentrations of these drugs. As shown in (Figure 6-2-B), the LC<sub>50</sub> of chlorpromazine on SH-SY5Y is 5 μM. However, there was an increase in the LC<sub>50</sub> in the differentiated SH-SY5Y cells to 10 μM. (Figure 6-3-B) also shows an increase of the LC<sub>50</sub> for trifluoperazine from 6 μM in the undifferentiated cells to 10 μM in the RA-differentiated cells.

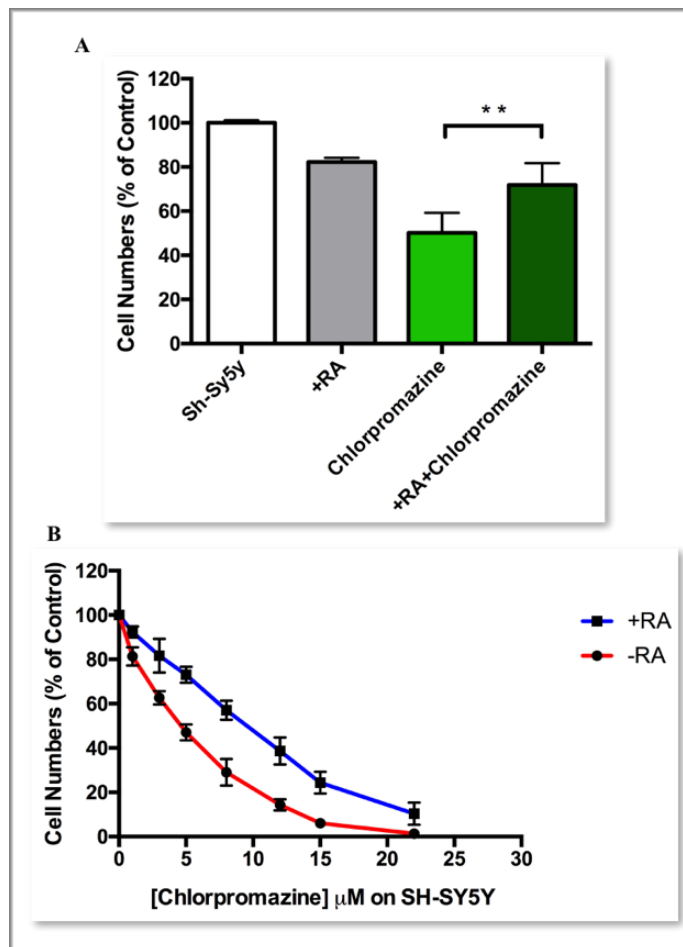


Figure 6-3: The effect of Chlorpromazine (FGA) on both differentiated and non-differentiated SH-SY5Y.

(A) shows the effects of RA on the cell viability of SH-SY5Y after 7 days of the treatment. Also shown is the effect of the LC50 for chlorpromazine (5  $\mu$ M) on untreated SH-SY5Y and differentiated SH-SY5Y cells. The results are presented as % to the control (non-treated cells) of mean  $\pm$  SD and repeated 3 times. (P value was statistically significant starting at \*\*  $P \leq 0.001$ , for the unpaired two-tailed t-tests.) (B) shows the dose-dependent cell viability effects of chlorpromazine on

both differentiated (blue) and non-differentiated SH-SY5Y (red). Data are the mean  $\pm$  SD of 3 repeats.

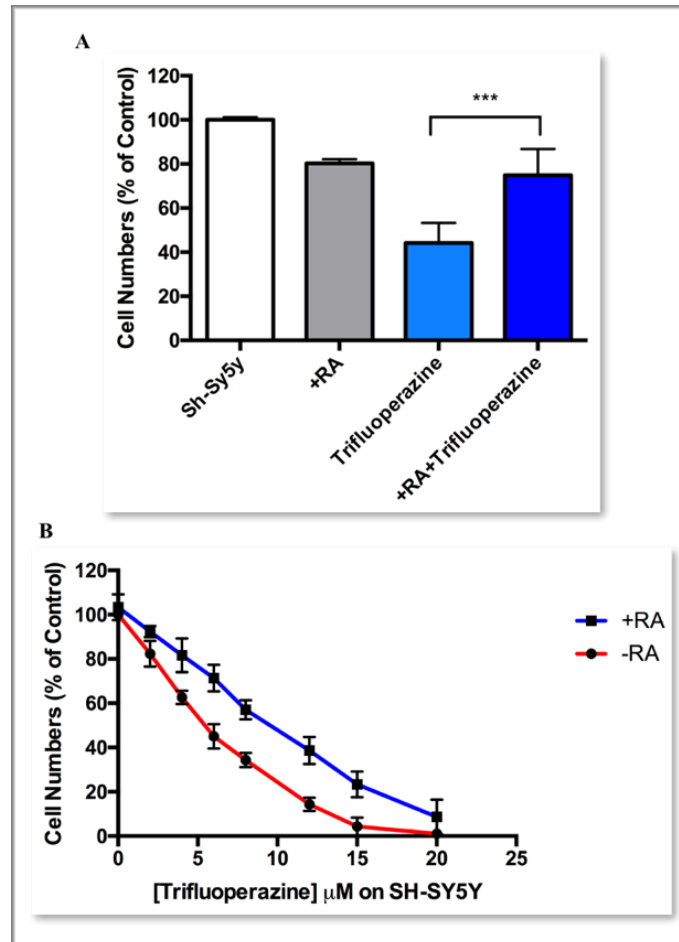


Figure 6-4: The effect of Trifluoperazine (FGA) on both differentiated and non-differentiated SH-SY5Y cells.

(A) shows the effects of RA on SH-SY5Y after 7 days of treatment and the effect of the  $LC_{50}$  for Trifluoperazine on undifferentiated SH-SY5Y and differentiated SH-SY5Y cells. The P value was determined to be  $***P \leq 0.001$  using two-tailed unpaired t-tests. Dose-dependent effects on the cell viability of Trifluoperazine for both differentiated (blue) and undifferentiated cells (red) are shown. Data represent the mean  $\pm$ SD of 3 determinations.

## 6.2 Discussion

This study aimed to investigate the effects of FGA on more “normal” neuronal-like cells by differentiating SH-SY5Y using RA. In previous chapters, the effects of FGA were studied in detail on undifferentiated SH-SY5Y cells, and the LC<sub>50</sub> of these drugs was determined. This study has shown observations similar to those of other studies on treating SH-SY5Y with RA in terms of morphology changes and in terms of the increased expression of neuronal marker GAP43 (Lopes et al., 2010; Cheung et al., 2009; Korecka et al., 2013). Comparing the toxicity of FGA on differentiated versus undifferentiated SH-SY5Y cells also showed significant differences. As seen in Table 6-1, the drugs had a more toxic effect on the undifferentiated SH-SY5Y cells compared to the differentiated cells. The effect of the drugs on differentiated cells were similar to the non-neuronal cells (COS7) This finding could be an indication that FGA might be able to selectively kill neuroblastoma cells compared to the more “normal” cells which are less sensitive to these drugs. Therefore, these drugs might be considered as a treatment for neuroblastomas. A study by Mu et al. (2014) found that thioridazine, which is a FGA drug, had an inhibitory effect on the cell viability of gastric cancer cells. Other research has reported that the risk of rectal cancer is reduced in both women and men using antipsychotic drugs (Dalton et al., 2004; Dalton et al., 2006). These observations might also support the anticancer properties of these drugs.

Table 6-1: The LC<sub>50</sub> of FGA on differentiated and undifferentiated SH-SY5Y using crystal violet assay.

	<b>Undifferentiated SH-SY5Y</b>	<b>Differentiated SH-SY5Y</b>	<b>COS7</b>
<b>Chlorpromazine</b>	6 $\mu$ M $\pm$ 3.6	10 $\mu$ M $\pm$ 6.11	12 $\pm$ 4.1 $\mu$ M
<b>Trifluoperazine</b>	5 $\mu$ M $\pm$ 5.5	11 $\mu$ M $\pm$ 6.1	10 $\pm$ 2.3 $\mu$ M

## **Chapter 7:**

# **General Discussion**

## **7. General Discussion and Future Work**

### **7.1 General Discussion**

Alzheimer's disease is a degenerative disorder of the brain which progresses slowly over time. The length of this disease differs within individuals, but on average its length is about 8.5 years from initial diagnosis of symptoms to death (Ellul et al., 2007). Agitation, aggression, hallucination, and delusion are some of the common symptoms exhibited by Alzheimer's disease patients (Tariot et al., 1995; Devanand et al., 1997; Jeste and Finkel, 2000; Paulsen et al., 2000). Antipsychotic drugs are reported to be among the most commonly used drugs to treat these symptoms and behaviours (Alexopoulos et al., 2004; Schneider et al., 1990). In the UK, primary care antipsychotic drugs are often prescribed to elderly people with dementia (Marston et al., 2014). Although there are many documented reviews about the side effects of antipsychotic drugs, less attention has been paid to the effect of these drugs on the Alzheimer's patients.

The drugs used in my study belong to both generations (chlorpromazine and trifluoperazine are FGAs, and olanzapine and quetiapine are SGAs), and they are considered to be the most prescribed antipsychotic medications in the UK (Marston et al., 2014).

Given the highly neurotoxic nature of the FGAs as described in my study, one of the suggestions I would like to make is that clinicians follow the recommendations made by the study of Peters et al. (2015), in that FGAs should not be prescribed to

patients with neurodegenerative diseases such as Alzheimer's disease. The findings from my study highlighted that both generations of the antipsychotics have a more toxic effect on neuronal cells (SH-SY5Y cells) than on non-neuronal cells (COS7 cells). The findings also indicated that FGAs have a far greater toxic effect on neuronal cells than SGAs.

After undertaking a systematic investigation of the mechanisms of cell death induced by these antipsychotic drugs, it was concluded that each generation has a different mechanism of cell death. Generally, cell death induced by both generations of antipsychotics mainly occurs through apoptosis. However, the study has shown that cell death induced by the FGAs is reduced after the inhibition of caspase-8. This finding indicates that apoptosis cell death by the FGAs is occurring through the extrinsic pathway. In contrast, cell death induced by the SGAs was found to occur through the intrinsic pathway after the activation of caspase-9. Regulated necrosis was also induced to a small degree after treating the cells with the FGAs, but not after treating with the SGAs. In addition, there was no evidence that autophagy plays a role in antipsychotic drug induced cell death.

The data presented in this study demonstrated the involvement of  $\text{Ca}^{2+}$  in cell death induced by these antipsychotic drugs. That was deduced by observing a decrease in drug-induced cell death after the use of BAPTA-AM (a  $\text{Ca}^{2+}$  chelator) and the overexpression of SERCA  $\text{Ca}^{2+}$  pumps (to remove  $\text{Ca}^{2+}$  from the cytosol). Increases in the expression of the  $\text{Ca}^{2+}$  pump SERCA2b in COS7 shows a protection against the antipsychotic drugs. The suggestion of the involvement of ER stress generated

by these types of drugs was also proven after experiments showed that the FGAs caused an elevation of the ER stress response marker CHOP. A recent study by Cano-Gonzalez et al. (2018) showed that the ER-stress response and activation of caspase-8 (independent of ligand) are linked via the CHOP pathway (Figure 7-1). These results directly support the results from the present study that cell death induced by the FGAs occurs through a caspase-8 dependent pathway, independent of ligand binding.

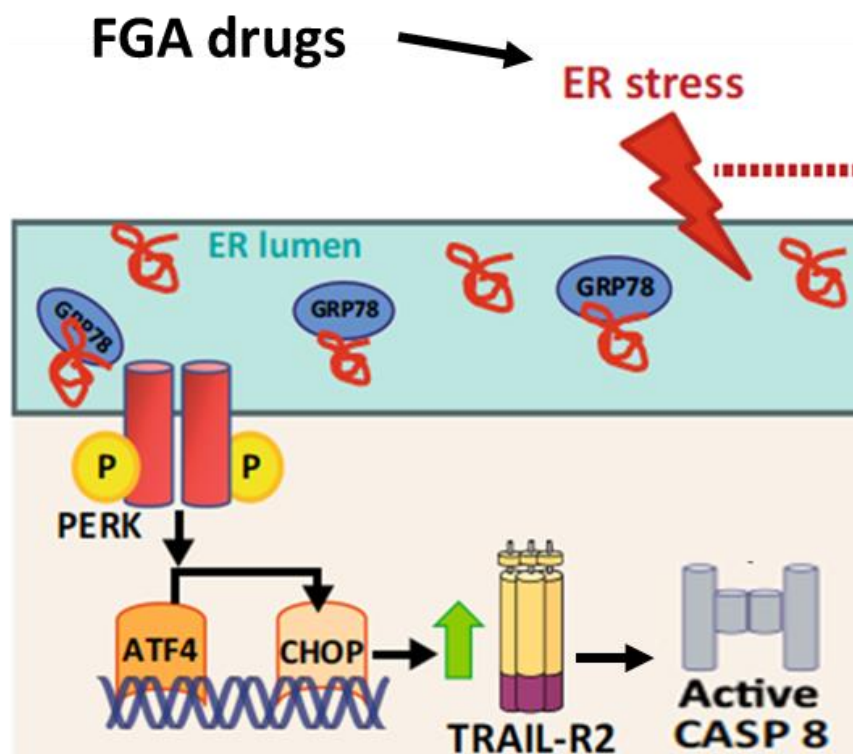


Figure 7-1: ER stress induced apoptosis (modified from Cano-Gonzales et al., 2018).

Overexpression of SERCA gave substantial protection in cells treated with FGAs. The effect on SGA toxicity was smaller, albeit still significant. SPCA overexpression showed no protection against cell death induced by either generation of the drugs. These results could be explained by the previous findings of this study, namely that cell death by SGAs is due to the caspase-9 activated apoptosis pathway, wherein ER stress does not need to be involved, and SPCA has an effect on intracellular  $[Ca^{2+}]$  levels, but does not affect the ER stress response. Treating the cells with FGAs caused possible 'co-localisation' between SERCA2b and the mitochondria. This could well be due to the increase in mitochondria-ER contact sites that is caused by cellular stress (Ilacqua et al., 2017), which can be induced by these antipsychotic drugs.

This study also suggested that RGN could help protect against the FGAs on COS7 cells. This suggestion could be in response that RGN is reducing ER stress. A study by Yamaguchi et al. (Izumi and Yamaguchi, 2004b) showed that RGN protects against thapsigargin, which is a classic ER stress response inducer. That finding could suggest that there is a link between RGN and ER stress protection. Additionally, Lai et al. (2011) also showed that RGN overexpression was also able to act as a transcription regulator and increase the expression of SERCA. As this study also indicated that SERCA protects against drug-induced cell death, this could be another mechanism of protection by RGN.

In summary, the major aims of this study were firstly to investigate the effect of both generations of antipsychotic drugs on brain and kidney cell lines. Secondly, to

identify the mechanism of cell death caused by these drugs. Then to identify if its calcium dependent, and whether increasing the level of Ca<sup>2+</sup> pumps and RGN could afford some protection. Finally investigating the effect of the same drugs on differentiated versus undifferentiated SH-SY5Y cells.

There were 3 major novel findings of this study. Firstly, cell death induced by antipsychotic drugs used in this study were mainly apoptosis with the involvement of regulated necrosis but not autophagy. In addition, FGA were more neurotoxic than the SGA tested. Secondly, calcium is involved in inducing cell death and the overexpression of calcium pumps can give some protection against cell death caused by these drugs. Thirdly, the FGA drugs are more neurotoxic to undifferentiated versus differentiated SH-SY5Y cells, and this could be further investigated as a therapeutic agent to treat neuroblastomas.

## 7.2 Future Work

Since this research has shown the toxicity of antipsychotic drugs and determined some of the mechanisms of cell death induced by these drugs. There are four recommended areas for further exploration.

- The results of this study indicated the involvement of extrinsic pathway by the FGA. Therefore, investigating the role of caspase-8 in more detail would be of interest.
- RGN and SERCA2b were shown to have an effect on the protection against the cytotoxicity by these drugs. Therefore, it is important to explore in more detail any cytosolic redistribution and co-localization of these proteins with other organelles during drug exposure.
- The ER stress response was shown to be a factor in cell death by these drugs. This should be further explored with SH-SY5Y cells.
- Future work could investigate the effects of other FGA drugs on neuroblastoma cells to see if they have a larger therapeutic window between undifferentiated and differentiated cell states.
- In As this study was limited to the use of 2 cell lines, future investigations using primary neuronal cells would be more beneficial
- Future studies could also consider investigating the effects of these drugs on animals and studying the physiological changes in their brain

## **Chapter 8:**

# **References**

## 8. References

- Abada, A. and Elazar, Z. (2014). Getting ready for building: signaling and autophagosome biogenesis. *EMBO reports*, 15(8), pp.839-852.
- Alberdi, A., Jimenez-Ortiz, V. and Sosa, M. (2001). The calcium chelator BAPTA affects the binding of assembly protein AP-2 to membranes. *Biocell*, 25(2), pp.167-172.
- Alexopoulos, G., Streim, J., Carpenter, D. and Docherty, J. (2018). Using antipsychotic agents in older patients. *Journal of Clinical Psychiatry*, 65.
- Al-Mousa, F. (2011). *Neurotoxicity of environmental pollutants*. Ph.D. thesis. University of Birmingham.
- Al-Mousa, F. and Michelangeli, F. (2012). Some commonly used brominated flame retardants cause Ca<sup>2+</sup>-ATPase inhibition, beta-amyloid peptide release and apoptosis in SH-SY5Y neuronal cells. *PloS one*, 7(4), p.33059.
- Alnemri, E., Livingston, D., Nicholson, D., Salvesen, G., Thornberry, N., Wong, W. and Yuan, J. (1996). Human ICE/CED-3 Protease Nomenclature. *Cell*, 87(2), p.171.
- Angstman, K., Miser, J. and Franz, W. (1990). Neuroblastoma. *Am Fam Physician*, 41(1), pp.238-244.
- Anon, (2015). [online] Available at: <http://droualb.faculty.mjc.edu> [Accessed 10 Nov. 2015].
- Antebi, A. and Fink, G. (1992). The yeast Ca(2+)-ATPase homologue, PMR1, is required for normal Golgi function and localizes in a novel Golgi-like distribution. *Molecular Biology of the Cell*, 3(6), pp.633-654.
- Apoptosis, Cytotoxicity and Cell Proliferation. (2008). 4th ed. Mannheim: Roche Diagnostics GmbH.
- Arnot, J., McCarty, L., Armitage, J., Toose-Reid, L., Wania, F. and Cousins, I. (2009). An evaluation of hexabromocyclododecane (HBCD) for persistent organic pollutant (POP) properties and the potential for adverse effects in the environment. Submitted to European Brominated Flame Retardant Industry Panel (EBFRIP), 26.

- Ashkenazi, A. (2008). Directing cancer cells to self-destruct with pro-apoptotic receptor agonists. *Nature Reviews Drug Discovery*, 7(12), pp.1001-1012.
- Axe, E., Walker, S., Manifava, M., Chandra, P., Roderick, H., Habermann, A., Griffiths, G. and Ktistakis, N. (2008). Autophagosome formation from membrane compartments enriched in phosphatidylinositol 3-phosphate and dynamically connected to the endoplasmic reticulum. *The Journal of Cell Biology*, 182(4), pp.685-701.
- Ban, T. (2007). Fifty years chlorpromazine: a historical perspective. *Neuropsychiatric disease and treatment*, 3(4), p.495.
- Bandelow, B., Wedekind, D., Pauls, J., Broocks, A., Hajak, G. and R  ther, E. (2000). Salivary Cortisol in Panic Attacks. *American Journal of Psychiatry*, 157(3), pp.454-456.
- Baron, S., Vangheluwe, P., Sep  lveda, M., Wuytack, F., Raeymaekers, L. and Vanoevelen, J. (2010). The secretory pathway Ca<sup>2+</sup>-ATPase 1 is associated with cholesterol-rich microdomains of human colon adenocarcinoma cells. *Biochimica et Biophysica Acta (BBA) - Biomembranes*, 1798(8), pp.1512-1521.
- Beasley, C., Tollefson, G., Tran, P., Satterlee, W., Sanger, T. and Hamilton, S. (1996). Olanzapine versus Placebo and Haloperidol. *Neuropsychopharmacology*, 14(2), pp.111-123.
- Berger, E., Galadari, H. and Gottlieb, A. (2007). Successful treatment of Hailey-Hailey disease with acitretin. *Journal of drugs in dermatology*, 6(7), pp.734-736.
- Berridge MJ. (2008). Cell Signalling Biology. Module-10. Cellular processes. Portland Press Limited. [Available]: [www.cellsignallingbiology.org](http://www.cellsignallingbiology.org).
- Bezprozvanny, I. and Mattson, M. (2008). Neuronal calcium mishandling and the pathogenesis of Alzheimer's disease. *Trends in Neurosciences*, 31(9), pp.454-463.
- Bhattacharyya, D. and Sen, P. (1999). The effect of binding of chlorpromazine and chloroquine to ion transporting ATPases. *Mol Cell Biochem*, 198(1-2), pp.179-185.

- Blair, D. and Dauner, A. (1992). Extrapyramidal Symptoms Are Serious Side-effects of Antipsychotic and Other Drugs. *The Nurse Practitioner*, 17(11), pp.56,62,63,64,67.
- Bootman, m. L., p. (2001). Calcium signalling and regulation of cell function. Encyclopedia of life sciences.
- Boucher, J., Macotela, Y., Bezy, O., Mori, M., Kriauciunas, K. and Kahn, C. (2010). A Kinase-Independent Role for Unoccupied Insulin and IGF-1 Receptors in the Control of Apoptosis. *Science Signaling*, [online] 3(151), pp.ra87-ra87. Available at: <http://dx.doi.org/10.1126/scisignal.2001173> [Accessed 3 Oct. 2014].
- Bradford, M. (1976) A Rapid and Sensitive Method for the Quantitation of Microgram Quantities of Protein Utilizing the Principle of Protein-Dye Binding. *Analytical Biochem.* 72:248-254.
- Brini, M. and Carafoli, E. (2009). Calcium Pumps in Health and Disease. *Physiological Reviews*, 89(4), pp.1341-1378.
- Brini, M., Cali, T., Ottolini, D. and Carafoli, E. (2012). Intracellular Calcium Homeostasis and Signaling. *Metal Ions in Life Sciences*, pp.119-168.
- Brini, M., Cali, T., Ottolini, D. and Carafoli, E. (2014). Neuronal calcium signaling: function and dysfunction. *Cellular and Molecular Life Sciences*, 71(15), pp.2787-2814.
- Brisse, H., McCarville, M., Granata, C., Krug, K., Wootton-Gorges, S., Kanegawa, K., Giammarile, F., Schmidt, M., Shulkin, B., Matthay, K., Lewington, V., Sarnacki, S., Hero, B., Kaneko, M., London, W., Pearson, A., Cohn, S. and Monclair, T. (2011). Guidelines for Imaging and Staging of Neuroblastic Tumors: Consensus Report from the International Neuroblastoma Risk Group Project. *Radiology*, 261(1), pp.243-257.
- Bulotta, A., Farilla, L., Hui, H. and Perfetti, R. (2004). The role of GLP-1 in the regulation of islet cell mass. *Cell Biochemistry and Biophysics*, 40(S3), pp.65-77.
- Cali, T., Ottolini, D. and Brini, M. (2012). Mitochondrial Ca<sup>2+</sup> and neurodegeneration. *Cell Calcium*, 52(1), pp.73-85.

- Calì, T., Ottolini, D. and Brini, M. (2012). Mitochondrial Ca<sup>2+</sup> and neurodegeneration. *Cell Calcium*, 52(1), pp.73-85.
- Cano-González, A., Mauro-Lizcano, M., Iglesias-Serret, D., Gil, J. and López-Rivas, A. (2018). Involvement of both caspase-8 and Noxa-activated pathways in endoplasmic reticulum stress-induced apoptosis in triple-negative breast tumor cells. *Cell Death & Disease*, 9(2).
- Carafoli E. (2002). Calcium signaling: a tale for all seasons. *Proc Natl Acad Sci USA*. 99(3):1115-22.
- Carafoli, E. (2003). Timeline: The calcium-signalling saga: tap water and protein crystals. *Nature Reviews Molecular Cell Biology*, 4(4), pp.326-332.
- Carafoli, E. (2007). The unusual history and unique properties of the calcium signal. *Calcium - A Matter of Life or Death*, pp.3-22.
- Catts, V. and Catts, S. (2000). Apoptosis and schizophrenia: is the tumour suppressor gene, p53, a candidate susceptibility gene?. *Schizophrenia Research*, 41(3), pp.405-415.
- Catts, V., Catts, S., O'Toole, B. and Frost, A. (2008). Cancer incidence in patients with schizophrenia and their first-degree relatives – a meta-analysis. *Acta Psychiatrica Scandinavica*, 117(5), pp.323-336.
- Cell Viability Assays. In: G. Sittampalam, N. Coussens, K. Brimacombe, A. Grossman, M. Arkin, D. Auld, C. Austin, M. Glicksman, J. Inglese, P. Iversen, Z. Li, J. McGee, O. McManus, L. Minor, A. Napper, J. Peltier, T. Riss, J. Trask, J. Weidner, M. Wildey, M. Xia and X. Xu, ed., *Assay Guidance Manual*. [online] Eli Lilly & Company and the National Center for Advancing Translational Sciences. Available at: <https://ncats.nih.gov/expertise/preclinical/agm> [Accessed 22 Jul. 2018].
- Chaabane, W., User, S., El-Gazzah, M., Jaksik, R., Sajjadi, E., Rzeszowska-Wolny, J. and Łos, M. (2012). Autophagy, Apoptosis, Mitoptosis and Necrosis: Interdependence Between Those Pathways and Effects on Cancer. *Archivum Immunologiae et Therapiae Experimentalis*, 61(1), pp.43-58.
- Chakraborti, S. and Bahnson, B. (2010). Crystal Structure of Human Senescence Marker Protein 30: Insights Linking Structural, Enzymatic, and Physiological Functions,. *Biochemistry*, 49(16), pp.3436-3444.

- Chan, F., Moriwaki, K. and De Rosa, M. (2013). Detection of Necrosis by Release of Lactate Dehydrogenase Activity. *Methods in Molecular Biology*, pp.65-70.
- Chan, F., Shisler, J., Bixby, J., Felices, M., Zheng, L., Appel, M., Orenstein, J., Moss, B. and Lenardo, M. (2003). A Role for Tumor Necrosis Factor Receptor-2 and Receptor-interacting Protein in Programmed Necrosis and Antiviral Responses. *Journal of Biological Chemistry*, 278(51), pp.51613-51621.
- Chang, H. and Yang, X. (2000). Proteases for Cell Suicide: Functions and Regulation of Caspases. *Microbiology and Molecular Biology Reviews*, 64(4), pp.821-846.
- Chemspider.com, (2014). *Chlorpromazine* / *C17H19ClN2S* / *ChemSpider*. [online] Available at: <http://www.chemspider.com/Chemical>
- Chemspider.com, (2014). *Olanzapine* / *C17H20N4S* / *ChemSpider*.
- Chemspider.com, (2014). *trifluoperazine* / *C21H24F3N3S* / *ChemSpider*. [online] Available at: <http://www.chemspider.com/Chemical-Structure.5365.html> [Accessed 1 Oct. 2014].
- Cheung, k. H., shineman, d., muller, m., cardenas, c., mei, l., yang, j., tomita, t., iwatsubo, t., lee, v. M. & foskett, j. K. (2008). Mechanism of ca<sup>2+</sup> disruption in alzheimer's disease by presenilin regulation of insp3 receptor channel gating. *Neuron*, 58, 871-83.
- Chipuk, J., Fisher, J., Dillon, C., Kriwacki, R., Kuwana, T. and Green, D. (2008). Mechanism of apoptosis induction by inhibition of the anti-apoptotic BCL-2 proteins. *Proceedings of the National Academy of Sciences*, 105(51), pp.20327-20332.
- Cho, Y., Challa, S., Moquin, D., Genga, R., Ray, T., Guildford, M. and Chan, F. (2009). Phosphorylation-Driven Assembly of the RIP1-RIP3 Complex Regulates Programmed Necrosis and Virus-Induced Inflammation. *Cell*, 137(6), pp.1112-1123.
- Clapham, D. (1995). Calcium Signaling. *Elsevier Inc*, 80(2), pp.259-268.
- Clapham, D. (2007). Calcium Signaling. *Cell*, 131(6), pp.1047-1058.
- Clyburn, L., Stones, M., Hadjistavropoulos, T. and Tuokko, H. (2000). Predicting caregiver burden and depression in Alzheimer's disease. *The Journals of*

*Gerontology Series B: Psychological Sciences and Social Sciences*, 55(1), pp.S2-13.

- Coen, R., Swanwick, G., O'boyle, C. And Coakley, D. (1997). Behaviour Disturbance And Other Predictors Of Carer Burden In Alzheimer's Disease. *International Journal Of Geriatric Psychiatry*, 12(3), Pp.331-336.
- Corbett, A., Burns, A. and Ballard, C. (2014). Don't use antipsychotics routinely to treat agitation and aggression in people with dementia. *BMJ*, 349(nov03 1), pp.g6420-g6420.
- Cowdry, R. and Gardner, D. (1988). Pharmacotherapy of borderline personality disorder: alprazolam, carbamazepine, trifluoperazine, and tranlycypromine. *Archives of General Psychiatry*, 45(2), pp.111--119.
- Dahan, d., spanier, r. & rahamimoff, h. (1991). The modulation of rat brain na(+)-ca<sup>2+</sup> exchange by k<sup>+</sup>. *J biol chem*, 266, 2067-75.
- Dalton, S., Johansen, C., Poulsen, A., Nørgaard, M., Sørensen, H., McLaughlin, J., Mortensen, P. and Friis, S. (2006). Cancer risk among users of neuroleptic medication: a population-based cohort study. *British Journal of Cancer*, 95(7), pp.934-939.
- Dalton, S., Laursen, T., Mellekjær, L., Johansen, C. and Mortensen, P. (2004). Risk for Cancer in Parents of Patients With Schizophrenia. *American Journal of Psychiatry*, 161(5), pp.903-908.
- Dalton, S., Mellekjær, L., Thomassen, L., Mortensen, P. and Johansen, C. (2005). Risk for cancer in a cohort of patients hospitalized for schizophrenia in Denmark, 1969–1993. *Schizophrenia Research*, 75(2-3), pp.315-324.
- Daniel, D., Zimbhoff, D., Potkin, S., Reeves, K., Harrigan, E. and Lakshminarayanan, M. (1999). Ziprasidone 80 mg/day and 160 mg/day in the Acute Exacerbation of Schizophrenia and Schizoaffective Disorder A 6-Week Placebo-Controlled Trial. *Neuropsychopharmacology*, 20(5), pp.491-505.
- Degterev, A., Hitomi, J., Gemscheid, M., Ch'en, I., Korkina, O., Teng, X., Abbott, D., Cuny, G., Yuan, C., Wagner, G., Hedrick, S., Gerber, S., Lugovskoy, A. and Yuan, J. (2008). Identification of RIP1 kinase as a specific cellular target of necrostatins. *Nature Chemical Biology*, 4(5), pp.313-321.

- Degterev, A., Hitomi, J., Gemscheid, M., Ch'en, I., Korkina, O., Teng, X., Abbott, D., Cuny, G., Yuan, C., Wagner, G., Hedrick, S., Gerber, S., Lugovskoy, A. and Yuan, J. (2008). Identification of RIP1 kinase as a specific cellular target of necrostatins. *Nature Chemical Biology*, 4(5), pp.313-321.
- Degterev, A., Huang, Z., Boyce, M., Li, Y., Jagtap, P., Mizushima, N., Cuny, G., Mitchison, T., Moskowitz, M. and Yuan, J. (2005). Chemical inhibitor of nonapoptotic cell death with therapeutic potential for ischemic brain injury. *Nature Chemical Biology*, 1(2), pp.112-119.
- Demuro, a., parker, i. & stutzmann, g. E. (2010). Calcium signaling and amyloid toxicity in alzheimer disease. *J biol chem*, 285, 12463-8.
- Deter, R. (1967). INFLUENCE OF GLUCAGON, AN INDUCER OF CELLULAR AUTOPHAGY, ON SOME PHYSICAL PROPERTIES OF RAT LIVER LYSOSOMES. *The Journal of Cell Biology*, 33(2), pp.437-449.
- Devanand, D., Jacobs, D., Tang, M., Del, C., Sano, M., Marder, K., Bell, K., Bylsma, F., Brandt, J., Albert, M. and Stern, Y. (1997). The Course of Psychopathologic Features in Mild to Moderate Alzheimer Disease. *Archives of General Psychiatry*, 54(3), pp.257-263.
- Dibben, C., Khandaker, G., Underwood, B., O'Loughlin, C., Keep, C., Mann, L. and Jones, P. (2016). First-generation antipsychotics: not gone but forgotten. *BJPsych Bulletin*, 40(02), pp.93-96.
- Dikic, I. and Elazar, Z. (2018). Mechanism and medical implications of mammalian autophagy. *Nature Reviews Molecular Cell Biology*, 19(6), pp.349-364.
- Divac, N., Prostran, M., Jakovcevski, I. and Cerovac, N. (2014). Second-Generation Antipsychotics and Extrapyramidal Adverse Effects. *BioMed Research International*, 2014, pp.1-6.
- Dodo, K., Katoh, M., Shimizu, T., Takahashi, M. and Sodeoka, M. (2005). Inhibition of hydrogen peroxide-induced necrotic cell death with 3-amino-2-indolylmaleimide derivatives. *Bioorganic & Medicinal Chemistry Letters*, 15(12), pp.3114-3118.

- Duncan, R., Goad, D., Grillo, M., Kaja, S., Payne, A. and Koulen, P. (2010). Control of Intracellular Calcium Signaling as a Neuroprotective Strategy. *Molecules*, 15(3), pp.1168-1195.
- Duprez, L., Wirawan, E., Berghe, T. and Vandenabeele, P. (2009). Major cell death pathways at a glance. *Microbes and Infection*, 11(13), pp.1050-1062.
- Dwyer, D., Lu, X. and Bradley, R. (2003). Cytotoxicity of conventional and atypical antipsychotic drugs in relation to glucose metabolism. *Brain Research*, 971(1), pp.31-39.
- Earnshaw, W., Martins, L. and Kaufmann, S. (1999). Mammalian caspases: structure, activation, substrates, and functions during apoptosis. Annual review of biochemistry, 68(1), pp.383--424.
- Ebashi, F. and Ebashi, S. (1962). Removal of Calcium and Relaxation in Actomyosin Systems. *Nature*, 194(4826), pp.378-379.
- Ellul, J., Archer, N., Foy, C., Poppe, M., Boothby, H., Nicholas, H., Brown, R. and Lovestone, S. (2006). The effects of commonly prescribed drugs in patients with Alzheimer's disease on the rate of deterioration. *Journal of Neurology, Neurosurgery & Psychiatry*, 78(3), pp.233-239.
- Elwess, N., Filoteo, A., Enyedi, A. and Penniston, J. (1997). Plasma Membrane Ca<sup>2+</sup> Pump Isoforms 2a and 2b Are Unusually Responsive to Calmodulin and Ca<sup>2+</sup>. *Journal of Biological Chemistry*, 272(29), pp.17981-17986.
- English, A. and Voeltz, G. (2013). Endoplasmic Reticulum Structure and Interconnections with Other Organelles. *Cold Spring Harbor Perspectives in Biology*, 5(4), pp.a013227-a013227.
- Falzer, P., Moore, B. and Garman, D. (2008). Incorporating clinical guidelines through clinician decision-making. *Implementation Science*, 3(1), p.13.
- Fan, Z., Beresford, P., Oh, D., Zhang, D. and Lieberman, J. (2003). Tumor suppressor NM23-H1 is a granzyme A-activated DNase during CTL-mediated apoptosis, and the nucleosome assembly protein SET is its inhibitor. *Cell*, 112(5), pp.659--672.
- Favaloro, B., Allocati, N., Graziano, V., Di Ilio, C. and De Laurenzi, V. (2012). Role of Apoptosis in disease. *Aging*, 4(5), pp.330-349.

- Feng, S., Yang, Y., Mei, Y., Ma, L., Zhu, D., Hoti, N., Castanares, M. and Wu, M. (2007). Cleavage of RIP3 inactivates its caspase-independent apoptosis pathway by removal of kinase domain. *Cellular Signalling*, 19(10), pp.2056-2067.
- Feoktistova, M., Geserick, P. and Leverkus, M. (2016). Crystal Violet Assay for Determining Viability of Cultured Cells. *Cold Spring Harbor Protocols*, 2016(4), p.pdb.prot087379.
- Festjens, N., Vanden Berghe, T. and Vandenabeele, P. (2006). Necrosis, a well-orchestrated form of cell demise: Signalling cascades, important mediators and concomitant immune response. *Biochimica et Biophysica Acta (BBA) - Bioenergetics*, 1757(9-10), pp.1371-1387.
- Festjens, N., Vanden Berghe, T., Cornelis, S. and Vandenabeele, P. (2007). RIP1, a kinase on the crossroads of a cell's decision to live or die. *Cell Death and Differentiation*, 14(3), pp.400-410.
- Foster, R. (2001). *Basic Pharmacology, chapter 5 Drug action on the central nervous system*. UK: Arnold, pp.236-239.
- Frandsen, A., and Schousboe, A. (1991). Dantrolene prevents glutamate cytotoxicity and  $Ca^{2+}$  release from intracellular stores in cultured cerebral cortical neurons. *J neurochem*, 56, 1075-8.
- Fuentes-Prior, P. And Salvesen, G. (2004). The protein structures that shape caspase activity, specificity, activation and inhibition. *Biochem. J.*, 384(2), pp.201-232.
- Fujita, t. (1999). Senescence marker protein-30 (smp30): structure and biological function. *Biochem biophys res commun*, 254, 1-4.
- Fujita, t., mandel, l., shirasawa, t., hino, o., shirat, t. & maruyama, n. (1995). Isolation of cDNA clone encoding human homolog of senescence marker protein-30 (smp-30) and its location on the x-chromosome. *Biochimica et biophysica acta-gene structure and expression.*, 1263, pp.249-252.

- Fujita, t., shirasawa, t., uchida, k. & maruyama, n. (1996). Gene regulation of senescence marker protein-30 (smp30): coordinated up-regulation with tissue maturation and gradual down-regulation with aging. *Mech ageing dev*, pp.87, 219-29.
- Garraway, S. and Hochman, S. (2001). Pharmacological characterization of serotonin receptor subtypes modulating primary afferent input to deep dorsal horn neurons in the neonatal rat. *British Journal of Pharmacology*, 132(8), pp.1789-1798.
- Gass'o, P., Mas, S., Molina, O., Bernardo, M., Lafuente, A. and Parellada, E. (2012). Neurotoxic/neuroprotective activity of haloperidol, risperidone and paliperidone in neuroblastoma cells. *Progress in Neuro-Psychopharmacology and Biological Psychiatry*, 36(1), pp.71--77.
- Gelder, M., Cowen, P. and Harrison, P. (2006). *Shorter Oxford textbook of psychiatry*. Oxford: Oxford University Press.
- Gil-Ad, I., Shtauf, B., Levkovitz, Y., Dayag, M., Zeldich, E. and Weizman, A. (2004). Characterization of Phenothiazine-Induced Apoptosis in Neuroblastoma and Glioma Cell Lines: Clinical Relevance and Possible Application for Brain-Derived Tumors. *Journal of Molecular Neuroscience*, 22(3), pp.189-198.
- Gil-Ad, I., Shtauf, B., Levkovitz, Y., Dayag, M., Zeldich, E. and Weizman, A. (2004). Characterization of Phenothiazine-Induced Apoptosis in Neuroblastoma and Glioma Cell Lines: Clinical Relevance and Possible Application for Brain-Derived Tumors. *Journal of Molecular Neuroscience*, 22(3), pp.189-198.
- Glick, D., Barth, S. and Macleod, K. (2010). Autophagy: cellular and molecular mechanisms. *The Journal of Pathology*, 221(1), pp.3-12.
- Goddard, E. (1959). Trifluoperazine in psychoneurotic outpatients. *Canadian Medical Association journal*, 81(6), pp.467-470.
- Godoy, J., Rios, J., Zolezzi, J., Braidy, N. and Inestrosa, N. (2014). Signaling pathway cross talk in Alzheimer's disease. *Cell Communication and Signaling*, 12(1), p.23.

- Golstein, P. and Kroemer, G. (2007). Cell death by necrosis: towards a molecular definition. *Trends in Biochemical Sciences*, 32(1), pp.37-43.
- Goping, I., Barry, M., Liston, P., Sawchuk, T., Constantinescu, G., Michalak, K., Shostak, I., Roberts, D., Hunter, A., Korneluk, R. and others, (2003). Granzyme B-induced apoptosis requires both direct caspase activation and relief of caspase inhibition. *Immunity*, 18(3), pp.355--365.
- Grant, P. (2015). Neurotransmitters. *International Encyclopedia of the Social & Behavioral Sciences*, pp.749-754.
- Green, D. R. (2011). Apoptosis: physiology and pathology. Cambridge: Cambridge University press.
- Gunteski-Hamblin, A., Clarke, D. and Shull, G. (1992). Molecular cloning and tissue distribution of alternatively spliced mRNAs encoding possible mammalian homologs of the yeast secretory pathway calcium pump. *Biochemistry*, 31(33), pp.7600-7608.
- Haavik, C. (1977). Profound hypothermia in mammals treated with tetrahydrocannabinols, morphine, or chlorpromazine. *Federation proceedings*, 36(12), pp.2595-2598.
- Hakem R, Hakem A, Duncan GS, Henderson JT, Woo M, Soengas MS, Elia A, de la Pompa JL, Kagi D, Khoo W, Potter J, Yoshida R, Kaufman SA, Lowe SW, Penninger JM, Mak TW. (1998). Differential requirement for caspase 9 in apoptotic pathways in vivo. *Cell*. 94:339-52.
- Hampel, H., Prvulovic, D., Teipel, S., Jessen, F., Luckhaus, C., FrÄ¶lich, L., Riepe, M., Dodel, R., Leyhe, T., Bertram, L., Hoffmann, W. and Faltraco, F. (2011). The future of Alzheimer's disease: The next 10 years. *Progress in Neurobiology*, 95(4), pp.718-728.
- Hans, J. (2008). *Apoptosis, Cytotoxicity and Cell Proliferation*. 4th ed. [ebook] Roche Diagnostics GmbH. Available at: [https://lifescience.roche.com/wcsstore/RASCatalogAssetStore/Articles/05242134001\\_05.08.pdf](https://lifescience.roche.com/wcsstore/RASCatalogAssetStore/Articles/05242134001_05.08.pdf) [Accessed 23 Jul. 2015].
- Hassan, M., Haikel, Y., Selimovic, D. and El-Khattouti, A. (2013). Crosstalk Between Apoptosis and Autophagy: Molecular Mechanisms and Therapeutic Strategies in Cancer. *JCD*, p.37.

- Hasselbach, W. and Makinose, M. (1961). The calcium pump of the "relaxing granules" of muscle and its dependence on ATP-splitting. 333, pp.518-28.
- He, S., Wang, L., Miao, L., Wang, T., Du, F., Zhao, L. and Wang, X. (2009). Receptor Interacting Protein Kinase-3 Determines Cellular Necrotic Response to TNF- $\alpha$ . *Cell*, 137(6), pp.1100-1111.
- Healy, M. (2009). *Psychiatric Drugs Explained*. 5th ed. London: Elsevier.
- Higgins, E. and George, M. (2013). *The neuroscience of clinical psychiatry*. 2nd ed. China: Lippincott Williams and Wilkins.
- Hilfiker, H., Guerini, D. and Carafoli, E. (1994). Cloning and expression of isoform 2 of the human plasma membrane Ca<sup>2+</sup> ATPase. Functional properties of the enzyme and its splicing products. *J Biol Chem.*, 269(42), pp.26178-83.
- Hill, S., Bishop, J., Palumbo, D. and Sweeney, J. (2010). Effect of second-generation antipsychotics on cognition: current issues and future challenges. *Expert Review of Neurotherapeutics*, 10(1), pp.43-57.
- Hippius, H. (1989). The history of clozapine. *Psychopharmacology*, 99(S1), pp.S3-S5.
- Hirsova, P. and Gores, G. (2015). Death Receptor-Mediated Cell Death and Proinflammatory Signaling in Nonalcoholic Steatohepatitis. *Cellular and Molecular Gastroenterology and Hepatology*, 1(1), pp.17-27.
- Holler, N., Zaru, R., Micheau, O., Thome, M., Attinger, A., Valitutti, S., Bodmer, J., Schneider, P., Seed, B. and Tschopp, J. (2000). Fas triggers an alternative, caspase-8-independent cell death pathway using the kinase RIP as effector molecule. *Nature Immunology*, 1(6), pp.489-495.
- Hu, Z., Bonifas, J., Beech, J., Bench, G., Shigihara, T., Ogawa, H., Ikeda, S., Mauro, T. and Epstein, E. (2000). Mutations in ATP2C1, encoding a calcium pump, cause Hailey-Hailey disease. *Nat Genet.*, 24(1), pp.61-5.
- Hui, H., Dotta, F., Mario, U. and Perfetti, R. (2004). Role of caspases in the regulation of apoptotic pancreatic islet beta-cells death. *Journal of Cellular Physiology*, 200(2), pp.177-200.

- Hukkanen, m., hughes, f. J., buttery, l. D., gross, s. S., evans, t. J., seddon, s., riveros-moreno, v., macintyre, i. & polak, j. M. (1995). Cytokine-stimulated expression of inducible nitric oxide synthase by mouse, rat, and human osteoblast-like cells and its functional role in osteoblast metabolic activity. *Endocrinology*, 136, pp.5445-53.
- Igney, F. and Krammer, P. (2002). Death and anti-death: tumour resistance to apoptosis. *Nature Reviews Cancer*, 2(4), pp.277--288.
- Izumi, T. and Yamaguchi, M. (2004). Overexpression of regucalcin suppresses cell death in cloned rat hepatoma H4-II-E cells induced by tumor necrosis factor-? or thapsigargin. *Journal of Cellular Biochemistry*, 92(2), pp.296-306.
- Jablensky, A. and Lawrence, D. (2001). Schizophrenia and Cancer. *Archives of General Psychiatry*, 58(6), pp.579-580.
- Jagtap, P. and Szabó, C. (2005). Poly(ADP-ribose) polymerase and the therapeutic effects of its inhibitors. *Nature Reviews Drug Discovery*, 4(5), pp.421-440.
- Jarrett, H. and Penniston, J. (1977). Partial purification of the Ca<sup>2+</sup>-Mg<sup>2+</sup> ATPase activator from human erythrocytes: Its similarity to the activator of 3'5'-cyclic nucleotide phosphodiesterase. *Biochemical and Biophysical Research Communications*, 77(4), pp.1210-1216.
- Jencks, W., Yang, T., Peisach, D. and Myung, J. (1993). Calcium ATPase of sarcoplasmic reticulum has four binding sites for calcium. *Biochemistry*, 32(27), pp.7030-7034.
- Jeste, D. and Finkel, S. (2000). Psychosis of Alzheimer's Disease and Related Dementias: Diagnostic Criteria for a Distinct Syndrome. *The American Journal of Geriatric Psychiatry*, 8(1), pp.29-34.
- Jouan-Lanhouet, S., Arshad, M., Piquet-Pellorce, C., Martin-Chouly, C., Le Moigne-Muller, G., Van Herreweghe, F., Takahashi, N., Sergent, O., Lagadic-Gossmann, D., Vandenabeele, P., Samson, M. and Dimanche-Boitrel, M. (2012). TRAIL induces necroptosis involving RIPK1/RIPK3-dependent PARP-1 activation. *Cell Death & Differentiation*, 19(12), pp.2003-2014.
- Kabeya, Y. (2000). LC3, a mammalian homologue of yeast Apg8p, is localized in autophagosome membranes after processing. *The EMBO Journal*, 19(21), pp.5720-5728.

- Kalai, M., Van Loo, G., Vanden Berghe, T., Meeus, A., Burm, W., Saelens, X. and Vandenabeele, P. (2002). Tipping the balance between necrosis and apoptosis in human and murine cells treated with interferon and dsRNA. *Cell Death & Differentiation*, 9(9), pp.981-994.
- Kandel, E., Schwartz, J. and Jessell, T. (2013). *Principles of neural science*. 5th ed. New York: McGraw-Hill, Health Professions Division.
- Kar, R., Singha, P., Venkatachalam, M. and Saikumar, P. (2009). A novel role for MAP1 LC3 in nonautophagic cytoplasmic vacuolation death of cancer cells. *Oncogene*, 28(28), pp.2556-2568.
- Kerr, J., Wyllie, A. and Currie, A. (1972). Apoptosis: a basic biological phenomenon with wide-ranging implications in tissue kinetics. *British journal of cancer*, 26(4), p.239.
- Kiernan, J. and Barr, M. (2005). *Barr's The human nervous system*. Philadelphia: Lippincott Williams & Wilkins.
- Kischkel, F., Hellbardt, S., Behrmann, I., Germer, M., Pawlita, M., Krammer, P. and Peter, M. (1995). Cytotoxicity-dependent APO-1 (Fas/CD95)-associated proteins form a death-inducing signaling complex (DISC) with the receptor. *The EMBO Journal*, 14(22), pp.5579-5588.
- Kondo, Y., Inai, Y., Sato, Y., Handa, S., Kubo, S., Shimokado, K., Goto, S., Nishikimi, M., Maruyama, N. and Ishigami, A. (2006). Senescence marker protein 30 functions as gluconolactonase in l-ascorbic acid biosynthesis, and its knockout mice are prone to scurvy. *Proc natl acad sci u s a*, 103, pp.5723-5728.
- Kovalevich, J. and Langford, D. (2013). Considerations for the Use of SH-SY5Y Neuroblastoma Cells in Neurobiology. *Neuronal Cell Culture*, pp.9-21.
- Kumar-Singh, S., Pirici, D., McGowan, E., Serneels, S., Ceuterick, C., Hardy, J., Duff, K., Dickson, D. And Van Broeckhoven, C. (2005). Dense-core plaques in tg2576 and psapp mouse models of alzheimer's disease are centered on vessel walls. *Am j pathol*, 167, pp.527-43.

- Lai, P., Yip, N. and Michelangeli, F. (2011). Regucalcin (RGN/SMP30) alters agonist- and thapsigargin-induced cytosolic  $[Ca^{2+}]$  transients in cells by increasing SERCA  $Ca^{2+}$ -ATPase levels. *FEBS Letters*, 585(14), pp.2291-2294.
- Lamb, C., Yoshimori, T. and Tooze, S. (2013). The autophagosome: origins unknown, biogenesis complex. *Nature Reviews Molecular Cell Biology*, 14(12), pp.759-774.
- Lauressergues, E., Bert, E., Duriez, P., Hum, D., Majd, Z., Staels, B. and Cussac, D. (2012). Does endoplasmic reticulum stress participate in APD-induced hepatic metabolic dysregulation?. *Neuropharmacology*, 62(2), pp.784-796.
- Lee, A. and East, J. (2001). What the structure of a calcium pump tells us about its mechanism. *Biochemical Journal*, 356(3), pp.665-683.
- Lee, W., Lee, W., Cheng, C., Chen, K., Chou, C., Chung, C., Sun, M., Cheng, H., Ho, M. and Lin, C. (2015). Repositioning antipsychotic chlorpromazine for treating colorectal cancer by inhibiting sirtuin 1. *Oncotarget*, 6(29).
- Levine, B. and Yuan, J. (2005). Autophagy in cell death: an innocent convict?. *Journal of Clinical Investigation*, 115(10), pp.2679-2688.
- Li, J. and Yuan, J. (2008). Caspases in apoptosis and beyond. *Oncogene*, 27(48), pp.6194-6206.
- Linkermann, A. and Green, D. (2014). Necroptosis. *New England Journal of Medicine*, 370(5), pp.455-465.
- Llinas, R. (1988). The intrinsic electrophysiological properties of mammalian neurons: insights into central nervous system function. *Science*, 242(4886), pp.1654-1664.
- Locksley, R., Killeen, N. and Lenardo, M. (2001). The TNF and TNF Receptor Superfamilies. *Cell*, 104(4), pp.487-501.
- Lodish, H., Berk, A., Zipursky, S., (2000). *Molecular Cell Biology*. 4th edition. New York: W. H. Freeman; Section 24.1, Tumor Cells and the Onset of Cancer.

- Lopez, O., Wisniewski, S., Becker, J., Boller, F. and DeKosky, S. (1999). Psychiatric Medication and Abnormal Behavior as Predictors of Progression in Probable Alzheimer Disease. *Archives of Neurology*, 56(10), p.1266.
- Los, M., Mozoluk, M., Ferrari, D., Stepczynska, A., Stroh, C., Renz, A., Herceg, Z., Wang, Z. and Schulze-Osthoff, K. (2002). Activation and Caspase-mediated Inhibition of PARP: A Molecular Switch between Fibroblast Necrosis and Apoptosis in Death Receptor Signaling. *Molecular Biology of the Cell*, 13(3), pp.978-988.
- Lu, M., Lawrence, D., Marsters, S., Acosta-Alvear, D., Kimmig, P., Mendez, A., Paton, A., Paton, J., Walter, P. and Ashkenazi, A. (2014). Opposing unfolded-protein-response signals converge on death receptor 5 to control apoptosis. *Science*, 345(6192), pp.98-101.
- Maat, D. (2014). *Structure of a Neuron*. [online] HubPages. Available at: <http://hubpages.com/hub/Structure-of-a-Neuron#slide7624067> [Accessed 2 Oct. 2014].
- MacLennan, D., Brandl, C., Korczak, B. and Green, N. (1985). Amino-acid sequence of a  $\text{Ca}^{2+}$  +  $\text{Mg}^{2+}$  -dependent ATPase from rabbit muscle sarcoplasmic reticulum, deduced from its complementary DNA sequence. *Nature*, 316(6030), pp.696-700.
- MacLennan, D., Brandl, C., Korczak, B. and Green, N. (1985). Amino-acid sequence of a  $\text{Ca}^{2+}$  +  $\text{Mg}^{2+}$  -dependent ATPase from rabbit muscle sarcoplasmic reticulum, deduced from its complementary DNA sequence. *Nature*, 316(6030), pp.696-700.
- Maes, M., Vanhaecke, T., Cogliati, B., Yanguas, S., Willebroods, J., Rogiers, V. and Vinken, M. (2014). Measurement of Apoptotic and Necrotic Cell Death in Primary Hepatocyte Cultures. *Methods in Molecular Biology*, 1250, pp.349-361.
- Malenka, R., Kauer, J., Perkel, D., Mauk, M., Kelly, P., Nicoll, R. and Waxham, M. (1989). An essential role for postsynaptic calmodulin and protein kinase activity in long-term potentiation. *Nature*, 340(6234), pp.554-557.
- Marston, L., Nazareth, I., Petersen, I., Walters, K. and Osborn, D. (2014). Prescribing of antipsychotics in UK primary care: a cohort study. *BMJ Open*, 4(12).

- Marston, L., Nazareth, I., Petersen, I., Walters, K. and Osborn, D. (2014). Prescribing of antipsychotics in UK primary care: a cohort study. *BMJ Open*, 4(12), p.e006135.
- Martinez, C., Jones, R. and Rietbrock, S. (2013). Trends in the prevalence of antipsychotic drug use among patients with Alzheimer's disease and other dementias including those treated with antidementia drugs in the community in the UK: a cohort study. *BMJ Open*, 3(1), p.e002080.
- Martín-Pérez, R., Palacios, C., Yerbes, R., Cano-González, A., Iglesias-Serret, D., Gil, J., Reginato, M. and López-Rivas, A. (2014). Activated ERBB2/HER2 Licenses Sensitivity to Apoptosis upon Endoplasmic Reticulum Stress through a PERK-Dependent Pathway. *Cancer Research*, 74(6), pp.1766-1777.
- Martinvalet, D., Zhu, P. and Lieberman, J. (2005). Granzyme A Induces Caspase-Independent Mitochondrial Damage, a Required First Step for Apoptosis. *Immunity*, 22(3), pp.355-370.
- Marty, A. and Zimmerberg, J. (1989). Diffusion into patch-clamp recording pipette of a factor necessary for muscarinic current response. *Cellular Signalling*, 1(3), pp.259-268.
- Masters, C., Bateman, R., Blennow, K., Rowe, C., Sperling, R. and Cummings, J. (2015). Alzheimer's disease. *Nature Reviews Disease Primers*, p.15056.
- Mattson, M. (2007). Calcium and neurodegeneration. *Aging Cell*, 6(3), pp.337-350.
- McCormack, J. and Denton, R. (1990). Intracellular calcium ions and intramitochondrial Ca in the regulation of energy metabolism in mammalian tissues. *Proceedings of the Nutrition Society*, 49(01), pp.57-75.
- McKhann, G., Drachman, D., Folstein, M., Katzman, R., Price, D. and Stadlan, E. (1984). Clinical diagnosis of Alzheimer's disease: Report of the NINCDS-ADRDA Work Group\* under the auspices of Department of Health and Human Services Task Force on Alzheimer's Disease. *Neurology*, 34(7), pp.939-939.

- Melino, G. and Vaux, D. (2010). *Cell death*. Chichester, West Sussex: John Wiley & Sons.
- Messner, B., Frotschnig, S., Steinacher-Nigisch, A., Winter, B., Eichmair, E., Gebetsberger, J., Schwaiger, S., Ploner, C., Laufer, G. and Bernhard, D. (2012). Apoptosis and necrosis: two different outcomes of cigarette smoke condensate-induced endothelial cell death. *Cell death & disease*, 3(11), p.424.
- Meyers, S. (2000). Developments in aquatic microbiology. *International Microbiology*, 3(4), pp.203-211.
- Michelangeli, F., Colyer, J., East, J. and Lee, A. (1990). Effect of pH on the activity of the Ca<sup>2+</sup> Mg<sup>2+</sup>-activated ATPase of sarcoplasmic reticulum. *Biochemical Journal*, 267(2), pp.423-429.
- Michelangeli, F., Ogunbayo, O. and Wootton, L. (2005). A plethora of interacting organellar Ca<sup>2+</sup> stores. *Current opinion in cell biology*, 17(2), pp.135--140.
- Mijaljica, D., Prescott, M. and Devenish, R. (2011). Microautophagy in mammalian cells: Revisiting a 40-year-old conundrum. *Autophagy*, 7(7), pp.673-682.
- Min, K., Seo, B., Bae, Y., Yoo, Y. and Kwon, T. (2014). Antipsychotic agent thioridazine sensitizes renal carcinoma Caki cells to TRAIL-induced apoptosis through reactive oxygen species-mediated inhibition of Akt signaling and downregulation of Mcl-1 and c-FLIP(L). *Cell Death & Disease*, 5(2), pp.e1063-e1063.
- Mizushima, N. and Komatsu, M. (2011). Autophagy: Renovation of Cells and Tissues. *Cell*, 147(4), pp.728-741.
- Mizushima, N. and Komatsu, M. (2011). Autophagy: renovation of cells and tissues. *Cell*, 147(4), pp.728--741.
- Mizushima, N. and Yoshimori, T. (2007). How to Interpret LC3 Immunoblotting. *Autophagy*, 3(6), pp.542-545.
- Mizushima, N., Yamamoto, A., Matsui, M., Yoshimori, T. and Ohsumi, Y. (2004). In Vivo Analysis of Autophagy in Response to Nutrient Starvation Using Transgenic Mice Expressing a Fluorescent Autophagosome Marker. *Molecular Biology of the Cell*, 15(3), pp.1101-1111.

- Mizushima, N., Yoshimori, T. and Levine, B. (2010). Methods in Mammalian Autophagy Research. *Cell*, 140(3), pp.313-326.
- Mizushima, N., Yoshimori, T. and Ohsumi, Y. (2011). The Role of Atg Proteins in Autophagosome Formation. *Annual Review of Cell and Developmental Biology*, 27(1), pp.107-132.
- Mortensen, P. (1987). Neuroleptic treatment and other factors modifying cancer risk in schizophrenic patients. *Acta Psychiatrica Scandinavica*, 75(6), pp.585-590.
- Mortensen, P. (1989). The incidence of cancer in schizophrenic patients. *Journal of Epidemiology & Community Health*, 43(1), pp.43-47.
- Mortensen, P. (1992). Neuroleptic medication and reduced risk of prostate cancer in schizophrenic patients. *Acta Psychiatrica Scandinavica*, 85(5), pp.390-393.
- Nakagawa, T., Sawada, N. and Yamaguchi, M. (2005). Overexpression of regucalcin suppresses cell proliferation of cloned normal rat kidney proximal tubular epithelial NRK52E cells. *International Journal of Molecular Medicine*, 16(4), pp.637-643.
- Nandra, K. and Agius, M. (2012). The differences between typical and atypical antipsychotics: the effects on neurogenesis. *Psychiatr Danub*, 24(Suppl 1), pp.95--99.
- Neher, E. and Sakaba, T. (2008). Multiple Roles of Calcium Ions in the Regulation of Neurotransmitter Release. *Neuron*, 59(6), pp.861-872.
- Nemeroff, C., Kinkead, B. and Goldstein, J. (2002). Quetiapine: preclinical studies, pharmacokinetics, drug interactions, and dosing. *The Journal of Clinical Psychiatry*, 63, pp.5-11.
- Neurobiology of essential fatty acids*. New York: Plenum Press.

- Nicotera, P., Leist, M. and Ferrando-May, E. (1999). Apoptosis and necrosis: different execution of the same death. *Biochemical Society Symposium*, 66, pp.69-73.
- NIDA (2017). *Impacts of Drugs on Neurotransmission*. [online] Drugabuse.gov. Available at: <https://www.drugabuse.gov/news-events/nida-notes/2017/03/impacts-drugs-neurotransmission> [Accessed 19 Jul. 2018].
- Niggli, V., Ronner, P., Carafoli, E. and Penniston, J. (1979). Effects of calmodulin on the (Ca<sup>2+</sup> + Mg<sup>2+</sup>)ATPase partially purified from erythrocyte membranes. *Archives of Biochemistry and Biophysics*, 198(1), pp.124-130.
- Nikoletopoulou, V., Markaki, M., Palikaras, K. and Tavernarakis, N. (2013). Crosstalk between apoptosis, necrosis and autophagy. *Biochimica et Biophysica Acta (BBA) - Molecular Cell Research*, 1833(12), pp.3448-3459.
- Noback, C. (2005). *The human nervous system*. Totowa, N.J.: Humana Press.
- Noback, C., Ruggerio, D., Demarest, R. and Strominger, N. (2005). *The Human Nervous System*. Totowa: Humana Press.
- Noback, C., Ruggerio, D., Demarest, R. and Strominger, N. (2005). *The Human Nervous System*. Totowa: Humana Press.
- Norbury, C. and Hickson, I. (2001). Cellular responses to DNA damage. *Annual review of pharmacology and toxicology*, 41(1), pp.367-401.
- Norman, A., Vanaman, T. and Means, A. (1987). *Calcium-binding proteins in health and disease*. San Diego: Academic Press.
- Ogunbayo OA, Michelangeli F. (2007). The widely utilized brominated flame retardant tetrabromobisphenol A (TBBPA) is a potent inhibitor of the SERCA Ca<sup>2+</sup> pump. *J Biol Chem*. 408(3):407-15.
- Omura, M. and Yamaguchi, M. (1999). Enhancement of neutral phosphatase activity in the cytosol and nuclei of regenerating rat liver: role of endogenous regucalcin. *J cell biochem*, 73, pp.332-341.
- Orrenius, S. and Nicotera, P. (1994). The calcium ion and cell death. *Journal of Neural Transmission. Supplementa*, 43(1-11).

- Ostinelli, E., Brooke-Powney, M., Li, X. and Adams, C. (2017). Haloperidol for psychosis-induced aggression or agitation (rapid tranquillisation). *Cochrane Database of Systematic Reviews*.
- Owens, D. (1994). New or old antidepressants? Benefits of new drugs are exaggerated. *BMJ*, 309(6964), pp.1281-1282.
- Oyadomari, S. and Mori, M. (2003). Roles of CHOP/GADD153 in endoplasmic reticulum stress. *Cell Death and Differentiation*, 11(4), pp.381-389.
- Ozasa, R., Okada, T., Nadanaka, S., Nagamine, T., Zyryanova, A., Harding, H., Ron, D. and Mori, K. (2013). The Antipsychotic Olanzapine Induces Apoptosis in Insulin-secreting Pancreatic  $\beta$  Cells by Blocking PERK-mediated Translational Attenuation. *Cell Structure and Function*, 38(2), pp.183-195.
- Paulsen, J., Salmon, D., Thal, L., Romero, R., Weisstein-Jenkins, C., Galasko, D., Hofstetter, C., Thomas, R., Grant, I. and Jeste, D. (2000). Incidence of and risk factors for hallucinations and delusions in patients with probable AD. *Neurology*, 54(10), pp.1965-1971.
- Pedersen, P. and Carafoli, E. (1987). Ion motive ATPases. I. Ubiquity, properties, and significance to cell function. *Trends in Biochemical Sciences*, 12, pp.146-150.
- Peter, M. and Krammer, P. (2003). The CD95(APO-1/Fas) DISC and beyond. *Cell Death Differ*, 10(1), pp.26-35.
- Peters, M., Schwartz, S., Han, D., Rabins, P., Steinberg, M., Tschanz, J. and Lyketsos, C. (2015). Neuropsychiatric Symptoms as Predictors of Progression to Severe Alzheimer's Dementia and Death: The Cache County Dementia Progression Study. *American Journal of Psychiatry*, 172(5), pp.460-465.
- Peuskens, J. (1995). Risperidone in the Treatment of Patients with Chronic Schizophrenia: a Multi-National, Multi-Centre, Double-Blind, Parallel-Group Study versus Haloperidol. *British Journal of Psychiatry*, 166(06), pp.712-726.
- Pichot, P. (1996) the discovery of chlorpromazine and the place of psychopharmacology in the history of psychiatry. In: Healy D, ed., *the Psychopharmacologists*. New York: Chapman & Hall, 1996, pp. 1-27.

- Pillai, H., Shende, A., Parmar, M., Thomas, J., Kartha, H., Taru Sharma, G., Ghosh, S. and Bhure, S. (2017). Detection and localization of regucalcin in spermatozoa of water buffalo (*Bubalus bubalis*): A calcium-regulating multifunctional protein. *Reproduction in Domestic Animals*, 52(5), pp.865-872.
- Pizzo, P., Poplack, D., Adamson, P., Blaney, S. and Helman, L. (2016). *Principles and practice of pediatric oncology*. Philadelphia: Wolters Kluwer, p.772.
- Popugaeva, E., Vlasova, O. and Bezprozvanny, I. (2015). Restoring calcium homeostasis to treat Alzheimer's disease: a future perspective. *Neurodegenerative Disease Management*, 5(5), pp.395-398.
- Potter, W. and Hollister, L. (2004). *Basic & Clinical pharmacology*. 9th ed. McGraw-Hill: Medical publishing division, pp.chapter 29, pp.462-481.
- Pozzan, T., Rizzuto, R., Volpe, P. and Meldolesi, J. (1994). Molecular and cellular physiology of intracellular calcium stores. *Physiol Rev.*, 74(3), pp.595-636.
- Pradelli, L., BÃ©nÃ©teau, M. and Ricci, J. (2010). Mitochondrial control of caspase-dependent and -independent cell death. *Cell. Mol. Life Sci.*, 67(10), pp.1589-1597.
- Proskuryakov, S., Konoplyannikov, A. and Gabai, V. (2003). Necrosis: a specific form of programmed cell death?. *Experimental Cell Research*, 283(1), pp.1-16.
- Pu, F., Chen, N. and Xue, S. (2016). Calcium intake, calcium homeostasis and health. *Food Science and Human Wellness*, 5(1), pp.8-16.
- Rang, H., Ritter, J., Flower, R. and Henderson, G. (2016). *Rang and Dale's pharmacology*. Amsterdam: Elsevier.
- Reinhardt, T., Horst, R. and Waters, W. (2004). Characterization of Cos-7 cells overexpressing the rat secretory pathway Ca<sup>2+</sup>-ATPase. *Am J Physiol Cell Physiol*, 286(1), pp.164-9.
- Riedel, M., MÃ¼ller, N., Strassnig, M., Spellmann, I., Severus, E. and MÃ¶ller, H. (2007). Quetiapine in the treatment of schizophrenia and related disorders. *Neuropsychiatric Disease and Treatment*, 3(2), pp.219-235.

- Riedl SJ, Salvesen GS. (2007). The apoptosome: signalling platform of cell death. *Nat Rev Mol Cell Biol.* 5: 405-13.
- Riedl, S. and Salvesen, G. (2007). The apoptosome: signalling platform of cell death. *Nature Reviews Molecular Cell Biology*, 8(5), pp.405-413.
- Riss, T., Moravec, R., Niles, A., Duellman, S., Benink, H., Worzella, T. and Minor, L. (2004).
- Roach, H. and Clarke, N. (2000). Physiological cell death of chondrocytes in vivo is not confined to apoptosis. *The Journal of Bone and Joint Surgery*, 82(4), pp.601-613.
- Rosenheck, R., Leslie, D., Sindelar, J., Miller, E., Lin, H., Stroup, T., McEvoy, J., Davis, S., Keefe, R., Swartz, M. and others, (2006). Cost-effectiveness of second-generation antipsychotics and perphenazine in a randomized trial of treatment for chronic schizophrenia. *American Journal of Psychiatry*, 163(12), pp.2080-2089.
- Ross, C., Margolis, R., Reading, S., Pletnikov, M. and Coyle, J. (2006). Neurobiology of schizophrenia. *Neuron*, 52(1), pp.139-153.
- Rothschild, A., Bates, K., Boehringer, K. and Syed, A. (1999). Olanzapine response in psychotic depression. *The Journal of clinical psychiatry*, 60(2), pp.116-118.
- Rubinsztein, D., Bento, C. and Deretic, V. (2015). Therapeutic targeting of autophagy in neurodegenerative and infectious diseases. *The Journal of Experimental Medicine*, 212(7), pp.979-990.
- Rudolph, H., Antebi, A., Fink, G., Buckley, C., Dorman, T., LeVitre, J., Davidow, L., Mao, J. and Moir, D. (1989). The yeast secretory pathway is perturbed by mutations in PMR1, a member of a Ca<sup>2+</sup> ATPase family. *Cell*, 58(1), pp.133-145.
- Saelens, X., Festjens, N., Walle, L., Gurr, M., Loo, G. and Vandenabeele, P. (2004). Toxic proteins released from mitochondria in cell death. *Oncogene*, 23(16), pp.2861-2874.
- Sanders, R. and Gillig, P. (2012). Extrapyramidal Examinations in Psychiatry. *Innovations in Clinical Neuroscience*, 9(7-8), pp.10-16.

- Sarkar, S., Ravikumar, B. and Rubinsztein, D. (2009). Chapter 5 Autophagic Clearance of Aggregate-Prone Proteins Associated with Neurodegeneration. *Autophagy in Disease and Clinical Applications, Part C*, 453, pp.83-110.
- Schatzmann, H. (1966). ATP-dependent Ca<sup>++</sup>-Extrusion from human red cells. *Experientia*, 22(6), pp.364-365.
- Scheller, C., Knöferle, J., Ullrich, A., Prottengeier, J., Racek, T., Sopper, S., Jassoy, C., Rethwilm, A. and Koutsilieri, E. (2006). Caspase inhibition in apoptotic T cells triggers necrotic cell death depending on the cell type and the proapoptotic stimulus. *Journal of Cellular Biochemistry*, 97(6), pp.1350-1361.
- Schmidt, H., Pollock, J., Nakane, M., Förstermann, U. and Murad, F. (1992). Ca<sup>2+</sup>-calmodulin-regulated nitric oxide synthases. *Cell Calcium*, 13(6-7), pp.427-434.
- Schneider, L., Pollock, V. and Lyness, S. (1990). A Metaanalysis of Controlled Trials of Neuroleptic Treatment in Dementia. *Journal of the American Geriatrics Society*, 38(5), pp.553-563.
- Schneider, L., Tariot, P., Dagerman, K., Davis, S., Hsiao, J., Ismail, M., Lebowitz, B., Lyketsos, C., Ryan, J., Stroup, T., Sultzer, D., Weintraub, D. and Lieberman, J. (2006). Effectiveness of Atypical Antipsychotic Drugs in Patients with Alzheimer's Disease. *New England Journal of Medicine*, [online] 355(15), pp.1525-1538. Available at: [https://www.nejm.org/doi/full/10.1056/NEJMoa061240#article\\_references](https://www.nejm.org/doi/full/10.1056/NEJMoa061240#article_references) [Accessed 19 Jul. 2018].
- Seeman, P. (2004). Dopamine receptors and the dopamine hypothesis of schizophrenia. *Synapse*, 1(2), pp.133-152.
- Seida, J., Boylan, K., Newton, A. and Carrey, N. (2012). First- and second-generation antipsychotics for children and young adults. Rockville, MD: Agency for Healthcare Research and Quality.
- Sempere, L., Freemantle, S., Pitha-Rowe, I., Moss, E., Dmitrovsky, E. and Ambros, V. (2004). *Genome Biology*, 5(3), p.R13.
- Shen, W. (1999). A history of antipsychotic drug development. *Comprehensive Psychiatry*, 40(6), pp.407-414.

- Shi, Y. (2004). Caspase activation, inhibition, and reactivation: A mechanistic view. *Protein Science*, 13(8), pp.1979-1987.
- Shimizu, S., Yoshida, T., Tsujioka, M. and Arakawa, S. (2014). Autophagic Cell Death and Cancer. *International Journal of Molecular Sciences*, 15(2), pp.3145-3153.
- Shuster C. (2003). Vision learning. BIO-1 (2). [Available]: [http://www.visionlearning.com/library/module\\_viewer.php?mid=64](http://www.visionlearning.com/library/module_viewer.php?mid=64)
- Sigel, a., sigel, h. & sigel, r. K. O. 2013. Interrelations between essential metal ions and human diseases, dordrecht ; new york, springer.
- Silva, E., Braga, R., Avelino-Silva, T. and Gil Junior, L. (2011). Antipsychotics in Alzheimer's disease: A critical analysis. *Dementia & Neuropsychologia*, 5(1), pp.38-43.
- Skulachev, V. (2006). Bioenergetic aspects of apoptosis, necrosis and mitoptosis. *Apoptosis*, 11(4), pp.473-485.
- Slee, E., Adrain, C. and Martin, S. (2000). Executioner Caspase-3, -6, and -7 Perform Distinct, Non-redundant Roles during the Demolition Phase of Apoptosis. *Journal of Biological Chemistry*, 276(10), pp.7320-7326.
- Sommer, I., Slotema, C., Daskalakis, Z., Derks, E., Blom, J. and van der Gaag, M. (2012). The Treatment of Hallucinations in Schizophrenia Spectrum Disorders. *Schizophrenia Bulletin*, 38(4), pp.704-714.
- Sommer, I., Slotema, C., Daskalakis, Z., Derks, E., Blom, J. and van der Gaag, M. (2012). The Treatment of Hallucinations in Schizophrenia Spectrum Disorders. *Schizophrenia Bulletin*, 38(4), pp.704-714.
- Son, T. G., Zou, Y., Jung, K. J., Yu, B. P., Ishigami, A., Maruyama, N. & Lee, J. (2006). Smp30 deficiency causes increased oxidative stress in brain. *Mech ageing dev*, 127, pp.451-457.
- Squire, L. (2008). *Fundamental neuroscience*. Amsterdam: Elsevier / Academic Press.

- STECK, H. (1954). Extrapyramidal and diencephalic syndrome in the course of largactil and serpasil treatments. *Annales medico-psychologiques*, 112(2-5), pp.737-744.
- Steele, C., Rovner, B., Chase, G. and Folstein, M. (1990). Psychiatric symptoms and nursing home placement of patients with Alzheimer's disease. *American Journal of Psychiatry*, 147(8), pp.1049-1051.
- Strehler, E. and Zacharias, D. (2001). Role of alternative splicing in generating isoform diversity among plasma membrane calcium pumps. *Physiol Rev.*, 81(1), pp.21-50.
- Structure.2625.html?rid=71791261-71d6-43cd-a5f2-69aa3c600e0f [Accessed 1 Oct. 2014].
- Sudbrak, R. (2000). Hailey-Hailey disease is caused by mutations in ATP2C1 encoding a novel Ca<sup>2+</sup> pump. *Human Molecular Genetics*, 9(7), pp.1131-1140.
- Sugden D, Davidson K, Hough KA, Teh T. (2004). Melatonin, melatonin receptors and melanophores: a moving story. *Pigment Cell Res.* 17(5): pp. 454-460.
- Susin, S., Daugas, E., Ravagnan, L., Samejima, K., Zamzami, N., Loeffler, M., Costantini, P., Ferri, K., Irinopoulou, T., Prévost, M., Brothers, G., Mak, T., Penninger, J., Earnshaw, W. and Kroemer, G. (2000). Two Distinct Pathways Leading to Nuclear Apoptosis. *The Journal of Experimental Medicine*, 192(4), pp.571-580.
- Szulik, J. (2007). Antipsychotics in geriatric institutions. *Vertex*, 18(76), pp.454-460.
- Tanida, I., Ueno, T. and Kominami, E. (2008). LC3 and Autophagy. *Autophagosome and Phagosome*, pp.77-88.
- Tariot, P., Schneider, L. and Katz, I. (1995). Anticonvulsant and Other Non-neuroleptic Treatment of Agitation in Dementia. *Journal of Geriatric Psychiatry and Neurology*, 8(1), pp.S28-S39.
- Taylor, D., Mir, S. and Mace, S. (1999). Olanzapine in practice: a prospective naturalistic study. *Psychiatric Bulletin*, 23(3), pp.178--180.

- Thomas, R. (2009). The plasma membrane calcium ATPase (PMCA) of neurones is electroneutral and exchanges 2 H<sup>+</sup> for each Ca<sup>2+</sup> or Ba<sup>2+</sup> ion extruded. *The Journal of Physiology*, 587(2), pp.315-327.
- Tobisawa, M. and Yamaguchi, M. (2003). Inhibitory role of regucalcin in the regulation of nitric oxide synthase activity in rat brain cytosol: involvement of aging. *J Neurol Sci*, 209, pp.47-54.
- Toyoshima, C., Nakasako, M., Nomura, H. and Ogawa, H. (2000). Crystal structure of the calcium pump of sarcoplasmic reticulum at 2.6 Å resolution. *Nature*, 405(6787), pp.647-655.
- Tsujimoto, Y. and Shimizu, S. (2005). Another way to die: autophagic programmed cell death. *Cell Death and Differentiation*, 12, pp.1528-1534.
- Tsurusaki, Y. & Yamaguchi, M. (2002). Role of endogenous regucalcin in nuclear regulation of regenerating rat liver: suppression of the enhanced ribonucleic acid synthesis activity. *J Cell Biochem*, 87, pp.450-7.
- Vallianatou, K. (2016). Antipsychotics. *Medicine*, 44(12), pp.748–752.
- Van Baelen, K., Dode, L., Vanoevelen, J., Callewaert, G., De Smedt, H., Missiaen, L., Parys, J., Raeymaekers, L. and Wuytack, F. (2004). The Ca<sup>2+</sup>/Mn<sup>2+</sup> pumps in the Golgi apparatus. *Biochimica et Biophysica Acta (BBA) - Molecular Cell Research*, 1742(1-3), pp.103-112.
- Van Baelen, K., Vanoevelen, J., Callewaert, G., Parys, J., De Smedt, H., Raeymaekers, L., Rizzuto, R., Missiaen, L. and Wuytack, F. (2003). The contribution of the SPCA1 Ca<sup>2+</sup> pump to the Ca<sup>2+</sup> accumulation in the Golgi apparatus of HeLa cells assessed via RNA-mediated interference. *Biochemical and Biophysical Research Communications*, 306(2), pp.430-436.
- Van Meerloo, J., Kaspers, G. and Cloos, J. (2011). Cell Sensitivity Assays: The MTT Assay. *Methods in Molecular Biology*, pp.237-245.
- Vandecaetsbeek, I., Vangheluwe, P., Raeymaekers, L., Wuytack, F. and Vanoevelen, J. (2011). The Ca<sup>2+</sup> Pumps of the Endoplasmic Reticulum and Golgi Apparatus. *Cold Spring Harbor Perspectives in Biology*, 3(5), pp.a004184-a004184.

- Vandenabeele, P., Galluzzi, L., Vanden Berghe, T. and Kroemer, G. (2010). Molecular mechanisms of necroptosis: an ordered cellular explosion. *Nature Reviews Molecular Cell Biology*, 11(10), pp.700-714.
- Vanlangenakker, N., Berghe, T., Krysko, D., Festjens, N. and Vandenabeele, P. (2008). Molecular Mechanisms and Pathophysiology of Necrotic Cell Death. *Current Molecular Medicine*, 8(3), pp.207-220.
- Vanoevelen, J., Dode, L., Van Baelen, K., Fairclough, R., Missiaen, L., Raeymaekers, L. and Wuytack, F. (2005). The Secretory Pathway  $\text{Ca}^{2+}/\text{Mn}^{2+}$ -ATPase 2 Is a Golgi-localized Pump with High Affinity for  $\text{Ca}^{2+}$  Ions. *Journal of Biological Chemistry*, 280(24), pp.22800-22808.
- Vanoevelen, J., Dode, L., Van Baelen, K., Fairclough, R., Missiaen, L., Raeymaekers, L. and Wuytack, F. (2005). The Secretory Pathway  $\text{Ca}^{2+}/\text{Mn}^{2+}$ -ATPase 2 Is a Golgi-localized Pump with High Affinity for  $\text{Ca}^{2+}$  Ions. *Journal of Biological Chemistry*, 280(24), pp.22800-22808.
- Vaz, C., Maia, C., Marques, R., Gomes, I., Correia, S., Alves, M., Cavaco, J., Oliveira, P. and Socorro, S. (2014). Regucalcin is an androgen-target gene in the rat prostate modulating cell-cycle and apoptotic pathways. *The Prostate*, 74(12), pp.1189-1198.
- Vercammen, D., Beyaert, R., Denecker, G., Goossens, V., Van Loo, G., Declercq, W., Grooten, J., Fiers, W. and Vandenabeele, P. (1998). Inhibition of Caspases Increases the Sensitivity of L929 Cells to Necrosis Mediated by Tumor Necrosis Factor. *The Journal of Experimental Medicine*, 187(9), pp.1477-1485.
- Vercammen, D., Brouckaert, G., Denecker, G., Van de Craen, M., Declercq, W., Fiers, W. and Vandenabeele, P. (1998). Dual Signaling of the Fas Receptor: Initiation of Both Apoptotic and Necrotic Cell Death Pathways. *The Journal of Experimental Medicine*, 188(5), pp.919-930.
- Vucicevic, L., Misirkic-Marjanovic, M., Paunovic, V., Kravic-Stevovic, T., Martinovic, T., Ciric, D., Maric, N., Petricevic, S., Harhaji-Trajkovic, L., Bumbasirevic, V. and Trajkovic, V. (2014). Autophagy inhibition uncovers the neurotoxic action of the antipsychotic drug olanzapine. *Autophagy*, 10(12), pp.2362-2378.

- Vucicevic, L., Misirkic-Marjanovic, M., Paunovic, V., Kravic-Stevovic, T., Martinovic, T., Ciric, D., Maric, N., Petricevic, S., Harhaji-Trajkovic, L., Bumbasirevic, V. and Trajkovic, V. (2014). Autophagy inhibition uncovers the neurotoxic action of the antipsychotic drug olanzapine. *Autophagy*, 10(12), pp.2362-2378.
- Wajant, H., Pfizenmaier, K. and Scheurich, P. (2002). TNF-related apoptosis inducing ligand (TRAIL) and its receptors in tumor surveillance and cancer therapy. *APOPTOSIS*, 7(5), pp.449-459.
- Wallach, D. and Kovalenko, A. (2014). Keeping inflammation at bay. *eLife*, 3.
- Weiner, m. W., veitch, d. P., aisen, p. S., beckett, l. A., cairns, n. J., green, r. C., harvey, d., jack, c. R., jagust, w., liu, e., morris, j. C., petersen, r. C., saykin, a. J., schmidt, m. E., shaw, l., siuciak, j. A., soares, h., toga, a. W., trojanowski, j. Q. & alzheimer's disease neuroimaging, i. (2012). The alzheimer's disease neuroimaging initiative: a review of papers published since its inception. *Alzheimers dement*, 8, s1-68.
- Wiklund, E., Catts, V., Catts, S., Ng, T., Whitaker, N., Brown, A. and Lutze-Mann, L. (2010). Cytotoxic effects of antipsychotic drugs implicate cholesterol homeostasis as a novel chemotherapeutic target. *International Journal of Cancer*, 126(1), pp.28-40.
- Wojda, U., salinska, E. and Kuznicki, J. (2008). Calcium ions in neuronal degeneration. *Iubmb life*, 60, pp.575-590.
- Wootton, L., Argent, C., Wheatley, M. and Michelangeli, F. (2004). The expression, activity and localisation of the secretory pathway Ca<sup>2+</sup>-ATPase (SPCA1) in different mammalian tissues. *Biochimica et Biophysica Acta (BBA) - Biomembranes*, 1664(2), pp.189-197.
- Wuytack, F., Raeymaekers, L. and Missiaen, L. (2002). Molecular physiology of the SERCA and SPCA pumps. *Cell Calcium*, 32(5-6), pp.279-305.
- Xiang, M., Mohamalawari, D. and Rao, R. (2005). A Novel Isoform of the Secretory Pathway Ca<sup>2+</sup>,Mn<sup>2+</sup>-ATPase, hSPCA2, Has Unusual Properties and Is Expressed in the Brain. *Journal of Biological Chemistry*, 280(12), pp.11608-11614.

- Xiang, M., Mohamalawari, D. and Rao, R. (2005). A Novel Isoform of the Secretory Pathway Ca<sup>2+</sup>,Mn<sup>2+</sup>-ATPase, hSPCA2, Has Unusual Properties and Is Expressed in the Brain. *Journal of Biological Chemistry*, 280(12), pp.11608-11614.
- Yamaguchi, H. and Wang, H. (2004). CHOP Is Involved in Endoplasmic Reticulum Stress-induced Apoptosis by Enhancing DR5 Expression in Human Carcinoma Cells. *Journal of Biological Chemistry*, 279(44), pp.45495-45502.
- Yamaguchi, M. (2000). Mini review –role of regucalcin in calcium signalling. *Life science*, 66, pp. 1769-1780.
- Yamaguchi, M. (2000). Role of regucalcin in calcium signaling. *Life Sciences*, 66(19), pp.1769-1780.
- Yamaguchi, M. (2010). Regucalcin and metabolic disorders: osteoporosis and hyperlipidemia are induced in regucalcin transgenic rats. *Mol cell biochem*, 341, pp.119-133.
- Yamaguchi, M. (2011). Regucalcin and cell regulation: role as a suppressor protein in signal transduction. *Mol cell biochem*, 353, pp.101-137.
- Yamaguchi, M. (2012). Regucalcin, cell signaling-related protein: its multifunctional role in kidney cell regulation. *OA Biotechnology*, 1(1).
- Yamaguchi, M. (2012). Role of regucalcin in brain calcium signaling: involvement in aging. *Integrative Biology*, 4(8), pp.825-837.
- Yamaguchi, M. (2012). Role of regucalcin in brain calcium signaling: involvement in aging. *Integr biol (Camb)*, 4, pp.825-837.
- Yamaguchi, M. (2013). Calcium regulatory protein, regucalcin, may be a key molecule in brain disease. *Journal of molecular and genetic medicine*, 07.
- YAMAGUCHI, M. (2014). Regulatory role of regucalcin in heart calcium signaling: Insight into cardiac failure (Review). *Biomedical Reports*, 2(3), pp.303-308.
- Yamaguchi, M. 2005. Role of regucalcin in maintaining cell homeostasis and function (review). *Int j mol med*, 15, pp.371-89.

- Yamaguchi, M. and Daimon, Y. (2005). Overexpression of regucalcin suppresses cell proliferation in cloned rat hepatoma H4-II-E cells: Involvement of intracellular signaling factors and cell cycle-related genes. *Journal of Cellular Biochemistry*, 95(6), pp.1169-1177.
- Yamaguchi, M. and Isogai, M. (1993). Tissue concentration of calcium-binding protein regucalcin in rats by enzyme-linked immunoadsorbent assay. *Mol cell biochem*, 122, pp.65-68.
- Yamaguchi, M. and Yamamoto, T. (1978). Purification of calcium binding substance from soluble fraction of normal rat liver. *Chem pharm bull*, 26, pp.1918.
- Yamaguchi, M., Hanahisa, Y. and Murata, T. (1999). Expression of calcium-binding protein regucalcin and microsomal Ca<sup>2+</sup>-ATPase regulation in rat brain: attenuation with increasing age. *Molecular and Cellular Biochemistry*, 200(1/2), pp.43-49.
- Yamaguchi, M., Igarashi, A., Uchiyama, S. and Sawada, N. (2004). Hyperlipidemia is induced in regucalcin transgenic rats with increasing age. *International Journal of Molecular Medicine*, 14(4), pp.647-651.
- Yamaguchi, M., Osuka, S., Weitzmann, M., Shoji, M. and Murata, T. (2016). Increased regucalcin gene expression extends survival in breast cancer patients: Overexpression of regucalcin suppresses the proliferation and metastatic bone activity in MDA-MB-231 human breast cancer cells in vitro. *International Journal of Oncology*, 49(2), pp.812-822.
- Yamaguchi, M., Takakura, Y. & Nakagawa, T. (2008). Regucalcin increases ca<sup>2+</sup>-atpase activity in the mitochondria of brain tissues of normal and transgenic rats. *J cell biochem*, 104, pp.795-804.
- Youle, R. and Strasser, A. (2008). The BCL-2 protein family: opposing activities that mediate cell death. *Nature Reviews Molecular Cell Biology*, 9(1), pp.47-59.
- Zarain-Herzberg, A., MacLennan, D. and Periasamy, M. (1990). Characterization of rabbit cardiac sarco(endo)plasmic reticulum Ca<sup>2+</sup>(+)-ATPase gene. *J Biol Chem.*, 265(8), pp.4670-7.

- Zhang, D., Shao, J., Lin, J., Zhang, N., Lu, B., Lin, S., Dong, M. and Han, J. (2009). RIP3, an Energy Metabolism Regulator That Switches TNF-Induced Cell Death from Apoptosis to Necrosis. *Science*, 325(5938), pp.332-336.
- Zhang, J. and Ming, X. (2000). DNA fragmentation in apoptosis. *Cell research*, 10(3), pp.205--211.
- Zito, J., Safer, D., Gardner, J., Boles, M., Lynch, F. and others, (2000). Trends in the prescribing of psychotropic medications to preschoolers. *Jama*, 283(8), pp.1025--1030.